Development of Novel Inhibitors
of Human Dihydroorotate Dehydrogenase
as Antiviral Drug Candidates

-

Design, Synthesis and Pharmacological Evaluation

Dissertation
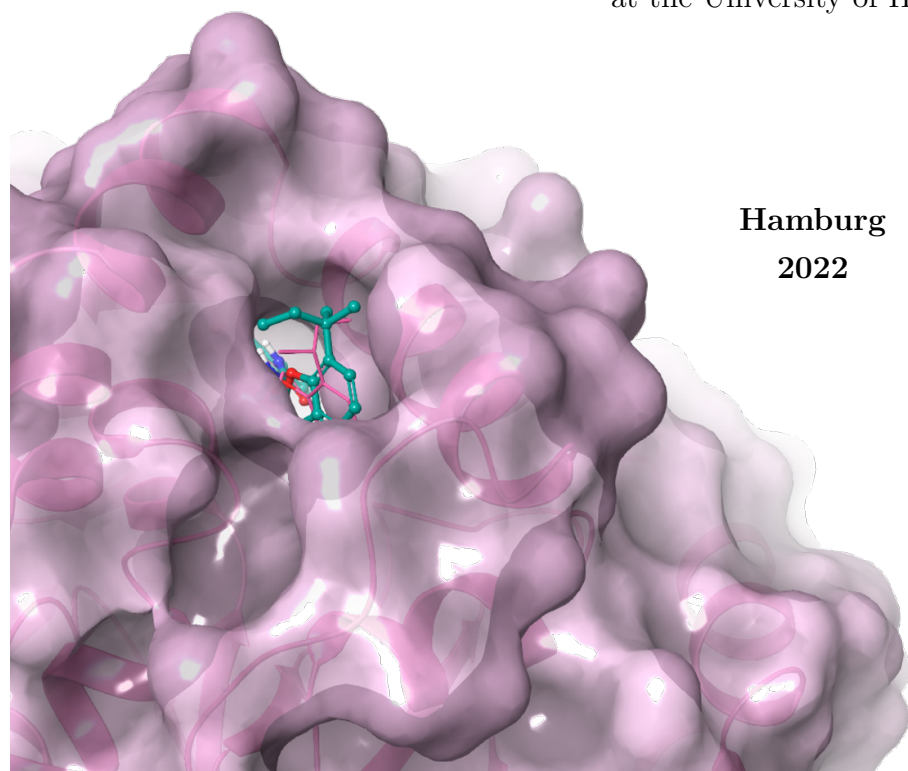
to obtain the Scientific Doctoral Degree

by

Nora Constanze Laubach (born Fohrmann)

presented to

the Department of Chemistry
of the Faculty of Sciences
at the University of Hamburg

Hamburg
2022

The present work was compiled in the research group of Prof. Dr. Chris Meier at the Institute of Organic Chemistry in the Department of Chemistry of the University of Hamburg between March 2017 and December 2020.

1st Reviewer: Prof. Dr. Chris Meier
2nd Reviewer: Prof. Dr. Johannes Kirchmair

Date of disputation: 22.04.2022
Date of print approval: 18.08.2022

≫*Du hast schon wieder Flausen im Kopf!*
Ich bin hier zufrieden und weiß überhaupt gar nicht
in welche Richtung ich fliegen müsste. So eine lange Reise ist viel zu gefährlich,
ich bleibe hier!≪*, erwiderte Kalle entschlossen.*

≫*Dann fliege ich eben alleine los.*
Ich weiß den Weg auch nicht, aber das wird bestimmt ein großes Abenteuer!≪

From Imke Hahn: Olaf will ans Meer. 2021.

Contents

Contents

List of publications

Patents

P1 Meier, C.; Fohrmann, N. C.; Rijono, D. DHODH inhibitors and their use as antiviral agents. European Patent Application, 2022/07/11 PCT/EP2022/069306.

P2 Meier, C.; Winkler, M.; Pfaff, K.; Fohrmann, N. C.; Querat, G.; de Lamballerie, X. DHODH inhibitors and their use as antiviral agents. International Patent Application, Publication date 2020/11/12. WO/2020/225330 A1.

Posters and oral presentations

P3 Fohrmann, N. C.; Gerber, L.; Oestereich, L.; Pfeffer, I.; Quérat, G.; Meier, C. Metabolic Stabilization of a Novel hDHODH Inhibitor with Potent Broad Spectrum Antiviral Activity. Poster Presentation and Oral Presentation at the 34th International Conference on Antiviral Research (ICAR) 2021 Virtual Meeting.

P4 Fohrmann, N. C.; Pfaff, K. Winkler, M.; Kirchmair, J.; Quérat, G.; Meier, C. Rational Design, Synthesis and Biological Evaluation of Novel hDHODH Inhibitors. Poster Presentation and Oral Presentation at the 11th Joint Meeting on Medicinal Chemistry (JMMC) 2019. Prague, Czech Republic.

P5 Fohrmann, N. C.; Pfaff, K.; Winkler, M.; Kirchmair, J.; Quérat, G.; Meier, C. Development of Novel hDHODH Inhibitors as Potent Broad Spectrum Antiviral Agents. Poster Presentation and Oral Presentation at the 32nd International Conference on Antiviral Research (ICAR) 2019. Baltimore, MA, USA.

Supervised bachelor theses

P6 Lydia Gerber, *Beiträge zur Synthese potentieller, metabolisch stabilisierter Inhibitoren der Dihydroorotat Dehydrogenase.* University of Hamburg, **2019**.

P7 Sarah Post, *Synthese von Heterozyklusderivaten als Bausteine für neue potentielle DHODH-Inhibitoren.* University of Hamburg, **2018**.

P8 Melanie Hofmann, *Synthese eines Benzodioxol-Derivats als Kernfragment für neue potentielle DHODH-Inhibitoren.* University of Hamburg, **2018**.

P9 Sahra Massoud, *Beiträge zur Synthese von Stickstoffheterozyklus-Derivaten eines metabolisch instabilen DHODH-Inhibitors.* University of Hamburg, **2017**.

List of abbreviations

Abb.	Abbildung
ADME	absorption, distribution, metabolism, elimination
ADP	atomic displacement parameters
AML	acute myeloid leukemia
A-orientation	active site-orientation
ATR	attenuated total reflection
aq	aqueous
a. u.	arbitrary units
AUC	area under the curve
BINAP	2,2'-bis(diphenylphosphino)-1,1'-binaphthalene
BuLi	butyllithium
cbc1	cytochrome c oxidoreductase
CAD	carbamoyl phosphate synthetase II, aspartate carbamoyltransferase & dihydroorotase enzyme complex
calc.	calculated
CC_{50}	halfmaximal cytotoxic concentration
CCHFV	Crimean-Congo hermorrhagic fever virus
CD4	cluster of differentiation 4
CD8	cluster of differentiation 8
CDP	cytidine diphosphate
CES	carboxylesterase
conc.	concentrated
COSY	homonuclear correlation spectroscopy
CoQ1	coenzyme Q1 (ubiquinone-1)
COVID-19	Corona virus disease 2019
CTP	cytidine triphosphate
CYP	cytochrome P450
DAD	diode array detection
DCPIP	2,6-dichlorophenolindophenol
demin.	demineralised
DHO	dihydroorotate
DHODH	dihydroorotate dehydrogenase
DMAP	4-(dimethylamino)pyridine
DMSO	dimethyl sulfoxide
DNA	deoxyribonucleic acid

dTTP	deoxy thymidine triphosphate
dCTP	deoxy cytidine triphosphate
DMF	*N,N*-dimethylformamide
E1cb	elimination, unimolecular, conjugate base
EA	ethyl acetate
EC_{50}	halfmaximal effective concentration
E. coli	*escherichia coli*
EBOV	Ebola virus
EI	electron ionisation
em	emission
eq.	equivalents
ESI	electrospray ionisation
et al.	*et alia* (and others)
Et_3N	triethylamine
exc	excitation
fig.	figure
FLD	fluorescence detection
FMN	flavin mononucleotide
$FMNH_2$	dihydro flavin mononucleotide
FLD	fluorescence detection
hDHODH	human dihydroorotate dehydrogenase
HEGA-8	octanoyl-*N*-hydroxyethylglucamide
HEPES	4-(2-hydroxyethyl)-1-piperazineethanesulfonic acid
HMBC	heteronuclear multiple bond correlation
HPLC	high performance liquid chromatography
HRMS	high resolution mass spectrometry
HSQC	heteronuclear single quantum coherence spectroscopy
HT	high throughput
IC_{50}	halfmaximal inhibitory concentration
IPTG	*iso*-propyl-β-D-thiogalactoside
IR	infrared
isocr.	isocratic
IV	intravenous
KO*t*Bu	potassium *tert*-butoxide
LASV	Lassa virus
LC/MS	liquid chromatography coupled to mass spectrometry

logD	distribution coefficient
+M-effect	positive mesomeric effect
MES	2-(N-morpholino)ethanesulfonic acid
MHC	major histocompatibility complex
MS	mass spectrometry
NADPH	nicotinamide adenine dinucleotide phosphate
NanoDSF	nano differential scanning fluorimetry
n. d.	not determined
NMR	nuclear magnetic resonance
NOESY	Nuclear Overhauser Effect spectroscopy
OMP	orotate monophosphate
ORO	orotate
PAMPA	parallel artificial membrane permeation assay
PBS	phosphate buffered saline
PD	pharmacodynamic
PDB	Protein Data Base
Pd/C	palladium on activated carbon
PE	petroleum ether
pfDHODH	*plasmodium falciparum* DHODH
PG	protecting group
pH	*potentia hydrogenii*
PK	pharmacokinetic
PO	peroral
PPB	plasma protein binding
QH$_2$	ubiquinol
quant.	quantitative
ref	reference
rt	room temperature
RNA	ribonucleic acid
S9	supernatant from centrifucation at 9000 g
SAR	structure-activity relationship
SARS-CoV	severe acute respiratory syndrome Coronavirus 2
SC	subcutaneous
SDS-PAGE	sodium dodecyl sulfate polyacrylamide gel electrophoresis
S$_N$2	nucleophilic substitution, bimolecular
SOC	super optimal broth with catabolites repression

Contents

1 Zusammenfassung

Die humane Dihydroorotat Dehydrogenase (hDHODH) ist ein prominentes Targetenzym für die Therapieentwicklung zur Behandlung von Autoimmunkrankheiten, Krebs und viralen Infektionen.[1,5,6,89,90] Als Schlüsselenzym der *de novo* Biosynthese von Pyrimidin-Nucleotiden ist sie für die Proliferation von Immun- und Krebszellen sowie die intrazelluläre Replikation von Viren unabdingbar.[1,7–12] Der in den meisten anderen Zellen dominierende, alternative *salvage pathway*, bei dem Nucleotide aus Metabolismusprodukten zurückgewonnen werden, verspricht zudem deren uneingeschränkte Funktion bei einer Hemmung des Biosynthesewegs und somit eine geringe Toxizität von hDHODH-Inhibitoren.[55] Bislang konnte jedoch nur die Zulassung eines einzigen hDHODH-Inhibitors zur Behandlung von Autoimmunkrankheiten erfolgen,[101,102] da sämtliche vielversprechende Wirkstoffkandidaten in klinischen Studien aufgrund hoher Toxizität oder geringer *in vivo*-Wirksamkeit scheiterten.[12] Um in Zukunft das gesamte therapeutische Potential von hDHODH Inhibitoren ausschöpfen zu können, ist die Entwicklung weiterer Wirkstoffkandidaten nach wie vor von großem Interesse.

Kürzlich wurde der hochpotente hDHODH-Inhibitor KP-CF39 **22** (IC_{50} = 7.1 nM, siehe Kapitel 5.2, S. 54-58) von unserer Forschungsgruppe entdeckt und darüber hinaus seine antivirale Breitbandaktivität festgestellt.[124,125] Im ersten Teil dieser Arbeit wurde der Inhibitor hinsichtlich seiner pharmakokinetischen Eigenschaften (siehe Kapitel 5.1, S. 45-50) untersucht. Hierfür wurden zunächst entsprechende Assays etabliert. Bei diesen Untersuchungen wurde neben seiner moderaten Lipophilie (logD = 2.65) und seiner guten Membranpermeabilität (P_{PAMPA} = 1.58·10⁻⁵ cm/s) seine geringe metabolische Stabilität ($S_{S9,1h}$ = 22 %) festgestellt. Mittels LC/MS-Analyse des gebildeten S9-Metabolitengemischs wurde eine metabolische Spaltung der Amidbindung identifiziert sowie die Entstehung von fünf weiteren Metaboliten, bei denen es sich vermutlich um Produkte von Hydroxylierungen am *sec*-Butyl-substituierten Phenolfragment handelte (siehe Kapitel 5.1.4, S. 50-53). Da die geringe metabolische Stabilität von KP-CF39 **22** seine Wirksamkeit in weiterführenden *in vivo*-Studien stark beeinträchtigen würde, wurden im Rahmen dieser Arbeit Optimierungen seiner Struktur vorgenommen. Seine röntgenkristallographisch ermittelte Bindepose diente dabei als Modellvorlage für das Struktur- und Liganden-basierte Design.

In einem ersten Ansatz erfolgte mittels klassischer Leitstrukturoptimierungsprozedur die rationale, schrittweise Modifikation von labilen Elementen der Struktur **22** in drei Zyklen aus Design, Synthese und pharmakologischer Bewertung (siehe Kapitel 5.3, S. 59-74). Die Amidbindung konnte in Zyklus 1 unter Erhalt der hDHODH-Inhibitionsstärke stabilisiert werden, indem sie zu einer Harnstofffunktion erweitert wurde. Dies

führte zu einer Verdopplung der metabolischen Stabilität. Im zweiten Zyklus konnte die metabolische Stabilität durch eine Substitution der *sec*-Butylgruppe gegen eine Trifluormethyleinheit auf 90 % erhöht werden, allerdings führte diese Modifikation auch zu einer achtfachen Reduktion der inhibitorischen Aktivität. Durch eine Modifikation des Linkers sowie eine Eliminierung des stereogenen Zentrums durch seine Erweiterung zur *tert*-Amylfunktion in Zyklus 3 ging der metabolisch stabile, hochpotente hDHODH Inhibitor CF278 **33c** (Abb. 2.1, IC_{50} = 9 nM) als vielversprechender Wirkstoffkandidat mit geeignetem *in vitro*-ADME-Profil ($S_{S9,1h}$ = 68 %, logD = 3.0, P_{PAMPA} = 0.6·10^{-5} cm/s) hervor.

Im letzten Teil dieser Arbeit wurde, ausgehend von dem aktiven 2-Amidobenzoat-Kernfragment, mittels rationalen Designs eine neue, metabolisch stabile Leitstruktur aufgebaut (siehe Kapitel 5.4, S. 107-123). Die schrittweise Erweiterung des Kernfragments erfolgte ebenfalls in drei Zyklen aus Design, Synthese und pharmakologischer Untersuchung. In den ersten beiden Zyklen wurde die Einführung cyclischer Substituenten an der Amidofunktion des Kerngerüsts untersucht, wobei sich das Naphthylfragment als besonders geeignet erwies. Um im dritten Zyklus durch Modifikationen am Anthranilsäurefragment eine fein abgestimmte Anpassung des Naphthyl-basierten Liganden an die hDHODH Bindetasche realisieren zu können, wurde er zunächst mit dem hergestellten Enzym (siehe Kapitel 5.2, S. 54-55) cokristallisiert und anschließend röntgenkristallographisch seine Bindepose bestimmt (siehe Kapitel 5.4.3, S. 117-119). Basierend darauf wurde im dritten Zyklus das Isonicotinsäure Derivat CF287 **97** (Abb. 2.1) entworfen, das sich als potenter hDHODH-Inhibitor (IC_{50} = 89 nM) mit überzeugenden pharmakokinetischen Eigenschaften ($S_{S9,1h}$ = 90 %, P_{PAMPA} = 0.7·10^{-5} cm/s, logD = 0.3) erwies.

Alle Zielverbindungen konnten über 1-9 Stufen in hohen Reinheiten und ausreichenden Mengen für die folgenden pharmakologischen Studien erhalten werden (siehe Kapitel 5.3.6, S. 79-106 und 5.4.5, S. 123-138). Für den Aufbau der Harnstoff- bzw. Carbamatfunktion der Zielverbindungen wurden verschiedene Methoden erprobt. Als robusteste Methode erwies sich eine Kupplungsreaktion zwischen geschütztem 2-Isocyanatobenzoat und den verschiedenen Aminen bzw. deprotonierten Heteroaromaten oder Alkoholen. Die anschließende Entschützung führte zu den Zielverbindungen. Während sich die Methylfunktion als geeignete Carboxy-Schutzgruppe für alle Kupplungsreaktionen mit Alkoholaten (S. 89-92) und sekundären Aminen (S. 127-130) erwies, war für die Kupplung primärer Amine der Einsatz einer Benzyl-Schutzgruppe notwendig (S. 100-105). Ihre Entfernung konnte im letzten Schritt ohne den Einsatz basischer Reagenzien realisiert werden, wodurch kein Basen-induzierter Ringschluss zu

den entsprechenden Quinazolindionderivaten erfolgte. Eine solche Cyclisierung war in Vorläuferverbindungen mit sekundärem Aminobaustein nicht möglich. Alle Alkohole und Amine, die nicht kommerziell erhältlich waren, wurden vor der Kupplung dargestellt (siehe Kapitel 5.3.6, S. 82-99). Die Phenoxyethylalkohole wurden aus den entsprechenden Phenolen durch Ethersynthesen erhalten, während die Benzofuranylmethylalkohole mittels *one-pot* Tandem-Sonogashira-Cyclisierungen aus den *ortho*-iodierten Phenolen hergestellt wurden. Die *ortho*-selektiven Iodierungen erfolgten zuvor regioselektiv nach einer literaturbekannten Methode über drei Schritte. Die Alkoholfunktionen beider Strukturklassen wurden anschließend über drei Stufen in Aminofunktionen umgewandelt, wobei die Mesylaktivierung der Benzofuranylmethylalkohole nicht erfolgreich war und stattdessen ihre Chlorierung vorgenommen wurde.

Schlussendlich gehen aus dieser Arbeit die beiden neuen, potenten hDHODH Inhibitoren CF278 **33c** und CF287 **97** hervor (Abb. 2.1), die sich beide durch ein günstiges *in vitro* ADME-Profil auszeichnen. Das Isonicotinsäurederivat **97** überzeugt zudem durch seine kompakte Struktur und seinen einfachen synthetischen Zugang und weist somit alle Charakteristika einer optimalen Leitstruktur auf, die künftig ein pharmakokinetisch fundiertes Wirkstoffdesign ermöglichen kann. Mit dem Anthranilsäurederivat CF278 **33c** wurde zudem ein neuer Wirkstoffkandidat entwickelt, der *in vitro* eine antivirale Breitbandaktivität im nanomolaren Bereich sowie eine stark hemmende Wirkung auf die Proliferation von Immunzellen zeigte (siehe Kapitel 5.3.4, S. 74-76). In ersten *in vivo* Experimenten wurde zudem seine pharmakokinetische Eignung bestätigt (siehe Kapitel 5.3.5, S. 76-78). Seine gute *in vivo*-Verträglichkeit und seine bemerkenswert hohe perorale Bioverfügbarkeit heben den hochpotenten Wirkstoffkandidaten CF278 **33c** aus dem Spektrum derzeit bekannter hDHODH-Inhibitoren hervor.

2 Abstract

The human dihydroorotate dehydrogenase (hDHODH) is a prominent enzyme, frequently targeted for the development of therapeutics against autoimmune diseases, cancer and viral infections.[1,5,6,89,90] Being involved in the *de novo* biosynthesis of pyrimidine nucleotides, its intact function is inevitable for the proliferation of immune and cancer cells as well as for intracellular viral replication.[1,7–12]At the same time, the alternative nucleotide salvage pathway, which is predominant in most other cells, preserves their function during a shutdown of the *de novo* biosynthesis and, thus, suggests low cytotoxicity of hDHODH inhibitors.[55] However, until now, only one hDHODH inhibitor has been approved for the treatment of autoimmune diseases,[101,102] as several promising drug candidates failed clinical trials due to high toxicity or low *in vivo* efficacy.[12] Consequently, the development of novel drug candidates remains of high interest, aiming to fully exploit the therapeutic potential of hDHODH inhibitors, once.

Recently, highly potent hDHODH inhibitor KP-CF39 **22** (IC_{50} = 7.1 nM, see chapter 5.2, p. 54-58) has been discovered in our research group as well as its broad spectrum activity against a panel of viruses.[124,125] Efforts of this work moreover revealed its widely suitable pharmacokinetic properties which were investigated in the first part of this thesis (see chapter 5.1, p. 45-50). For this purpose, according assays were established, before. KP-CF39 **22** was characterised by a moderate lipophilicity (logD = 2.65) and good membrane permeability (P_{PAMPA} = 1.58·10^{-5} cm/s) but poor metabolic stability ($S_{S9,1h}$ = 22 %). Via LC/MS analysis of the formed S9-metabolites mixture, a cleavage of the amide bond was identified, as well as the formation of four hydroxylation products, whose sites of metabolism were assumed to be located at the *sec*-butyl-substituted phenol fragment (see chapter 5.1.4, p. 50-53). Since this metabolic lability would severely limit the *in vivo* efficacy of KP-CF39 **22**, its structure was optimised, here. Its X-ray crystallographically determined binding pose served as a model template for the applied structure/ligand-based design.

In a first approach, labile elements in structure **22** were successively modified in three cycles of design, synthesis and pharmacological evaluation, by following a classical lead optimisation procedure (see chapter 5.3, p. 59-74). In cycle 1, a stabilisation of the amide bond was achieved by its inclusion into an ureido-function, which preserved hDHODH inhibition potency. This modification resulted in a twofold increase of overall-metabolic stability. Replacing the *sec*-butyl group by a trifluoro substituent in cycle 2 increased the metabolic stability to $S_{S9,1h}$ = 90 % but was accompanied with an eightfold loss of hDHODH inhibition potency. Through linker modification in

cycle 3 and a simultaneous elimination of the stereogenic center in the *sec*-butyl substituent by its replacement with a *tert*-amyl function, metabolically stable and highly potent benzofuranyl-based hDHODH inhibitor CF278 **33c** (figure 2.1, IC_{50} = 9 nM, $S_{S9,1h}$ = 68 %) finally emerged from the lead optimisation procedure as promising drug candidate with suitable *in vitro* ADME profile (logD = 3.0, P_{PAMPA} = $0.6 \cdot 10^{-5}$ cm/s). In the last part of this thesis, a novel lead structure was developed, starting from the active 2-amidobenzoate core scaffold (see chapter 5.4, p. 107-123). Its stepwise expansion was carried out in three cycles of design, synthesis and pharmacological evaluation. From the first two cycles, naphthyl emerged as most suitable cyclic substituent at the amido function of the core scaffold. Cocrystallisation of the according ligand with the prepared enzyme was followed by X-ray crystallographic determination of its binding pose (see chapter 5.2, p. 54-55 and 5.4.3, p. 117-119). Based on this, a finetuned adaption of the ligand structure to the binding pocket of hDHODH was enabled through modifications at the anthranilate arene in cycle 3. Thus, isonicotinic acid derivative **97** (figure 2.1) emerged as potent hDHODH inhibitor (IC_{50} = 89 nM) with druglike pharmacokinetic properties ($S_{S9,1h}$ = 90 %, P_{PAMPA} = $0.7 \cdot 10^{-5}$ cm/s, logD = 0.3).

All target compounds were synthesised in 1-9 steps in high purities and sufficient quantities for the following pharmacologic studies (see chapter 5.3.6, p. 79-106 and 5.4.5, p. 123-138). For ureido or carbamate formation, various methods were tested. The robustest method proved to be a coupling reaction between previously synthesised, protected 2-isocyanatobenzoate and various amines, deprotonated heteroarenes or alcoholates. Subsequent deprotection finally yielded the target compounds. For all coupling reactions with alcoholates (p. 89-92) and secondary amines (p. 127-130), a methyl group was successfully used to protect the carboxy function, whereas couplings of primary amines required the use of a benzyl protecting group, instead (p. 100-105). For its hydrogenolytic cleavage in the last step, no basic reagents were required and, thus, no cyclisation to the respective quinazolinediones occurred. In contrast, precursor structures from secondary amines were inert to such cyclisations. All alcohols and amines, that were not commercially available, were synthesised prior to coupling (see chapter 5.3.6, p. 82-99). Phenylalcohols were obtained from respective phenols in according ether syntheses, whereas benzofuranylmethylalcohols were synthesised via one-pot Tandem-Sonogashira cyclisations. Previous *ortho*-selective iodinations succeeded via three-step literature-known procedures. Subsequently, the alcohol moieties of both structure classes were converted to amino functions in three steps. Since the mesylation of benzofuranylmethylalcohols was not successful, chlorides were used as

reactive species, instead.

In conclusion, the two novel, potent hDHODH inhibitors CF278 **33c** and CF287 **97** emerge from this thesis (fig. 2.1), both characterised by a druglike *in vitro* ADME profile. CF287 **97** moreover convinces with its compact structure and its facile synthetic access, thus providing all charasteristics of an optimal lead structure on whose basis a pharmacokinetically founded drug design can be realised in the future. With the development of CF278 **33c**, a new drug candidate was created that showed nanomolar antiviral broad spectrum activity *in vitro* as well as strong inhibitory effects on the proliferation of immune cells (see chapter 5.3.4, p. 74-76). First *in vivo* experiments moreover revealed its pharmacokinetic suitability (see chapter 5.3.5, p. 76-78). Its good *in vivo* tolerability and its high peroral bioavailability raise CF278 **33c** above the pool of currently discovered hDHODH inhibitors.
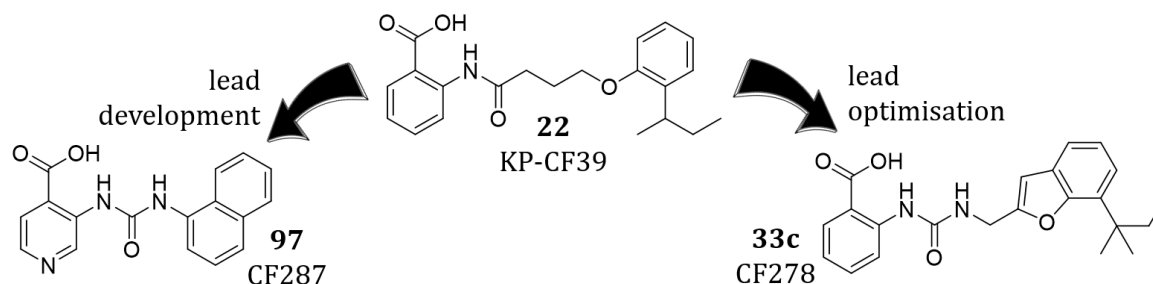

Figure 2.1: Structures of two novel hDHODH inhibitors, developed from common lead structure **22**.

3 Introduction

3.1 Motivation

The development of a drug from its discovery to its approval is a cost-intensive and time-demanding process. In this process, a conscious and thorough optimisation of the drug candidate's potency and pharmacological properties increases its chance to successfully pass clinical studies. Therefore, it is of particular interest and rewarding to develop substances that can be applied in more than one therapeutic area. Such a broad therapeutic application potential is attributed to inhibitors of the human enzyme dihydroorotate dehydrogenase (hDHODH), that show immunosuppressive as well as anticancer and antiviral activities.[1–6] hDHODH is involved in the *de novo* biosynthesis of pyrimidine nucleotides and, thus, its intact function is essential to provide rapidly proliferating cells, like activated T lymphocytes[7,8] and cancer cells[9,10] with building blocks for their replication, protein glycosylation, membrane lipid synthesis and extra-cellular signalling. Viruses also rely on an intact pyrimidine *de novo* synthesis pathway in the infected host cell,[11,12] since they are characterised by a fast replication. At the same time, the function of resting cells is independent of hDHODH activity, as their supply with pyrimidine nucleotides is realised by sole recycling of catabolised monophosphates via salvage pathway.[13]

In general, for antiviral therapy the inhibition of cellular enzymes has decisive advantages over targeting viral enzymes, despite their high potential to cause toxic effects in the host. Hence, they are rarely subject to mutations and the resulting formation of resistance. Furthermore, due to the high diversity of viral enzymes, their inhibition often only enables a one-drug-one-bug approach, whereas broad spectrum antiviral activity is likely to be achieved by the inhibition of cellular target enzymes, like hDHODH.[14,15]

Recently, newly emerging viruses have gained increasing attention. Their sudden appearance and fast spreading rate are the result of mutation events which can affect various properties of the virus, like its host specificity, virulence or caused symptoms and mortality, facilitating their distribution. Moreover, recent trends like globalisation, expanding populations and global warming further accelerate the spread and expand the distribution range of such emerging viruses and expose us to an omnipresent risk of developing fatal virus pandemics.[16,17] This risk recently became reality when in 2019 SARS-CoV-2 evolved the ability to infect humans and, thus, rapidly spread globally, resulting in the current fatal SARS-CoV-2 pandemic, which until now has claimed the lives of more than 5.5 million people.[18] The development of broad spectrum

antivirals is of high interest to enable a fast response to suddenly emerging viruses. Besides SARS-CoV-2 and Ebola virus, species of the order *Bunyavirales*, which include Lassa virus (LASV), Crimean-Congo hemorrhagic fever virus (CCHFV) and Toscana virus (TOSV) among many others, are considered extremely dangerous and capable of developing emergence potential, which could lead to another fatal pandemic.[19] Bunyavirus infections can induce life-threatening diseases in their hosts, ranging from fever to respiratory diseases, encephalitis, hepatitis and hemorrhagic fever. No drugs have been approved for the treatment of infections with bunyaviruses and their response to currently available broad spectrum antivirals like Ribavirin and Favipiravir is largely insufficient.[20] Thus, the development of further broad-spectrum antivirals is of high priority, in order to prepare for potential outbreaks of newly emerging viruses in the future.

Even though the high antiviral efficacy of hDHODH inhibitors in infected cell cultures hitherto failed to be transferred to infected organisms,[12] the persistency of the current SARS-CoV-2 pandemic has revived interest in achieving the approval of novel hDHODH inhibitors for antiviral application. Especially for the treatment of infections with immunopathogenic viruses, the simultaneous immunosuppressive potential of hDHODH inhibitors is expected to boost their antiviral potential.

3.2 Drug development - Strategies and fundamentals

Drug development is a comprehensive and cost-intensive process that takes many years and only in rare cases is successfully completed by drug approval. Individual steps of the complete drug development workflow are shown in figure 3.1. The process starts with the discovery of a biologically active substance with potential for therapeutic application (hit). Whereas the discovery of drugs was based on known natural products or serendipitous discoveries until the 20th century, nowadays, advanced technologies enable a targeted discovery of substances that are aimed to cause a specific therapeutic effect. For this purpose, large molecule libraries can be screened for a specific compound feature, either virtually (*in silico*) or by an automated high-throughput procedure (HT screening) that enables screenings of libraries consisting of real molecules (*in vitro*). Depending on the chosen screening method, compounds can be discovered that either bind to a specific target enzyme, cause a specific biological effect in cells
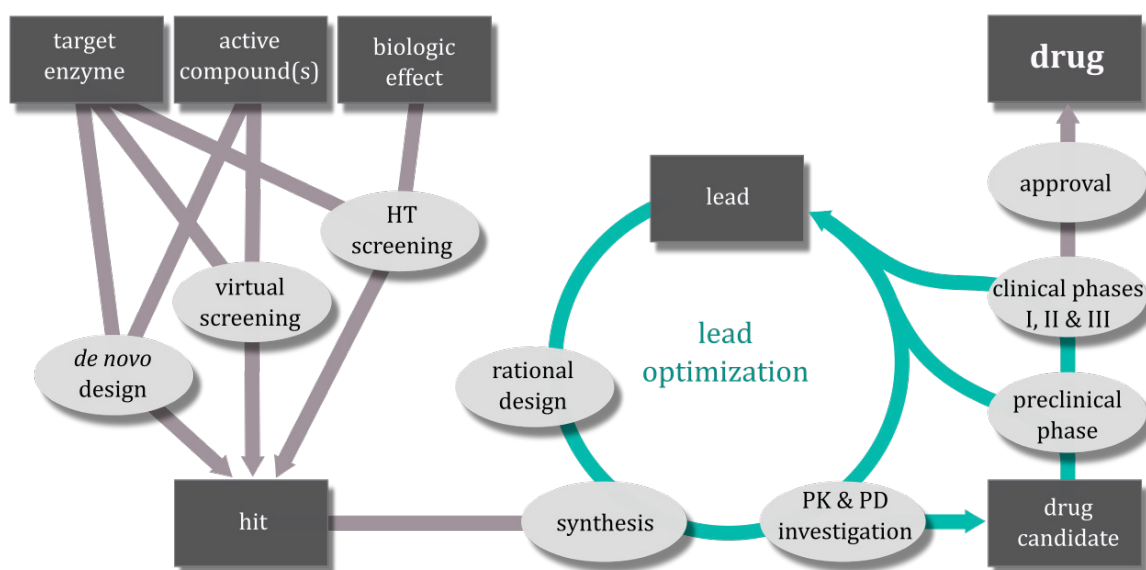
Figure 3.1: Drug development process including stages of hit discovery, hit-to-lead development, lead optimisation and drug approval.

or are similar to already known biologically active compounds regarding structure and consequently potentially regarding their action.[21] Alternatively, a *de novo* design of novel, potentially bioactive compounds can be performed, either inspired by the structural features of known active compounds (ligand-based design) or based on a high-resolution image of the molecular structure of the enzyme's binding site (structure-based design).[22] In the initial phase of drug development, any of these approaches results in the discovery of a compound that is intended to cause a certain biological effect and is called hit. After the synthesis of this compound, its pharmacokinetic (PK) and pharmacodynamic (PD) properties are investigated. Brought together, these investigations help predicting the compound's efficacy and tolerability in living organisms (*in vivo*). Depending on the results of these investigations, the structure either becomes a lead structure for the rational design of novel, structurally improved compounds or already enters the preclinical phase as drug candidate. However, the latter is rarely the case and often several cycles of lead optimisation are required to find a compound with suitable pharmacological properties. Such a drug candidate is then extensively tested for its efficacy and tolerability in living organisms during preclinical and clinical phases. A successful completion of all clinical phases leads to the drug's approval, whereas in case of failure, the drug candidate can reenter the optimisation cycle as novel lead.[23]

As the drug development process progresses, the associated costs increase and become maximal for clinical trials. Therefore, and not at least for ethical reasons, the probability

of preclinical and clinical failure must be minimised. This requires a thorough and conscientious investigation of the compound's pharmacokinetic (chapter 3.2.1) and pharmacodynamic (chapter 3.2.2) features as well as their optimisation (chapter 3.2.3).

3.2.1 Pharmacokinetics and their investigation

After being administered, drugs are exposed to processes of the organism. These processes are summarised under the term *pharmacokinetics* (PK) and critically determine the quantity of drug that reaches the target enzyme and becomes effective, also referred to by the term bioavailability. Pharmacokinetic processes are subdivided into the terms absorption, distribution, metabolism and elimination (ADME).[24]
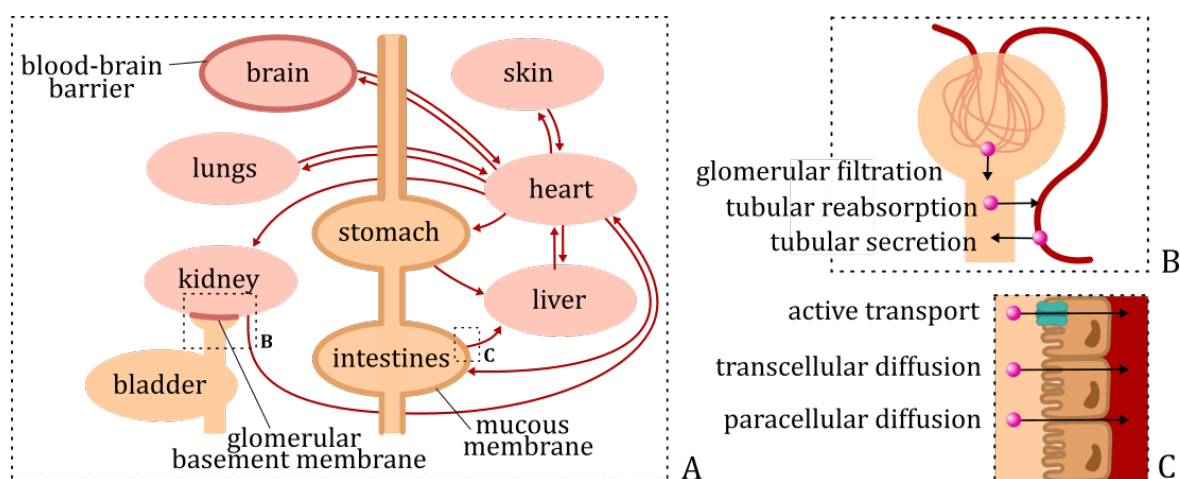
Figure 3.2: Pharmacokinetic exposure of a drug. A: Distribution, B: Renal elimination C: Gastrointestinal absorption.

Absorption and distribution

In order to reach its target site, the administered drug needs to enter blood circulation by a process called absorption. Depending on the route of administration, absorption occurs at different organs of the body. Apart from intravenous application, each administration route requires the drug to penetrate epithelial cell layers which protect the appropriate organ from harmful invaders. After oral uptake of a drug, which is the major route of administration, it can be absorbed through the mucous membrane of any organ in the gastrointestinal tract, whereby the small intestine is the most common site for absorption (fig. 3.2A).[25,26] Absorption processes through cell layers are either mediated by active transport systems or occur by passive diffusion in a paracellular or

transcellular manner (fig. 3.2C). The latter is the most common absorption mechanism for small molecule drugs with molecular weights above 200 g mol^{-1}. This mechanism requires the drug to diffuse through cellular lipid bilayers, a process which is driven by the drug's concentration gradient between the two compartiments.[27] In order to successfully cross these lipid layers, that are mostly lipophilic but to some extend hydrophilic, drugs must exhibit a certain degree of lipophilicity.[24] However, due to its concentration driven character, the rate and extent of absorption of an orally administered drug both strongly depend on its ability to previously dissolve in the aqueous environment of the gastrointestinal tract which is limited for highly lipophilic compounds.[27]

After absorption, the drug is distributed throughout the body via blood circulation or to a minor extent via the lymphatic system. Processes summarised under the term *distribution* include the drug's transport via the circular system as well as its transfer from of blood vessels to various tissues through capillary walls, cell membranes and special barriers, such as the blood-brain barrier (fig. 3.2A).
The quality of a drug's distribution is strongly affected by its solubility in aqueous medium. Poor aqueous solubility of a substance may, for example, lead to its deposition in blood vessels or organs which, as a result, not only limits its distribution but even can cause organ damage.[24] To evaluate a compound's solubility in the context of distribution processes, it needs to be considered that its molecules are partly bound to present proteins and lipids in an unspecific and reversible manner and consequently cannot freely diffuse in the solution. This plasma protein binding (PPB) can have a positive effect on the solubility of a compound since it reduces its concentration in the surrounding aqueous medium. However, PPB impedes the drug's passage through capillary walls, membranes and barriers into target tissues after circulatory transport.[28] Thus, PPB has a critical impact on the rate of drug distribution and its quantification is part of a complete pharmacokinetic profiling.

The drug's distribution in living organism is firstly investigated during preclinical studies in animal models. For this purpose, a certain period of time after drug administration, drug concentrations in distinct organs are measured. A realistic, encompassing prediction of drug distribution via *in vitro* assays is not yet possible. Nevertheless, the ability of a compound to cross membranes and barriers can be reliably investigated by *in vitro* assays which provide an important indication for predicting the absorption and distribution quality of a drug. Model systems for a transcellular passive permeation may be realised by the compound's diffusion through monolayers of certain biological cells

or an artificial membrane.[29] Besides drug properties, membrane permeability is affected by organ specific parameters like, for example, the respective surface area or membrane composition. In consideration of tissue specific scaling factors, *in vivo* absorption can be reliably predicted, when assuming a passive, transcellular permeation mechanism.[27] A further indication that helps estimating a compound's ability to be absorbed and distributed is its solubility in distinct solvents. Especially determining the compound's partition coefficient over different immiscible solvents at specific pH values can be helpful in order to predict the drug's blood-tissue-partitioning.[30, 31]

Metabolism and elimination

Whereas absorption and distribution processes contribute to the delivery of drugs to target organs, metabolism and elimination simultaneously aim their removal from the organism.

As blood passes the kidney during distribution processes, it is partly filtered in the glomerulus (fig. 3.2B, glomerular filtration). Whereas large molecules like proteins and blood cells remain in the blood fraction, small molecules like most drugs cross into the filtrate. Most of the filtrated substances are subsequently reabsorbed along renal tubules (tubular reabsorption), whereas substances that are too hydrophilic to get reabsorbed are excreted in the urine.[32] Hydrophilic drugs that have evaded the glomerular filtration process may be actively secreted from renal tubules (tubular secretion) in a process opposite to tubular reabsorption.[33]
The extent of plasma protein binding plays a crucial role for renal elimination of a drug, as protein bound drugs are not subject to these pathways. Thus, PPB strongly contributes to the drug's residence time in the organism.[34]

Lipophilic drugs as well as large, ionised drugs are not excreted via renal mechanisms. Whereas bilary secretion in the feces is the major route for large and ionised molecules,[35] the elimination of lipophilic substances requires previous biotransformation reactions to more hydrophilic compounds. These transformation reactions are referred to as drug metabolism and occur in blood plasma or organs, though the main location for metabolism is the liver.[24]
The liver is the first organ to be inevitably passed after gastrointestinal absorption of orally intaken substances. One of its original functions is to protect the organism from food toxins like, for example, exogenous hormones from other organisms that would interfere in human hormone balances, or toxins produced, for example, by plants for

protective reasons. Food toxins are mainly lipophilic, which enables not only their fast absorption from gastrointestinal tract and their unhindered penetration of membranes and barriers but also makes them resistant towards renal excretion mechanisms. Thus, as protection mechanism, before entering blood circulation they are metabolically converted to hydrophilic compounds.[36]

Metabolic reactions can be classified in two phases of biotransformation. Each of them is aimed to successively enhance hydrophilicity. Phase I metabolism reactions are mainly oxidation reactions biocatalysed by cytochrome P450 monooxygenases (CYPs), but also involve reductions and hydrolyses and the action of other enzymes like, for example, esterases and amidases. These phase I reactions usually introduce polar moieties to unpolar molecules. Phase II metabolic reactions add hydrophilic conjugates such as sugar molecules, salts or amino acids to compounds that already possess polar groups which can be the parent drug or the phase I metabolite. Compounds of sufficient hydrophilicity are released from cells by efflux pumps to be finally eliminated. This active transport often is refered to as metabolism phase III.[36]
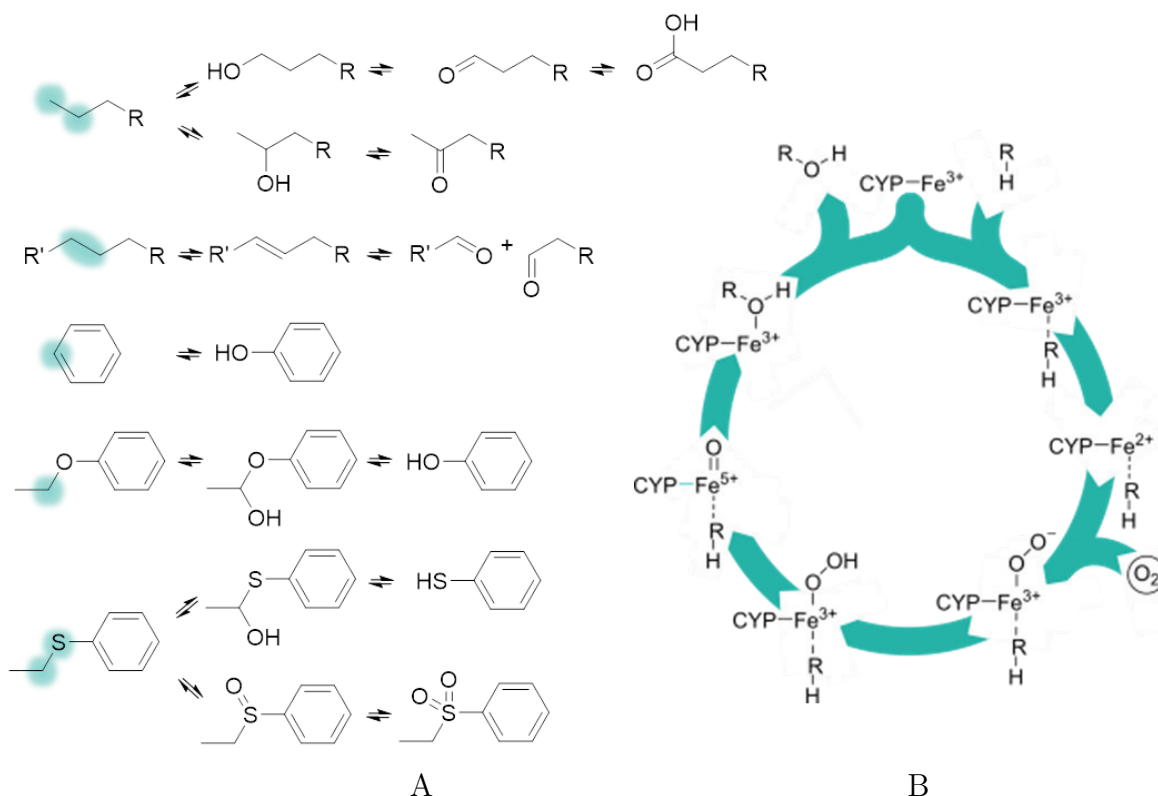

Figure 3.3: A: Selection of typical phase I metabolic reactions. B: Mechanism of CYP-catalyzed hydroxylation.

Figure 3.3 shows a selection of typical phase I metabolic reactions. Hydrocarbon atoms

are commonly hydroxylated to alcohols which are further oxidised to ketons or aldehydes and carboxylic acids. If a hydroxylation reaction results in an unstable product as it is the case for α-hydroxylations of alkylethers, alkyl thioethers or alkylamines, a spontaneous elimination of the respective alkyl aldehyde will result in the formation of dealkylated alcohols, thiols or amines (fig. 3.3A).[37] Besides, thioethers are likely to be oxidised to sulfoxides and sulfones.[38]

CYP catalyzed hydroxylations mainly occur at sterically accessible and electron-rich sites of the molecule, because they require its coordination to the Fe^{3+}-ion in the active site of the enzyme.[37] The general mechanism of CYP-catalyzed hydroxylation reactions is shown in figure 3.3B. Initially, the Fe^{3+}-ion in the active site of the enzyme coordinates to the hydrocarbon molecule, subsequently is reduced to Fe^{2+} and binds an oxygen molecule. Upon protonation and dehydration, a Fe^{5+} species is formed that reacts with the coordinated substrate under oxygen insertion. Finally the hydroxylated metabolite exits the binding site.[39]

In general, drug metabolism and elimination are desirable processes, since drug therapies should only temporarily intervene in natural processes of the organism. Otherwise, irreversible damage of organs or tissues can occur due to long-term shutdown of vital functions or due to drug accumulation. On the other hand, drug metabolism will become an issue if the metabolites have toxic potential. Often, the introduction of polar moieties to a compound is associated with a fatal enhancement of its reactivity. This can lead to irreversible reactions with cellular structures and thus cause cytotoxicity. Besides, metabolites can be produced that unexpectedly inhibit or activate other enzymes which can also result in toxicity.[40] For this reasons, a complete PK/PD profiling of a drug includes the identification and investigation of its metabolites. But even a simple loss of biological effect through metabolism is not desirable, especially if it occurs before the drug reaches its target tissue. Preventing this so called first pass effect is one important task of drug design, especially for orally administered drugs, as well as to find a suitable balance between the drug's sensibility towards metabolism and excretion.[41]

Several *in vitro* assays exist to investigate drug metabolism. For this purpose, compounds are either incubated with certain cells, subcellular fractions or isolated biotransforming enzymes.[42] However, it needs to be considered that organisms are able to upregulate their metabolic capability due to increased concentrations of lipophilic compounds,[43] resulting in a more pronounced metabolism *in vivo* than expected from *in vitro* assays.

3.2.2 Pharmacodynamics and their investigation

Whereas pharmacokinetics comprise processes of the organism to which the drug is exposed, the term *pharmacodynamics* (PD) refers to all actions a substance induces in an organism, including its desired therapeutic effects as well as toxic mechanisms.[24]

Even though drugs can have diverse mechanisms of action, most of them act by inhibiting the natural activity of specific enzymes, for example by binding to it as so called ligands. Usually, this binding event is of reversible nature, meaning that an equilibrium exists between enzyme-ligand-complex and both free ligand and free enzyme.[44] In dependence of the respective equilibrium position, the rate by which the enzyme converts its natural substrate is reduced through addition of the ligand. A measure which is often used to estimate the extent of such enzyme rate reduction or a drug's inhibitory activity is its IC_{50} value. This value reflects the concentration of a substance that is required to reduce the enzyme's rate of converting its natural substrate by half.[45] In case that instead of enzyme inhibition the compound's biological effect in a cell based-assay is regarded, the EC_{50} value is indicated as an analogous measure.

Besides the desired therapeutic effects, a drug can also perform toxic actions in the body. These may be related to the mechanism of action itself or result from an unintended simultaneous initiation of other mechanisms.[46] Either the drug itself or its metabolites can be responsible for such toxic mechanisms. However, above a certain concentration every substance becomes toxic. Analogous to the half-maximal inhibitory concentration, the CC_{50} (half-maximal cytotoxic concentration) value indicates the concentration at which a substance reduces the viability of a cell or organism by half. The term therapeutic index quantifies the concentration range of a drug in which it releases the desired therapeutic effect without immediately causing toxicity. It is calculated by dividing CC_{50} by EC_{50}.

3.2.3 Optimisation of pharmacokinetic and pharmacokdynamic properties by rational design

The process of rational drug design during lead optimisation aims to improve the compound's pharmacodynamic and pharmacokinetic properties by specifically modifying its structure.

A suitable pharmacokinetic profile is required for a drug to reach the target site in sufficient concentration. It is defined by the drug's ability to be dissolved in water, to cross membranes and to evade unspecific plasma protein binding, metabolism and early excretion (chapter 3.2.1). All these features are strongly affected by the drug's overall lipophilicity. Therefore, a decisive task in drug design is to find compounds with a good balance of being lipophilic enough to penetrate membranes and barriers but at the same time not being too lipophilic to allow its dissolution, to prevent unspecific plasma protein binding and to reduce metabolism. Since high lipophilicity of a compound often has positive effects on several *in vitro* pharmacokinetic and pharmacodynamic studies, issues concerning an insufficient desolvability often are not recognised in time or taken seriously, resulting later in the failure of *in vivo* studies. Besides lipophilicity, further drug features are important for an appropriate pharmacokinetic profile, especially for a proper membrane penetration, like its molecular size, polar surface area, ionisation, energy required for its desolvation and flexibility.[47] Moreover, the design of drugs that are able to cross barriers like, for example, the blood-brain barrier is highly demanding but nevertheless required for a sufficient distribution of corresponding brain-targeted drugs.[48]

Regarding pharmacodynamics, both a high inhibitory activity and a high therapeutic index of the drug are aimed (chapter 3.2.2) which can be realised by strong and highly specific molecular interactions between a drug and its target enzyme.
The strongest non-covalent molecular interactions are of ionic nature, also referred to as salt bridges (fig. 3.4, pink). Besides their strength, their long-range forces guide the free ligand to approach its binding site. Strong interactions also occur between aromatic systems (violet) that are aligned towards each other in certain arrangements. Hydrogen bonds (turquoise) are rather weak molecular interactions and require defined distances and bonding angles of the associated atoms. Their formation involves a previous cleavage of hydrogen bonds to water molecules in the original, solvated state of protein and ligand. Thus, hydrogen bonds usually do not significantly contribute to enthalpic gains of the system. But at the same time it will be enthalpically unfavourable if hydrogen bonding donors or acceptors at the surface of the protein are not saturated by a suitable counterpart in the ligand molecule, and vice versa, since desolvation costs nevertheless are incurred (fig. 3.4). Thus, a precise placing of hydrogen bonding partners in the structure of a ligand can strongly enhance its selectivity towards a specific target enzyme. Lipophilic interactions (green), when considered individually, are the weakest molecular interactions but will majorly contribute to binding affinity if they act on a

large surface. For this, not only enthalpic contributions are responsible, but entropic effects play a major role. The aggregation of two lipophilic surfaces increases the entropy of the system because it releases adjacent water molecules from a forced arrangement to move freely (fig. 3.4). By realizing an optimal shape complementarity between the lipophilic surfaces of protein and ligand, the important enthalpic and entropic gains of hydrophobic interactions can be maximised.
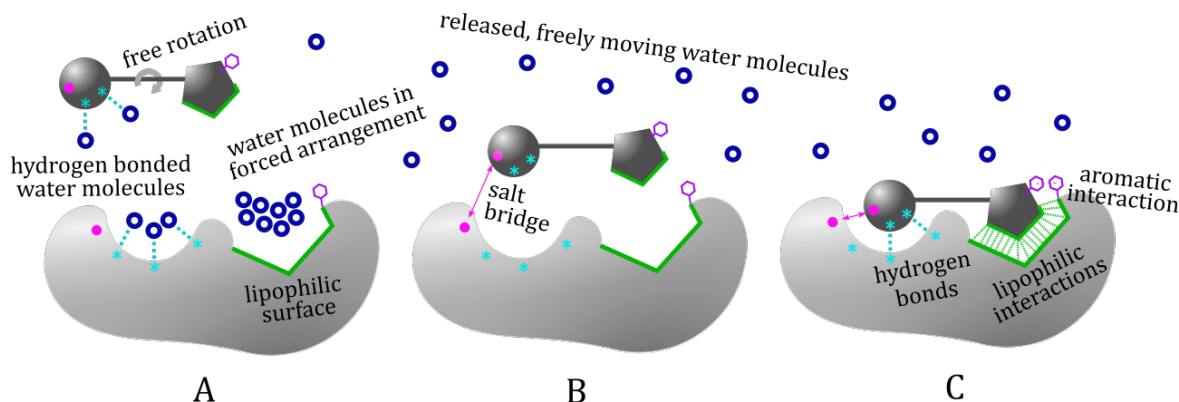

Figure 3.4: Enthalpic and entropic contributions to binding affinity. A: Solvated protein and ligand, B: desolvated ligand approaches desolvated protein, C: protein-ligand-complex.

Also for entropic reasons, a high rigidity of the ligand is advantageous, as it is associated with a reduced loss of degrees of freedom during binding process, compared to a flexible ligand.[49,50]

Besides the above mentioned *in vitro* assays (chapters 3.2.2 and 3.2.1), *in silico* tools exist for the prediction of several pharmacokinetic and pharmacodynamic properties of a specific compound. Such virtual tools strongly support rational drug design during lead optimisation. Structure optimisation procedures include an investigation of the scope of modifications that are tolerated for individual structural elements while maintaining the inhibitor's activity. To promote such SAR (Structure-Activity Relationship) approaches, computer-based molecular modeling techniques can be applied, providing first hints on possible structural modifications.

3.3 Topical context: the target enzyme human dihydroorotate dehydrogenase

3.3.1 DHODH function and biological context

Human dihydroorotate dehydrogenase (hDHODH) is a redox enzyme which is assigned to class 2 DHODHs that are present in eukaryotes and some gram-negative bacteria. In eukaryotes DHODH is located in the intermembrane space of mitochondria, associated to their inner membrane, whereas it is bound to cytosolic membranes of gram-negative bacteria.[51]

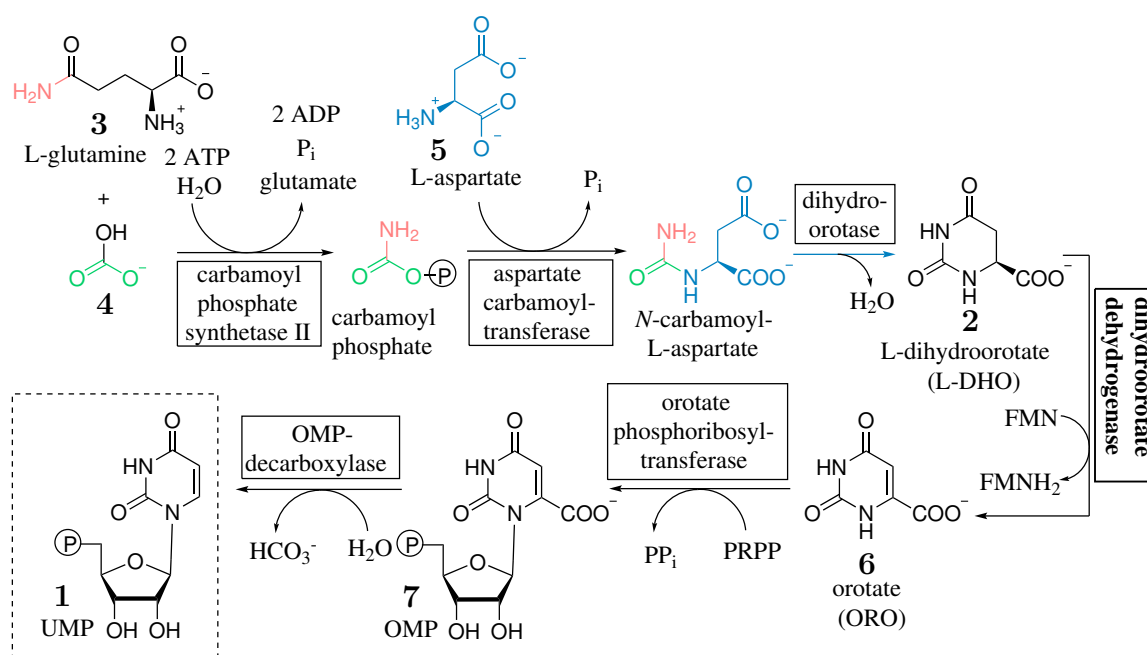**Involvement of DHODH in the *de novo* synthesis of pyrimidine nucleotides**

Figure 3.5: Biosynthesis of uridine monophosphate (UMP) **1**.

DHODH is involved in the six step *de novo* biosynthesis (fig. 3.5) of uridine monophosphate **1** (UMP) which subsequently is converted intracellularly to all different natural pyrimidine nucleotides.[12] In the first three steps, dihydroorotate **2** (DHO) is synthesised from L-glutamine **3**, bicarbonate **4** and aspartate **5**, catalyzed by multifunctional enzyme complex CAD.[52] After the successful ring formation, DHO **2** is oxidised to aromatic orotate **6** (ORO) in the fourth step, catalyzed by DHODH. In the final two

steps, ORO **6** is phosphoribosylated to orotate monophosphate **7** (OMP) which in turn is decarboxylated to UMP **1**.[53]

UMP **1** then serves as precursor for the intracellular synthesis of pyrimidine ribonucleoside triphosphates UTP and CTP as well as deoxyribonucleoside triphosphates dTTP and dCTP (fig. 3.6). Corresponding polymerases select these triphosphates as building blocks to synthesise deoxyribonucleic acids (DNA) and ribonucleic acids (RNA), respectively.[12] Besides their indispensibility for DNA and RNA synthesis, pyrimidine nucleotides are essential starting materials for protein glycosylation (UDP) and the biosynthesis of membrane lipids (CDP) and furthermore act as extracellular signal molecules, regulating diverse processes (uridine nucleotides).[13,54]

Alternative access to pyrimidine nucleotides via salvage pathway

The pyrimidine *de novo* synthesis pathway is energetically expensive. For this reason, most cells mainly produce their pyrimidine nucleotides via the more efficient salvage pathway, in which intracellularly present nucleosides are phosphorylated.[55] These nucleosides either have been ingested with food or originate from intracellular or extracellular catabolic pathways.[56] Diverse cellular processes involve the catabolic degradation of nucleic acid fragments, like for example DNA repair, RNA maturation, cell signaling or pathogen defense mechanisms.[57] In the course of catabolism, ribose and deoxyribose nucleic acids are stepwise degraded to their mononucleotides and their nucleosides. Whereas few nucleosides are further catabolised to be finally excreted, most of them are recycled via kinase-catalyzed phosphorylation to the corresponding triphosphates (salvage pathway) which serve as starting materials for the above mentioned processes.[55] Unlike purine bases, pyrimidine bases are rarely converted into the corresponding nucleosides by cellular processes.[12,58]

In different organs and cell lines the rate of the energetically unfavored pyrimidine *de novo* synthesis varies in dependence of the respective demand for nucleotides, due to intracellular enzyme levels and metabolic control mechanisms.[9,55] It was furthermore demonstrated that increasing intracellular uridine concentrations lead to a downregulation of pyrimidine *de novo* synthesis, as nucleotides in this case can be predominantly obtained via salvage pathway.[55,59] Resting cells are characterised by a low replication rate and thus uridine consumption is low. This results in a downregulation of pyrimidine *de novo* synthesis as enough pyrimidine nucleotides can be provided by salvage pathway. In contrast to that, rapidly proliferating cells, like T-cells, additionally depend on the

de novo synthesis pathway because the cellular uridine pool is not sufficient to cover the increased nucleotide demand via salvage pathway.[13]
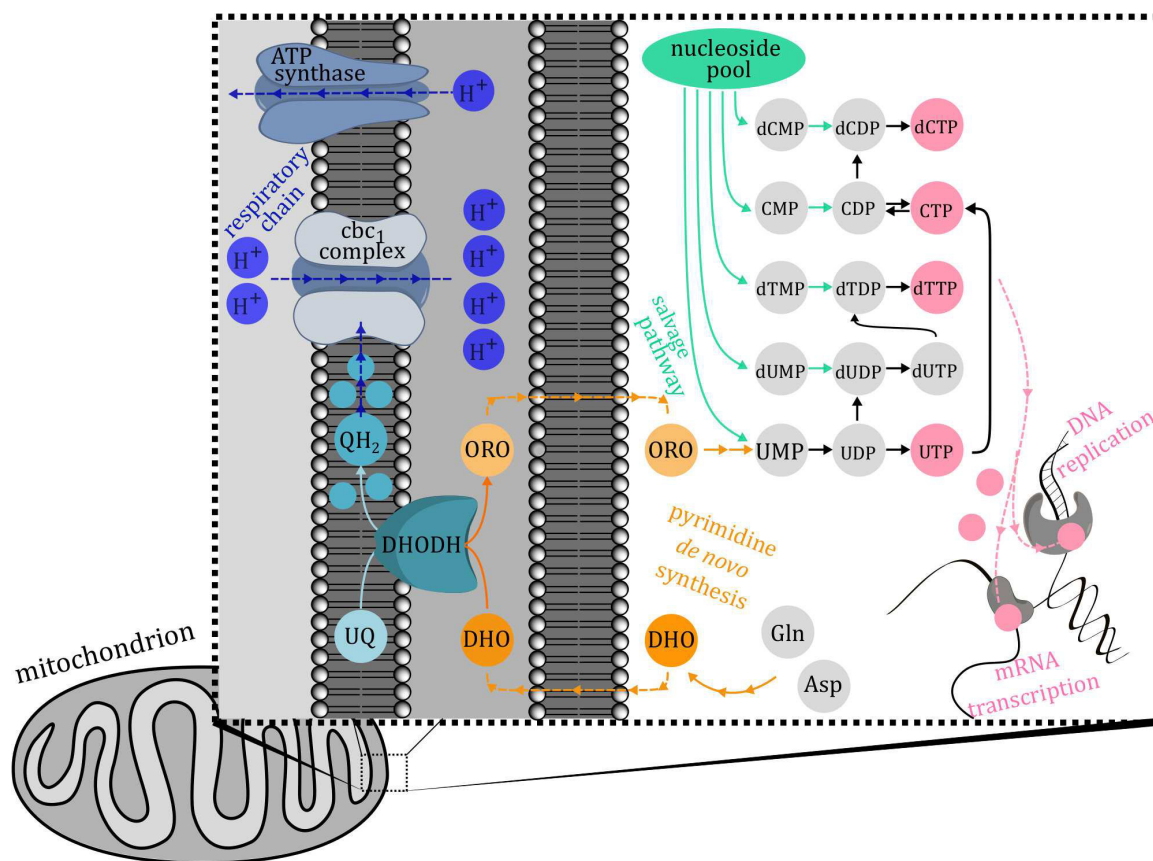

Figure 3.6: Involvement of mitochondrial DHODH in several cellular processes and alternative access to pyrimidine nucleotides via salvage pathway.

Involvement of mitochondrial DHODH in respiratory chain

Whereas all other enzymes of the UMP *de novo* biosynthesis are localised in the cytosol, DHODH is the only mitochondrial enzyme involved in this pathway. Consequently, its substrate DHO **2** and its reaction product ORO **6** need to pass the outer mitochondrial membrane. DHODH is simultaneously involved in the mitochondrial respiratory chain (fig. 3.6). After DHO **2** oxidation, the activity of the redox enzyme is recovered by a transfer of the excess electron to the enzyme's cosubstrate ubiquinone UQ **8**, thereby converting it to ubiquinol QH_2 **9** (see chapter 3.3.3 for details of the complete molecular mechanism of DHODH).[60] With the conversion of UQ **8** to QH_2 **9**, DHODH actively participates in electron transport processes within the mitochondrial respiratory chain by contributing a small part to a huge pool of QH_2 **9** molecules. QH_2 **9** then binds to

ubiquinol cytochrome *c* oxidoreductase (cbc1 complex), an enzyme of the mitochondrial respiratory chain, and thus enters its so called Q cycle. Reoxidation of two QH_2 molecules provides cbc1 complex with four electrons and four protons. Whereas all four protons are released into intermembrane space of the mitochondrion, the electrons are partly used for reduction of two substrate molecules and for the reoxidation of one generated UQ **8** molecule under simultaneous uptake of two protons from the inner of the mitochondrion (fig. 3.6).[61] As a result, an electrochemical proton gradient is generated across the inner mitochondrial membrane which is reinforced by other enzymes of the respiratory chain (not shown). The resulting membrane potential drives mitochondrial ATP production by ATP synthase that converts the energy, obtained by a backflow of protons, into ATP phosphate bond energy.[62] Consequently, the activity of DHODH depends on an intact respiratory chain and vice versa. Although a variety of enzymes contributes to the QH_2 **9** pool that is converted by cbc1 complex, it was shown that a depletion of hDHODH activity lead to a slight loss of activity of cbc1 complex and thus induced mitochondrial dysfunction.[63]

3.3.2 The role of the *de novo* synthesis pathway in diseases

Not only T lymphocytes are characterised by a high replication rate but also cancer cells and virally infected cells. Consequently, they depend on an upregulated *de novo* pyrimidine synthesis not only for DNA and RNA synthesis, but also for membrane lipid biosynthesis and protein glycosylation (see chapter 3.3.1). Thus, several infections, cancer and diseases, that affect the immune system, are highly dependent on an intact function of enzymes involved in pyrimidine *de novo* synthesis.[1]

Autoimmune diseases

The immune system protects the body from invading pathogens. Shortly after infection, so called pattern recognition receptors detect pathogen-specific molecular patterns.[64] This triggers diverse immune defense mechanisms, like an unspecific inflammation reaction or the activation of T lymphocytes that is shown in figure 3.7.
Dendritic cells are numerously present in surface tissues. The activated pattern recognition receptors induce the maturation of these dendritic cells (1) which, as a result, take up surrounding antigens via phagocytosis (2) and present them on their cell surfaces via MHC (major histocompatibility complex) molecules (3). A continuous drainage of tissue fluids caused by the inflammation flushes the activated dendritic cells into

nearby lymph nodes.[65] Various T lymphocytes that patrol the peripheral lymphoid tissue, each having a unique sort of antigen receptor on its surface, attach to the MHC complexes and scan the presented antigens. Only a successful interaction between a T cell receptor and its specific antigen causes activation of the T lymphocyte (4), which consequently proliferates strongly and finally develops effector functions (5).[66]
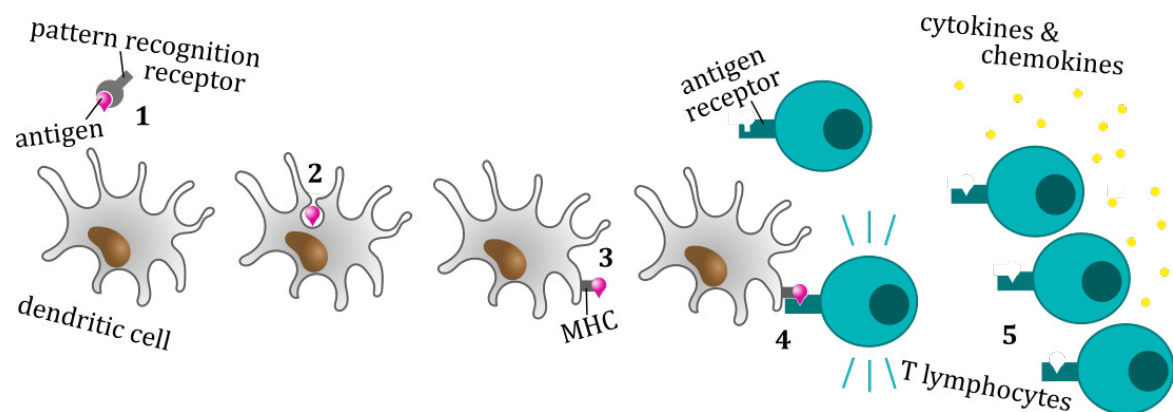

Figure 3.7: T lymphocyte activation. 1: Pathogen recogniton, 2: antigen uptake (phagocytosis), 3: antigen presentation, 4: T lymphocyte activation, 5: T lymphocyte proliferation and release of cytokines and chemokines.

Depending on their specialisation, T lymphocytes trigger different signalling cascades after being activated. Whereas activated T killer cells directly become cytotoxic and destroy the corresponding infected cells, activated T helper cells secrete cytokines, which in turn activate other cells to destroy infected cells. These two classes of T lymphocytes differ in the nature of their cell surface proteins.[67] Whereas T helper cells carry CD4 proteins on their surfaces, T killer cells are characterised by their CD8 proteins.[65]

Activated dendritic cells do not only take up exogenous but also endogenous antigens which they also present on the surface. In order to prevent T lymphocyte activation by endogenous antigens, those T lymphocytes which would interact with endogenous substances induce apoptosis during their development in the thymus. But the tolerance of weak interactions between T cell receptors and endogenous antigens during selection in the thymus results in an extensive repertoire of foreign antigens which can be recognised by T lymphocytes at the expense of some degree of self-reactivity.[68,69] This weak self-reactivity plays a decisive role in the development of autoimmune diseases. For insufficiently understood reasons, the patient's immune system responds to endogenous antigens and triggers an immune response causing chronic damage to the affected organ or the entire body.

Infections are assumed to be one cause of autoimmune diseases. One possible explanation for this is that some pathogens are able to adapt their antigens to the host's antigens by immune invasion and thus trigger activation of weakly self-reactive T lymphocytes resulting in an autoimmune response.[66] Also, T lymphocytes that express dual receptors on a single cell and thus have dual reactivity for foreign and endogenous antigens could favour autoimmune diseases.[70]

It was shown that T lymphocyte proliferation after their activation requires an intact pyrimidine *de novo* synthesis. An inhibition of pyrimidine *de novo* synthesis was shown to deplete the pyrimidine pool of T lymphocytes by 70 % that before underlay an eightfold increase due to lymphocyte activation.[7] Furthermore, inhibitors of enzymes involved in this pathway were shown to induce apoptosis of replicating T lymphocytes.[8] Both effects contribute to the immunosuppressive activity of inhibitors of the pyrimidine *de novo* synthesis that can be used for the treatment of autoimmune diseases or transplant rejection.[71]

Viral infections

As viruses are primitive in structure and cannot replicate on their own, they specifically manipulate infected host cells to transform into virus production factories. Infected cells consequently dedicate their enzymes, building blocks and cofactors to the production of virus particles, only. Due to the increased demand for nucleotides, virally infected cells up-regulate their *de novo* synthesis pathways.[12]

Despite the enormous diversity of existing viruses, in general they infect and use host cells in a similar manner which is shown in figure 3.8. Viral infections are initiated by the attachment of a virus particle to a host cell membrane (1) by specifically binding to a cellular receptor molecule. After entering the host cell (2) via endocytosis, fusion with or penetration through the cellular membrane, the virus releases its genome (3). This uncoating process can be initiated by a conformational change of the particle itself or by the release of viral transporter proteins. As different virus species vary widely regarding their composition and genome structure, also their replication strategies strongly differ.[72] Viruses that are composed the most simple only consist of a genome strand and a protein coat. The simpler the viral composition, the more does replication depend on the host machinery. As an example, in positive-strand RNA viruses the genome has the polarity of a messenger RNA and thus is directly translated by cellular processes to viral proteins like the viral RNA dependent RNA polymerase. This polymerase in

turn synthesises a complementary strand serving as matrix for genome replication. In contrast, negative-strand viruses need to contain and release viral polymerases for initial synthesis of a messenger RNA. DNA viruses need to either bring their own DNA-polymerase or use host enzymes for replication.[73] After gene expression and replication have occurred (4), the produced building blocks are assembled to new virus particles (5) which mature to infectious viruses and finally are released from the cell (6) to infect further cells.[72]
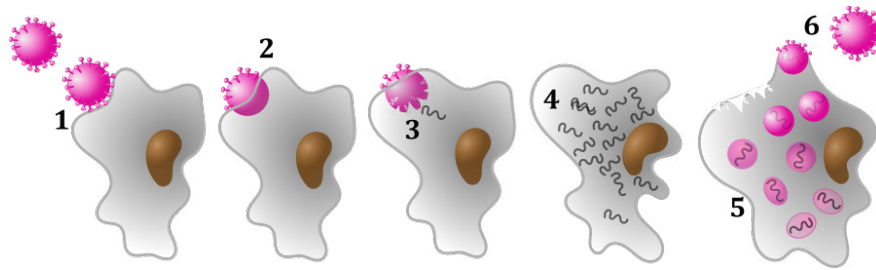
Figure 3.8: Viral infection of a host cell. 1: Attachment, 2: entry, 3: uncoating, 4: replication, 5: assembly, 6: maturation and budding.

Various protective host mechanisms lead to a disposal of infected cells and thus an elimination of the virus from the organism. They can either be lysed as a result of their morphological changes, initiate their own apoptosis or be detected and destroyed by immune cells. Often, these cell damages furthermore result in necrosis in the adjacent, non-infected tissue.[74]

Whereas most viral infections are endured without drastic damage to host tissues and organs, some viruses are able to evade early immune responses, which results in a chronic infection that in the further course can lead to organ failure and death.[75] Otherwise, in many cases the overacting, virally triggered immune response is the major cause for fatal tissue and organ damages. Often, T lymphocytes are involved in such viral immunopathologic mechanisms, for example when damaging cells infected with non-cytopathic viruses or when inducing an exaggerated release of inflammatory cytokines, also known as cytokine storm, that results in massive organ damage and failure. Moreover, the virally induced hyperactivation of T lymphocytes can lead to immune exhaustion, resulting in chronic infections.[75] Thus, in the fight against viral infections with immunopathological mechanisms, immunosuppressants offer an important therapeutic tool to prevent organ failure or the occurrence of chronic infections in patients.[76,77]

Thus, an intracellular upregulation of pyrimidine *de novo* synthesis is not only crucial for viral replication itself, but also plays an important role for T lymphocyte-induced

immunopathological mechanisms. It was shown that an inhibition of the pyrimidine *de novo* synthesis not only suppresses the replication of T lymphocytes[7,8] and the replication of a broad range of viruses,[11,12] but moreover results in an activation of innate immune responses,[78,79] which benefits its potential for antiviral therapy.

Cancer

Tumor cells are characterised by an uncontrolled, excessive proliferation and cell growth as well as a loss of their apoptotic control. These attributes are caused by several mutations of the genome which occur either randomly or triggered by stimulation with various external influences, like irradiation or reactive substances. Via cell division such mutations are locally passed on and result in the formation of a tumor. If tumor cells spread into other tissues, malignant tumors will develop, also known as cancer. Since cellular mechanisms exist that detect and repair mutations or induce apoptosis of the cell before its division in order to prevent such tumor formation, the simultaneous occurrence of certain genome mutations is required to cause cancer.[80] In more than half of all human tumor cells, the p53 gene is deactivated by mutations, resulting in the loss of their apoptotic activity.[81]

The excessive proliferation and growth of cancer cells requires adequate nucleotide pools which are mainly supplied by pyrimidine *de novo* synthesis.[9,10] It was furthermore shown that tumor suppressors and oncogenes, which are factors that promote abnormal cell growth in cancer cells, directly regulate the *de novo* synthesis of pyrimidine nucleotides.[9,82] Apart from its suppressing effect on cancer cell proliferation, an inhibition of the pyrimidine *de novo* synthesis was shown to furthermore result in a reactivation of their p53 gene and thus restoring their apoptotic activity.[83] These two parallel effects explain the anticancer potential of inhibitors of enzymes which are involved in the pyrimidine *de novo* synthesis.[10,84]

Parasitic infections

Besides mammals, several bacteria also produce their pyrimidine nucleotides via the *de novo* biosynthesis route and therefore possess a class 2 DHODH. Contrary to their mammal hosts, bacteria have no opportunity to produce pyrimidine nucleotides via an alternative salvage pathway. Thus, bacterial DHODH is a popular target enzyme for the effective treatment of parasitic infections like *Helicobacter pylori* or *Plasmodium falciparum* which cause stomach ulcer and malaria, respectively. Furthermore, since

the structure of bacterial DHODH slightly differs from its mammal counterpart, a high specifity of ligands towards the bacterial enzyme can be realised.[6] However, at the same time the bacterial enzyme, in contrast to hDHODH, is susceptible to mutations which poses the risk of drug resistance. Currently, one selective *Pf*DHODH inhibitor is under clinical development for the treatment of malaria.[85]
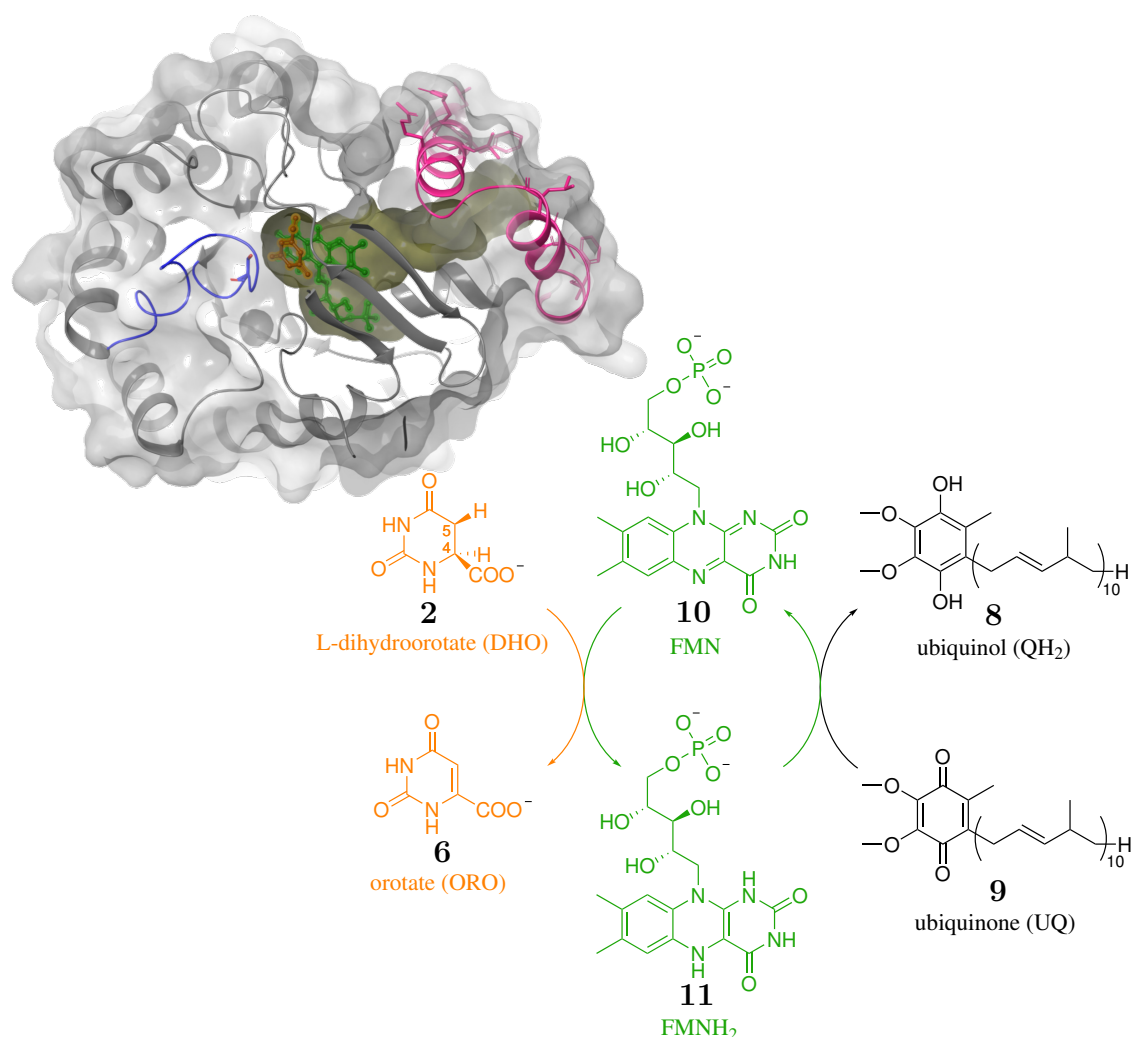
3.3.3 Structure and catalytic mechanism of DHODH

Figure 3.9: Crystal structure (PDB: 2PRM[86]) and molecular mechanism of hDHODH.

The structure of hDHODH (fig. 3.9), as well as of other class 2 DHODHs, is composed of eight circularly arranged alpha helices that enclose a central barrel of eight beta sheets and five shorter beta sheets, arranged above and below the barrel (grey, not all visible in fig. 3.9). The active site of the enzyme is localised in the center of the barrel where the cofactor flavin mononucleotide **10** (FMN, green) is tightly bound next to the binding

site of the substrate dihydroorotate **2** (DHO, orange). Two seperately localised alpha helices (pink) form a tunnel leading from the active site to the protein surface. At the tunnel entrance, the helices are made up of amino acids with hydrophobic sidechains (pink) pointing to the protein surface which plunges into the hydrophobic inner of the mitochondrial membrane. The negatively charged headgroups of the membrane phospholipids interact with a fringe of positively charged residues (not shown) of the two alpha helices, thereby contributing to the enzyme's anchorage in the membrane.[87] Among class 2 DHODHs, high sequence identity exists. Class 1 DHODHs on the other hand can be found in the cytosol of kinetoplasts as well as some species of yeast and lack the two membrane associated alpha helices.[51]

Oxidation of the bound substrate DHO **2** is initiated by Ser215 (blue) that serves as catalytical base, abstracting a proton from DHO's C-5 position. Direct hydride transfer from the C-4 position of DHO **2** to FMN **10** results in the formation of orotate **6** (ORO). Lys255 (not shown) presumably provides the second proton for converting the cofactor FMN **10** to dihydro flavin mononucleotide **11** (FMNH$_2$).[87] In order to regenerate the original enzyme redox activity, FMNH$_2$ **11** is reoxidised to the active cofactor FMN **10** by donating its electrons to cosubstrate ubiquinone **8** (UQ), presumably in a single-electron transfer mechanism.[88] For this redox reaction, UQ **8** reaches FMNH$_2$ **11** through the tunnel leading from the inner of the mitochondrial membrane to the active site of the enzyme. It is assumed that the interaction of UQ **8** with the enzyme induces an opening movement of a loop (blue), thereby releasing ORO **6** from the active site of the enzyme directly into the intermembrane space of the mitochondrium and uptaking a new substrate **2**.[87] Ubiquinol **9** (QH$_2$), the reduced form of UQ **8**, finally leaves the enzyme through the tunnel into the inner of the mitochondrial membrane. The products ORO **6** and QH$_2$ **9** are further converted in pyrimidine *de novo* synthesis or mitochondrial respiratory chain, respectively (see chapter 3.3.1).

3.4 State-of-the-art: Inhibitors of hDHODH as therapeutics

An intact pyrimidine *de novo* synthesis is essential for the development of autoimmune diseases, cancer or various infections (see chapter 3.3.2). Therefore, an inhibition of this pathway, for example by hDHODH-inhibition, is a promising approach for the therapeutic treatment of these diseases.[1,5,6,89,90] At the same time, the function of

resting cells is preserved, as their comparibly low pyrimidine demand is covered via the salvage pathway (see chapter 3.3.1).

Mechanisms for DHODH inhibition and known hDHODH inhibitors

DHODH activity can be inhibited by occupying the binding site of either the substrate dihydroorotate **2** or the cosubstrate ubiquinone **8** with a ligand molecule. Ligands competing with dihydroorotate **2** for its binding site are severely limited in both shape and pharmacophore features. A comparatively strong binding structural analog of dihydroorotate **2** is dihydro-5-azaorotate that exhibits a third amino function replacing its methylene moiety. Contrary to that, ubiquinone's binding site offers a wide scope for the *de novo* design of so called redox silent ubiquinone antagonists, resulting in a tremendous structural variance of inhibitors.[91] Figure 3.10 shows an X-ray structure of hDHODH in complex with such ubiquinone antagonist (yellow) as well as a selection of structurally diverse hDHODH inhibitors that bind at the same site. All shown inhibitors are or were involved in clinical trials.
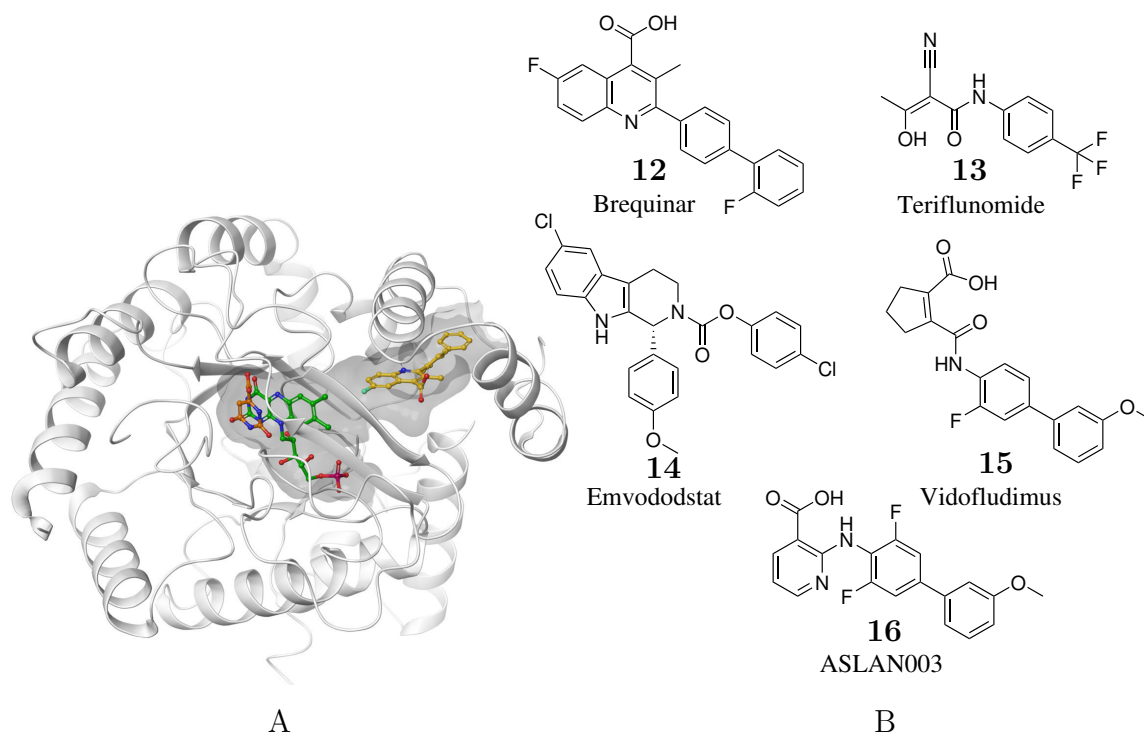
Figure 3.10: A: X-ray cocrystal structure of hDHODH (PDB 1D3G[87]) in complex with its natural substrate (orange), its reduced cofactor $FMNH_2$ **11** (green) and a brequinar analogue (yellow), B: selection of known, structurally diverse hDHODH inhibitors.

Brequinar **12** was discovered in 1985 as compound with anticancer potential. Its activity was attributed to the inhibition of DHODH one year later.[92,93] Since then it has been evaluated in several phase I and II trials for the treatment of patients with various cancer types[94–99]. Due to toxic effects that appeared when administering brequinar **12** at doses that were required to induce an antitumoral effect, no clinical study could be successfully completed. Nevertheless, with IC_{50} values of 5 to 10 nM brequinar **12** is one of the most potent known inhibitors of hDHODH and therefore is used as reference compound in several assays.[4]

Teriflunomide **13** is a less potent hDHODH inhibitor with an IC_{50} value of 300 nM in the isolated enzyme.[100] Unfortunately, it is associated with liver toxicity, presumably occuring due to its long plasma half life of two weeks. Nevertheless, it has been approved under the trade name Aubagio® for the treatment of multiple sclerosis in 2013.[101] Already in 1998, its isooxazole prodrug leflunomide has been approved under the name Arava® for the treatment of rheumatoid arthritis. Moreover, it has been successfully used for the off-label treatment of transplant rejection.[102] Thirteen years before, immunomodulating properties of the compound, that was former applied as pesticide, were established for the first time.[71,103] Its mechanism of action was elucidated in 1995.[104]

A very promising hDHODH inhibitor is Emvododstat **14** that was discovered in 2016 as potential anticancer agent was furthermore shown to inhibit the expression of vascular endothelial growth factor (VEGF) A in tumor cells.[105] Interestingly, its IC_{50} value in hDHODH is slightly above 1 µM in the recombinant enzyme only but around 20 nM in isolated mitochondria. This observation was explained with the requirement of membrane lipids for a realistic depiction of its hDHODH activity.[106] Even though Emvododstat **14** failed to successfully complete a phase II study in patients with Kaposi's sarcoma, due to a low response rate that could not surpass current standard-of-care chemotherapy,[107] it is currently being investigated in a phase III study in patients hospitalised with COVID-19.[108]

Cyclopentene carboxylic acid derivative Vidofludimus **15** and nicotinic acid derivative ASLAN003 **16** are further hDHODH inhibitors that inhibit the enzyme with IC_{50} values of 134 nM[109] and 35 nM, respectively. They are currently tested in phase II trials in patients with acute myeloid leukemia (vidofludimus **15**)[110] or primary sclerosing cholangitis (ASLAN003 **16**)[111]. The calcium carboxylate analogue of Vidofludimus **15** even has entered clinical phase III for the treatment of COVID-19.[112]

Limitations regarding the *in vivo* use of hDHODH inhibitors

hDHODH inhibitors exhibit an extensive and versatile efficacy *in vitro*. Since the elucidation of the mechanism of action of Brequinar **16** and Teriflunomide **13**, hDHODH inhibitors have been under continuous investigation. However, many promising hDHODH inhibitors failed to complete clinical phase II in humans, due to an insufficient *in vivo* efficacy. A possible explanation for this issue is an unexpectedly robust uridine supply in organisms, thus enabling also rapidly proliferating cells to solely cover their demand for pyrimidine nucleotides via salvage pathway. As evidence for this, it was shown that an activation of uridine salvage through inhibition of pyrimidine *de novo* synthesis only resulted in a modest perturbation of plasma uridine concentrations.[12,113,114] However, on the one hand, this problem does not occur for the therapeutic use of DHODH inhibitors as immunosuppressives, as it can be seen for Teriflunomide **13**. An explanation for this may be that uridine salvage is less dominant in lymphocytes, compared to other cell types.[12] On the other hand, the successfully proceeding clinical trials of hDHODH inhibitors for use as antivirals[108,112] and anticancer[111] agents raise hope for their future approval as drugs. Anyway, due to the large diversity of virus species and cancer cell types, a therapeutic application of DHODH inhibitors as antivirals or anticancer agents is still conceivable, despite no hDHODH inhibitors were accordingly approved in the past.

One fact that must be considered already in preclinical testing of hDHODH inhibitors is that the protein sequence slightly differs from that of other species and thus also the corresponding binding affinities do. As an example, Vidofludimus **15** strongly inhibits human DHODH with an IC_{50} value of 134 nM, whereas it has only moderate activity in rat DHODH (IC_{50} = 1200 nM) and very low activity in mouse DHODH (IC_{50} = 10300 nM). Thus, a suitable animal model should be carefully selected to prevent false failure of the drug candidate already in the preclinical studies.

Besides, the inhibition of hDHODH has been tentatively associated with long-term health effects like for example clinical characteristics of Miller syndrome, which presumably is caused by mutations of the hDHODH gene which develop as a consequence of hDHODH inhibition.[115–117] Furthermore, decreasing uridine levels as a result of hDHODH inhibition, and thus activation of salvage pathway, may lead to hepatic microvesicular steatosis due to an imbalanced protein acetylation.[118]

All in all, the development of hDHODH inhibitors is risky and not as straight forward as it seems to be at first glance. However, the discovery of the role of hDHODH as

potential target enzyme for the treatment of acute myeloid leukemia (AML)[3,119] as well as last years SARS-CoV-2 pandemic has reawakened interest and ambition to develop novel hDHODH inhibitors and achieve their approvals.

Structural features and binding modes of known hDHODH inhibitors

A comparison of known hDHODH inhibitors that act as ubiquinone antagonists (see fig. 3.10) reveals similarities regarding their overall structures. They all consist of a small hydrophilic and a large lipophilic part, illustrating the amphiphilic character of their binding site.[120] Nonpolar residues spike the enzyme surface at the entrance of the tunnel leading from the inner of the mitochondrial membrane to the enzyme's active site. This allows the mainly lipophilic cosubstrate ubiquinone **8** to reach the active site for electron transfer.[121] The lipophilic part of the inhibitor unspecifically interacts with these nonpolar residues and thus for a high binding affinity, its shape should optimally match the shape of the binding site.[122] At the site before the tunnel merges with FMN binding site (fig. 3.10), it narrows and is composed of polar as well as charged side chains, like for example Arg136, Gln47, Thr360 and Tyr356. These act as anchoring points for specific interactions with hydrophilic moieties of the inhibitors. A small hydrophobic cavity built by Val134 (not shown) and Val143 forms a cap on this polar area.[120] Figure 3.11 provides detailed insights in the inhibitor binding site of hDHODH cocrystallised with two different inhibitors.

A   B
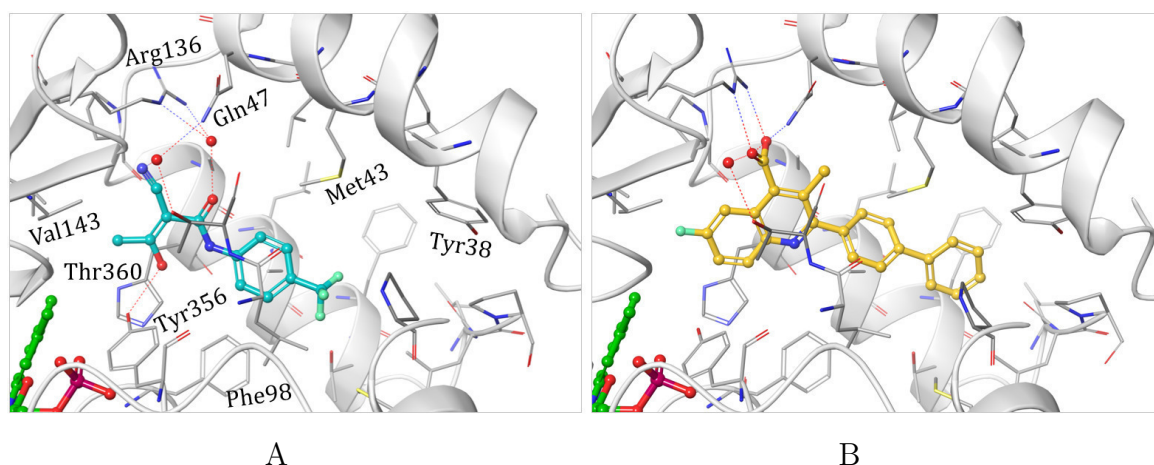
Figure 3.11: Molecular arrangement of hDHODH inhibitors in their binding sites. X-ray structures of hDHODH cocrystallised with A: Teriflunomide **13** (PDB 1D3H[87]) or B: a Brequinar analogue (PDB 1D3G[87]).

Teriflunomide **13** (fig. 3.11A, blue) directly interacts with Tyr356 via its enolic hydroxy moiety. Furthermore, two water molecules participate in a hydrogen bonding network

between ligand and enzyme by binding to the isonitrile and carboxy moiety of teri-flunomide **13** as well as further polar side chains of the binding pocket. Contrary to other inhibitors, its lipophilic surface which is accessible for hydrophobic interactions with the enzyme is comparably small.

Figure 3.11B shows an X-ray structure of hDHODH cocrystallised with an analogue of Brequinar **12** (yellow). Brequinar has an aromatic carboxylate moiety that strongly interacts with the positively charged guanidino moiety of Arg136 via a salt bridge and thus firmly anchors the ligand to the polar part of the binding pocket. The optimal arrangement of the carboxy moiety towards the guanidino moiety under simultaneous compatibility of brequinar's large lipophilic surface with the binding pocket build the basis for brequinar's strong binding affinity. The enzyme's binding pocket offers space for a cocrystallised water molecule that mediates an interaction between Thr360 and the carboxy moiety of brequinar which in turn interacts with Gln47 via another hydrogen bond. The small hydrophobic cavity is served by the annelated arene.

Development of novel, anthranilic acid-based hDHODH inhibitors
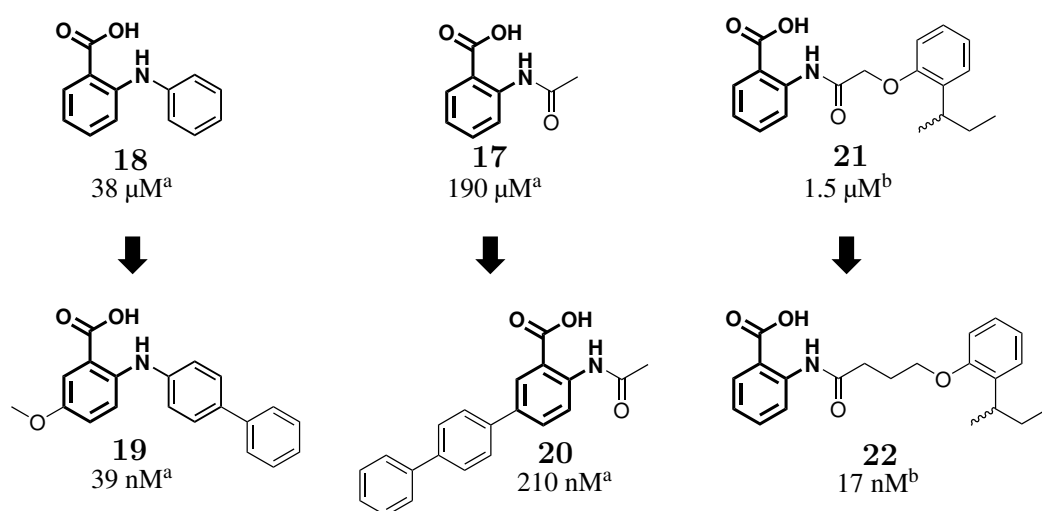
Figure 3.12: Structures and IC_{50} values of literature-known hDHODH inhibitors with anthranilic acid core fragment, [a]) discovered by FRITZSON *et al.*[123] or [b]) MEIER *et al.*[124, 125].

The aromatic carboxy group is a motif that is very common among hDHODH inhibitors. In particular, anthranilic acid derivatives like ASLAN003 **16** have shown high potential. Series bearing this anthranilic acid motive have been discovered by FRITZSON *et al.*[123], ZENG *et al.*[126] and our research group[124, 125]. Structures of selected examples

of these series and their IC_{50} values, determined in isolated hDHODH, are shown in figure 3.12.

In a compound screening, FRITZSON *et al.*[123] discovered the hDHODH-inhibition potential of the two anthranilic acid analogues **17** and **18** in 2010. Fenamic acid derivative **18** served as lead structure for the design of highly potent inhibitor **19**, whereas inhibitor **20** was developed from *N*-(alkylcarbonyl)anthranilic acid derivative **17**.

Independently of this, recently, a series of hDHODH inhibitors with 2-amidobenzoic acid core fragment was developed in our research group.[124,125] Hit structure **21** was discovered in a high throughput screening of a chemical library consisting of 30,040 compounds in simian vero E6 cells infected with toscana virus. In a SAR approach, extending the linker by two methylene groups (fig. 3.13, KP-CF39 **22**) lead to a strong increase in antiviral activity from $IC_{50} = 670$ nM to 70 nM.

The antiviral potential of KP-CF39 **22** was investigated against a broad range of further RNA viruses[124,125] and the results are visualised in the bar graph in figure 3.13.
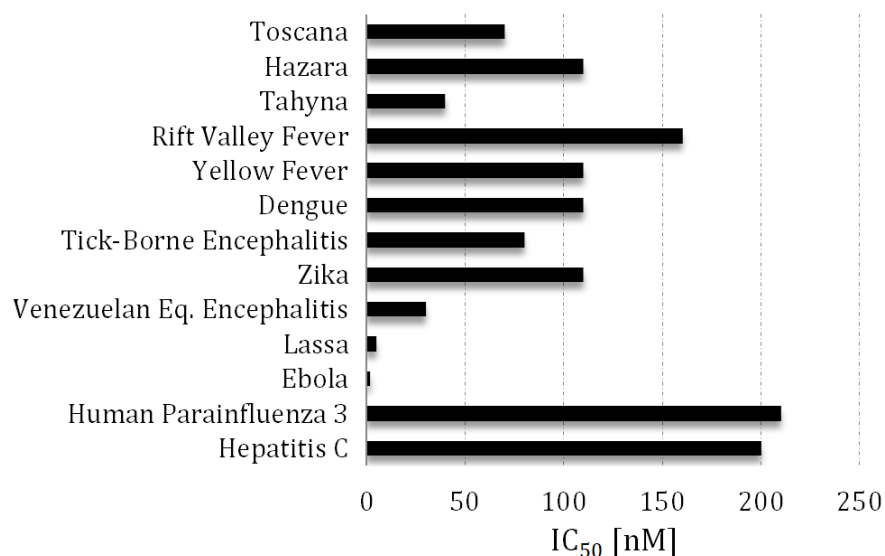
Figure 3.13: Antiviral broad spectrum activity of KP-CF39 **22**.

The inhibitor showed strong antiviral activity in nanomolar range against many different RNA viruses, including examples of the Bunyavirales order and other prominent virus species classified as dangerous emerging viruses by the World Health Organization (WHO)[19]. This broad spectrum antiviral activity was attributed to strong hDHODH inhibition, with $IC_{50} = 17$ nM in the isolated, recombinant enzyme.[125]

4 Objectives

In the past years hDHODH inhibitors have shown high potential for the treatment of several diseases.[1,5,6,89,90] However, although one hDHODH inhibitor has been successfully approved as drug for the therapy of autoimmune diseases[101,102] and other are currently being investigated in clinical phases II and III,[108,110–112] their application has often been linked to some severe issues in the past. Accordingly, numerous clinical trials failed due to high toxicity or low *in vivo* efficacy,[12] especially when the inhibitors were applied as antiviral agents (chapter 3.4). In order investigate whether these issues might be target-related or whether it will be possible to once exploit their full performance spectrum, the development of novel, pharmacologically promising hDHODH inhibitors as well as their antiviral assessment is highly rewarding. Thus, the general aim of this thesis was to support the development of further, highly potent hDHODH inhibitors. Focus was put on attaining suitable pharmacokinetic properties and low toxicity, with respect to the future investigation of their therapeutic potential *in vivo*. Especially viral infections with immunopathogenic mechanism were targeted, for which hDHODH inhibitors appear particular promising (chapter 3.3.2).

Due to its strong inhibitory potency on isolated hDHODH and its broad-spectrum antiviral activity (see chapter 3.4), KP-CF39 **22** was chosen as a lead structure for the main part of this thesis. Especially against Lassa virus, KP-CF39 was found to be highly active with $EC_{50} = 5$ nM, recently (see fig. 3.13).[124,125] Although the pathogenesis of Lassa virus has not been elucidated in detail, there is evidence that overreactions of the immune system are also involved in their fatal outcome.[135] A putative immunosuppressive effect of KP-CF39 **22** that remained to be investigated, may synergistically reinforce its antiviral potency *in vivo*.

The first aim of this thesis was to investigate and analyse the pharmacokinetic properties of KP-CF39 **22** (chapter 5.1). Based on the results of this investigation, a drug candidate with suitable pharmacokinetic properties for future antiviral *in vivo* studies was aimed to be developed. For this purpose, lead structure KP-CF39 **22** was to be rationally modified in classical lead optimisation cycles (chapter 5.3), following the procedure shown in figure 4.1, while aiming to maintain its high inhibitory potency towards the enzyme as well as the virus. At the same time, the stereogenic centre in the molecule should be eliminated, which has been shown to be non-essential for inhibition in previous works.[122,125] The X-ray structure of the complex of hDHODH and KP-CF39 **22**[125] was selected to serve as basis for a computer-assisted ligand design. New synthesis routes needed to be developed to enable efficient derivative syntheses of the new designs. The designs were planned to be evaluated based on their IC_{50}

values in the isolated enzyme. For this purpose, an enzyme assay had to be established after prior expression and purification of the recombinant hDHODH (chapter 5.2). Pharmacokinetic properties were to be investigated by appropriate experiments, that were envisaged to be established within this thesis (chapter 5.1). Finally, a selection of inhibitors was aimed to be evaluated regarding their antiviral activity and immuno-suppressive properties, in order to be able to identify the best for *in vivo* investigation in mice.

Figure 4.1: A: Main aim of this thesis: Lead optimisation of KP-CF39 **22** to a drug candidate for preclinical investigation.
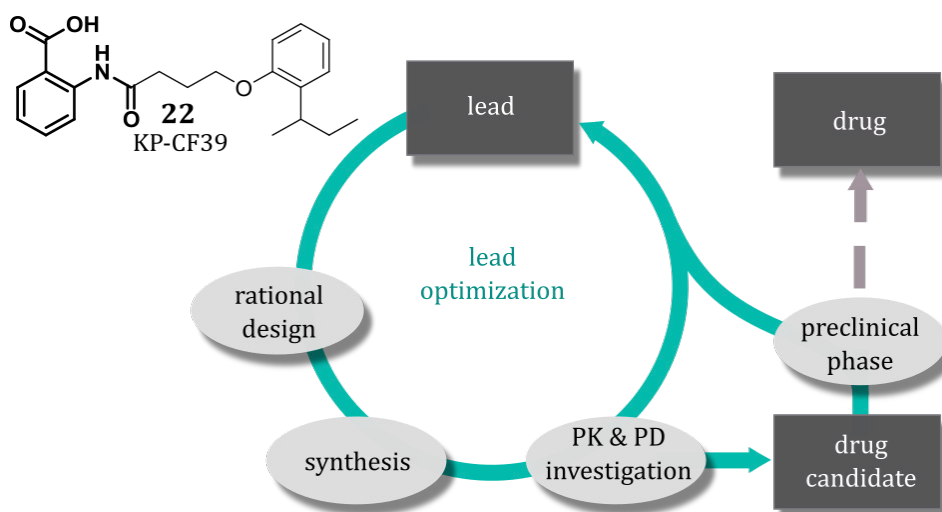
In the last part of this thesis, a novel lead structure was intended to be developed, starting from the active central anthranilic acid core fragment. In contrast to lead structure KP-CF39 **22**, whose sole pharmacodynamic evaluation impacted its original development, the novel lead structure was aimed at already exhibiting suitable pharma-cokinetic properties and exhibiting characterics of an optimal lead structure on whose basis a pharmacokinetically founded drug design can be realised in the future.

5 Results and discussion

5.1 Pharmacokinetic investigation of KP-CF39 and assay establishment

Prior to the *in vivo* administration of a substance, an *in vitro* investigation of its pharmacokinetic properties is recommended, in order to estimate its bioavailability. Therefore, the pharmacokinetic *in vitro* profile of KP-CF39 **22** (racemic mixture) was explored at the outset of this thesis. Parts of the results were published in [P2]. The fluorescence emission capability of KP-CF39 **22**, which was observed to be proportional to its concentration (see figure 5.1A), benefited the compound's quantification in all pharmacokinetic studies. It is induced by the fluorescent anthranilate core scaffold.

5.1.1 Lipophilicity

The lipophilicity of KP-CF39 **22** was investigated first, in order to initially assess its druggability. For this purpose, the compound's distribution in an emulsion of 1-octanol and PBS buffer was determined, which was achieved after one hour mixing, realised by continuously rotating the reaction tube (fig. 5.1A).

$$y = 0.132x + 0.001$$
$$R^2 = 0.997$$
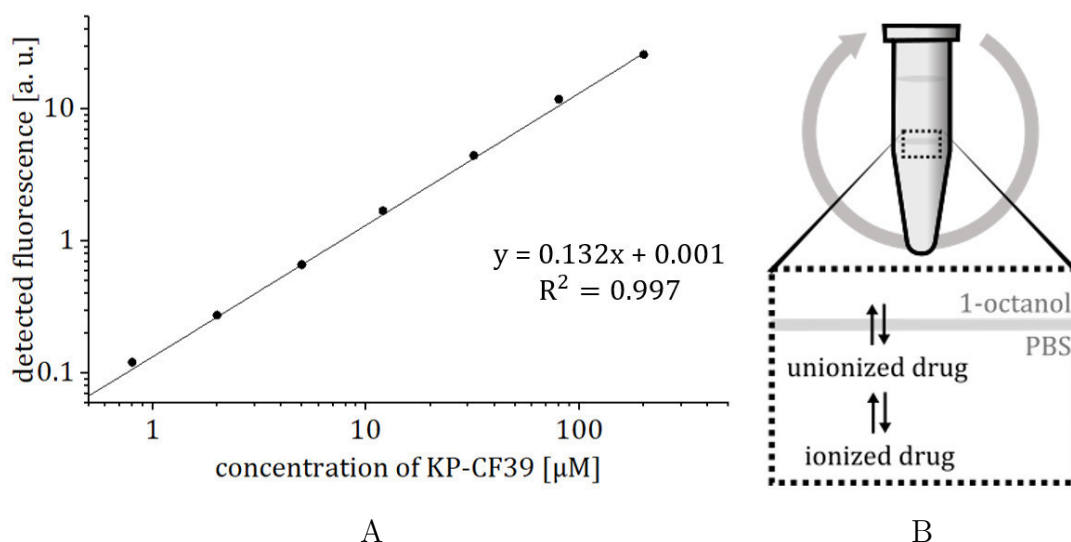
Figure 5.1: A: Linear correlation between the concentration and the fluorescence emission ($\lambda_{\text{exc}} = 300$ nm, $\lambda_{\text{em}} = 460$ nm) of a KP-CF39 **22** solution series in PBS buffer with specification of the regression formula and the agreement (R^2) of the measured values. B: Experimental setup for determining the distribution coefficient.

In the experiment, the organic solvent 1-octanol is originally meant to mimic the hydrophobic core of a biomembrane, whereas the aqueous media inside or outside the cell is modelled by aqueous PBS buffer.[127] Thus, in addition to determining the compound's lipophilicity, this experiment also serves to estimate its ability to permeate biomembranes. In general, if the substance is able to pass from the aqueous into the organic phase to a certain extent, an effective transfer through the lipid core of the membrane is prognosticated.

Contrary to the logP value (octanol/water participation), the logD value considers potential ionisation of the test substances at pharmacological conditions,[127] as PBS buffer maintains a pH value of 7.4 during the experiment. It is assumed that ionisable compounds, such as KP-CF39 **22**, generally only pass from the aqueous phase into the organic phase in their unionised form (fig. 5.1A).[127] However, it was shown that carboxylic acids are able to partition into octanol also in their pharmacologically predominant ionised forms, when sodium is present and acts as counterion.[128] Whether this concept can be transferred to the passage of biological membranes still remains unclear.

The experiment was performed in duplicates and the resulting decrease in inhibitor concentration in the aqueous phase was quantified by high performance liquid chromatography (HPLC) analysis. The distribution coefficient of KP-CF39 **22** was derived via equation 2 (see experimental section 6). KP-CF39 **22** exhibited a logD value of 2.65 $\pm$ 0.01. As a reference, the lipophilicity of caffeine was investigated under the same conditions and was calculated to -0.076 $\pm$ 0.005. This value is in good agreement with the value of -0.07, reported in the literature[129].

A sufficient biomembrane permeation is attributed to compounds with positive logD values and thus certain hydrophilicity.[127] However, substances that are highly lipophilic (logD > 3) may get stuck in the membrane. Thus, the lipophilicity of KP-CF39 **22** lies within a range which is suitable for pharmacological use. In general, the optimal lipophilicity for inhibitors of hDHODH is comparatively high, since they reach their binding site in the target enzyme exclusively from the inside of the mitochondrial membrane and the binding site is quite hydrophobic. The ability to be liposoluble thus limits the ability for hDHODH inhibition in the cell. Nevertheless, it is imperative to consider that excessive lipophilicity may limit other pharmacokinetic processes besides membrane permeation (see chapter 3.2.3).

5.1.2 Membrane permeation

To study the ability of KP-CF39 **22** to penetrate membranes, a parallel artificial membrane permeation assay (PAMPA) was performed. Whereas logD determination was mainly intended to estimate the lipophilicity, since its prediction on membrane permeation is limited, the PAMPA actually enabled an investigation of the compound's permeation through an artificial membrane.

The artificial membrane consists of a hydrophobic filter material, pretreated with a lipid-containing, organic solvent. Its penetration is supposed to mimic a passive, transcellular permeation (chapter 3.2.1) of biomembranes in the gastrointestinal tract, which is the most common absorption mechanism for orally administered small molecule drugs.[29] In case that active transport mechanisms shall be considered, it would be necessary to use real biomembranes, such as in the Caco-2 assay[130]. However, Caco-2 assays are very laborious, whereas PAMPA plates are commercially available as 96 well plates, already contain the membrane and only need to be thawed, prior to use. Moreover, Caco-2 assays are poorly reproducible and can mispredict compounds' permeabilites, for example, when transport proteins have been either over- or underexpressed.[29] Additionally, the PAMPA enables a high throughput investigation of several compounds under the same conditions, which is very useful for the comparison of derivatives and thus for this thesis.
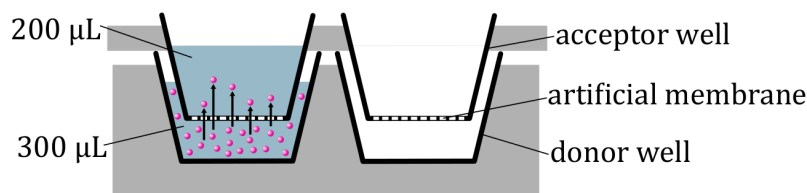
Figure 5.2: Experimental setup for determining the PAMPA permeation.

Figure 5.2 shows the PAMPA plate setup. It consists of two single plates which were filled with buffer solutions prior to the experiment. The test substance KP-CF39 **22** was added to the donor wells only and the plates were plugged together to initiate permeation. This allowed molecules of the test substance to permeate from the donor wells through the bottoms of the acceptor plate, each consisting of an artificial membrane, in upward direction. Five hour incubation was followed by analysing the compound concentration decrease in the donor wells by fluorescence spectrophotometry. The effective PAMPA permeation P_{pampa} of KP-CF39 **22** was calculated by equation 3 (see experimental section 6) to $(1.582 \pm 0.258) \cdot 10^{-5}$ cm/s. As a reference, the permeability of caffeine was investigated under the same conditions and was calculated

to $(0.823 \pm 0.143) \cdot 10^{-5}$ cm/s. This value is in accordance with the literature value of $(1.12 \pm 0.29) \cdot 10^{-5}$ cm/s.[131]

According to a publication of STOCKDALE *et al.*[132], permeation values ranging from $2\text{-}10 \cdot 10^{-6}$ cm/s are considered moderate and the compound's permeability improves as the values increase. Thus, KP-CF39 **22** showed good membrane permeability.

5.1.3 Plasma protein binding

The non-specific interaction of KP-CF39 **22** with plasma proteins was found to be very high with a value of 99 %, determined by TechMed[ILL] (Strasburg) (see [P2][124] for experimental details). Nevertheless, this value is still below 100 %, which means that unbound molecules are still available for a specific inhibition of the target enzyme, although they are few. As described in chapter 3.2.1, high PPB can also have positive effects, such as a reduced metabolic transformation.

5.1.4 Stability and metabolite investigation

KP-CF39 **22** was shown to be highly stable in mouse blood plasma in an investigation by TechMed[ILL] (Strasburg) (see [P2][124] for experimental details). They determined its plasma stability to 94 ± 6 % after 2 h incubation.

In order to investigate the stability of KP-CF39 **22** in presence of liver enzymes, a metabolism assay was established as part of this thesis, realised by an incubation of the test substance with liver S9 fraction.

S9 fractions can be commercially purchased or obtained by an ultracentrifugation of liver homogenates at 9000 g and subsequent selection of the supernatant. During this process, which is shown in figure 5.3, nuclei, debris, mitochondria and lysozymes are removed, so that S9 fractions contain microsomes as well as cytosolic components of the liver. Whereas microsomes contain CYP450 enzymes which catalyse most phase I metabolism reactions, enzymes involved in phase II metabolism reactions are present in the cytosolic fraction only.[136] An even more realistic representation of metabolism would be achieved by incubating the test substance with hepatocytes that exhibit a full complement of metabolic enzymes in addition to intact cellular compartments. However, in contrast, S9 assays are much cheaper and less laborious and still provide a comprehensive analysis of a substance's metabolism.[137]
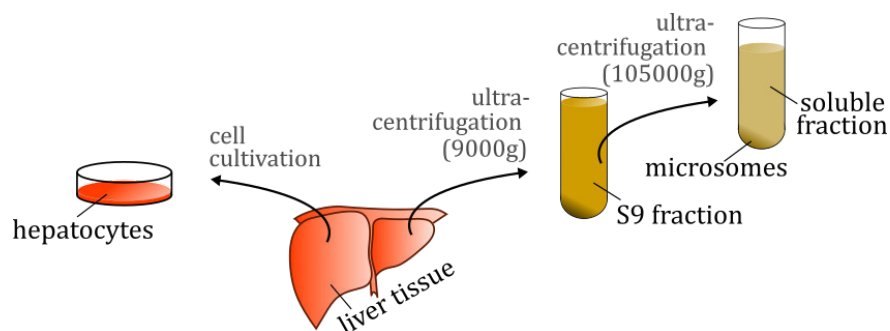
Figure 5.3: Preparation of S9 fraction, microsomes and hepatocytes.

Initially, the phase I metabolism of KP-CF39 **22** was investigated, following a protocol of MAITI *et al.*[138]. Rat liver S9 fraction was treated with magnesium chloride and NADPH in phosphate buffer and the resulting mixture was preincubated at 37 °C before the test substance was added. Figure 5.4A shows the assay setup. Immediate sampling of a reference aliquot (0 h) was followed by 3 h incubation at 37 °C, during which two further aliquots were sampled after 1 h and at the end of incubation. Immediately after sampling, the aliquots were analysed via HPLC and LC/MS. The experiment was performed in triplicates.
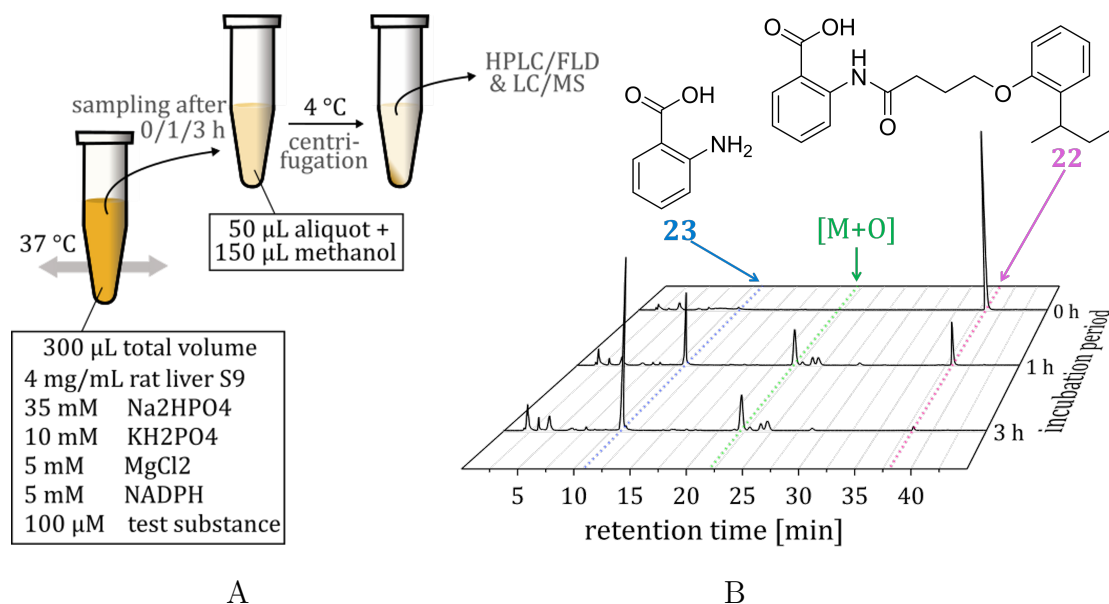
Figure 5.4: A: Experimental setup for determining the metabolic stability in rat S9 mix.
B: HPLC-chromatograms (FLD, λ_{exc} = 300 nm, λ_{em} = 407 nm) obtained after a 0 h, 1 h and 3 h incubation of KP-CF39 **22** with rat S9 mix.

Figure 5.4B shows the fluorescence chromatograms that were recorded during HPLC analysis of the three solutions. Besides a high sensitivity of fluorescence detection, components of the S9 mix do not appear in the chromatograms, as they are not

fluorescent. Thus, fluorescent test compounds are of particularly advantage in this assay.[139] However, it should be noted, that only metabolites are detected, that bear the fluorescent anthranilic acid fragment.

In this thesis, the metabolic compound stability is indicated by its percentage amount remaining after 1 h incubation in rat liver S9 mix (S_{S9}), quantified by HPLC-analysis (equation 4, see experimental section 6). KP-CF39 **22** exhibited a metabolic stability of 21.8 %. As a reference, the metabolic stability S_{S9} of fluorescent, literature-investigated 7-ethoxycoumarin was determined to $S_{S9} = 47.8 \pm 6.1$ % and 7-hydroxycoumarin was detected as sole fluorescent metabolite. This is in good agreement with the stability range of 50-65 %[140] indicated in the literature.

With 21.8 %, the metabolic stability of KP-CF39 **22** is rather low. Even though a drug's slow biotransformation is desirable and thus the metabolic stability should not reach 100 %, such low metabolic stability suggests an almost complete elimination of the compound during the first liver passage. Consequently, the target organ would not be reached at all.

For reference purposes, the experiment was repeated, without the addition of inhibitor. HPLC-analysis revealed that all peaks with retention times below ten minutes (see fig. 5.4) can be assigned to the metabolising mixture. Moreover, an incubation of KP-CF39 **22** with heat-inactivated S9 mix showed that its lability is mainly due to the activity of the metabolising enzymes in the mixture. The stability of KP-CF39 **22** in heat-inactivated S9 mix was determined to 91 % after 1 h incubation.
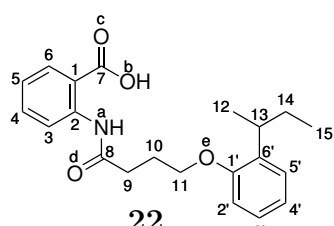
At this point, phase II metabolism, which requires the addition of further reagents, was not investigated yet.

The metabolites of KP-CF39 **22** were identified by LC/MS analysis of the mixture using the same retention conditions on the same column. Due to the lower sensitivity of this detection method, only an analysis of the highest peaks at retention times of 11 and 23 min was possible.

For the peak at 23 min retention time, a mass peak increased by the mass of oxygen was found, suggesting hydroxylation of KP-CF39 **22**. Its slight asymmetry suggests that two hydroxylation products eluted with almost identical retention time. Presumably, the three smaller peaks in the retention range from 20 to 25 min can also be attributed to hydroxylation products, due to their similar retention. In total, four to five hydroxylation products were assumed to have formed in the course of the compound's metabolism.

Mass spectrometric metabolite identification did not allow a location of the hydroxylation site in the structure of KP-CF39 **22**. For this reason, the *in silico* tool FAME 3[141] was applied to the structure of KP-CF39 **22** in order to predict its most probable metabolism sites. FAME 3 was developed by KIRCHMAIR *et al.* and predicts the probabilities for individual atoms in a query molecule to become sites of phase 1 and phase 2 metabolism.[141] The results are shown in figure 5.5. With probabilities ranging from 19 to 28 %, hydroxylations of the *sec*-butyl carbon atoms were predicted to be most probable. Due to their better steric accessibility, the two methyl groups were more likely to be hydroxylated. Hydroxylation of the linking alkyl chain was predicted less probable with values ranging from 11 to 15 %. Among the aromatic carbon atoms, only C-4 and C4' were predicted to be hydroxylated with probabilities above 10 %. Thereby, hydroxylation at the phenoxyarene was predicted to be more probable due to its higher electron density.

Atom	Predicted probability [%]
O-b	76.0
C-15	27.9
C-14	27.2
C-12	24.3
C-13	19.6
C-4'	15.9
C-9	14.4
C-4	12.8
C-8	11.6
N-a	11.6
C-11	11.2

Figure 5.5: Output for the *in silico* prediction of metabolism sites for KP-CF39 **22** using FAME 3[141]. Only probability values > 10 % are shown in the table.

The metabolite that was eluated at a retention time of 11 min (see fig. 5.4B) was identified as anthranilic acid **23** by LC/MS analysis. A co-injection of this compound to the mixture confirmed this. However, it was found that the fluorescence intensity, that was emitted by anthranilic acid at the detected wavelength, was about three times higher than that of KP-CF39 **22** at similar concentrations. Thus, the peak height in the chromatogram (fig 5.4) suggests a higher amount of this metabolite in the mixture than was actually present. The actual ratio was not determined here. Anthranilic acid **23** has formed due to a cleavage of the amide bond.

Amides are generally considered to be chemically stable and therefore prominent motives in pharmaceutical drug structures but are also beared in biomolecules such as peptides and proteins. For a targeted degradation of these biomolecules during enzymatic digestion, amidases and peptidases use catalytic mechanisms to weaken the amide bond through an interplay of different amino acid residues, thus enabling the nucleophilic attack of an activated water molecule and thus effective amide cleavage.[142] For this interplay, a specific spatial arrangement of these involved residues is required, which was described in detail by SYRÉN *et al.*[143] Peptidase or amidase-catalysed amide cleavage is therefore a highly selective process that only occurs at specific locations in designate amino acid sequences. Thus, unnatural amides are usually no substrates.[144] Esterases, on the other hand, are less selective, as their original biological function is to metabolise xenobiotics and endobiotics.[145] While they mainly catalyse the cleavage of ester bonds, amides can also be their substrates.[146] Figure 5.6 shows the assumed mechanism for amide cleavage catalysed by an carboxylesterase (CES) with KP-CF39 **22** as a substrate. The shown mechanism was derived from the mechanism proposed by SATOH and HOSOKAWA[147] for the CES-catalysed cleavage of ester bonds.
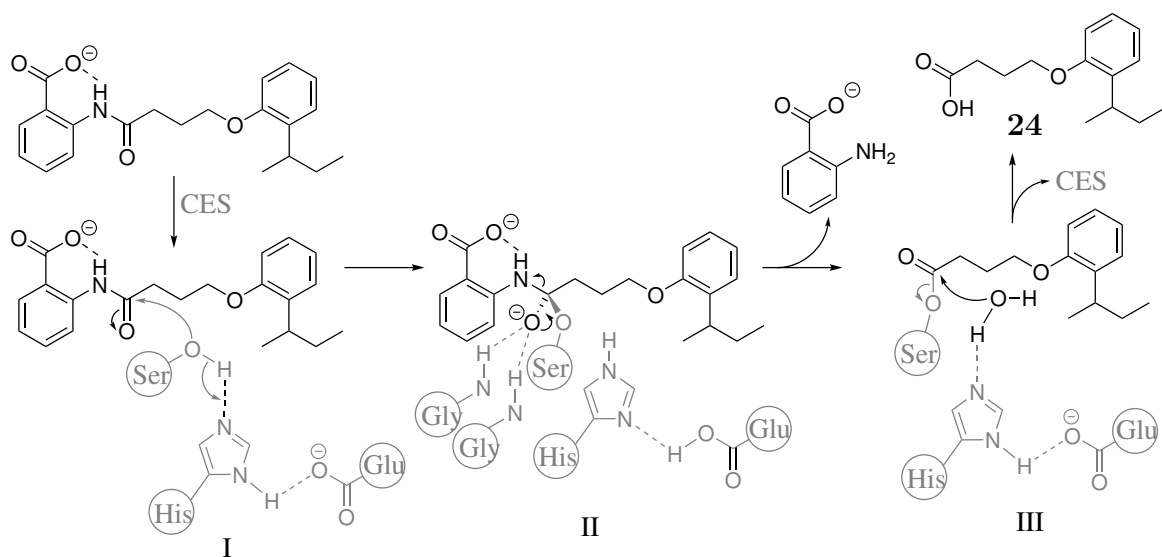
Figure 5.6: Proposed mechanism for the carboxylesterase (CES)-catalysed hydrolysis of KP-CF39 carboxylate. Side chains of the protein are colored in grey.

The active site of hydrolases bears a so-called catalytic triad, consisting of a nucleophile, a base and an acid. In carboxylesterases, the acidic glutamate polarises an adjacent histidine, which in turn deprotonates serine that consequently is activated for a nucleophilic attack on the amide carbon atom of the substrate (I). This nucleophilic attack results in the formation of a tetrahedral intermediate (II), in which the negatively

charged oxygen is stabilised by two glycine residues that form a so-called oxyanion hole. A subsequent proton transfer from the protonated histidine to the thus eliminated anthranilate results in the formation of ester complex III, in which a water molecule is hydrogen bonded to histidine. A final nucleophilic attack of the thus activated water on the activated ester leads to the release of carboxylic acid **24** under recovery of enzymatic activity.

Whereas esters are efficiently cleaved under CES-catalysis, amides are usually converted much slower, due to the reduced electrophilicity of their carbonyl carbon atom.[148] The rapid amide cleavage that was observed during metabolic transformation of KP-CF39 **22** must be favoured by certain effects. Since the carboxy moiety turns into a carboxylate anion under physiological pH, its electron-withdrawing capacity is neutralised. Consequently it does not enhance electrophilicity at the carbonyl carbon atom to facilitate nucleophilic attacks of the nucleophilic side chain or a water molecule. However, the carboxylate anion forms an intramolecular hydrogen bond to the amide proton (see fig. 5.6). SYRÉN *et al.*[143] showed that amide hydrogen bonding enables amide cleavage in amidases by facilitating nitrogen inversion. This inversion is necessary because the immobile catalytic base is responsible for both the deprotonation of serine in the course of its nucleophilic attack on the substrate's carbonyl carbon, and for the protonation of the amine that is eliminated from the tetrahedral intermediate.[143] The hydrolysis mechanism in amidases is, apart from this detail, similar to that of esterases, shown in figure 5.6. Based on this evidence, it was suggested that the intramolecular hydrogen bond in anthranilate derivative KP-CF39 **22** was responsible for its rapid metabolisation.

Overall, the stability of KP-CF39 **22** towards Phase I metabolism was low, due to hydrolysis of the amide bond as well as hydroxylation of the *sec*-butyl moiety. Consequently, bioavailability was expected to be insufficient for an *in vivo* investigation of its antiviral potency. Except this, KP-CF39 **22** was shown to have suitable pharmacokinetic properties.

5.2 Preparation and purification of recombinant hDHODH and enzyme assay establishment

For the lead structure optimisation procedure (see fig. 4.1A), an enzyme assay had to be established in order to enable evaluation of the designed compounds and comparison of their potencies with that of initial lead compound KP-CF39 **22**. This chapter deals with the production and preparation of recombinant hDHODH and the establishment of the enzyme assay for IC_{50} calculation.

5.2.1 Enzyme expression, purification and evaluation

Expression and purification of the enzyme was performed under the friendly support of I. PFEFFER (EMBL Hamburg), following a protocol of DAS *et al.*.[149] The expression plasmid pET28a-hDHODH$_{29-396}$ was kindly provided by H. MUNIER-LEHMANN.[150] Besides a gene for the desired truncated, His6$_6$-tagged enzyme it contained a kanamycin resistence gene.

Initially, the plasmids were transferred into competent E.coli cells via heatshock transformation and the plasmid-bearing bacterial colonies were allowed to grow on Kanamycin-treated LB-Agar plates and later terrific broth medium at 37 °C. Thereby, the added antibiotic realised a selective growth of plasmid-containing cells. Subsequently, the protein's natural cofactor flavin mononucleotide **10** was added to the mixture to ensure its immediate incorporation into the protein structure during its expression, which was induced by the addition of isopropyl-β-D-thiogalactoside (IPTG). After 20 hour incubation at 16 °C, the cells were harvested by centrifugation. 37 g cells were obtained from 6 L expression volume.

The harvested cells were lysed by sonication to release the expressed enzyme, followed by centrifugation in order to remove cellular debris. The enzyme's solubilisation was thereby ensured through the addition of the detergent Triton-X 100.[151] The supernatant was purified via HisTrap Ni^{2+} affinity column chromatography, which was enabled by the introduced His$_6$-tag, followed by final size exclusion chromatography. During all purification steps, protein-containing fractions were quickly identified due to the yellow colour of the incorporated cofactor FMN (figure 5.7B). Analysis of the amount and purity of enzyme in the mixtures was performed by SDS PAGE. Figure 5.7A shows the final gel that visualises the overall progress during protein purification. After the

last purification step, the recombinant protein was obtained in high purity. In total, 350 µL of a 28.6 mg/mL protein solution were obtained.

Enzyme folding was analysed by nano differential scanning fluorimetry (nanoDSF). During constant temperature increase, the emitted fluorescence of the prepared protein in presence (green) and absence (blue) of the inhibitor KP-CF39 **22** was monitored. Figure 5.7C shows that upon heating the prepared protein unfolded its structure, which was indicated by an increase in fluorescence intensity as result of the exposition of fluorescent protein residues like tryptophane and tyrosine.[152] By the addition of ligand KP-CF39 **22**, the protein's melting temperature was increased by 14.8 °C, due to its stabilising effect. Thus, an intact, folded structure of the prepared protein was indicated by this experiment.
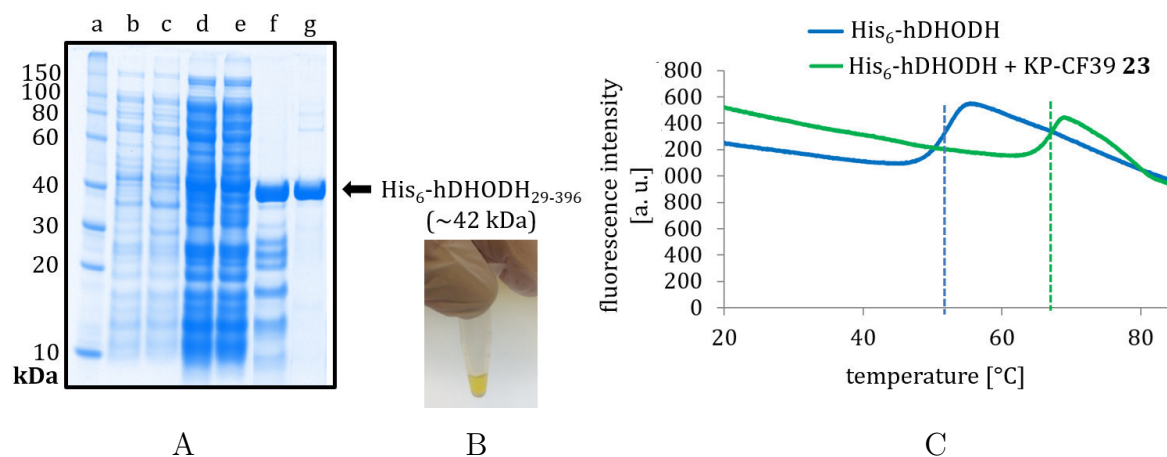
Figure 5.7: A: SDS-PAGE-analysis of protein quantity and purity after cell harvesting (b), sonication (c: pellet, d: soluble fraction), concentration (f), HisTrap chromatography (e) and size exclusion chromatography (g). B: Yellow coloration of the enzyme due to FMN-incorporation. C: nanoDSF-melting curves of the prepared protein with (green) and without (blue) inhibitor addition (FLD, λ_{exc} = 280 nm, λ_{em} = 330 nm).

5.2.2 Enzyme inhibition assay

The enzyme assay was established based on a protocol[150] which was published by MUNIER-LEHMANN *et al.*. Accordingly, to visualise enzymatic activity, the blue redox indicator 2,6-dichlorophenolindophenol **25** (DCPIP) was included into the redox reaction cycle of hDHODH, as shown in figure 5.8. Instead of the cofactor ubiquinone (see chapter 3.3.3), its short-chained analogue CoQ1 **26** was used, which is accordingly reduced to the corresponding ubiquinol derivative **27**. CoQ1 **26** then is recovered by a

reduction of DCPIP **25** to its colourless form **28**. Consequently, by observing the loss of colour, the enzymatic substrate conversion can be followed.

A   B
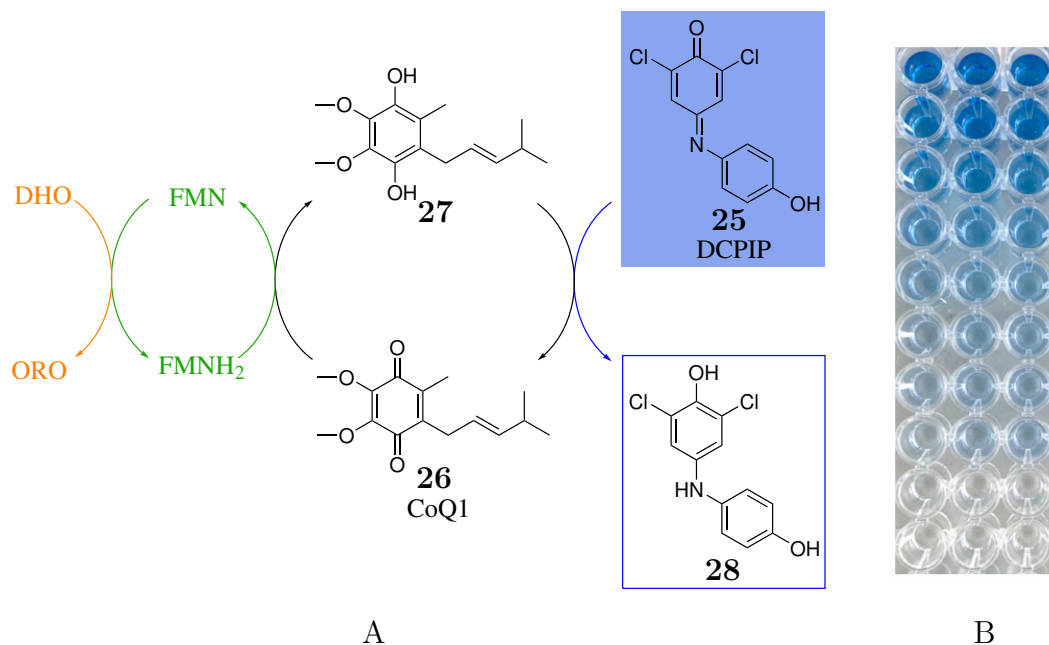
Figure 5.8: A: Inclusion of DCPIP reduction into the redox cycle of DHODH.
B: Blue colouring of a DCPIP **25** dilution series.
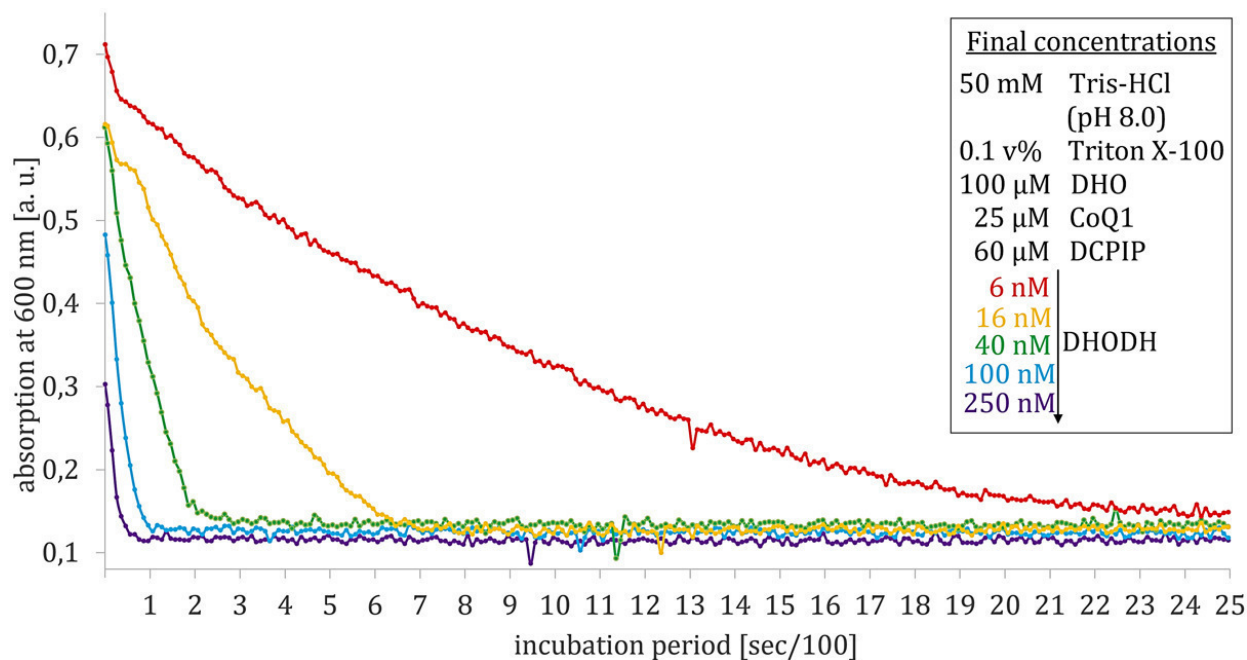
Figure 5.9: Decrease in absorption at 600 nM due to DCPIP **25** conversion at different DHODH concentrations.

In order to investigate a suitable enzyme concentration for the assay, which is not given in the literature protocol,[150] DCPIP conversion was followed at five different enzyme concentrations in the absense of the inhibitor under the conditions stated in figure 5.9. This was realised by spectrophotometrically monitoring the decrease in absorbance at a wavelength of 600 nm. Since FMN was already included in the enzyme structure, it was not added separately. The results of this first experiment are shown in figure 5.9 and moreover indicate an intact enzymatic function.

With progressing incubation period, the ratio of unreacted DCPIP **25** to enzyme, present in the mixture, decreases. Consequently, it becomes less probable that DCPIP **25** molecules will hit an enzyme molecule. This can be observed as a flattening of all curves to a minimum absorption value. The enzymatic conversion rate can be determined from the initial linear range which is therefore also referred to as the initial enzyme rate. Such initial linear ranges were observed for enzyme concentrations of 40 nM (green), 100 nM (blue) and 250 nM (violet). Apparently, protein concentrations of 6 nM and 16 nM were too low for reflecting the initial conversion rate as linear ranges, at least for these fixed substrate concentrations. Moreover, it can be observed that the detected start absorption value decreases with increasing enzyme concentration. This is related to the period of time which passes between enzyme addition and recording of the first measuring point. The initial enzyme rate can be determined best for the longest linear range, which was observed for an enzyme concentration of 40 nM, here. In further experiments, a prolongation of the linear range was achieved at an optimal enzyme concentration of 35 nM.

To determine the IC_{50} value of KP-CF39 **22**, the following procedure proved to be most robust: The inhibitor was added in nine different concentrations to a 96 well plate, followed by a prepared substrate mix that contained the other ingredients (see fig. 5.8). DCPIP conversion was initiated by the simultaneous addition of 80 µL enzyme solution to each well to give total volumes of 200 µL. The recorded absorption curves are shown in figure 5.10A. The initial enzyme rate v_c (0-200 sec) was determined for each inhibitor concentration and plotted against the concentration. The experiment was performed in triplicates. Figure 5.10 shows the resulting IC_{50} curve with logarithmic concentration plotting. The enzymatic activities v_c/v_0 were calculated for visualisation purposes, here. The IC_{50} value was determined as the curve's inflection point by non-linear fitting to equation 1 (see experimental section 6). This resulted in an IC_{50} value of 7.1±0.6 nM for KP-CF39 **22**.
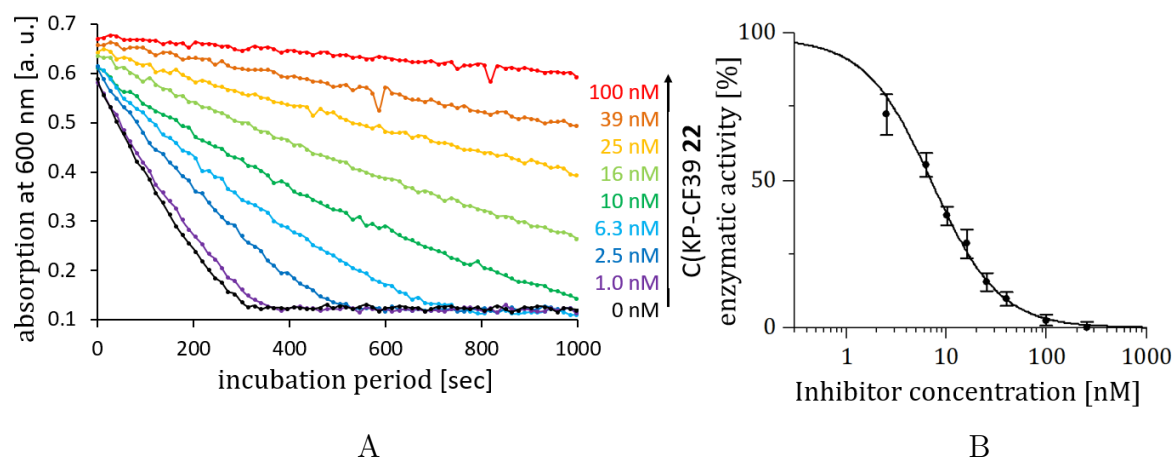
Figure 5.10: **A**: Absorption curves (600 nm), monitored during enzymatic conversion of DCPIP **25** at different concentrations of the inhibitor KP-CF39 **22**. **B**: Graphic plot of the calculated residual enzymatic activities against present inhibitor concentrations.

As reference, the IC_{50} value of the known, highly potent inhibitor Brequinar **12** was determined analogously. It was calculated to 14.7 ± 1.4 nM which agrees roughly with published values of 10 nM[153] or 8.4 nM[150]. Consequently, KP-CF39 **22** was shown to be an even slightly stronger inhibitor compared to Brequinar **12**, at least in the isolated, recombinant enzyme under the stated conditions.

5.3 Lead optimisation

In order to stabilise KP-CF39 **22** against biotransformation, its labile structure fragments (see chapter 5.1.4) were modified successively, supported by a rational, structure-based ligand design approach. Parts of this work were submitted in [P1].

The X-ray structure of a cocrystallised complex of KP-CF39 **22** in recombinant hD-HODH was kindly provided by M. LAURSEN and K. PFAFF.[125] A section of this structure is shown in figure 5.11A. Both enantiomers of the added racemic mixture of KP-CF39 **22** occupied the binding site equimolarly in the irradiated cocrystal. Therefore, the resulting electron density map corresponds to a superposition of both enantiomers whose binding poses are almost identical. This fact moreover explains their similar antiviral activities (see chapter 4).

A   B
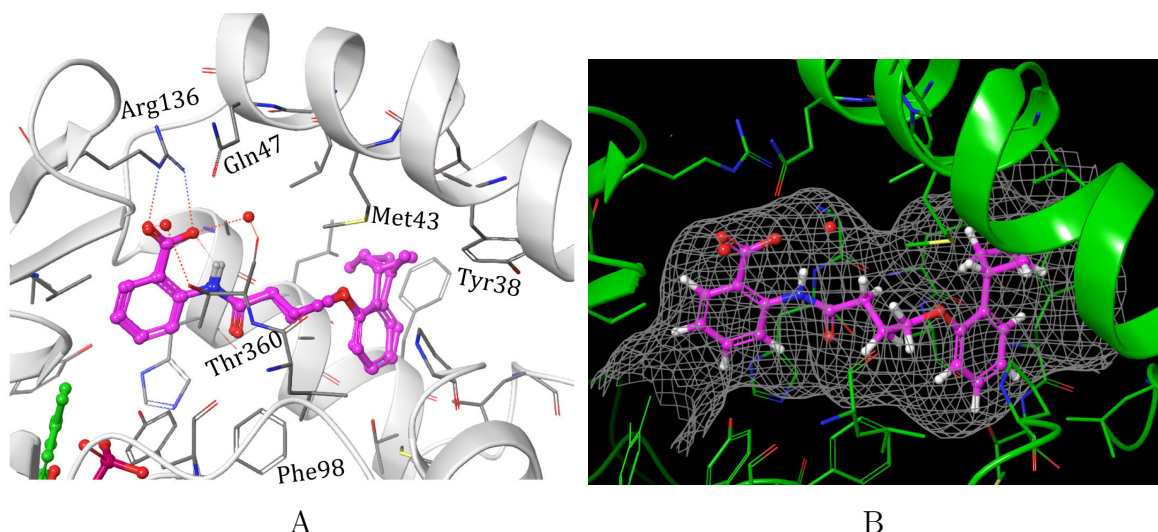
Figure 5.11: Binding pose of KP-CF39 **22** in a cocrystal complex with recombinant hDHODH, determined via X-ray crystallography.

Analogous to Teriflunomide **13**, Brequinar **12** (see fig. 3.11 for comparison) and many other known hDHODH inhibitors, KP-CF39 **22** binds to the enzyme's hydrophobic access tunnel for ubiquinone. Similar as in the discussed binding pose of Brequinar **12** (see chapter 3.4), a salt bridge between the carboxy group of KP-CF39 **22** and Arg136 anchors the ligand firmly in the binding pocket and thus strongly contributes to its high binding affinity.

Contrary to Brequinar **12**, the rotational mobility of the carboxy group in KP-CF39 **22** is restricted by its intramolecular hydrogen bonding with the amide proton. This resulted in a slight rotatory adaption of the sidechain of Arg136. This intramolecular

interaction is expected to have advantageous effects on binding entropy of the enzyme-ligand complex: Less degrees of freedom were lost during the binding process, compared to a ligand with freely rotating functions. Moreover, the solvation of these interacting functions in aqueous medium was reduced, which in turn lead to lower energetic desolvation costs prior to binding.

The changed arrangement of the carboxy moiety, compared to Brequinar **12**, lead to the inclusion of a second crystallised water molecule. Both shown water molecules participate in a hydrogen bonding network between enzyme and ligand and consequently improve binding enthalpy of the complex.

Ultimately, the ligand's high binding affinity is attributed to its large lipophilic surface and good shape compatibility with the surface of the binding pocket, enabled by the flexibility of the butyryl linker. The binding pose almost perfectly matches the predictive docking pose obtained in a previous study[122], for which the enzyme-ligand-surface compatibility was described in more detail.

5.3.1 Optimisation cycle 1: Amide bond stabilisation

Although the *ortho*-arrangement of carboxy and amino function seems to facilitate metabolic cleavage of the amide bond due to the formed intramolecular hydrogen bond (see chapter 5.1.4), it also proved to create a suitable core fragment for highly potent hDHODH inhibitors (see chapter 3.4). The attached amido-carbonyl function not only increases rigidity of the ligand while optimally fitting into the binding pocket, but also facilitates synthetic accessibility of the inhibitors. Thus, instead of substituting the amide function, a strategy was developed to stabilise it. For this purpose, two approaches were applied.

As first approach, a steric shielding moiety was introduced to the structure, in order to reduce the amide's accessibility for metabolising enzymes.

In figure 5.11B, the protein surface is visualised as grey mesh. It can be seen that the binding pocket does not offer large space for sterically demanding moieties in adjacent positions of the 2-amido functionality. Thus, only small substituents, like for example a methyl group, will be tolerated. The C-3 carbon atom of the anthranilate arene appeared to be most suitable for such substitution. A newly introduced, methyl substituent at this position will point towards the thus shielded amido function and moreover was expected not to clash with the protein surface. Thus, methyl-modified structure **29** (figure 5.12) resulted as first design of optimisation cycle 1.
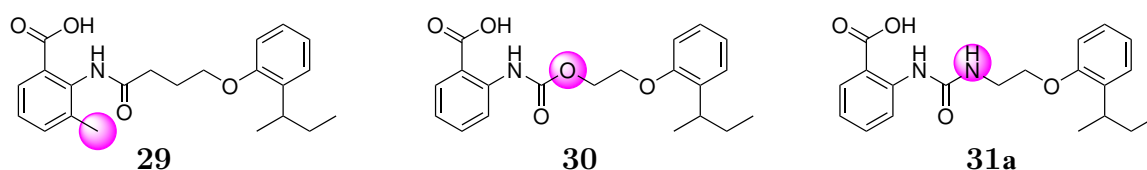
Figure 5.12: Structures of three designed molecules with stabilised amide bond. Modified structure elements are highlighted.

In a second approach, the amide bond was chemically stabilised. Carbamate and urea functionalities are prominent bioisosteres of amides which are frequently used in drug design and still contain the amido functionality. The positive mesomeric effect of the respective additional heteroatom increases electron density at the carbonyl carbon atom and thus reduces its reactivity towards hydrogenolysis by metabolising enzymes.[154] Carbamate **30** and ureide **31a** emerged as two further designs of the first optimisation cycle.

The synthesis of these three compounds as well as all other designs of this chapter is discussed at its end (chapter 5.3.6).

The three synthesised compounds **29**, **30** and **31a** were investigated regarding their metabolic stabilities, first. For this purpose, each of them was incubated with S9 mix, following the procedure that was described for KP-CF39 **22** (chapter 5.1.4). The resulting HPLC chromatograms are shown in figure 5.13 and 5.14.
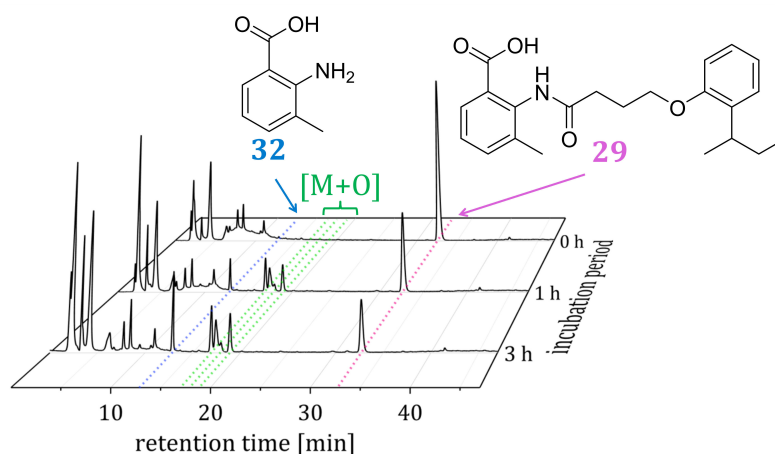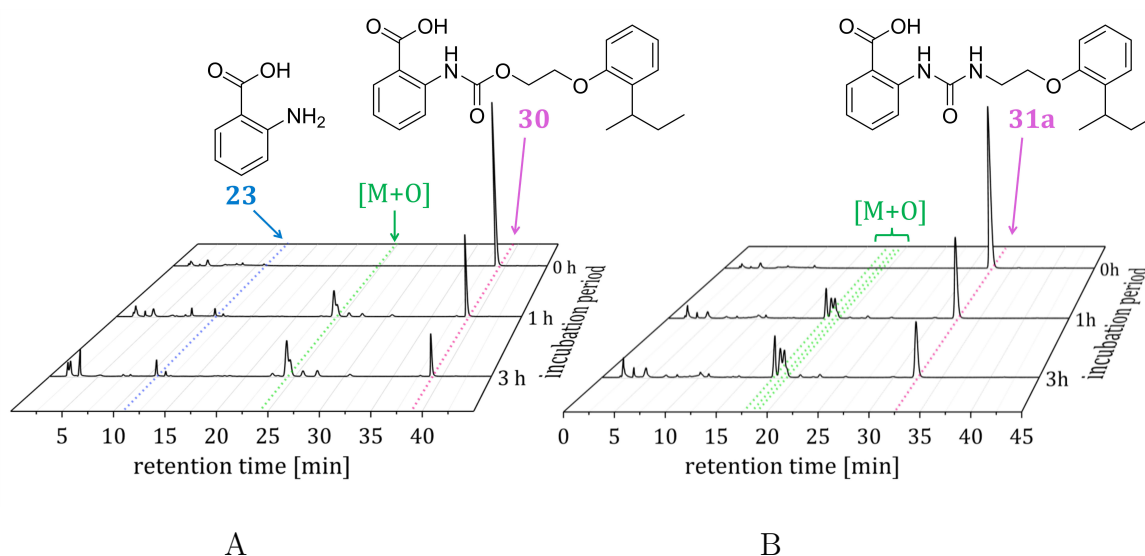

Figure 5.13: HPLC-chromatograms (FLD, λ_{exc} = 300 nm, λ_{em} = 407 nm) obtained after a 0 h, 1 h and 3 h incubation of compound **29** with rat S9 mix. The declared metabolites were identified by LC/MS analysis.

The methyl modification in derivative **29** (fig. 5.13) strongly reduces its fluorescence emission, which is why the signal noise from the S9 mix at early retention times appears higher than for the others. For methylated derivative **29** (fig. 5.13), similar as for lead structure KP-CF39 **22**, several metabolites were detected in the retention time range of 17-19 min (green), which have been identified as hydroxylation products [M+O] by LC/MS analysis. However, regarding the task of this optimisation cycle, the most relevant peak appeared at a retention time of 12.9 min (blue). The associated metabolite is 3-methylanthranilic acid **32**, whose identity has been indicated by LC/MS analysis and confirmed by HPLC-coinjection. Apparently, the shielding effect of the introduced methyl moiety was not sufficient to completely inhibit cleavage of the amide bond. Nevertheless, the metabolic stability was increased to 49.1 % after one-hour incubation and thus doubled, in comparison to that of lead structure KP-CF39 **22**. In table 5.1 the determined metabolic stabilities of the three derivatives are compared with each other as well as with that of KP-CF39 **22**.

Table 5.1: Metabolic stabilities (S_{S9}, percentage compound amount remaining within 1 h incubation in rat S9 mix), hDHODH-inhibition (IC_{50}), lipophilicities (logD) and permeabilities (P_{PAMPA}) of the three compounds designed in optimisation cycle 1 as well as lead structure **22** for comparison.

Compound	S_{S9} [%]	IC_{50} [nM] (hDHODH)	logD	P_{PAMPA} [cm/s]
KP-CF39 **22**	21.8 ± 1.5	7.1 ± 0.6	2.65 ± 0.01	$(1.58 \pm 0.26) \cdot 10^{-5}$
methyl analogue **29**	49.1 ± 3.0	219 ± 2	1.73 ± 0.01	$(7.35 \pm 3.43) \cdot 10^{-6}$
carbamate **30**	43.8 ± 1.2	25 ± 2	2.65 ± 0.01	$(1.26 \pm 0.09) \cdot 10^{-5}$
ureide **31a**	48.9 ± 2.0	17 ± 1	2.05 ± 0.01	$(5.85 \pm 0.69) \cdot 10^{-6}$

With 43.8 %, the metabolic stability of carbamate **30** is slightly below that of methylated derivative **29** but still much higher compared to that of initial lead compound **22**. An inspection of its chromatograms (fig. 5.14A), which were recorded during the S9 assay, reveals that even the more stable carbamate unit was cleaved to a small extend, resulting in the formation of anthranilic acid **23**.

Figure 5.14: HPLC-chromatograms (FLD, $\lambda_{exc} = 300$ nm, $\lambda_{em} = 407$ nm) obtained after a 0 h, 1 h and 3 h incubation of A: carbamate **30** and B: ureide **31a** with rat S9 mix. The declared metabolites were identified by LC/MS analysis.

Only the amide's inclusion into an urea functionality (compound **31a**, fig. 5.14B) prevented its metabolic cleavage to full extend and resulted in a metabolic stability of 48.9 %.

Next, the effect of the three modifications on hDHODH-inhibition potency was investigated. For this purpose, their IC_{50} values were determined, again following the procedure which was described in chapter 5.1.4. With an IC_{50} value of 219 nM, methylated derivative **29** can still be classified as strong binding hDHODH ligand, but inhibits its activity with a thirtyfold weaker potency than KP-CF39 **22**. A possible explanation for this could be that the methyl group forces the phenylamido fragment into an altered, non-planar conformation, thus weakening its interaction with the enzyme. This altered conformation may also be considered as the cause for its strikingly lower lipophilicity (tab. 5.1). The introduction of a methyl substituent would normally result in an increase in overall lipophilicity and thus a higher logD value. It is conceivable that the steric demand of the methyl function forced a disruption of the intramolecular hydrogen bond and thus improved its solubility in aqueous environment.

With IC_{50} values of 25 and 17 nM, carbamate **30** and ureide **31a** both are highly potent inhibitors of hDHODH. Apparently, an extension of the rigid core fragment by a heteroatom was well tolerated in the binding pocket. In particular, the probably introduced hydrogen bond donor of derivative **31a** seems to have positively affected binding affinity. This may have been caused by an additionally formed hydrogen bond

to the water molecule, which was co-crystallised in the X-ray structure of KP-CF39 (see fig. 5.11) above its amide bond.

The urea function moreover decreased the compound's lipophilicity to a logD value of 2.05. This reduced lipophilicity led to a worsened membrane penetration of $5.85 \cdot 10^{-6}$ cm/s which is considered as moderate value. For carbamate **30** no significant change was found regarding both lipophilicity and permeability, compared to lead compound **22**.

Consequently, due to the strong loss in hDHODH inhibition potency, the approach of introducing a 3-methyl modification for sterical protection was discarded at this point. Compound **31a** with ureido modification was selected as novel lead structure for the following optimisation cycle, because of its fully stabilised amide bond and its highest hDHODH inhibition potency among the three designs of cycle 1. At this point, permeability was assigned a lower importance.

5.3.2 Optimisation cycle 2: Modification of the *sec*-butyl moiety

Starting from novel lead structure **31a**, the aim for optimisation cycle 2 was to prevent its metabolic hydroxylation. For this purpose, the *sec*-butyl substituent at the phenoxy ring was modified, which was assumed to act as site of hydroxylation (see chapter 5.1) and moreover bears a stereogenic center. The investigation of chiral drug candidates in preclinical and clinical studies is significantly more elaborate than that of non-chiral compounds, since all enantiomers must be investigated comprehensively, both individually and as racemic mixtures. Therefore, stereogenic centers should be avoided in drug candidate structures, as far as they are not essential for their efficacy.

In previous efforts of K. PFAFF *et al.*[125], modifications at the 2-position of the phenoxy scaffold in the original, amide-based lead structure **22** have already been investigated in order to establish structure-activity relationships. PFAFF *et al.*[125] showed that the stereogenic *sec*-butyl group is no essential element for the compound's high potency. Antiviral activities of 2-*tert*-pentyl and 2-cyclohexyl analogues were comparable to those of 2-*sec*-butyl lead compound KP-CF39 **22**.[125]

However, from a pharmacological point of view, both *tert*-pentyl and cyclohexyl are rather unsuitable substituents, due to their strong susceptibility towards metabolic hydroxylation. The structurally related trifluoromethyl or morpholino substituent both appear more appropriate drug structure elements.

For drug design, fluorine substituents are generally considered privileged structural units whose introduction can significantly advance optimising the compound's pharmacodynamic and pharmacokinetic properties.[155] Because of their comparable atomic sizes, fluorine atoms have been frequently used to substitute carbon-bonded hydrogen atoms in the course of drug development.[155] The C-F bond is not only considerably more stable itself towards metabolic reactions, compared to the C-H bond. Moreover, due to their high electronegativity, fluorine substituents withdraw electron density from adjacent structural elements and consequently also impede their CYP-catalysed hydroxylation (see chapter 3.2). Furthermore, a molecule's lipophilicity increases when a fluorine substituent is introduced. This can boost binding affinity, in case of a convenient positioning.[155]

Trifluoromethyl moieties are prominent substitutes for methyl groups in drug design.[155] However, exchanging the entire *sec*-butyl or *tert*-pentyl group against a trifluoromethyl substituent will probably result in a reduced lipophilic surface area of the molecule, which may have a negative effect on binding affinity to the enzyme. Nevertheless, compound **31d** emerged as one design of this optimisation cycle, not at least because of its convenient synthetic accessibility.
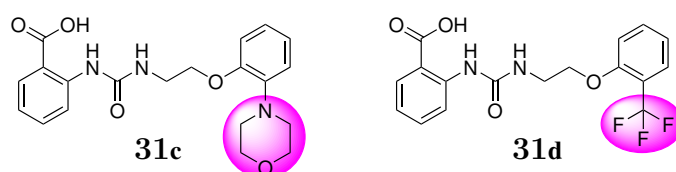
Figure 5.15: Structures of two stabilised designs from optimisation cycle 2. Modified structure elements are highlighted.

As second design, morpholino derivative **31c** was selected. Both designed structures are shown in figure 5.15. Morpholino substituents can be considered as cyclohexyl isosteres with desirable drug-like properties. The morpholino scaffold frequently occurs in drug structures with suitable pharmakokinetic profiles. Its chemical features provide morpholino derivatives with a balanced lipophilicity and thus higher binding selectivites and a lower susceptibility towards metabolic transformation. Moreover they are attributed with a facile synthetic accessibility.[156]

Compared to trifluoromethyl derivative **31d**, morpholino-bearing compound **31c** was assumed to provide a better surface compatibility with the binding pocket, due to its larger spatial demand and its structural similarity to the highly potent 2-cyclohexyl-derivative of KP-CF39 **22**, discovered by PFAFF *et al.*[122,125].

5 Results and discussion

Both synthesised compounds were investigated regarding their metabolic stabilities, hDHODH inhibition potencies, lipophilicities and permeabilities, following the previously described procedures (see chapter 5.1). The results are listed in table 5.2.

Both modifications drastically reduced the compounds' susceptibility towards metabolic transformations. The determined stabilities of about 90 % already have reached the desired range and would enable potential *in vivo* investigations.

Both novel compounds are significantly less lipophilic, compared to their lead compound. Nevertheless, the determined logD values of 0.34 and 1.28 are still in a range that suggests good absorption in the gastrointestinal tract (see chapter 5.1). However, only poor (compound **31d**) to moderate (compound **31c**) membrane permeabilities P_{PAMPA} have been determined.

Table 5.2: Metabolic stabilities (S_{S9}, percentage compound amount remaining within 1 h incubation in rat S9 mix), hDHODH-inhibition (IC_{50}), lipophilicities (logD) and permeabilities (P_{PAMPA}) of the two compounds designed in optimisation cycle 2.

Compound	S_{S9} [%]	IC_{50} [nM] (hDHODH)	logD	P_{PAMPA} [cm/s]
Trifluoromethyl analogue **31d**	89.8 ± 2.5	144 ± 10	1.28 ± 0.02	$(2.15 \pm 0.71) \cdot 10^{-6}$
Morpholino analogue **31c**	86.8 ± 4.2	2031 ± 153	0.34	$(2.50 \pm 0.95) \cdot 10^{-7}$

Regarding hDHODH inhibition potency, the morpholino modification led to a strong deterioriation. This may be related to the decreased lipophilic interaction surface. With an IC_{50} value of about 2 µM, it is still considered a weak inhibitor. Nevertheless, this severe drop in inhibition potency disclosed the morpholino moiety as unsuitable modification of the *sec*-butyl group, here. Compared to lead compound **31a**, the trifluoromethyl modification was also associated with a foreseen but not drastic loss of inhibition potency by factor 8.5 to an IC_{50} value of 144 nM.

Despite its worsening effect on inhibition potency, the strongly stabilising effect revealed the trifluoromethyl moiety as suitable modification, especially under consideration of the limited availability of 2-substituted phenol starting materials. Consequently, fluorinated compound **31d** emerged as novel lead structure of this optimisation cycle.

5.3.3 Optimisation cycle 3: Linker modification

The aim for optimisation cycle 3 was to improve the moderate hDHODH binding affinity of novel lead structure **31d**, while preserving its high metabolic stability. For this purpose, modifications in the flexible linker fragment that connects the ureido function with the phenoxy fragment were investigated in a structure-based, computer-aided drug design approach. Initially, as basis for this, the binding pose of lead structure **31d** was predicted, by virtually docking its energy-minimised structure into a docking grid of hDHODH, using Glide[157]-docking. The docking grid was previously prepared from the cocrystal X-ray structure of hDHODH with bound KP-CF39 **22**.

The Glide docking method generates a variety of rotamers of a query molecule and subsequently fits them into the previously defined binding pocket. Van der Waals distances to the protein are considered in this coarse initial positioning, which is subsequently refined by energy-minimisation of the torsion angles. The resulting docking poses are then ranked in terms of their docking scores. Those scores indicate estimated free binding enthalpy values of the complexes, which have been calculated by summing up individual energy contributions associated with existing specific interactions between protein and ligand. Originally, these energy contributions have been empirically derived from a training data set in which interactions found in X-ray structures are assigned to corresponding binding affinities.[49, 157]
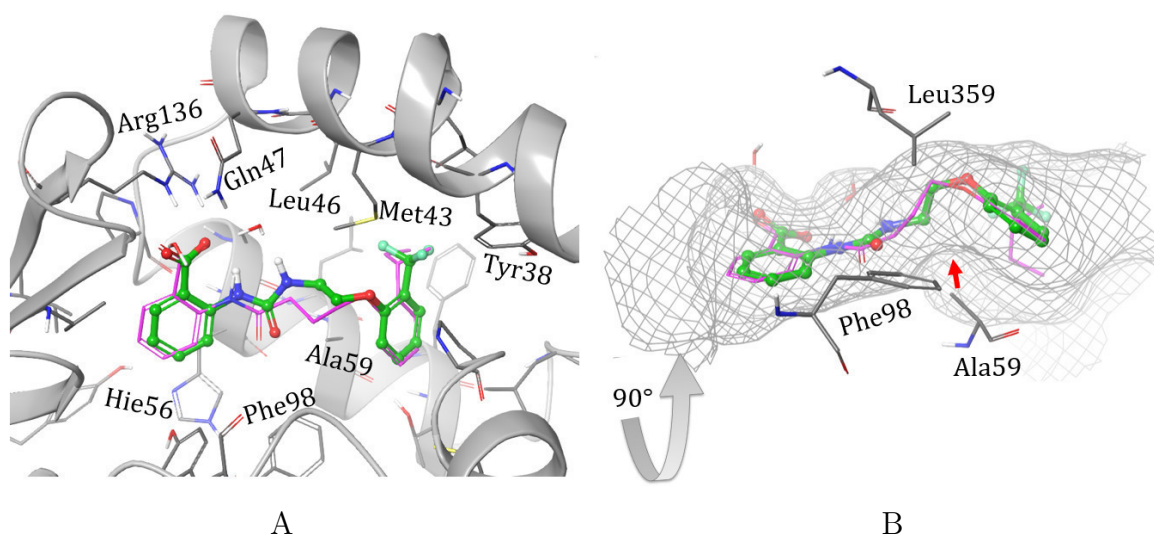
Figure 5.16: Docking pose of lead structure **31d** (green) overlaid to the binding pose of KP-CF39 **22** (pink) in its crystallised binding site of hDHODH, shown from different viewing directions.

5 Results and discussion

In figures 5.16A and B, the docking pose of lead structure **31d** (green) is shown, overlaid to the crystallised pose of KP-CF39 **22** (pink). The two poses are almost congruent. However, due to an additional expected interaction of the newly introduced ureido function with the crystallised water molecule, the arrangements of both linker fragments in the binding pocket slightly differ (see fig. 5.16A). However, the positioning of the phenoxy arene is not affected. This indicates that the binding pocket offers room for modifications in the linker fragment.

Various modifications of the linker fragment were investigated *in silico* by docking the designed, energy-minimised structures into the prepared grid. Structures that appeared promising ligands are shown in figure 5.17 and were selected for synthesis.
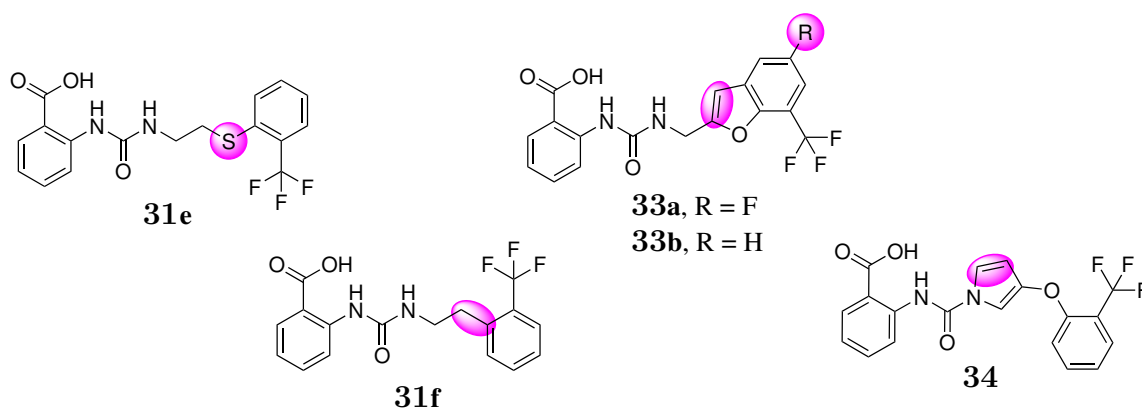
Figure 5.17: Structures of five designs with modified linkers from optimisation cycle 3. Modified structure elements are highlighted.

In structure **31e**, the phenoxy oxygen of the lead structure was isosterically replaced by a sulfur atom. Its highest ranked output docking poses do not differ much from those of phenoxy lead structure **31d**. Nevertheless, the C-S-C-bond lengths are longer and the respective angle smaller. Moreover, the sulfur atom is larger and less polar than the oxygen atom. These measures were expected to result in an increased lipophilic surface area of thioether **31e**, compared to ether **31d**, suggesting a higher binding affinity for the sulfur modification.

Another promising and similar set of docking poses was obtained for structure **31f**, in which the heteroatom was eliminated.

Figure 5.18A shows an overlay of each two highest ranked docking poses of lead structure **31d** (green) and its derivatives **31e** (brown) and **31f** (blue). Whereas the change in arrangement due to heteroatom elimination (structure **31f**) is weak, major

differences can be observed for the oxygen-sulfur-replacement (structure **31e**) regarding the positioning of the aromatic systems.
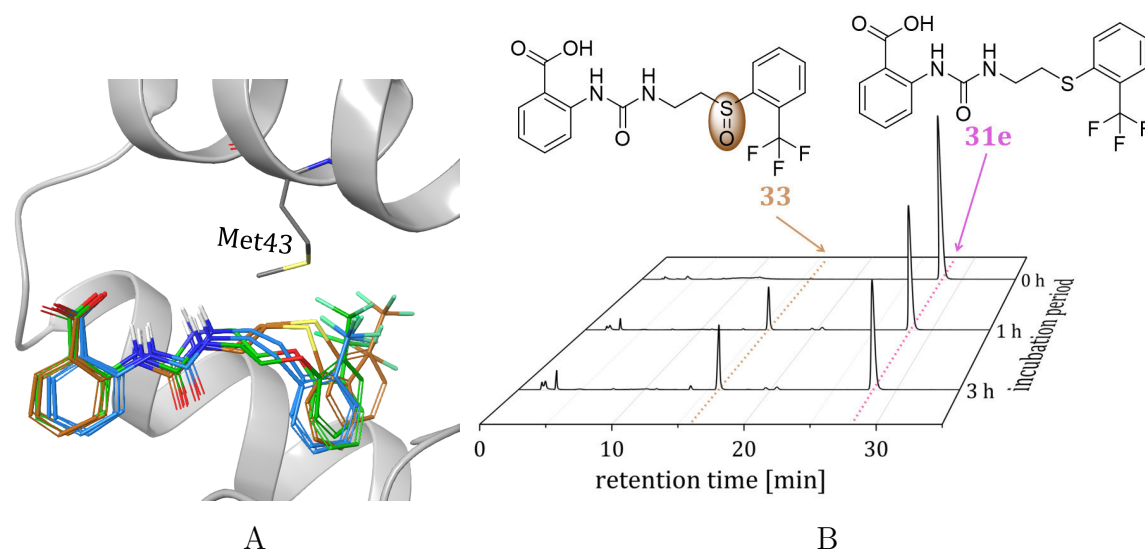
Figure 5.18: A: Docking poses of lead structure **31d** (green) and its derivatives **31e** (brown) and **31f** (blue). For every structure the two highest ranked docking poses are visualised. (For orientation in the binding pocket see fig. 5.16). B: HPLC-chromatograms (FLD, $\lambda_{\text{exc}} = 300$ nm, $\lambda_{\text{em}} = 407$ nm) obtained after a 0 h, 1 h and 3 h incubation of compound **31e** with rat S9 mix. The declared metabolite **35** was identified by LC/MS analysis and subsequent coinjection.

Table 5.3: Metabolic stabilities (S_{S9}, percentage compound amount remaining within 1 h incubation in rat S9 mix), hDHODH-inhibition (IC$_{50}$), lipophilicities (logD) and permeabilities (P_{PAMPA}) of three compounds designed in optimisation cycle 3.

Compound	S_{S9} [%]	IC$_{50}$ [nM] (hDHODH)	logD	P_{PAMPA} [cm/s]
Thiophenoxy analogue **31e**	71.4 ± 2.1	35 ± 2	1.61 ± 0.01	$(2.73 \pm 0.21) \cdot 10^{-6}$
Phenethyl analogue **31f**	96.6 ± 1.5	1168 ± 47	1.36 ± 0.01	$(2.50 \pm 0.46) \cdot 10^{-6}$
Benzofuranyl analogue **33b**	92.0 ± 2.3	91 ± 4	1.96 ± 0.01	$(3.23 \pm 0.23) \cdot 10^{-6}$

The determined pharmacokinetic data of these two novel, synthesised designs are listed in table 5.3. Compared to phenoxy analogue **31d** ($IC_{50} = 144$ nM), the thio modification in compound **31e** resulted in a four-fold increase in inhibition potency to 35 nM whereas a decrease by factor 8 to 1168 nM was observed for compound **31f**. Apparently, the oxygen-sulfur exchange (compound **31e**) achieved the above presumed effects, resulting in an increased binding affinity. The decrease in potency due to elimination of the heteroatom (compound **31f**) may be related to a loss of the ligand's potential interaction with the sulfur atom of the Met43 residue (visualised in fig. 5.18). Contrary to oxygen atoms, carbon-bonded sulfur atoms can interact with electron-donating systems, due to their energetically low $\sigma^{\star}$-orbitals. These interactions are comparable to hydrogen bonds and can be formed with oxygen atoms, sulfur atoms, halogen atoms and aromatic systems.[158] The spatial proximity of the phenoxy heteroatom to Met43 as well as the observed loss of inhibition potency as a result of its elimination indicated relevance of such interaction for highly affine ligands.

The S9 assay revealed compound **31f** to be highly stable with 96.6 %. Metabolite analysis of phenoxy lead compound **31d** showed that one hydroxylation product was still formed, whereas no metabolites were detected for derivative **31f**. Despite the strong electron-withdrawing effect of the trifluoromethyl substituent, the phenoxy-oxygen's +M-effect in lead compound **31d** apparently activated the arene for metabolic hydroxylation.
Contrary to that, the sulfur-modification dropped metabolic stability to 71.4 %. The recorded assay chromatograms are shown in figure 5.18B. The formation of one main metabolite was observed, for which a mass increased by the weight of oxygen was found via LC/MS-analysis. The oxidation to sulfoxides is a prominent metabolic reaction of thioethers[38] (see chapter 3.2). Whereas α-hydroxylation and subsequent cleavage (see chapter 3.2) was neither observed for the investigated phenoxy derivatives, nor for this thiophenoxy derivative **31e**, sulfoxide-formation was here confirmed by coinjection of synthesised sulfoxide **35**. Unfortunately, no inhibitory effect of sulfoxide **35** was observed, even at high concentration of 10 µM.

Nevertheless, all pharmacokinetic data, including the moderate PAMPA-permeability of $2.73 \cdot 10^{-6}$ cm/s, as well as the strong hDHODH inhibition potency of $IC_{50} = 35$ nM indicate strong potential of sulfur-bearing ligand **31e**.

Another approach which was applied in this optimisation cycle, intending to improve binding affinity by modifying the linker fragment, was its rigidisation. However, the design of rigid ligands is challenging, as their shape needs to perfectly match the binding site shape to enable binding. Moreover, a more detailed investigation of the binding pocket has revealed a kink which can be seen in figure 5.16B (red arrow), which shows the binding site from below. Adapting rigid linker fragments to this sharp bend proved to be a highly challenging drug design task. Many different modifications were tried *in silico* but only two of them appeared promising. Their structures **33b** and **34** are shown in figure 5.17 and their docking poses in figures 5.19A and B.
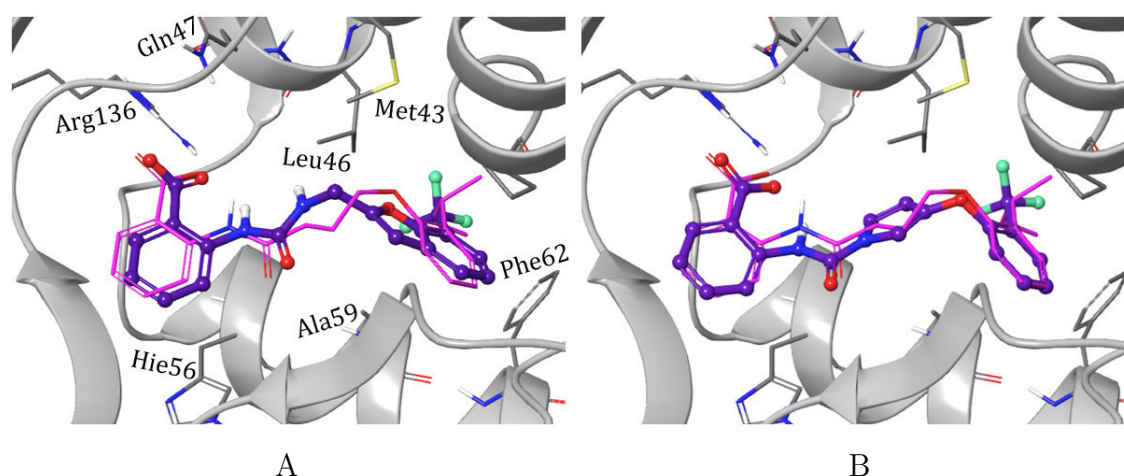
Figure 5.19: Docking poses of A: benzofuranyl-bearing structure **33b** (violet) and B: pyrrole-bearing structure **34** (violet), both overlaid to the binding pose of KP-CF39 **22** (pink, thin tubes) in its crystallised binding site of hDHODH.

In benzofuranyl derivative **33b** (fig. 5.19A), the positioning of both arenes slightly differs from that of the crystallised ligand, whereas they are almost congruent for pyrrole derivative **34** (fig. 5.19B). Nevertheless, both docking poses were regarded highly promising.

The discussion for pyrrole derivative **34** will be continued in chapter 5.4. Here, only investigations of the benzofuranyl modification are discussed. The synthesis of this design **33b** was initially facilitated by introducing a fluorine substituent in *meta* position to the trifluoromethyl substituent (compound **33a**), but was later successfully carried out even in its absence.

Synthesised benzofuranyl derivatives **33a** and **33b** were investigated regarding their hDHODH inhibition potencies. With IC_{50} = 91 nM, benzofuranyl derivative **33b** is slightly more potent than its lead structure **31d** (144 nM). This confirms the introduction of a benzofuranyl scaffold as successful rigidising modification of the linker

fragment. However, this potency increase may also be related to the additional carbon atom in the structure and the associated increase in lipophilicity.

Fluorine substitution (structure **33a**) decreased inhibition potency to an IC_{50} value of about 230 nM. For this reason, the pharmacokinetic properties of protonated derivative **33b** were investigated, only. The results are also listed in table 5.3. Besides its very high metabolic stability of 92 %, a slight improvement of PAMPA permeability, probably due to the related incease in lipophilicity, was found which, however, still was moderate.

The high potency of the original, *sec*-butyl substituted ligands (compounds **22** and **31a**) could not be reproduced with the trifluoromethyl modification. Therefore, in the following, it was investigated whether the benzofuranyl scaffold also provides stabilising effects in presence of aliphatic substituents. But instead of introducing a *sec*-butyl substituent, the non-chiral *tert*-amyl moiety with an additional methyl group was chosen as substituent, resulting in structure **33c**. Furthermore, the analogous phenoxy compound **31b** was synthesised and investigated, in order to enable a separate examination of effects which are solely attributed to the additionally introduced methyl group of the *tert*-amyl substituent. Both structures are shown in figure 5.20.
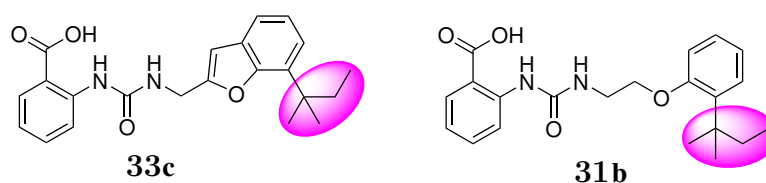
Figure 5.20: Structures of two designs with *tert*-amyl substituent from optimisation cycle 3.

The results of their pharmacological investigation are listed in table 5.4. Modifying the *sec*-butyl (compound **31a** table 5.1) to a *tert*-amyl substituent (compound **31b**) resulted in a halved hDHODH inhibition potency to an IC_{50} value of 33 nM. Moreover, the introduction of the additional methyl group increased lipophilicity from logD = 2.05 to 2.55 and led to a marginal metabolic destabilisation (48.9 to 45.7 %). At the same time, PAMPA permeability was not affected.

Considering the crucial, aforementioned advantages of removing the chiral centre, the *tert*-amyl moiety proved to be a suitable modification of the *sec*-butyl substituent, in total.

Table 5.4: Metabolic stabilities (S_{S9}, percentage compound amount remaining within 1 h incubation in rat S9 mix), hDHODH-inhibition (IC_{50}), lipophilicities (logD) and permeabilities (P_{PAMPA}) of two further compounds from optimisation cycle 3.

Compound	S_{S9} [%]	IC_{50} [nM] (hDHODH)	logD	P_{PAMPA} [cm/s]
2-*tert*-amyl phenoxy analogue **31b**	45.7 ± 1.6	33 ± 4	2.55	$(5.93 \pm 0.32) \cdot 10^{-6}$
5-*tert*-amyl-benzofuranyl analogue **33c**	68.2 ± 1.5	9.2 ± 2.5	2.98	$(5.75 \pm 0.15) \cdot 10^{-6}$

The benzofuranyl modification (compound **33c**) led to a strong increase in metabolic stability to 68.2 %. In figure 5.21, the respective assay chromatograms of both compounds are shown. Massspectrometric analysis revealed four hydroxylated metabolites for both compounds. However, hydroxylation seemed to proceed slower for benzofuranyl derivative **33c**, indicated by the smaller integrals of the metabolites' peaks and the slower decrease of the molecule peak.
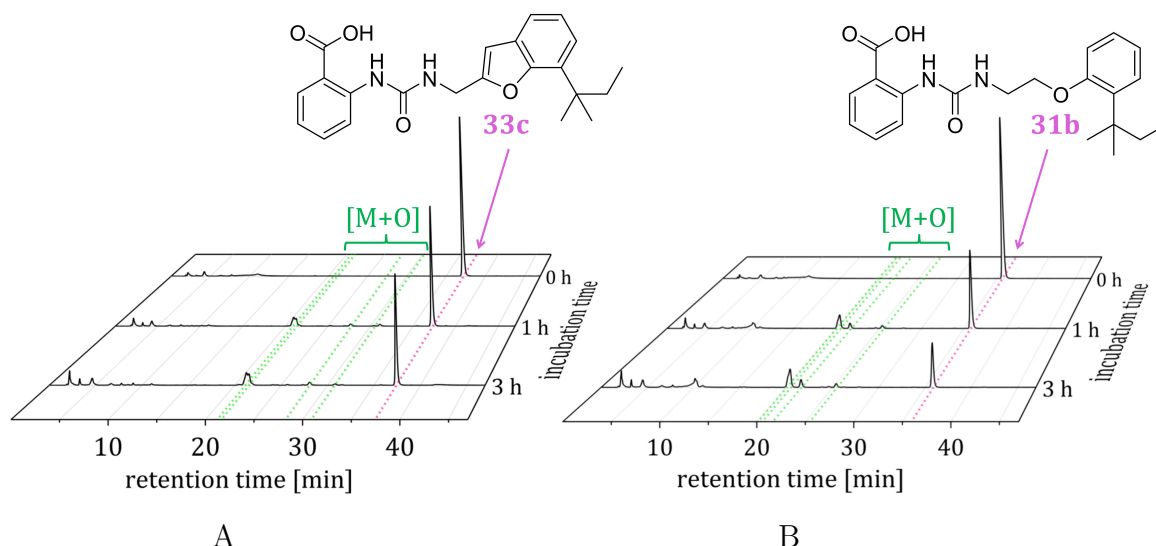
Figure 5.21: HPLC-chromatograms (FLD, $\lambda_{exc} = 300$ nm, $\lambda_{em} = 407$ nm) obtained after a 0 h, 1 h and 3 h incubation of compounds **33c** and **31b** with rat S9 mix.

Surprisingly, the addition of reagents that induce Phase II-metabolism (glutathione and UDP glucuronic acid), carried out in a seperate experiment, resulted in a similar metabolites-profile and equal values for the stability of compound **33c**. Thus, phase II metabolism (glucuronidation) was assumed not to be relevant for this compound. As a reference, the phase II metabolism of fluorescent, literature-investigated 7-hydroxy-coumarin was investigated and its stability was determined to $S_{S9} = 4.9$ % under the formation of one main metabolite which was assumed to be its glucuronate.

Moreover, the benzofuranyl modification resulted in a highly potent hDHODH inhibitor with an IC_{50} value of 9.2 nM. This strong potency has reached the value of initial inhibitor KP-CF39 **22** for the first time. The recorded IC_{50} curve is shown in figure 5.22A. Its concentration range is narrow, so that 90 % inhibition is already achieved at an inhibitor concentration below 50 nM.
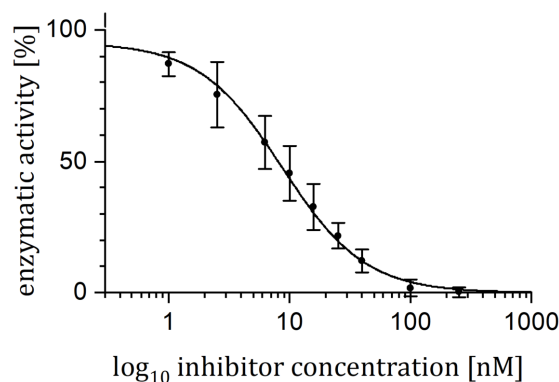
Figure 5.22: Investigation of hDHODH inhibition (IC_{50} curve) for optimised inhibitor **33c**.

The benzofuranyl modification showed no significant effect on PAMPA-permeability, which is still in the moderate range. However, compared to the analogous trifluoromethyl compound **33b**, an improvement can be noticed.

Overall, compound **33c** emerged from the whole structure optimisation procedure as best drug candidate with highly satisfying pharmacological properties.

5.3.4 Antiviral and immunosuppressive potencies *in vitro*

A selection of the developed inhibitors was tested in cell-based assays for their antiviral and immunosuppressive activities, particularly focusing on the best candidates **31e** and **33c**. The compounds' inhibitory effects on T-lymphocyte proliferation (CD4- and CD8-cells) were investigated by A. LEHMANN and F. HAAG at University Medical Center

Hamburg-Eppendorf. Antiviral assays were performed by L. OESTEREICH *et al.* at Bernhard Nocht Institute for Tropical Medicine in Hamburg (Crim Congo Hemorrhagic Fever Virus (CCHFV), Ebola Virus (EBOV) and Lassa Virus (LASV) in Vero cells) and by J. NEYTS, S. KAPTEIN and C. COLLARD at Rega Institute in Leuven (Yellow Fever Virus (YFV) in Huh-7 cells). All results are listed in table 5.5.

Table 5.5: Immunosuppression and antiviral data (EC_{50}) for selected compounds from chapter 5.3. (n. d. = not determined)

Compound	CD4	CD8	YFV (Huh-7)	CCHFV (Vero)	EBOV (Vero)	LASV (Vero)
22	150 nM	160 nM	276 nM	n. d.	2 nM[124]	5 nM[124]
31a	n. d.	n. d.	402 nM	900 nM	135 nM	164 nM
31d	n. d.	n. d.	4.7 µM	n. d.	n. d.	8.1 µM
31e	5.24 µM	5.96 µM	1.23 µM	n. d.	n. d.	2.3 µM
33b	n. d.	n. d.	1.28 µM	n. d.	n. d.	1.0 µM
33c	312 nM	415 nM	75.8 nM	100 nM	14 nM	35 nM

Three of the compounds were tested in CD4- and CD8-T-lymphocytes and all of them showed anti-proliferative effects. For benzofuranyl derivative **33c** this effect was weaker than for initial lead compound KP-CF39 **22** but nevertheless, the determined EC_{50} value is in nanomolar range.

Within the antiviral data, the high broad-range potency of novel benzofuranyl derivative **33c** is remarkable. Especially EBOV and LASV replication were strongly inhibited by this compound with low EC_{50} values of 14 and 35 nM, respectively. When comparing these with the even higher potencies of KP-CF39 **22** it must be considered that different cell batches were used for the respective investigations of the initial lead compound. However, the lower membrane permeability of benzofuranyl derivative **33c** compared to KP-CF39 **22** may also be plausible explanation for this difference.

The other compounds' lower activities are in line with their higher IC_{50} values determined in the isolated enzyme. Somewhat disappointing was thioether **31e**, which strongly inhibited activity of the isolated hDHODH (IC_{50} = 35 nM) but showed only micromolar EC_{50} values. This striking observation may be explained by its comparably low lipophilicity. The lipophilicity is indeed an important measure for hDHODH inhibitors to achieve high enzymatic binding affinity, but is even more crucial in cell-based assays. Intracellularly, the enzyme is bound to the mitochondrial membrane (see chapter 3.3.1) and thus, binding of the ligand can only proceed after membrane

intercalation. Consequently, a low lipophilicity of the ligand impedes its entry into the binding site.

Regarding cell toxicity, the addition of some compounds significantly reduced cell viability even at low micromolar concentrations. Compound concentrations that halved cell viability (CC_{50} values) are listed in table 5.6.

Table 5.6: Toxicity data (CC_{50} [µM]) for compounds from tab. 5.5.

Cell line	22	31a	31d	31e	33b	33c
Huh-7	61.7	>100	>100	>100	>100	69.7
Vero	19[124]	>1	15.6	4.4	>4	>1

For a suitable safety profile, a drug's CC_{50} value should exceed the EC_{50} value by factor 10.[159] This therapeutic window is not maintained for the LASV activities of compounds **31d**, **31e** and **33b** in Vero cells, whereas all other compounds meet the criteria. The cytotoxic effect of all compounds in Huh-7 cells was determined to be comparably low.

5.3.5 Pharmacological investigation of CF278 *in vivo*

Because of its highly promising pharmacodynamic and pharmacokinetic *in vitro* properties, drug candidate **33c**, from now on referred to as CF278, was further investigated for its pharmacological behaviour *in vivo*. These experiments were performed by K. Rox at the Helmholtz Centre for Infection Research in Braunschweig.

In order to complement the *in vitro* ADME profile of CF278 **33c**, its stability and plasma protein binding (PPB) were determined in two species (human and mice), first. The compound proved to be highly stable in plasma, with long half-lives of 914 min (mouse) and 555 min (human) and exhibited high PPB of 98.52 % (mouse) and 99.87 %. As discussed for initial lead compound KP-CF39 **22**, these high percentages are probably associated with the compound's high lipophilicity and may certainly benefit the compound's *in vivo* behaviour, due to the above mentioned positive effects on metabolism and excretion (see chapter 5.1).

In addition, the compound was tested for potential cytotoxic effects in HepG2, CHO and A549 cell lines. No significant influence on cell viability was observed for concentrations of up to 100 µg/mL.

All in all, the overall pharmacologic *in vitro* properties appeared suitable for *in vivo* experiments.
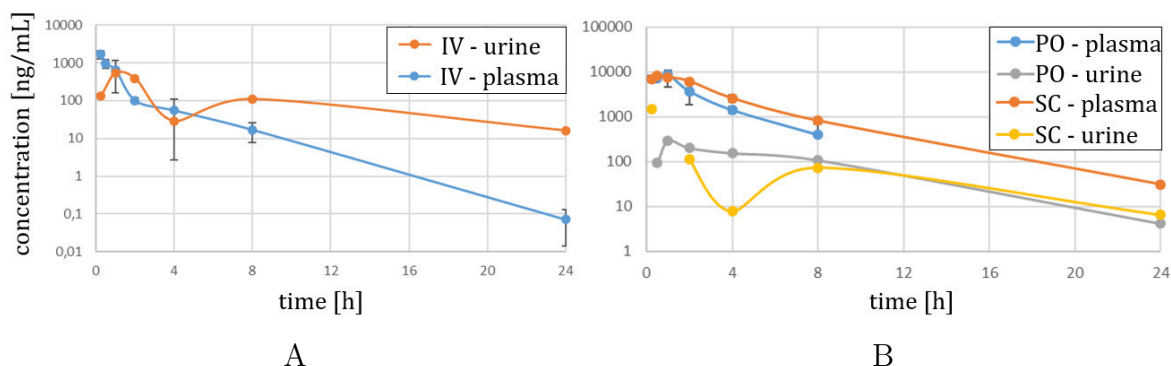
Figure 5.23: Concentrations of CF278 **33c** detected in plasma and urine after its A: intravenous (IV) and B: peroral (PO) or subcutaneous (SC) administration to three mice, each. The graphs were kindly provided by K. Rox.

In order to investigate the pharmacology of CF278 **33c** *in vivo*, the compound was administered to mice (male, CD-1), using different application routes.

Starting with an intravenous administration route, a low dose of 5 mg/kg of CF278 **33c** was injected into the veins of three mice, each. Subsequently, the compound concentration in blood plasma and excreted urine was quantified at different time points for 24 h. The plotted data are shown in figure 5.23A. Moreover, table 5.7 lists several pharmacokinetic parameters that were obtained from these graphs or calculated on their basis.

High initial plasma levels c_0 of 2452 ng/mL were detected. The volume of distribution V_D of 2.05 l/kg suggests a good compound distribution, also to tissues and organs. Regarding excretion of the compound, a two-phase elimination kinetic was observed: A quick initial elimination rate was followed by slower excretion after four hours. A possible explanation for this may be that the enzymes that were involved in the compound's excretion became saturated after this period of time. A half-life of slightly less than half an hour was calculated for the first phase of elimination. This moderate half-life is associated with correspondingly moderate values for the mean residence time *MRT* of one molecule in the organism, the area under the (plasma concentration) curve $AUC_{0\text{-}t}$ and a moderate clearance *Cl*. However, the concentration courses indicate that the molecule was excreted in its unmetabolised form only.

Table 5.7: Pharmacokinetic data obtained from the *in vivo* experiment with CF278 **33c**. The listed values were determined by K. Rox.

Administration route	intravenous	peroral	subcutaneous
c_{adm} [mg/kg]	5	30	30
c_0 or c_{max} [ng/mL]	2452 ± 221	8928 ± 778	8806 ± 1105
V_D or V_D/F[l/kg]	2.05 ± 0.2	3.91 ± 1.9	3.94 ± 1.0
$t_{1/2}$ [h]	0.46 ± 0.2	2.10 ± 1.3	3.21 ± 0.2
MRT [h]	0.66 ± 0.3	2.77 ± 1.3	3.70 ± 0.3
AUC_{0-t} [ng/mL·h]	1632 ± 736	20756 ± 2487	36113 ± 6076
Cl/F [mL/min/kg]	57.26 ± 20.7	22.73 ± 4.2	14.06 ± 2.4

Additionally, a peroral and a subcutaneous application route were both examined in three mice, each. Via these routes, the administration of higher concentrations (30 mg/kg) was possible and, moreover, longer half-lives were expected, due to a retarded compound absorption in the respective entry organ. Figure 5.23B shows the recorded concentration curves.

Again, no dose linearity was observed, probably due to the above mentioned reasons. However, the suggested depot-effect was actually observed for both routes, resulting in lower relative urine concentrations and extended half-lives of 2.10 and 3.21 h (see tab. 5.7). At the same time, high initial plasma concentrations were achieved for both routes.

As represented by all these results, both administration routes proved suitable for future *in vivo* efficacy studies. Furthermore, no toxic effects were observed.

Remarkably, a high peroral bioavailability F of more than 100 % was calculated. High bioavailabilities indicate poor biotransformation of the compound during the first liver passage and thus high compound concentrations that are available for being distributed in the organism. Moreover, a good bioavailability critically facilitates future drug formulation development. However, in this case, it is also attributed to the fact that CF278 did not exhibit dose linearity. Thus, overall, very good absorption and dissolution of the compound were indicated, in line with a possible saturation of metabolic and elimination pathways.

Even though highly potent and pharmacologically suitable drug candidate **33c** has been synthesised in a quantity of 250 mg, which will be sufficient for initial *in vivo*-efficacy experiments, its synthetic access proved to be elaborate (see chapter 5.3.6). For this reason, it was investigated whether hDHODH inhibition potency may be preserved when modifying the ureido function to a carbamate moiety (figure 5.24), as the synthetic access to carbamate **36** has been considerably less laborious (see chapter 5.3.6).

This modification only slightly reduced the compound's inhibition potency to an IC_{50} value of 13 $\pm$ 1 nM. Consequently, carbamate derivative **36** also proved to be a highly potent inhibitor of hDHODH, whose further pharmacologic properties have not yet been investigated. Based on the pharmacokinetic properties of carbamate **30**, a lower metabolic stability but higher membrane permeability is expected, compared to ureide **33c**.
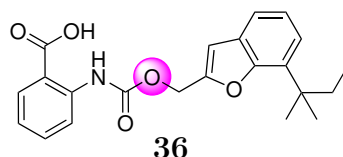
Figure 5.24: Structure of carbamate derivative **36**.

5.3.6 Synthesis

The 3-methyl analogue **29** of KP-CF39 **22** was synthesised according to the standard procedure[122,125] that has been established in our research group and has already been discussed in detail in the literature. As shown in figure 5.25, *sec*-butylphenol **37a** was coupled to the butyryl linker, using bromobutanoate **38** in the first step. After saponification of formed ethyl ester **24**, the carboxyl moiety of compound **39** was coupled to the modified methylanthranilate building block **40** via an acid chloride-activated amide synthesis approach. A final saponification of the obtained methyl ester **41** afforded inhibitor **29** in an overall yield of 38 % in 4 steps. The yields of the first two synthesis steps agree with those reported for compound **39**.[122] The following coupling with methyl-modified amine **40** and saponification both were achieved in a moderate yield of 65 % which is also in agreement with yields reported for analogous reactions with methyl anthranilate.[124,125]
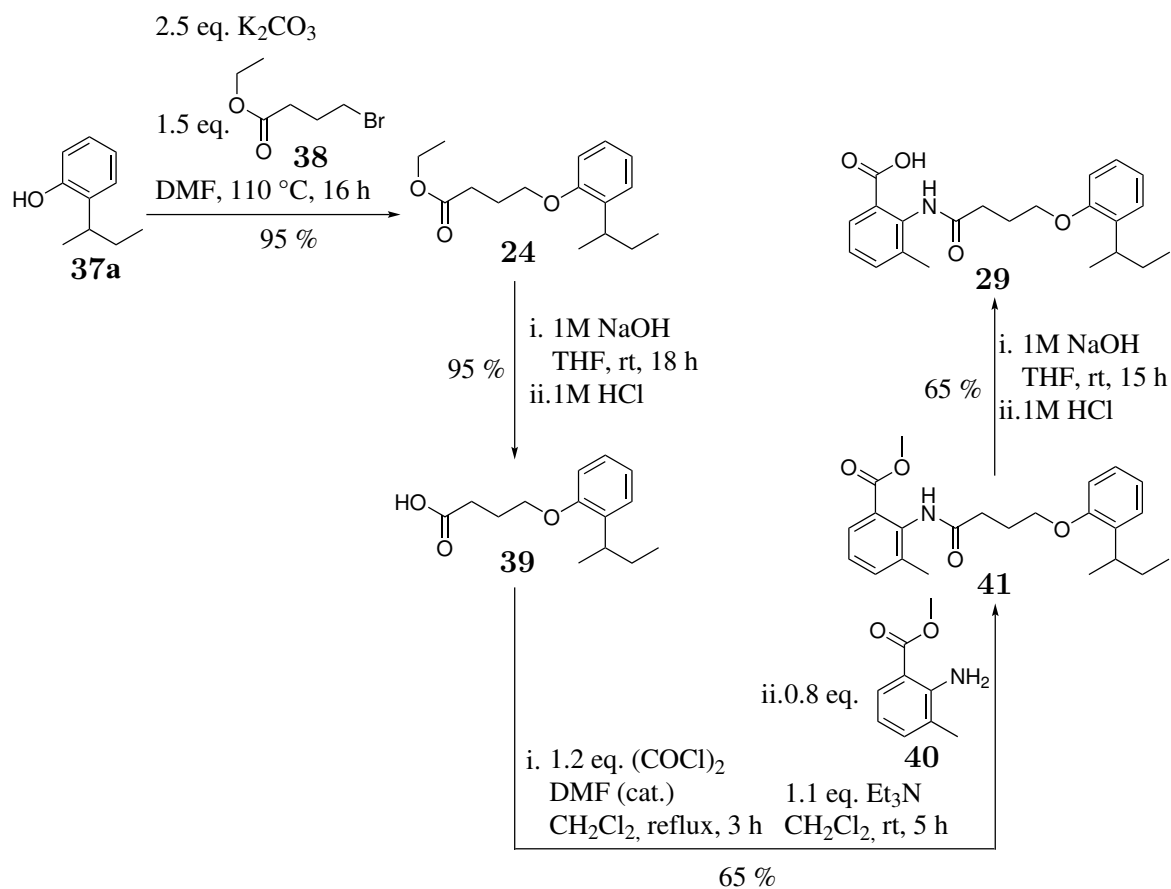
Figure 5.25: Procedure, conditions and yields for the synthesis of 2-amido-3-methylbenzoic acid derivative **29**.

All carbamates and ureides that have been discussed in this chapter can be assigned to one of the two general structures shown in figure 5.26. The development of their synthesis routes started with defining retrosynthetic cuts which are also shown in the figure.
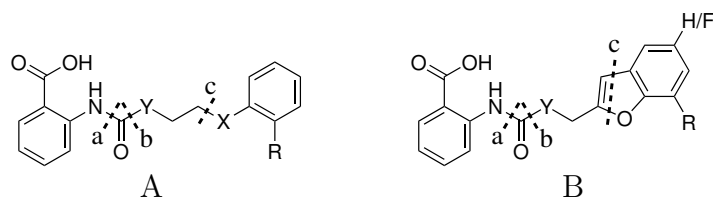
Figure 5.26: Retrosynthesis cuts for target compounds with A: phenoxy and B: benzofuranyl scaffold.

Both structures consist of four building blocks: Anthranilic acid, a carbonyl group, a linker and a phenol derivative. In order to enable a simple and fast access to the invidual derivatives, it would have been most appropriate to introduce the various substituted phenols (cut c) as last building block to the structures. However, this synthesis approach

was not considered promising for phenolic derivatives (see fig. 5.26A), as the respective ureido- or carbamate-containing precursor structures were intended to cyclise to the respective oxoimidazolidines or oxooxazolidines.[125] For derivatives with benzofurane structure (see fig. 5.26B), this synthesis route proved unsuccessful, either, as will be discussed later.

Alternative synthesis routes with an altered step order are shown in figure 5.27. A protecting group (PG) was intended to prevent side reactions that may have occurred at the carboxylic acid moiety of the anthranilate fragment during coupling reactions. Therefore, the final synthesis step for all ureides (**31a-e**, **33a-c**) as well as carbamates (**30**, **36**) was the removal of this protecting group. Both protected precursor structures were derived from three coupling elements which are connected by bonds a and b. The protected anthranilate as well as the carbonylation reagent were commercially available, whereas amines **42a-e** or **43a-c** or alcohols **44a-e** or **45a-c** needed to be synthesised before. The amines were intended to be obtained from the respective alcohols, which were retrosynthetically derived from a coupling (cut c) of phenols **37a-f** or their iodination products **46a-c** with the respective linker.
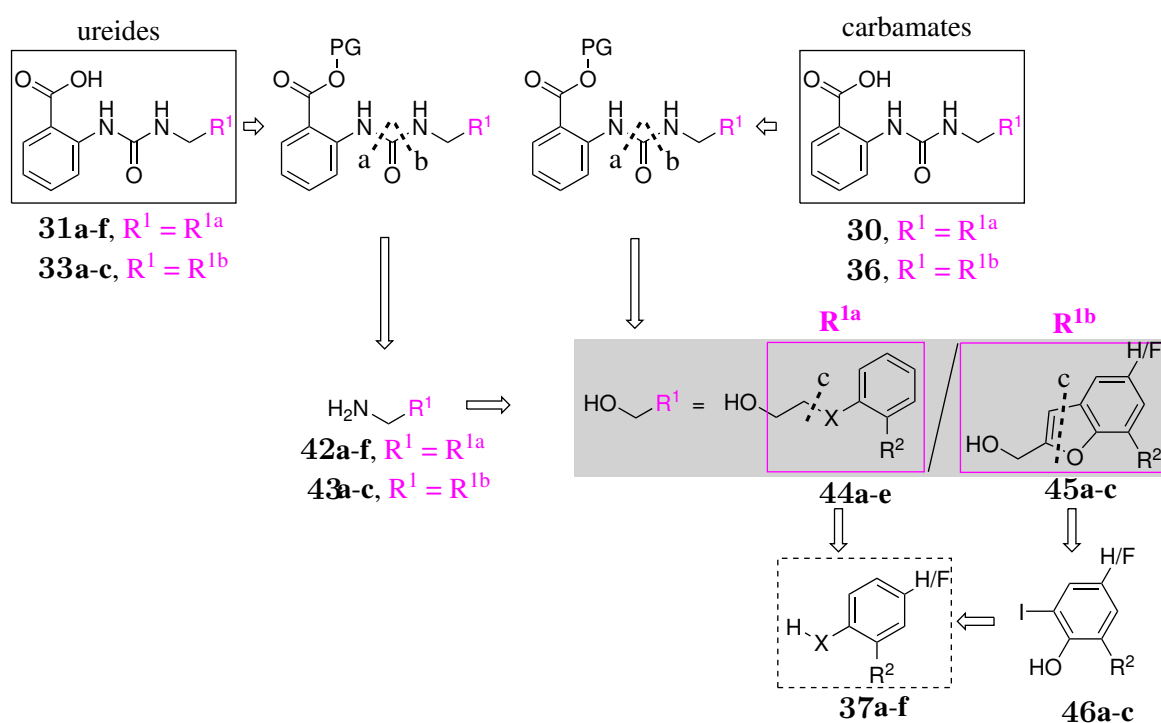
Figure 5.27: Retrosynthesis scheme for ureides **31a-e** and **33a-c** as well as carbamates **30** and **36**.

The development of a suitable synthesis route was significantly supported by

L. GERBER as part of her bachelor thesis [P6].[160]

Syntheses of alcohols 44a-e and 45a-c

i. 2.5 eq. K$_2$CO$_3$
   DMF, rt, 15 min

ii. 2.5 eq. HO⏜Br
   47

TBAI (cat.)
DMF, 110 °C, 24 h

37a-e → **44a-e**
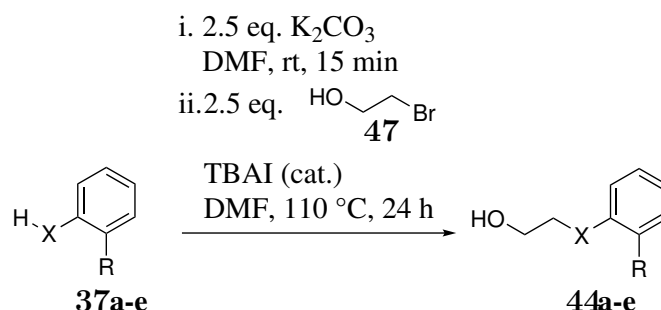
Figure 5.28: Conditions for the syntheses of alcohols **44a-e**.

Table 5.8: Yields obtained for the syntheses of 2-phenoxyethanol derivatives **44a-d** and 2-thiophenoxyethanol derivative **44e** (fig. 5.28).

X	R	Starting material	Yield	Product
O		**37a**	98 %	**44a**
O		**37b**	52 %	**44b**
O		**37c**	quant.	**44c**
O		**37d**	80 %	**44d**
S		**37e**	90 %	**44e**

Alcohols **44a-e** were obtained under the reaction conditions shown in figure 5.28. Initially, the corresponding phenol **37a-d** or thiophenol **37e** was dissolved in *N,N*-dimethylformamide (DMF) and deprotonated with potassium carbonate. Subsequently, after adding 2-bromoethanol **47** in excess and tetrabutylammonium iodide (TBAI) in a catalytical amount, the mixtures were stirred at 110 °C for 24 h. Conversion of the starting materials was followed by thin-layer chromatography. Aqueous workup and chromatographic purification gave alcohols **44a-e** in yields that are listed in table 5.8.

The given yields reflect the completeness of phenol conversion and differ due to adjustments in the synthesis procedure: It was observed that the phenol derivative was completely converted, in case that bromoethanol **47** had been slowly added to the reaction mixture after a reaction temperature of 110 °C had been reached. This procedure was followed for the syntheses of compounds **44a,c** and **e** and resulted in very good to quantitative yields. In contrast, adding bromoethanol **47** before heating led to lower yields for compounds **44b** and **d**, attributed to incomplete phenol conversions. A possible explanation for this observation may be that bromoethanol molecules reacted with each other in intermolecular nucleophilic substitution reactions at high temperatures. These side reactions seem to have occurred, when an excess of bromoethanol **47** was present in the heating mixture, wheras the reagent was apparently able to react successively with the deprotonated phenol component in a S_N2 reaction, when being slowly added at high temperatures. The catalyst TBAI was added to convert the bromide in reagent **47** to a more reactive iodide.

The syntheses of benzofurane-bearing alcohols **45a-c** started with an *ortho*-iodination of the corresponding phenolic starting materials (see fig. 5.27).

Due to their +M-effect, OH-substituents direct electrophilic aromatic substitution reactions to their *ortho* and *para* positions, whereas electron-withdrawing fluorine-substituents favour *meta* substitution. Accordingly, compound **37f** was iodinated selectively in the only favoured protonated position in a good yield of 73 % using the reaction conditions shown in figure 5.29, followed by workup and purification.

Moreover, the figure shows a couple of approaches that aimed the *ortho*-iodination of disubstituted trifluoromethylphenol **37d**. Its reaction with iodine monochloride under identical conditions lead to the formation of three products. Besides *ortho*- and *para*-substituted iodines **46b** and **48**, double-iodinated compound **49** was isolated as main product. Its percentage molar amount in the crude product mixture was determined to 76 %. Apparently, the -I-effect of the firstly introduced iodine substituent favoured a second electrophilic attack of the arene. Only 4 % of the mixture were identified as desired product **46b**. The reaction was repeated, using 0.6 equivalents of iodine monochloride in order to prevent double iodination, but the yield of *ortho*-product **46b** could not be significantly improved.
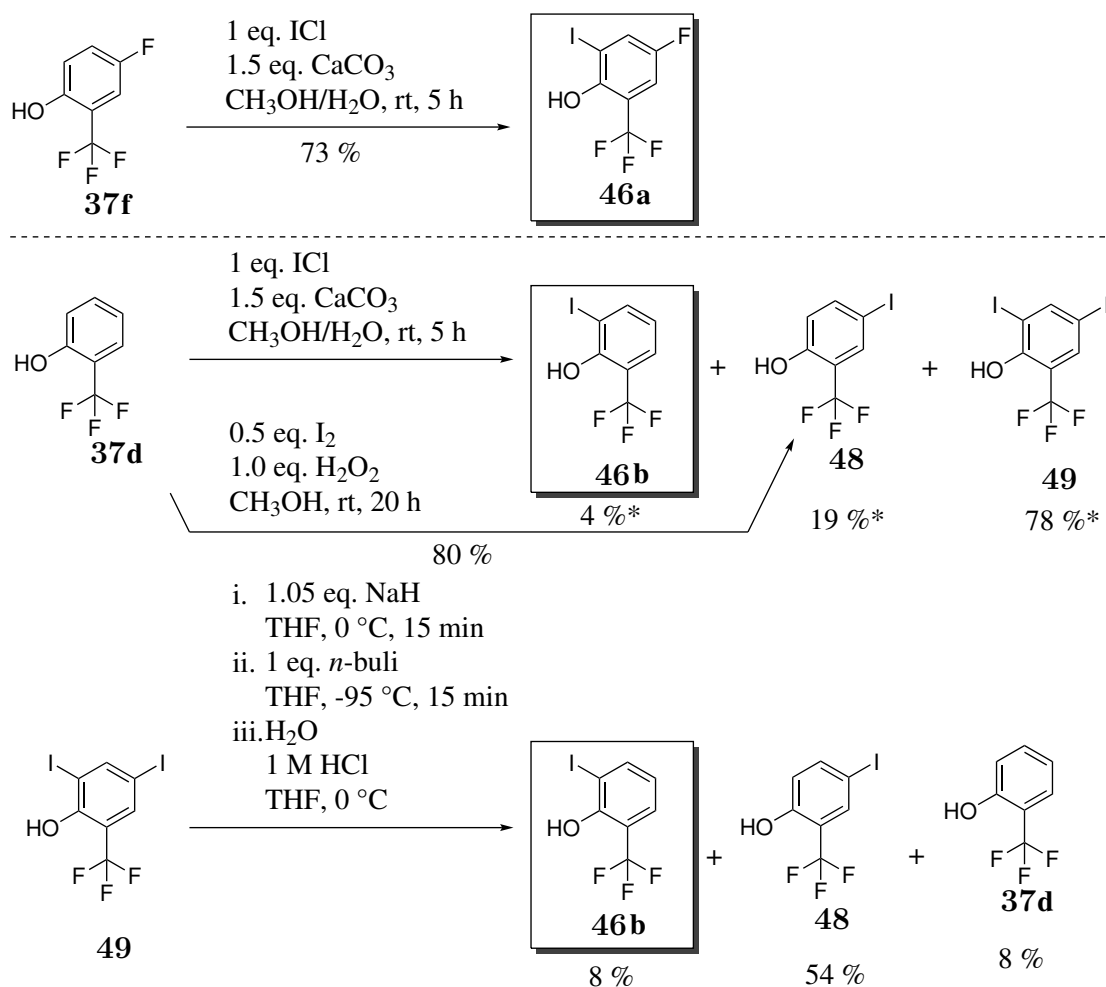
Figure 5.29: Conditions for the successful synthesis of iodophenol derivative **46a** and unsuccessful attempts for the regioselective *ortho*-iodination of phenol derivative **37d** (*: percentage amount in the crude product mixture).

Since this method did not yield desired product **46b** in sufficient quantity, a method for the selective synthesis of *ortho*-iodinated phenols was searched in the literature. GALLO *et al.*[161] promised a regioselective *ortho*-iodination of phenols when using hypoiodous acid as reagent, prepared *in situ* by adding iodine and hydrogen peroxide. The regioselectivity of this reaction was explained by an interaction of hypoiodous acid with the aromatic hydroxy group, resulting in iodination of the adjacent position, only.[162] However, instead, the published reaction conditions resulted in a regioselective iodination of the *para*-position of compound **48** in a yield of 80 % (see fig. 5.29).

Another approach was published by HORNE *et al.*[163] who reported a regioselective deiodination of the *para*-position of 2,4-diiodophenols. By converting the diiodophenol to its sodium phenolate using sodium hydride, the steric shielding effect of the sodium ion

was reported to enable a regioselective halogen-lithium exchange at the *para*-position. Lithiation was followed by acidic workup, to afford *para*-deioninated phenol **46d**.[163] However, contrary to that, a favoured deiodination of the *ortho*-position was observed instead for compound **49**. Apparently, the lithiation reagent even interacted with the aromatic hydroxyl group.
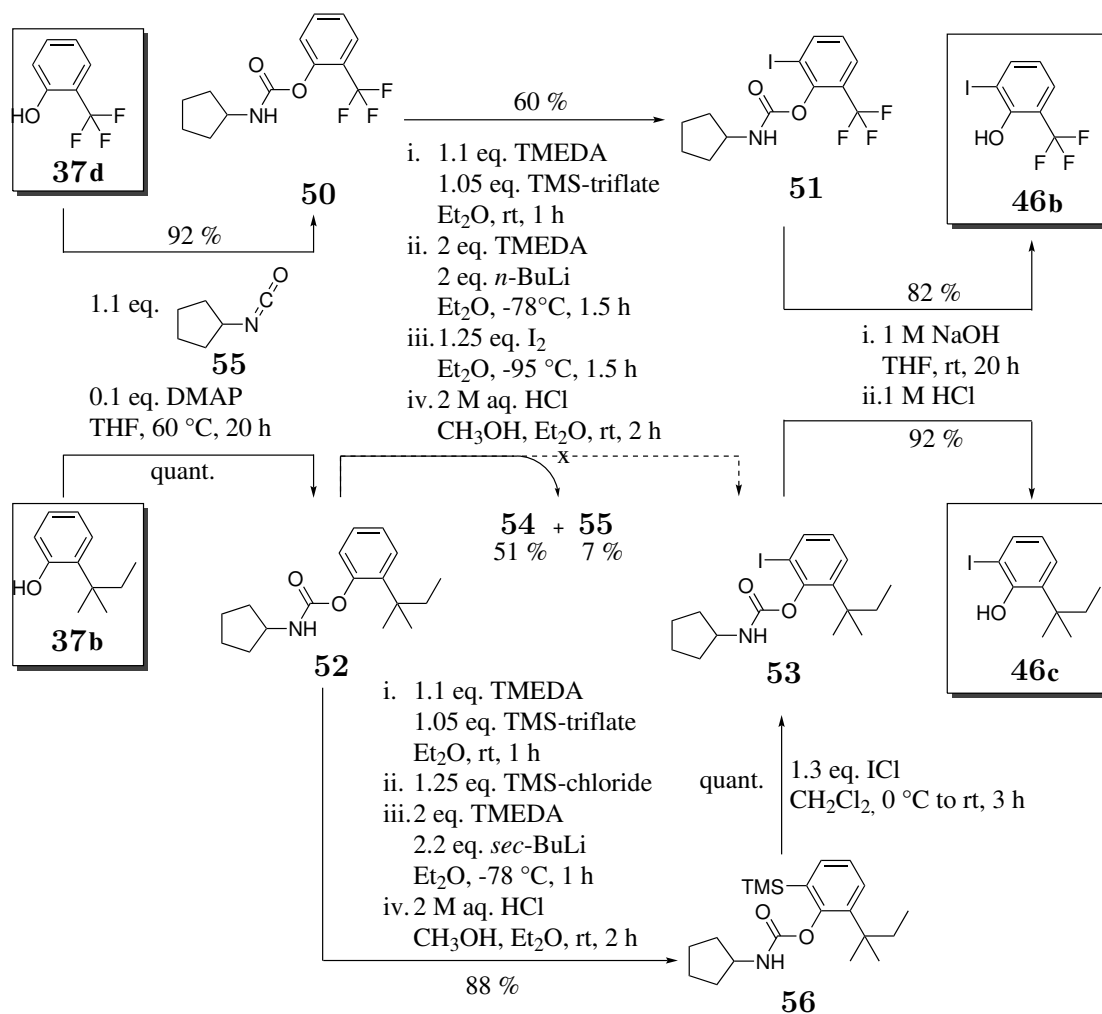
Figure 5.30: Scheme for the successful *ortho*-iodination of phenols **37d** and **b**, adapted from KAUCH *et al.*

KAUCH *et al.*[164, 165] published an *ortho*-selective phenol iodination method that uses the well-known concept of *ortho*-directed lithiation,[166] followed by lithium-halogen exchange. Following the protocol of KAUCH *et al.* (figure 5.30), regioselective *ortho*-iodinations of phenols **37d** and **b** were finally achieved in high yields.

The synthesis procedure started with converting the aromatic hydroxy group to a carbamate function, here using cyclopentyl isocyanate **57** as electrophile. For this purpose,

4-(dimethylamino)pyridine (DMAP) was added in catalytic amounts. Its nucleophilic addition to isocyanate **57** resulted in an increased electrophilicity.[167] Under elimination of DMAP, carbamate **50** was formed. The compound was obtained in a very good yield of 92 % after acidic workup and column-chromatographic purification. Analogously, the corresponding *tert*-amyl-substituted carbamate **52** was obtained in a quantitative yield. The next four steps were performed in one-pot synthesis procedures, as described by KAUCH,[164] and realised a selective iodination of the *ortho*-position of carbamates **50** and **52**. In the first step, the carbamoyl nitrogen atom was protected with a trimethylsilyl (TMS) group, using TMS-triflate. Tetramethylethylenediamine (TMEDA) was used as base and formed a salt with the eliminated triflic acid.[164] Through the addition of *n*-butyllithium (*n*-BuLi) in the second step, the *ortho*-position of the arene was lithiated. In this step, TMEDA was added to act as deaggregation additive, enabling rapid conversion of the lithiation reagent.[168]

The regioselectivity of this reaction step was achieved by an interaction of the lithium atom with the carbonyl oxygen atom of the carbamate substituent. Consequently, solely the adjacent *ortho*-position was deprotonated and consequently bound to the lithium atom. The formed intermediate complex **I** is shown in figure 5.31.[164]
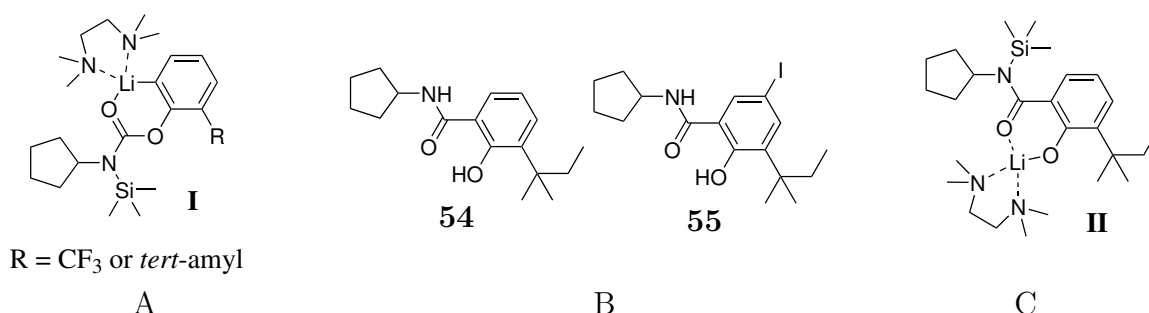
Figure 5.31: Structures of A: intermediate complex **I** formed after lithiation in presence of TMEDA; B: products **54** and **55** (see fig. 5.30); C: intermediate complex **II** formed after Fries-rearrangement.

The introduced lithium substituent activated its aromatic position for an electrophilic aromatic substitution reaction with the subsequently added iodine. By treating the mixture with aqueous hydrochloric acid solution in the last step, the protecting TMS group was eliminated which preserved the carbamate function from being cleaved during previous reaction steps.[164] Final aqueous workup and column-chromatographic purification yielded *ortho*-iodinated, trifluoromethyl-substituted carbamate **51** by 60 %. Compared to the yields that were published for derivatives which bear distinct 2-substituents and a isopropylcarbamate moiety instead,[164] this yield appears rather moderate. This might

be due to the strong electron-withdrawing effect of the trifluoromethyl group, which resulted in a reduced reactivity of the arene.

However, this reaction sequence did not afford the desired product **53**. Instead, compound **54** was obtained in a yield of 51 % as well as traces of its iodinated product **55**, whose structures are shown in figure 5.31B. KAUCH *et al.* later observed an analogous competitive reaction product for a structurally similar compound with 2-*tert*-butyl substituent.[165] Apparently, the electron-donating effect of the alkyl-substituents induced an *ortho*-Fries-rearrangement in the formed intermediate complex I after lithiation (see fig. 5.31). Accordingly, the amido moiety migrated to the adjacent aromatic position, resulting the formation of intermediate complex **II** (figure 5.31C). The formed O-Li bond was intended to be the driving force of this rearrangement.[169] Subsequent addition of iodine resulted in a electrophilic aromatic substitution reaction which proceeded slowly, due to the missing lithium-activation. Final treatment with hydrochloric acid resulted in the formation of products **54** and **55** which both were isolated and identified via NMR- and IR-spectroscopy and mass spectrometry.

In order to prevent this rearrangement, KAUCH *et al.*[165] established a modified synthesis sequence which is also shown in figure 5.30. In deviation from the other procedure, trimethylsilyl (TMS)-chloride was used as electrophile and was added to the reaction mixture prior to treatment with the lithiation reagent. Thus, immediately after having formed, intermediate **I** reacted with TMS-chloride in an electrophilic aromatic substitution reaction (*in situ* quenching effect).[165] Consequently, no Fries arrangement proceeded and TMS derivative **56** was isolated as sole product after acidification, aqueous workup and column-chromatographic purification in a very good yield of 88 %. A subsequent *ipso*-substitution quantitatively yielded the desired iodide **53** through the addition of iodine monochloride.

Both *ortho*-iodinated phenols **46b** and **c** were finally obtained by saponification reactions of their respective carbamates **58** and **53** in very good yields of 82 and 92 %, respectively (see fig. 5.30). Thus, overall yields of 45 % and 81 % were achieved for the *ortho*-selective iodination of phenols **37b** and **c**, respectively.

Subsequently, all three iodophenols **46a-c** were successfully converted with 2-propynol **59** to corresponding benzofuran-2-ylmethanol derivatives **45a-c**. The according reaction conditions have been adopted from a literature protocol of BOTTA *et al.*,[170] are shown in figure 5.32 and afforded good yields of 75 to 87 % (table 5.9) after workup and purification.

The first step of this reaction underlay the classical mechanism of a palladium- and

copper-catalysed Sonogashira-Hagihara cross-coupling[171] and resulted in the formation of alkyne intermediates **60a-c**. Subsequently, these intermediates cyclised to benzofuranes **45a-c** *in situ* via a nucleophilic addition of the phenol oxygen atom to the outer alkyne carbon atom. The use of the non-nucleophilic base 1,1,3,3-tetramethylguanidine (TMG) thereby realised a one pot procedure of both synthesis steps.[172]
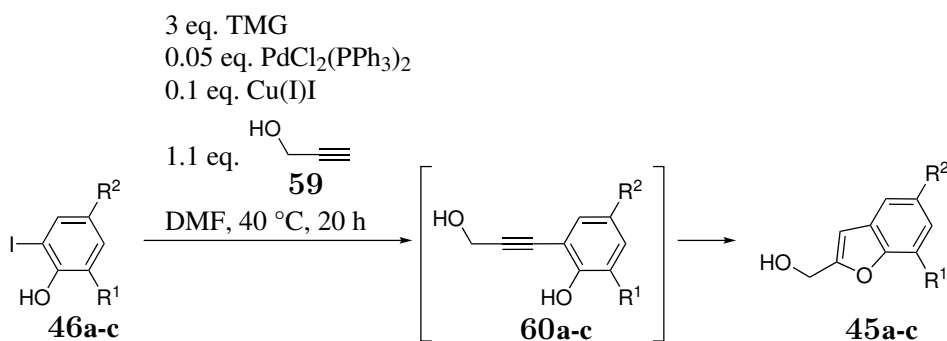
Figure 5.32: Conditions for the one-pot Sonogashira-Hagihara coupling with subsequent cyclisation to benzofuran-2-ylmethanol derivatives **45a-c**.

Table 5.9: Yields obtained for the syntheses of benzofuran-2-ylmethanol derivatives **45a-c** (fig. 5.32).

R^1	R^2	Yield	Product
	F	75 %	**45a**
	H	84 %	**45b**
	H	87 %	**45c**

Thinlayer chromatographic analysis of the crude products revealed a complete conversion for 2-*tert*-amyl phenol **46c**, only. This observation is consistent with the observed, slight yield discrepancy. Presumably, longer reaction times would have also resulted in complete conversions of phenols **37a** and **b**. However, from all three reaction mixtures one additional product was isolated in traces. Due to its similar R_f values and a similar signal patterns in the ^{1}H-NMR spectra, an incomplete cyclisation of all intermediates **60a-c** was assumed.

However, all alcohols were synthesised in sufficient quantity for further reactions.

Syntheses of carbamates 30 and 36
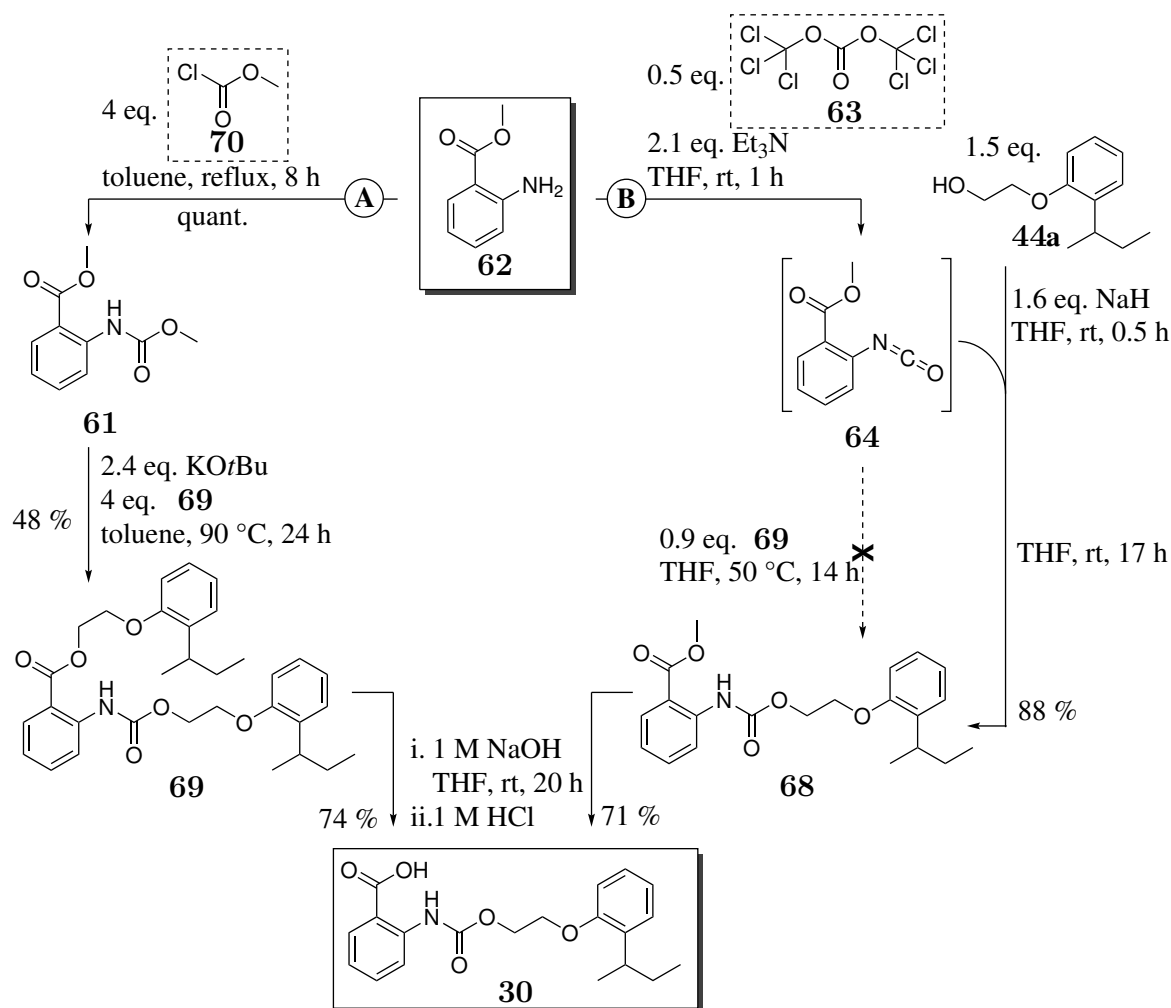
Figure 5.33: Two synthesis routes to carbamate **30**.

In general, the synthesis of carbamates is performed by coupling an amine and an alcohol with a carbonylation reagent. For the synthesis of carbamate **30** two different carbonylation reagents were tested via routes A and B which are shown in figure 5.33. Methyl-protected anthranilic acid was used as starting material for both routes.

On route A, a plain chloroformate moiety was coupled as carbonylation reagent to the amino function of methyl anthranilate **62**, followed by transesterification with the phenoxyethoxymoiety. The first reaction step on this route was an addition-elimination reaction of methyl anthranilate **62** with methyl chloroformate **70**. Carbamate **61** was thereby obtained in quantitative yield without workup or purification. For the following transesterification reaction, a substitution of both methanolate moieties in the structure was expected. Therefore, the addition of at least two equivalents of alcohol **44a** was

required. Furthermore, the leaving methanolate molecule was expected to steadily resubstitute the newly introduced alcoholate moiety in a competitive reaction. In order to reduce this competitive reaction, molecular sieves (4 Å) were added to the reaction mixture to absorb released methanolate. Moreover, an excess of 4 equivalents of alcohol **44a** was used in total. However, apparently, these efforts were insufficient to achieve a complete conversion of starting material **61** after stirring at 90 °C for 24 hours, which was revealed by thin-layer chromatography. Nevertheless, compound **69** was successfully separated from the starting materials as only product in a yield of 48 % by column-chromatographic purification. In the final step, the ester function of the molecule was saponified, which succeeded selectively under standard conditions in a good yield of 74 %. Yield losses were associated to an incomplete conversion of the reactant here, too.

Over the three steps of route A, an overall yield of 36 % was achieved. In order to reduce the number of steps, the use of sodium hydroxide as base in the second step might have directly yielded carboxylic acid **30** in a higher overall yield. However, in order to prevent the use of alcohol **44a** in excess, synthesis route B was tried as alternative.

On route B, triphosgene **63** was used as carbonylation reagent. In the first step, it was added in an amount of 0.5 equivalents to methylanthranilate **62**, followed by slow addition of 2.1 equivalents of triethylamine (Et₃N). The formal mechanism that presumably resulted in the formation of isocyanate **64** is shown in figure 5.34.
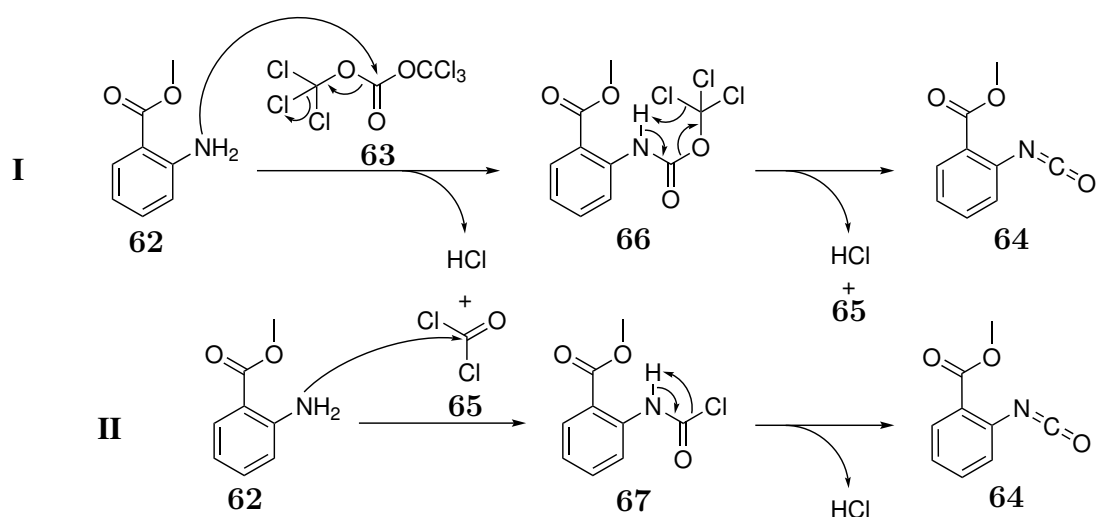
Figure 5.34: Mechanism for the carbonylation of methylanthranilate **62** using triphosgene **63**.

The reaction started (**I**) with a nucleophilic addition of amine **62** to the carbonyl carbon atom of triphosgene **63**. In this step, trichloromethanol was released and spontaneously decomposed to phosgene **65** and hydrogen chloride. The added base triethylamine (not shown) trapped the released hydrogen chloride and moreover removed hydrogen chloride from structure **66** in the second step, resulting in the formation of isocyanate **64**, triethylammonium hydrochloride (not shown) and another phosgene molecule **65**. Simultaneously (**II**), a second methyl anthranilate molecule **62** nucleophilically added to one of the released phosgene molecules **65** and thereby was converted to chloride **67**. Subsequent elimination of hydrogen chloride by triethylamine led to the formation of a second isocyanate molecule **64**. Taken together, two molecules of methyl anthranilate **62** were converted with one molecule of triphosgene **63** to two molecules of isocyanate **64** under consumption of three molecules of triethylamine and release of one phosgene molecule **65**.

After one hour stirring, volatile components, including released and unconverted phosgene **65**, were removed from the reaction mixture. Unfortunately, a subsequent addition of alcohol **44** (see fig. 5.33, dashed arrow) did not lead to the desired formation of carbamate **68** but alcohol **44a** was quantitatively reisolated. Apparently, the alcohol's nucleophilicity was insufficient for a reaction with isocyanate **64**. Therefore, in a second approach, alcohol **44a** was previously deprotonated with sodium hydride. The formed alcoholate was added to isocyanate **64**, after excess base had been removed. 17 h stirring, aqueous workup and column-chromatographic purification gave carbamate **68** in a very good yield of 88 %. As last step, the protecting methyl group was removed by saponification in a good yield of 71 %. Thus, with a good overall yield of 62 % and the use of 1.5 equivalents of alcohol **44a** only, route B proved to be well suited for the synthesis of carbamate **30**.

Therefore, a similar procedure was applied for the synthesis of carbamate **36**, which is shown in figure 5.35. Because of the laborious synthetic access to alcohol **45c**, it was used as deficiency component for the synthesis of methyl ester **71**. This deviation may explain the lower yield of 79 %, compared to that of methyl ester **68** (88 %, see 5.33). The deprotection in the second step succeeded in a yield of 71 %. Besides target compound **36**, one by-product was isolated via column-chromatographic purification, which was identified as alcohol **45c**. Apparently, the carbamate function was also hydrogenolysed. The reason for this side reaction, which was not observed for the synthesis of carboxylic acid **30**, may be the reduced electron density resulting from ether oxygen-insertion into a benzofuranyl scaffold.
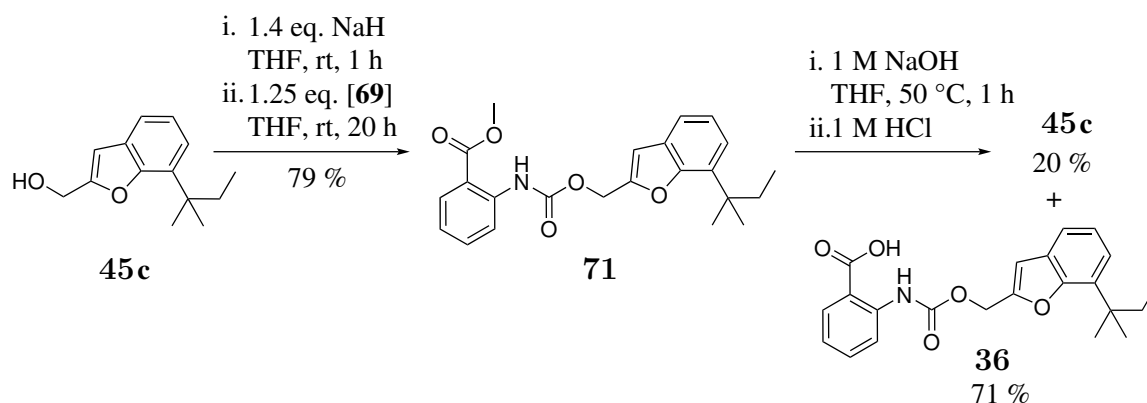
Figure 5.35: Scheme for the synthesis of carbamate **36**.

With 56 %, the overall yield for the two-step synthesis of target compound **36** was slightly lower, compared to that obtained for target compound **30**. However, both carbamates were obtained in sufficient quantities for following pharmacological investigations (see chapter 5.3.1 and 5.3.3, respectively).

Syntheses of amines 42a-e and 43a-c

For the synthesis of ureido-based target compounds **31a-f** and **33a-c**, the respective amino building blocks were required. Apart from commercially purchased amine **42f**, all amines **42a-e** and **43a-c** were obtained from their previously synthesised alcohol derivatives.

The conversion of primary hydroxy to amino moieties is a frequently performed approach in organic syntheses. Standard procedures consist of three steps, that involve an initial alcohol activation by converting the hydroxy moiety to a good leaving group, followed by nucleophilic introduction of a nitrogen bearing moiety and final transformation to the desired amino function.[173, 174]

The procedure which was applied for the synthesis of amines **31a-f** and **33a-c** is shown in figure 5.36. As a nucleophilic source of nitrogen, sodium azide was selected, as resulting azido moieties could be transferred to amines by simple hydrogenation in the last step (transformation). Mesylates were considered suitable precursor compounds for this substitution (nucleophilic N-introduction), as they could be easily obtained from the alcoholic starting materials (activation).
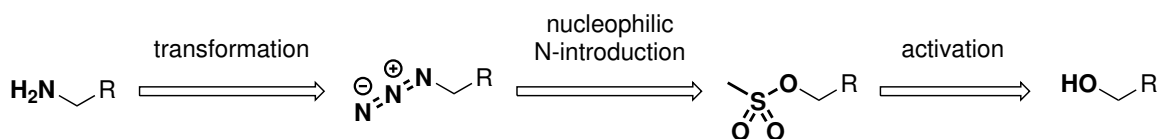
Figure 5.36: Retrosynthetic procedure for the synthesis of amines from alcohols.

Azides **72a-e** and **73a-c** were synthesised following a protocol[175] of YAMAKOSHI *et al.*. The according reaction conditions (**I** and **II**) as well as those for the final hydrogenation (**III**) to amines **42a-e** and **43a-c** are shown in figure 5.37. In table 5.10, obtained yields for the syntheses of azides **72** and amines **42** with (thio)-phenoxy scaffold are listed, whereas those for benzofuranyl-containing azides **73** and amines **43** are shown in table 5.11.
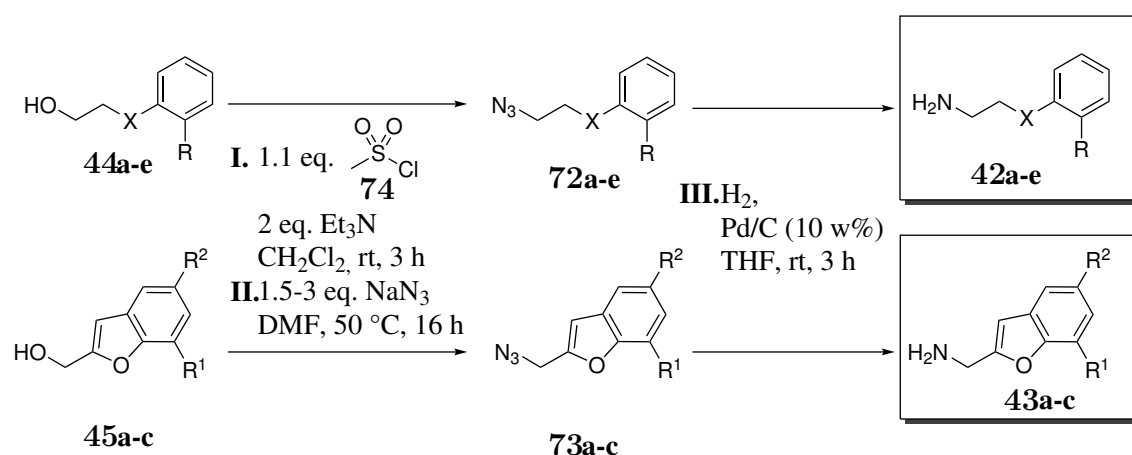
Figure 5.37: Reaction conditions for the two-step syntheses of amines **42a-e** and **43a-c**.

For the syntheses of phenoxyethylazides **72a-e**, methanesulfonyl chloride **74** was added to alcohols **44a-e** under basic conditions in step **I** (see fig. 5.37 and tab. 5.10). After aqueous workup, mesylates **75a-e** were obtained in very good to quantitative yields. Without purification, they were converted to the corresponding azides **72a-e** in step **II** by the addition of sodium azid in an S_N2 mechanism. Good yields of 80-89 % were achieved for this second synthesis step so that azides **72a-e** with (thio)phenoxyethyl scaffold were obtained in good overall yields of 72-83 %, starting from their respective alcohols **44a-e**.

Table 5.10: Yields obtained for the syntheses of 2-phenoxy and 2-thiophenoxy ethylamine derivatives **42a-e** (fig. 5.37).
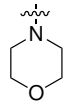
X	R	Yield step I	Yield step II	Yield step III	Products
O	(propyl)	quant.	84 %	90 %	**72/42a**
O	(isobutyl)	90 %	80 %	83 %	**72/42b**
O	(morpholine N)	95 %	89 %	90 %	**72/42c**
O	F-C(F)-F	97 %	86 %	98 %	**72/42d**
S	F-C(F)-F	97 %	80 %	88 %	**72/42e**

Table 5.11: Yields obtained for the syntheses of benzofuran-2-yl methylamine derivatives **43a-c** (fig. 5.37).

R^1	R^2	Yield step I & II	Yield step III	Product
F-C(F)-F	F	51 %	85 %	**73/43a**
F,F,F	H	59 %	79 %	**73/43b**
(isopropyl)	H	26 %	62 %	**73/43c**

Contrary to that, the two-step syntheses of azides **73a-c** with benzofuranyl scaffold were achieved in only low to moderate yields of 26-59 %, applying the same reaction conditions (steps **I** & **II**, see fig. 5.37 and tab. 5.11). Thin-layer chromatographic reaction monitoring of step **I** revealed an incomplete conversion of all three benzofuranylethyl alcohols **45a-c** and, moreover, the formation of two products, each. Exemplarily, the crude product mixture of converted alcohol **45c** was purified via column chromatography. Besides reisolated starting material **45c**, only the observed main product could be isolated. Subsequent analysis revealed that this product contained no mesyl moiety. The second, less dominantly formed product disappeared during column chromatography. Perhaps this minor product was the desired but highly reactive mesylate **76c**, which was hydrolysed to starting material **45c** during column chromatography. The ^{1}H NMR

spectrum of the isolated, non-mesylated main product is shown in figure 5.38A. For comparison, the ^{1}H NMR spectrum of successfully synthesised mesylate **75b** with phenoxyethyl scaffold is shown in figure 5.38B.
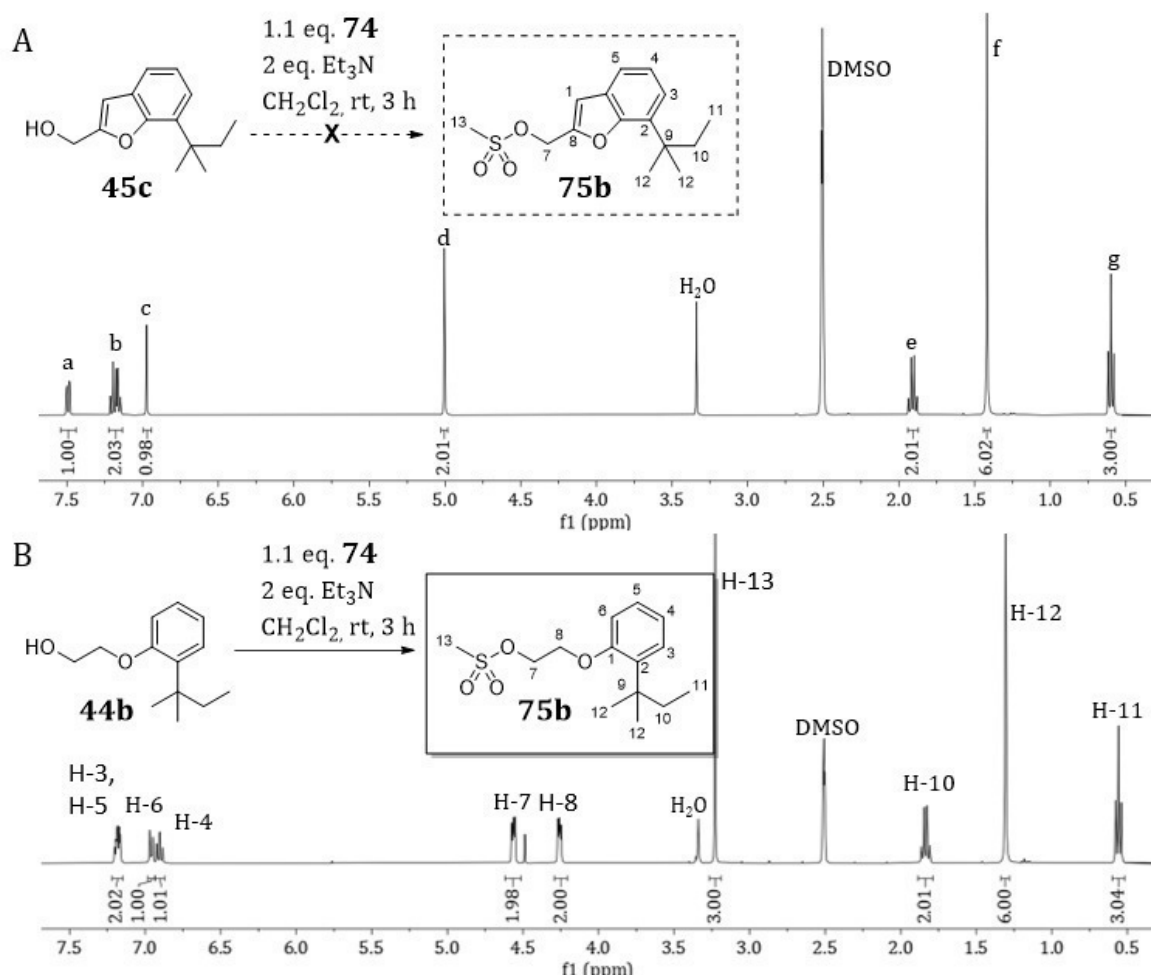
Figure 5.38: ^{1}H NMR spectra of the products formed after addition of mesyl chloride **74** under basic conditions to starting materials **45c** (A) or **44b** (B) (400 MHz, 25 °C, DMSO-d_6). A: Expected mesylate **76c** was not formed. B: Expected mesylate **75b** was formed.

For both products, signals of the *tert*-amyl-protons (H-10 to H-12) can be found below a chemical shift of 2.0 ppm and all expected aromatic proton signals above 6.5 ppm. The ethyl linker of mesylate **75b** is represented as two coupling triplets at 4.3 and 4.6 ppm (see fig. 5.38B, H-7 and H-8), whereas a singlet at 5.0 ppm (fig. 5.38A, H-d) might have been assigned to the methylene linker (H-7) of mesylate **76c**. However, the singlet of the mesylate-methyl moiety with an intensity of 3 protons can be found at 3.2 ppm for compound **75b** (see fig. 5.38B, H-13), whereas it is missing in the other

95

spectrum (see fig. 5.38A).

IR spectroscopy and EI-mass spectrometry were used complementarily, in order to identify the formed product. The according spectra as well as the identified structure are shown in figure 5.39.
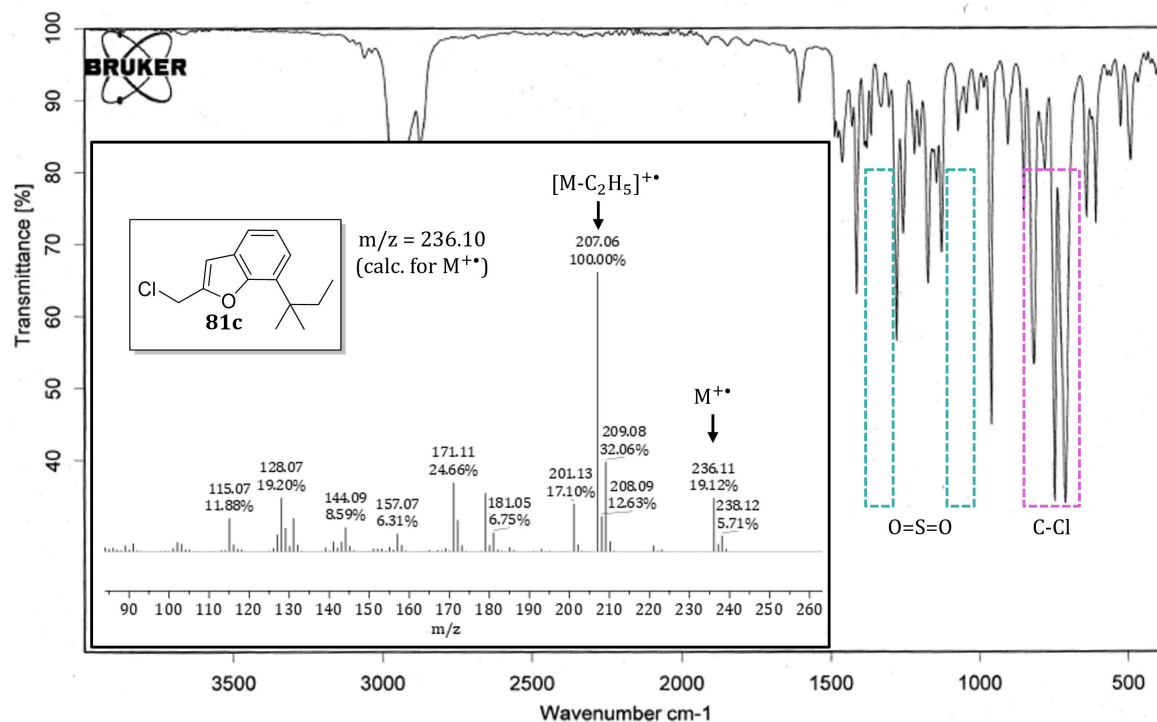
Figure 5.39: IR-spectrum, EI-mass spectrum (inlet) and structure of formed chloride **77c**.

O=S=O stretching vibration signals were expected to occur in the IR spectrum at 1120-1160 and 1300-1350 cm^{-1} (turquoise boxes).[176] Their absense confirmed that mesylate **76c** was not formed. Instead, strong bands between 600-900 cm^{-1} (pink box) indicate the formation of a carbon-halogen bond.[176]

The isotope pattern of individual signals in the EI-mass spectrum moreover indicate a chlorinated product. Finally, the signal at m/z = 236.11 could be assigned to the molecule ion of structure **77c**, which is in good agreement with the calculated value of 236.10.

DING *et al.* proposed a mechanism for such chlorination reactions which occur frequently when benzyl alcohols are converted with mesyl chloride **74**.[177] The postulated mechanism derived from this for the formation of chloride **77c** is shown in figure 5.40.
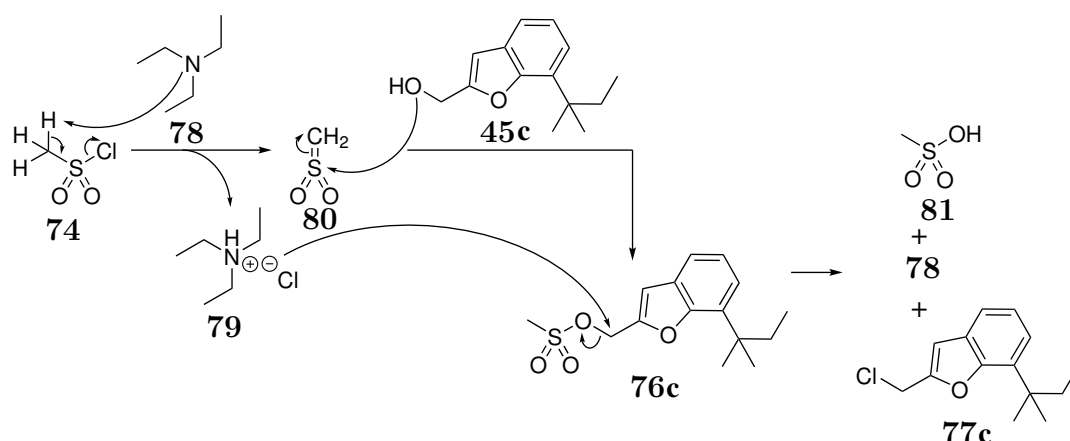
Figure 5.40: Reaction mechanism for the mesylation followed by chlorination of benzofuranylethanol derivative **45c**.

Accordingly, alcohol **45c** was initially converted to mesylate **76c**, following the common mesylation mechanism. In the first reaction step, triethylamine **78** deprotonated the added mesyl chloride **74** in an E1cb mechanism under formation of sulfene **80** and triethylammonium hydrochloride **79**. Subsequently, in an S_N2-reaction with sulfene **80**, the hydroxy moiety of alcohol **45c** was converted to a mesylate group.[178] Compared to phenoxyethyl mesylates **75a-e**, the α-position of benzofuranylmethyl mesylates **76a-c** is more electrophilic. This increased electrophilicity led to a nucleophilic addition of the chloride in triethylammonium hydrochloride **79** to this α carbon atom in the next step. Thus, chloride **77c** and methanesulfonic acid **81** were formed under the recovery of triethylamine.[177]

Chloride **77c** was obtained in a low yield of 29 % (see figure 5.41). However, it proved to be an appropriate starting material for the following azidation, either, which succeeded in a high yield of 91 %. Even though chloride formation was also observed for the analogous alcohols **45a** and **b** under mesylation conditions, azides **73a** and **b** were obtained in significantly higher yields (step **I** & **II**, see tab. 5.11). A probable reason for this may have been their increased electrophilicity, due to the fluorine substituents, which apparently resulted in a better conversion to chlorides **77a** and **b**.

Intending to increase the yield of azide **72c** over these two steps, an alternative, prominent chlorination approach using thionylchloride **82** was applied. According reaction conditions are also shown in figure 5.41. The addition of thionylchloride **82** to alcohol **45c** gave chloride **77c** after aqueous workup and columnchromatographic purification in a good yield of 80 %.
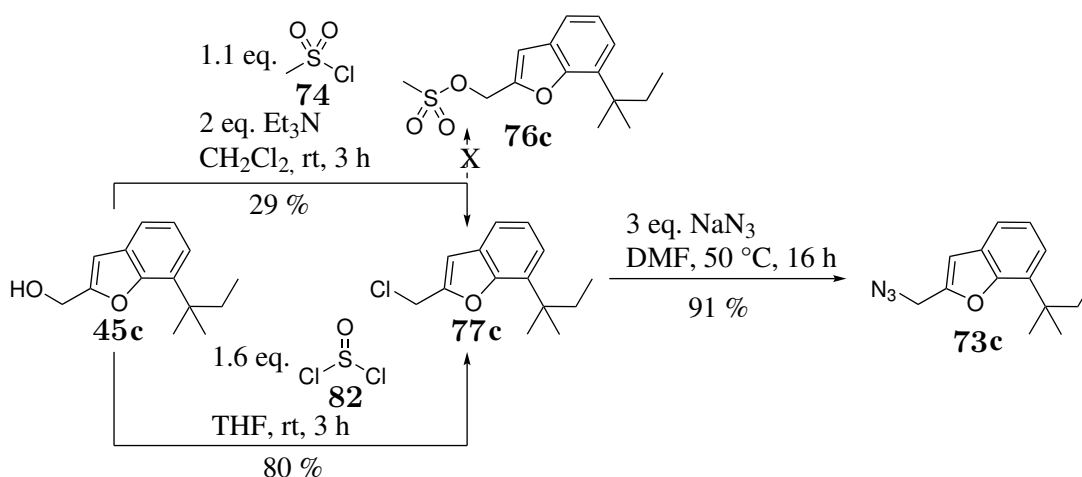
Figure 5.41: Alternative approach for the synthesis of azide **73c**.

Initially, alcohol **45c** reacted with thionylchloride **82** via an addition-elimination mechanism to a chlorosulfite intermediate, which subsequently was converted to chloride **77c** in an S_N2 reaction with the eliminated chloride.[179]

The improved access to chloride **77c** resulted in a good conversion of alcohol **45c** to azide **73c** in a yield of 73 % over two steps.
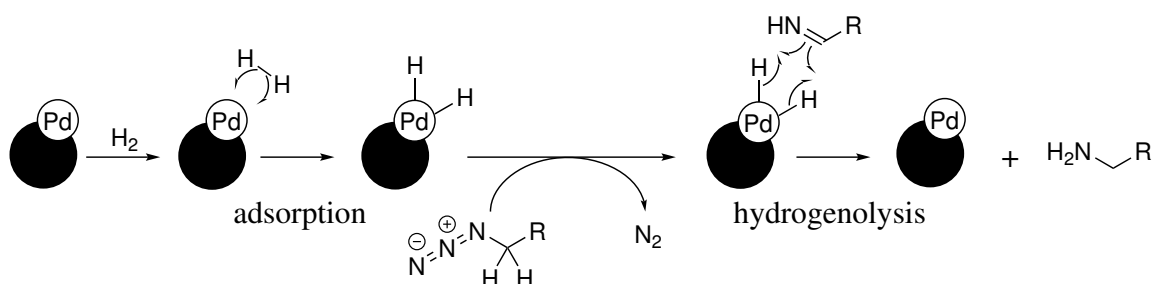
Figure 5.42: Postulated mechanism for the palladium-catalysed hydrogenation of azides.

Next, in step **III** (see fig. 5.37), amines **42a-e** and **43a-c** were finally synthesised by palladium-catalysed hydrogenation of the formed azides **72a-e** and **73a-c**. The corresponding, postulated mechanism, which was derived from literature observations and assumptions,[180,181] is shown in figure 5.42. The reaction was initiated by the approximation of a hydrogen molecule from the gas phase to a carbon-dispersed palladium atom. Homolytic cleavage of the hydrogen bond resulted in covalent interactions of both hydrogen atoms with palladium, in a process called adsorption. In presence of the palladium catalyst, azides are assumed to be converted to their imines under elimination of molecular nitrogen.[180,181] In the last step, the two adsorbed hydrogens were presumably transferred to the imine, resulting in the formation of an amine.

All amines **42a-e** and **43a-c** were successfully obtained in moderate to very good yields of 62-98 % (see tab. 5.10 and 5.11). Except for the synthesis of amine **42d**, the formation of one side-product was observed during each hydrogenation reaction. However, the strongly decreased polarity of this side-product enabled the products' facile separation via column chromatography. For the hydrogenation of benzofuranyl derivative **43c**, this by-product formation was particularly prominent: it was obtained in a yield of 35 %, which explains the moderate yield of the respective amine **43c**. The structure and ESI$^+$-mass spectrum of the formed by-product **83** are shown in figure 5.43.
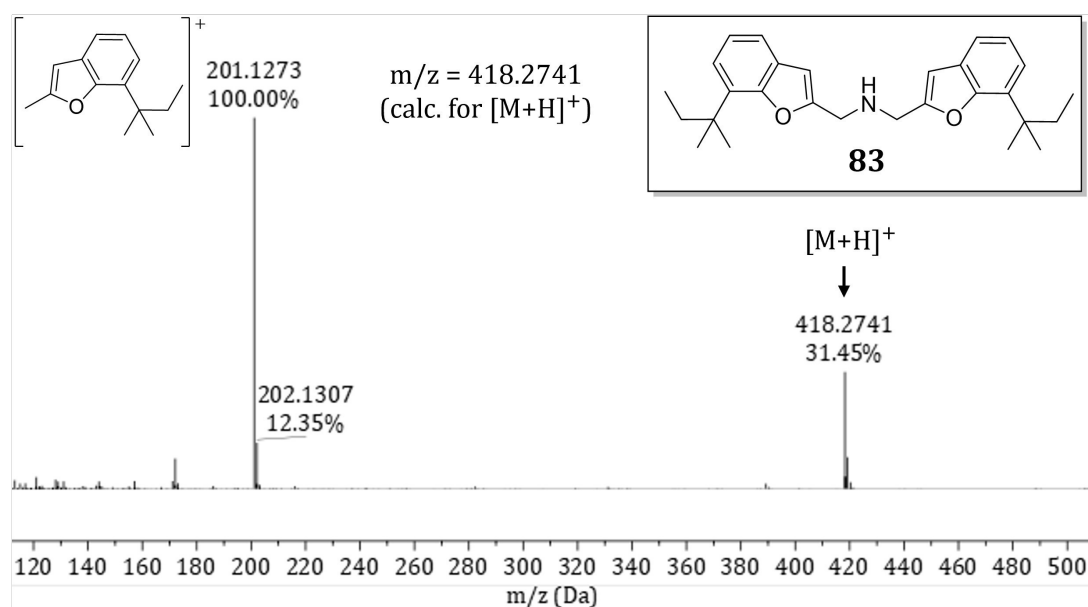
Figure 5.43: ESI$^+$-mass spectrum and structure of secondary amine **83**, which formed as side-product during the hydrogenolysis of azide **73c**.

The formation of secondary amines during azide-hydrogenolysis using palladium on activated carbon under hydrogen atmosphere is reported in the literature.[182] Probably, the formation of these dimers resulted from a nucleophilic addition of a formed primary amine to an imine intermediate (see fig. 5.42). A reduced reaction temperature,[182] higher amounts of added catalyst and smaller reaction scales may have conceivably resulted in a reduced dimerisation and thus higher yields of the desired primary amines. Alternatively, different reduction approaches may have been applied in order to obtain higher yields, in particular for amines **43a-c** with benzofuranyl scaffold. However, all amines were obtained in sufficient amounts for following coupling reactions.

Syntheses of ureides 31a-f and 33a-c

For the subsequent coupling and deprotection to ureido-based target compounds, synthesis route B (see fig. 5.33) was applied, which successfully yielded carbamates **30** and **36** (see fig. 5.33). As amines exhibit higher nucleophilicities compared to their alcohol analogues, they were simply added to freshly prepared isocyanate **64** without previous activation. Figure 5.44 shows an initial synthesis attempt, in which methyl anthranilate **62** and amine **42a** were used as starting materials.
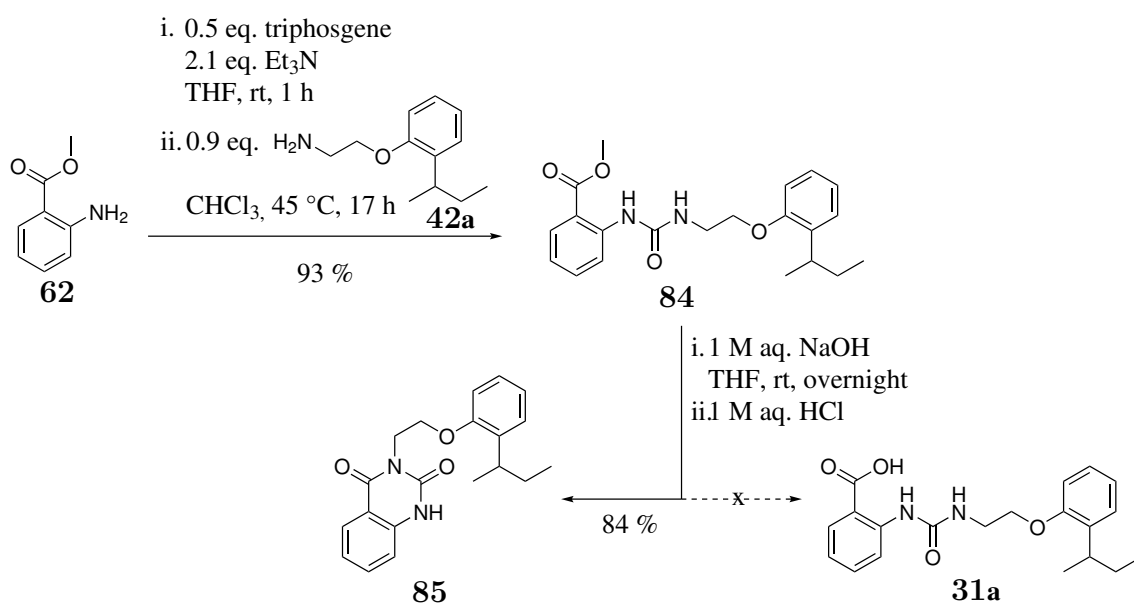
Figure 5.44: Scheme for the failed synthesis of ureide **31a** under quinazoline formation instead.

The initial coupling reaction succeeded in a very good yield of 93 %, calculated in relation to the limiting amount of added amine. This yield is in line with yields that were obtained for the analogous carbamate coupling. However, final deprotection of methyl ester **84** under basic conditions resulted in its undesired cyclisation to quinazolinedione **85**, that was obtained as only product in a yield of 89 %.

Quinazoline formation was initially indicated by the unusually low polarity of the product, which became apparent during thin-layer chromatographic reaction monitoring. Moreover, in the ESI$^+$ and ESI$^-$-spectra, molecule peaks with m/z values of the desired carboxylic acid **31a** reduced by the mass of water were found. Cyclisation product **85** was ultimately identified via 2D NMR spectroscopy. The HMBC spectrum of the product is shown in figure 5.45. The red circled signals indicate a coupling of both carbonyl carbon atoms (C-a and C-b) with the α-proton (H-c) of the amino building block, which confirmed the formation of structure **85**.
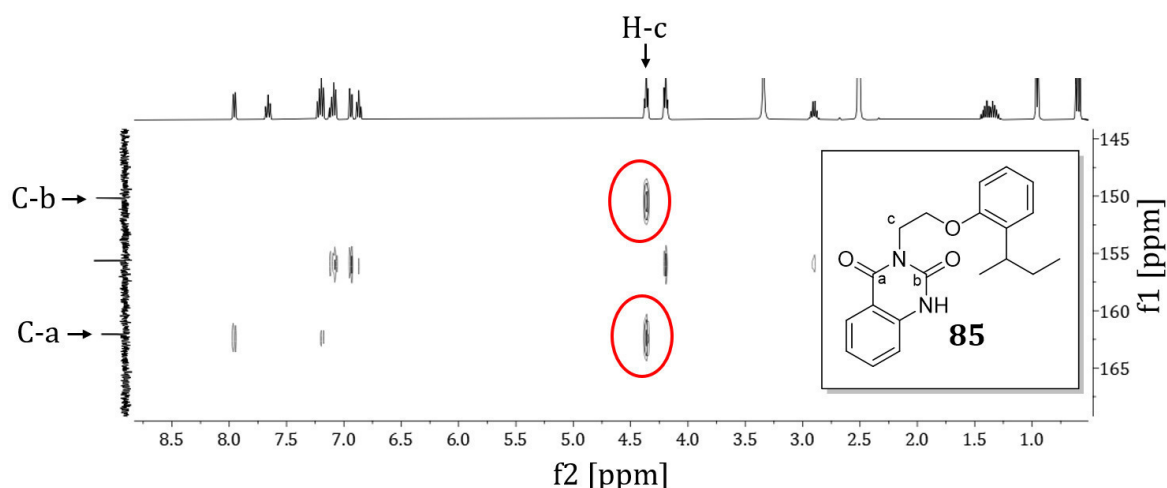
Figure 5.45: HMBC-NMR spectrum of the cyclised hydrolysis product **85**.

The postulated reaction mechanism that resulted in the formation of quinazoline **85** is shown in figure 5.46. Before the desired ester hydrolysis could have proceeded, the hydroxide ion had deprotonated the ureido moiety. Due to its resulting increase in nucleophilicity, the deprotonated nitrogen atom intramolecularly added to the carboxy carbon atom, resulting in the formation of a six-membered, annulated ring under elimination of methanolate.
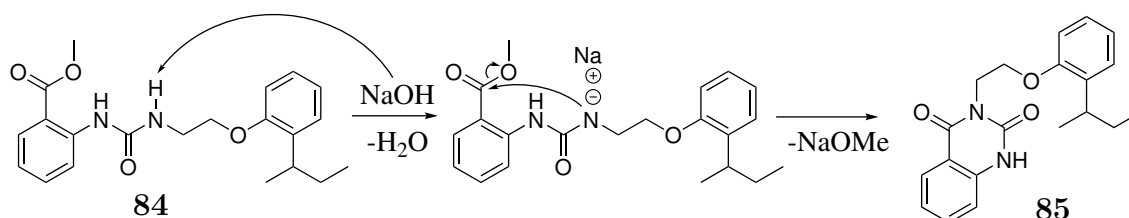
Figure 5.46: Mechanism of quinazoline formation under basic conditions.

Even the use of rather mild lithium hydroxide[183] in an equimolar amount resulted in the sole formation of quinazoline **85** and no carboxylic acid **31a** was formed.

Due to the observed base-lability of ureido-based methyl esters, benzyl was tried as alternative protecting group, as it can be cleaved without basic conditions.
The benzyl function is a widely used protecting group for alcohols, amines as well as carboxylic acids. A standard method for its cleavage is the hydrogenolysis using palladium on activated carbon under elimination of toluene. The assumed mechanism was derived from the literature[184] and is shown in figure 5.47. An insertion of the carbon-immobilised palladium into the oxygen-carbon-bond of benzylesters (oxidative

addition) was followed by previously described hydrogen adsorption (see fig. 5.42). Finally, toluene **86** and the carboxylic acid were reductively eliminated from the catalyst.
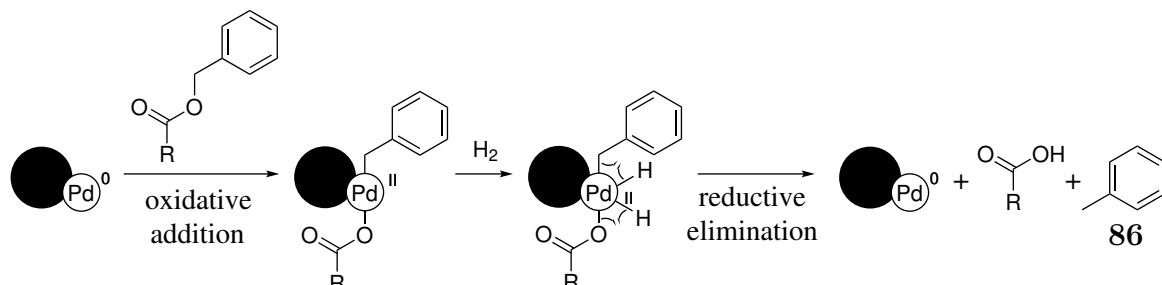
Figure 5.47: Postulated mechanism for the Pd/C-catalysed hydrogenolysis of benzylesters.

The use of benzyl anthranilate **87** as starting material enabled the synthesis of all desired ureido-based target compounds **31a-f** and **33a-c**. The according synthesis scheme is shown in figure 5.48 and the corresponding yields are listed in table 5.12 for compounds **31a-f** with phenoxy scaffold and in table 5.13 for compounds **33a-c** with benzofuranyl scaffold.
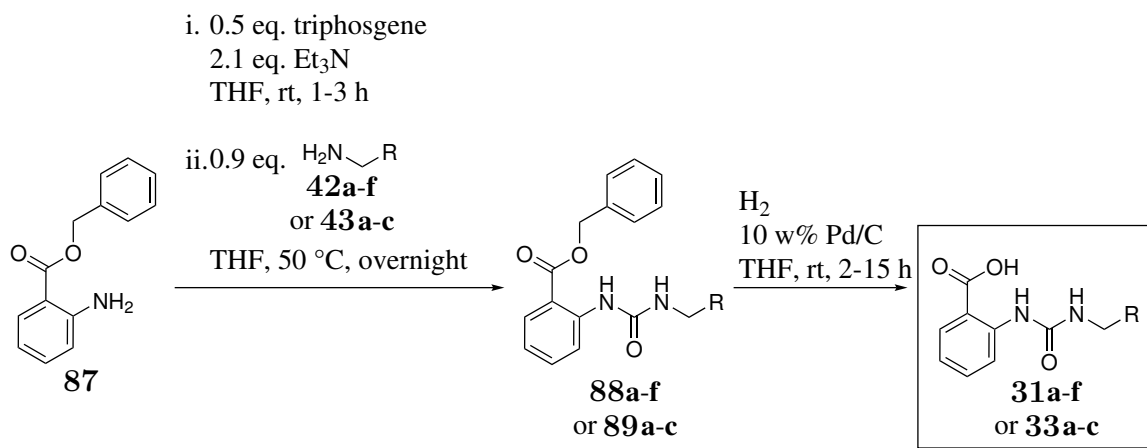
Figure 5.48: Reaction conditions for the coupling and final deprotection of all ureido-based target compounds.

Benzylesters **88a-f** and **89a-c** were successfully synthesised in moderate to very good yields under the established reaction conditions. In some cases, depending on the respective ester structure, column-chromatographic separation from the excess benzyl-anthranilate **87** was challenging. This partly explains the yield differences. Moreover, the reaction time of the isocyanate synthesis (step i., see figure 5.48) strongly influenced
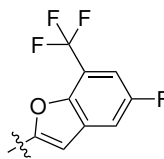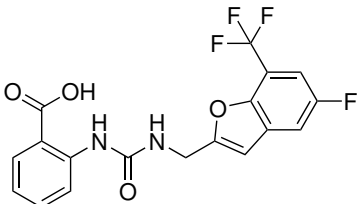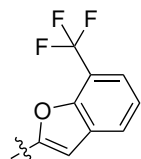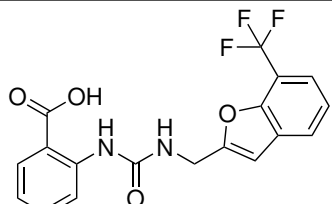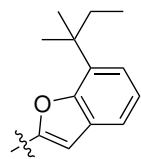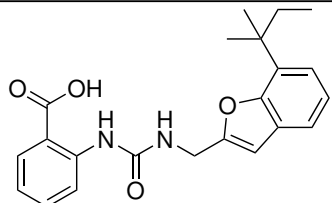
the yield. Stirring for 45 minutes before addition of amine **42f** was apparently not sufficient for a complete conversion of benzyl anthranilate **87**. Contrarily, an almost quantitative conversion was achieved for amine **90b**, that was added after three hour stirring. Nevertheless, all benzylesters were obtained in sufficient amounts for final deprotection by hydrogenolysis.

Table 5.12: Yields obtained for the coupling and final deprotection of ureido-based target compounds **31a-f** with phenoxy scaffold (fig. 5.48). (*: 50 w% Pd/C used)

R	Amine	Yield step 1	Product step 1	Yield step 2	Product step 2
	42a	76 %	**88a**	92 %	**31a**
	42b	99 %	**88b**	quant.	**31b**
	42c	80 %	**88c**	80 %	**31c**
	42d	62 %	**88d**	79 %	**31d**
	42e	62 %	**88e**	41 %*	**31e**
	42f	44 %	**88f**	71 %	**31f**

Table 5.13: Yields obtained for the coupling and final deprotection of ureido-based target compounds **33a-c** with benzofuranyl scaffold (fig. 5.48).

R	Amine	Yield step 1	Product step 1	Yield step 2	Product step 2
	43a	80 %	**89a**	98 %	**33a**
	43b	80 %	**89b**	quant.	**33b**
	43c	81 %	**89c**	93 %	**33c**

Good to quantitative yields were obtained for this last deprotection step for all ureido-based target compounds, except thiophenoxy derivative **31e**. The common hydrogenolysis conditions (see fig. 5.48) resulted in a very poor conversion of benzyl ester **88e**, which, however, could be significantly increased by the addition of higher amounts of catalyst. The use of 50 w% Palladium on activated carbon finally gave target compound **31e** in 41 % yield after 15 h stirring. It is known that palladium(II) readily coordinates to sulfur atoms. This interaction is crucial for the palladium-complexation of many sulphur-bearing ligands.[185] Since the poor conversion was unique to this derivative **88e** among all benzylesters, it may be assumed that such coordination led to catalyst saturation, which impeded hydrogenation.

For the hydrogenolysis to target compound **33c** it is strongly recommended to stop the reaction immediately after complete conversion of ester **89c**, which was already achieved after two hours. Synthesis attempts with longer reaction times resulted in a partial hydrolygenolysis of the benzofuranyl scaffold. Separation of the resulting by-

product from the product was almost impossible, due to the almost identical polarities. The ^{1}H NMR spectrum of synthesised target compound **33c** is shown in figure 5.49 and proves its high purity.
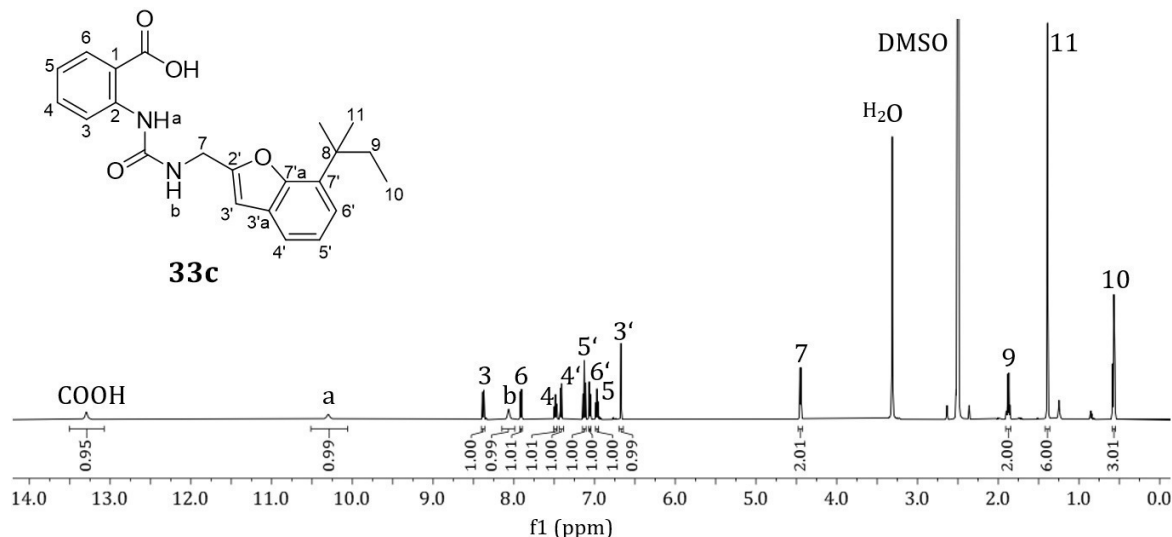
Figure 5.49: The ^{1}H-NMR spectrum of highly pure target compound **33c** (500 MHz, 25 °C, DMSO-d_6).
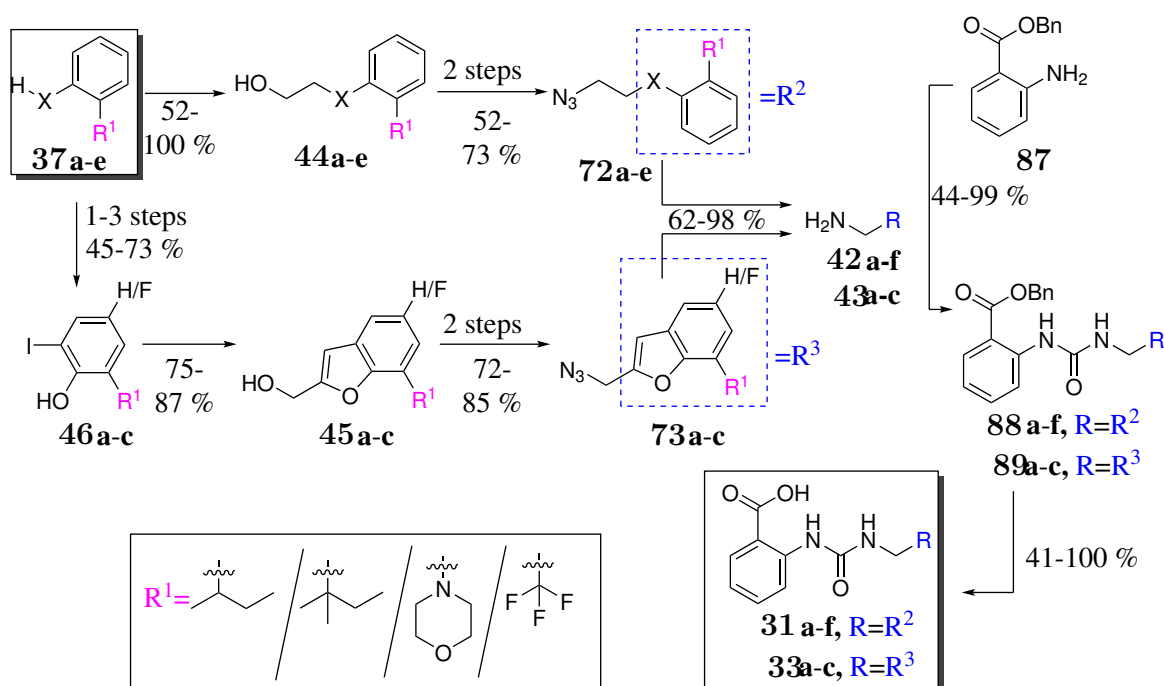
Figure 5.50: Synthesis overview of all ureides.

Figure 5.50 gives an overview over all synthesis steps to ureido-based target compounds,

105

which were discussed in this chapter. In total, all ureides **31a-e** and **33a-c** were
obtained in six to nine synthesis steps in satisfying yields and high purities. Among all
target compounds with phenoxy scaffold, the best overall yield of 52 % was obtained
for 2-*sec*-butylphenoxy derivative **31a**, whereas the worst overall yield of 16 % was
obtained for thio derivative **31e**, each over six steps. The access to potent benzofuranyl
derivatives **33b** and **c** via nine synthesis steps was rather elaborate. Nevertheless, they
were obtained in good overall yields of 14 and 20 %, respectively.

An opposite introduction of coupling elements, as shown in figure 5.51 and mentioned at
the beginning of the chapter, would have significantly accelerated the synthetic access
to benzofuranes **33a-c**. Introducing the alkynyl linker to the protected anthranilate **87**
in the first step succeeded by the addition of propargylamine **91** in a moderate yield of
67 %. However, the basic conditions that were required for the subsequent benzofurane
formation were expected to result in an already familiar cyclisation of ester **92** to
quinazolinedione derivative **93**. For this reason, this synthesis route was discarded, as
already indicated at the beginning of this chapter.
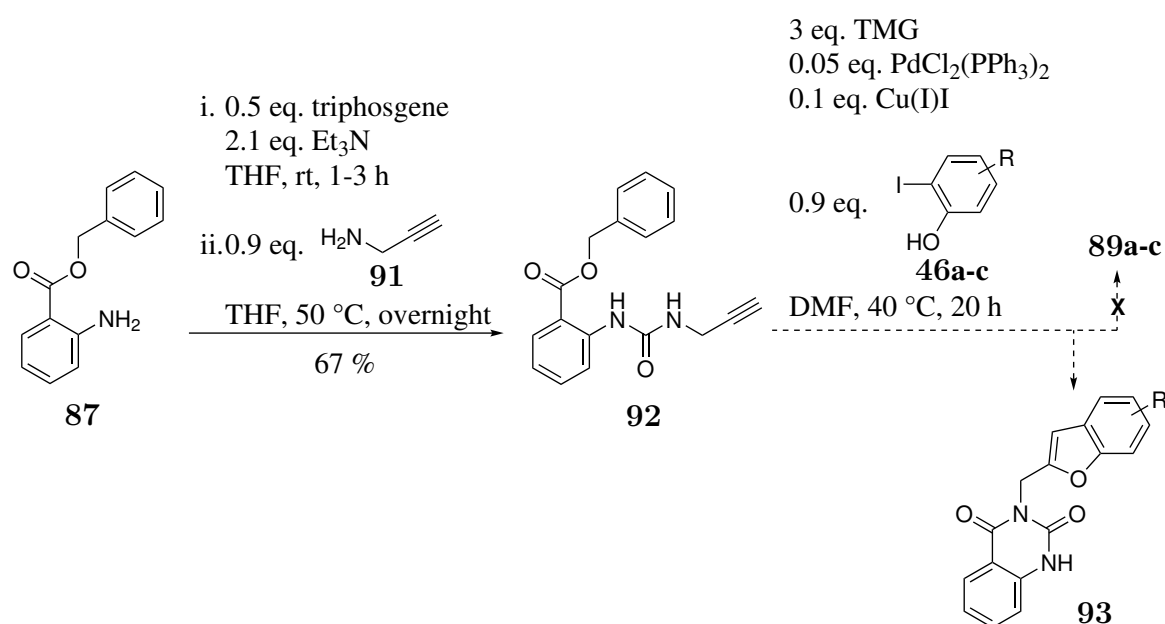
Figure 5.51: Alternative, discarded route which was set up but failed to accelerate the
synthetic access to benzofuranyl-based target compounds.

5.4 Development of a novel hDHODH inhibitor lead structure

Compound **33c** has proven to be a highly potent hDHODH inhibitor with suitable pharmacokinetic profile. However, its synthetic access was elaborate and derivatisation possibilities for further adjustments are limited.

Ideally, for a profitable drug development, the lead structure should already exhibit suitable pharmacokinetic properties and extensive possibilities for derivatisation, besides a certain biological effect. Furthermore, lead structures should be characterised by a low molecular weight, so that subsequent lead optimisation and drug formulation procedures can be thoroughly carried out without immediately reaching molecular weight limits. Thus, when designing a lead structure, the number of pharmacophore features should be reduced to the minimum required to satisfy these demands.

Following these rules, in the last part of this thesis a novel lead structure was developed. It was intended to serve as solid basis for the development of further highly potent and druggable hDHODH inhibitors, in the future. For this purpose, the inhibitor structure was kept as compact as possible, while particular emphasis was placed on metabolic stability, from the outset. Parts of this work were submitted in [P1].

The 2-amidobenzoate motif (fig. 5.52) was chosen as core scaffold for the development of this lead structure, as it has proven to be a convenient element of highly potent hDHODH inhibitors in the past (chapter 3.4).[123,124] An intramolecular hydrogen bond connecting the amide hydrogen and the carboxyl oxygen restricts the conformational flexibility of the anthranilate ring which has an entropically favorable effect on binding affinity (see chapter 5.3). The rotationally restricted amide group extends the rigidity of this core fragment and moreover strengthens the intramolecular hydrogen bond, by withdrawing electron density from the NH-bond. Furthermore the introduction of an amide moiety facilitates synthetic accessibility of the final inhibitors.
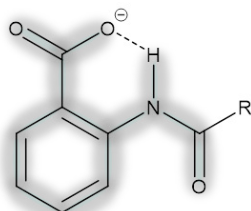
Figure 5.52: Structure of the rigid 2-amidobenzoate core fragment. Bonds shaded in grey are rotationally restricted.

In the ligand binding pocket of hDHODH, the amidobenzoate fragment can be oriented in two different directions, as became apparent by comparing the X-ray cocrystal structure of KP-CF39 **22** in hDHODH (see chapter 5.3) and the published structure of bound compound **18** (see chapter 3.4, PDB 2WV8). Excerpts of these two crystal structures, showing each amidobenzoate fragment only, are shown in figures 5.53A and B, respectively. The amido moiety is either directed towards the surface of the binding pocket, like in KP-CF39 **22** (S-orientation, fig. 5.53A), or points towards the active site, like in ligand **18** (A-orientation, fig. 5.53B). Depending on the respective orientation, the angle, formed between the carboxylate moiety of the ligand and the guanidino unit of Arg136, varies strongly. A slight rotation of arginine's side chain allows the formation of a salt bridge in both cases.
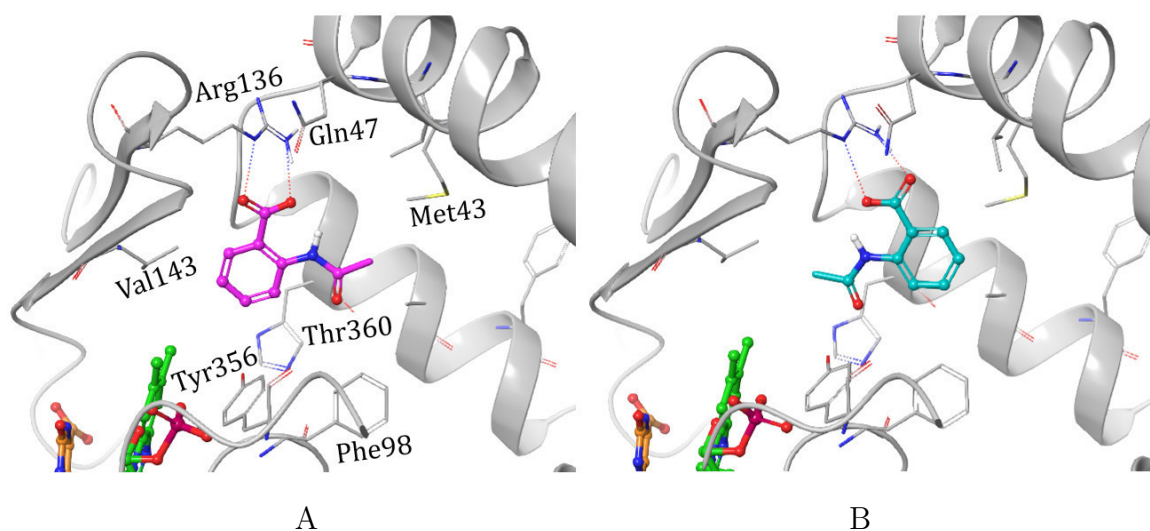
Figure 5.53: Two possible orientations of the 2-amidobenzoate core fragment in the ubiquinone binding site of hDHODH. A: S-orientation: amido moiety points at protein surface, excerpt of X-ray structure from hDHODH-KP-CF39 **22** complex, B: A-orientation: amido moiety points at active site, excerpt of X-ray structure from hDHODH-**18** complex.

In A-orientation (fig. 5.53B), only small substituents are tolerated at the amide's α-position. The aromatic 5-position is likely to be substituted with large, lipophilic moieties to achieve high binding affinities. Corresponding structure-activity relationships have been investigated by FRITZSON *et al.* and in our research group.[123,186] The introduction of larger amido-α-substituents forces the fragment to arrange in S-orientation (fig. 5.53A). In this case, a third substitution at the arene is not necessary for a high binding affinity of the ligand, since lipophilic fragments can be coupled directly to the amide. Moreover, the non-substituted part of the arene fits well into the

shape of the binding pocket. Avoiding a third substituent at the anthranilate core brings several advantages. On the one hand, it facilitates synthetic access to the corresponding inhibitors and on the other hand, it keeps the structure smaller, which is advantageous in the perspective of lead structure development.

For these reasons, the construction of a compact, novel lead structure was based on an S-oriented 2-amidoanthranilate.

In three cycles of design, synthesis and evaluation, a potent lead structure was gradually built up, starting from this core scaffold. In each cycle, a pre-selection of proper fragments or modifications was made by computer-assisted molecular modelling, prior to synthesis of these designs. For molecular modeling, the X-ray structure of the KP-CF39 **22**-hDHODH complex (see chapter 5.3) was used, initially. The structural modifications were finally evaluated regarding their effect on hDHODH inhibition strength. The best inhibitors of each cycle entered the next design cycle, in which they were expanded, analogously.

The synthesis of all compounds will be discussed at the end of this chapter.

5.4.1 Cycle 1 of lead structure development

In cycle 1, the structural margin of amido substituents that fit into the binding site was explored. With the aim to keep the structure compact and rigid, different ring fragments were selected as substituents. Therefore, not only different aliphatic and
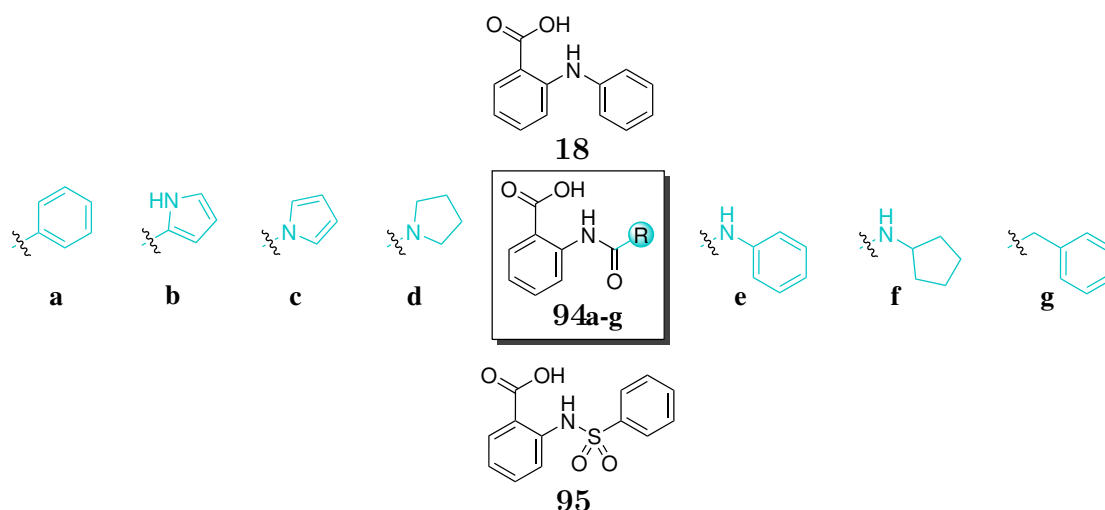
Figure 5.54: Structures of target compounds that were selected for the initial investigation of the binding pocket space in cycle 1.

aromatic rings of different sizes were coupled, but furthermore, it was investigated whether the binding pocket offers sufficient space to directly couple ring fragments to the amido function or whether the insertion of a spacer between amido function and ring would be necessary. Figure 5.54 shows the series of compounds that were selected for the initial investigation of space in the binding pocket. In structures **94a-d**, different ring fragments are attached directly to the amido moiety. Besides the 6-membered phenyl substituent (**94a**), pyrrole was selected as example of a 5-membered arene, either coupled via its α-carbon atom (**94b**) or via its nitrogen atom (**94c**). Pyrrolidine (**94d**) was chosen as small representative of an aliphatic ring system. Moreover, with compounds **94e-g** the effect of a linker extension on binding affinity was investigated. The amido linker was either exchanged by a ureido linker (**94e,f**) or extended with a more flexible methylene function (**94g**).

The amido moiety in 2-amidobenzoic acids has been identified as site of metabolism (see chapter 5.1). It has been successfully stabilised by converting the amides to corresponding ureido derivatives. Nevertheless, here, amides **94a,b** and **g** were selected besides the ureido derivatives, intending to better investigate the binding pocket in cycle 1. Moreover, a direct attachment of ring fragments to the amido function (compounds **94a** and **b**) may imaginably serve as sterical protection towards hydrolysis. Besides ureides, sulfonamides are also regarded as metabolically stable alternatives of amides. Therefore, sulfonamide **95** was chosen as representative to investigate whether replacing the amide against a sulfonamide (**95**) will be tolerated in the binding pocket.

FRITZSON's[123] fenamic acid derivative **18** was used as reference substance.

With molar masses of less than 280 g/mol, all compounds of cycle 1 are rather small with small lipophilic surfaces. As the hDHODH ubiquinone binding site is composed of predominantly lipophilic amino acids (chapter 3.4), binding affinity was expected to improve with increasing lipophilicity of the ligands. For these reasons, rather low inhibitory activities were expected for all compounds of cycle 1. The IC_{50} value of reference compound **18** was determined to 38 µM by FRITZSON *et al.*.[123] Similar inhibitory activities were expected for all compounds of this cycle.

IC_{50} values depend on various factors, such as the exact concentrations of the protein and other ingredients in the mixture. For this reason, the determination of individual IC_{50} values was regarded rather unsuitable for an accurate comparison of the nine compounds. Instead, the percentage inhibition of hDHODH in the presence of each compound at a final concentration of 10 µM was determined. This not only allowed a parallel measurement of all nine compounds under the same conditions in double

evaluation, but also saved time and material. The obtained, plotted results are shown in figure 5.55.
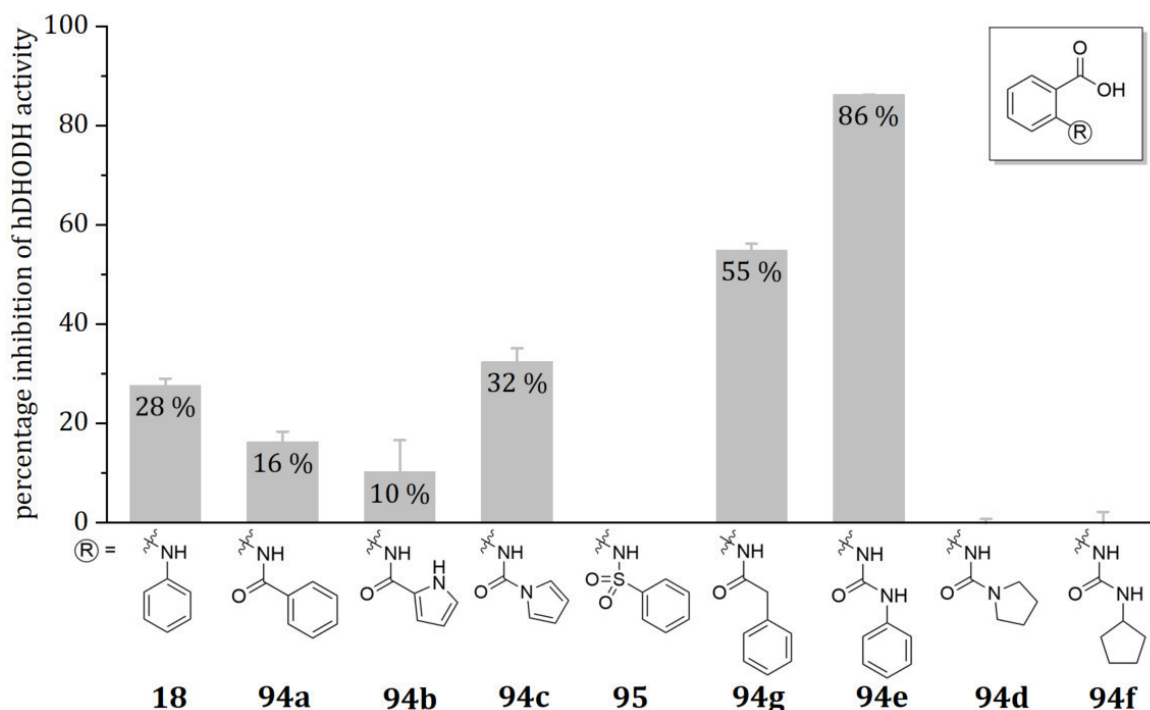
Figure 5.55: Percentage inhibition of hDHODH activity in presence of all compounds designed and synthesised in cycle 1. 50 mM Tris-HCl, pH 8.0, 0.1 % Triton X-100, 100 nM L-DHO, 25 nM CoQ1, 60 nM DCPIP, 10 µM test compounds, 25 °C.

Through the addition of the individual compounds (10 µM), enzyme activity was inhibited by 0 to 86 %. For reference compound **18** the enzymatic activity was inhibited by 28 %. This result is in good agreement with its reported IC$_{50}$ value of 38 µM[123].

A direct attachment of different ring substituents to the amide function was indeed tolerated in the binding pocket, as the inhibition values for compounds **94a**,**b** and **c** show. The strongest inhibition in this series was obtained for pyrrole derivative **94c**, which inhibited the enzymatic activity by 32 % and thus was similarly active as reference compound **18**. Compared to phenyl derivative **94a** (16 %), the smaller pyrrole ring apparently fitted better into the binding pocket. However, when the pyrrole substituent was attached to the amide function via its carbon atom at 2-position, the inhibition strength dropped to 10 %. One explanation for this may be that the accessible, polar amino function of compound **94b** interrupted the lipophilic interaction surface between ligand and enzyme, resulting in a lower binding affinity.

For sulfonamide **95**, no enzymatic inhibition was observed at the tested concentration of 10 µM. An attempt to dock this molecule into the binding pocket of hDHODH (see chapter 5.3 for details of the docking studies) was neither successful. Intending to find a rational explanation for this, the docking study was repeated with a ligand structure, in which the phenyl substituent was replaced by a smaller methyl substituent. The resulting docking pose is shown in figure 5.56A, viewing from the direction of the binding pocket opening.
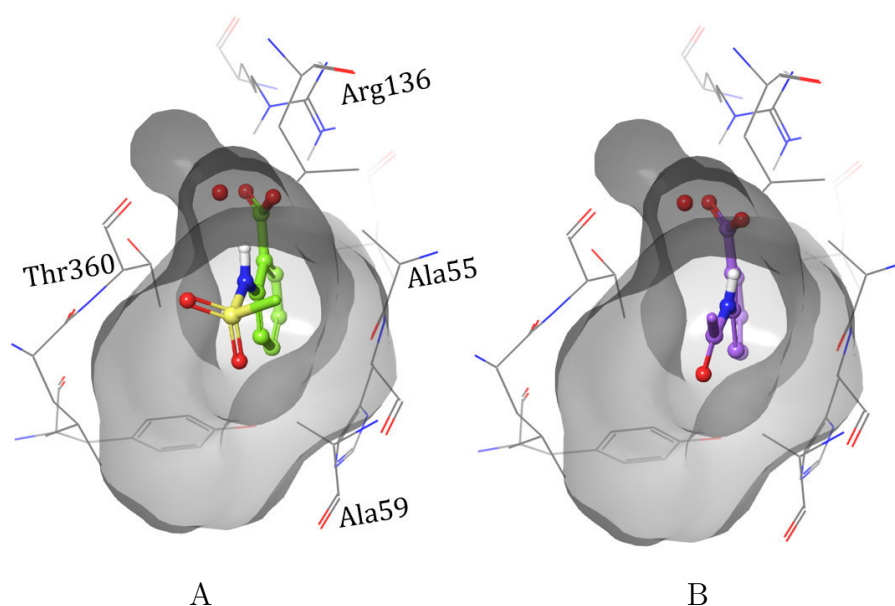
Figure 5.56: Glide Docking pose of A: 2-(methylsulfonamido)benzoate and B: 2-(methylamido)benzoate in the hDHODH binding site of KP-CF39 **22**. The protein surface is visualised in grey.

In carboxamides (fig. 5.56B), the α-substituent is oriented planar with the amide group. Thus, the substituent was expected to point towards a larger cavity in the binding pocket of hDHODH, that apparently offers enough space for a cyclic substituent. Contrary to that, α-substituents of sulfonamides are not oriented planar with the anthranilate arene and the amide group, but protrude from this plane at an angle of about 60°. As a result, the substituent either points towards Thr360 or Ala55 (see fig. 5.56A). Due to the short distance to these protein residues, larger substituents are expected to clash with these protein residues. Presumably, this was the reason why phenylsulfonamide **95** did not bind to the enzyme.

The inhibition data shown in figure 5.55 also indicate that extending the amide linker (compounds **94g** and **e**) significantly improved binding affinity. The ureido linker proved to be particularly suitable, as ureide **94e** induced an enzymatic inhibition of

86 %. Its docking pose is shown in figure 5.57B, whereas in figure 5.57A the docking pose of the respective amide **94a** can be seen.
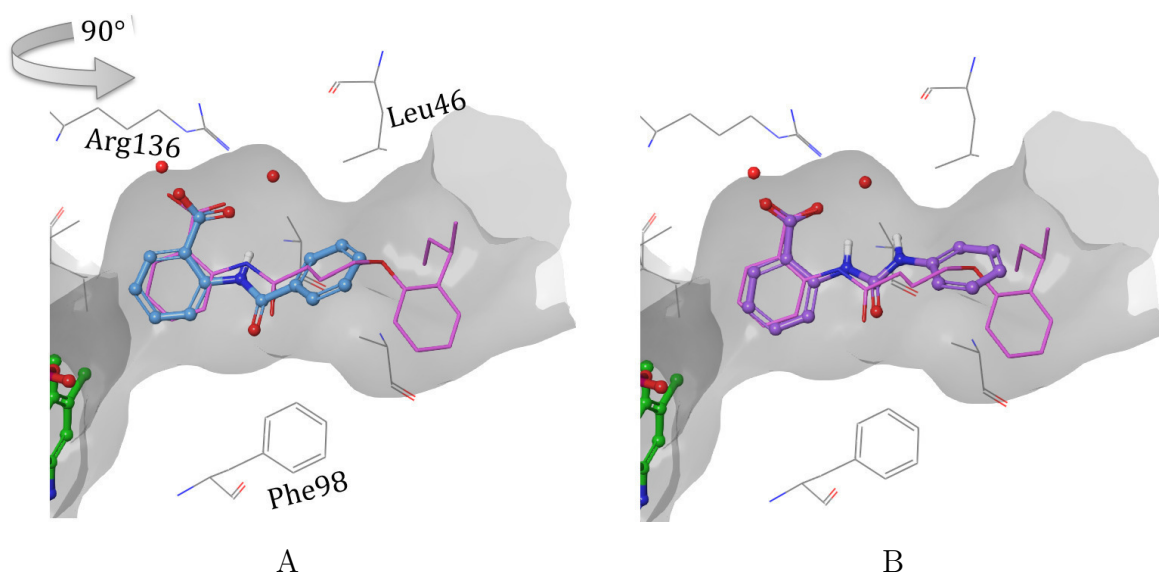
Figure 5.57: Docking poses of A: 2-benzamidobenzoate **94a** and B: 2-(3-phenylureido)benzoate **94e** in the hDHODH binding site of KP-CF39 **22** (pink, thin tubes).

The side chains of Leu46, Phe98 and Ala55 (not shown) constrict the binding pocket at the site where the α-position of the amide was expected to be located. As a result, sterically demanding α-substituents, such as the phenyl substituent in **94a**, are assumed to push the anthranilate out of its beneficial arrangement towards Arg136 (see fig. 5.57A). Due to the longer ureido linker, the phenyl substituent in **94e** (see fig. 5.57B) was expected to be placed in a larger cavity behind this constriction and thus to preserve the advantageous interaction between carboxylate and Arg136. Moreover, an additional hydrogen bond will presumably form between the ureido function and the trapped water molecule to further enhance binding affinity, as discussed in chapter 5.1.

For compounds **94d** and **f** with aliphatic substituents, no enzymatic inhibition was detected at the tested concentration. Apparently, these spatially more demanding, non-aromatic rings do not fit into the narrow binding pocket of hDHODH.

Consequently, phenylureido derivative **94e** has emerged as best inhibitor of cycle 1 with an enzymatic inhibition of 86 % at a concentration of 10 µM. However, considering its size, pyrrole carboxamide **94c** also appeared suitable as novel lead structure. Therefore, both structures were passed on to cycle 2 to get structurally expanded, aiming to achieve a stronger binding affinity.

5.4.2 Cycle 2 of lead structure development

In cycle 2, the phenyl substituent in compound **94e** and the pyrrole substituent in compound **94c** were each extended by an annulated benzene, first. The purpose of this was to fill the bulge of the binding pocket behind the constriction. The resulting chemical structures as well as their docking poses in the virtual binding pocket of hDHODH are shown in figure 5.58A and B.
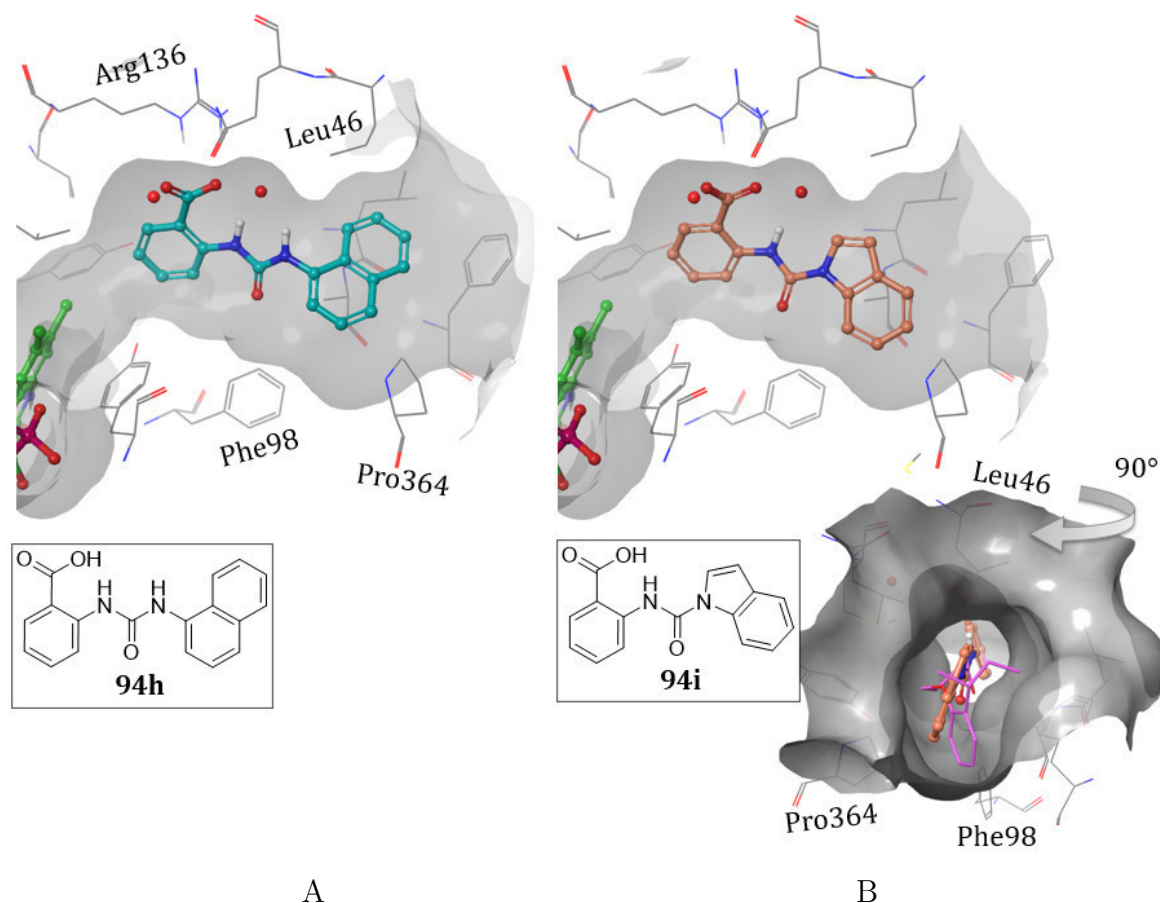
Figure 5.58: Docking poses of A: naphthyl derivative **94h** (turquoise) and B: indole derivative **94i** (orange) in the hDHODH binding site of KP-CF39 (pink, thin tubes).

Both, naphthyl derivative **94h** and indole derivative **94i** appear to fill the pocket better than their respective, non-annulated precursor compounds. Thus, these two structures were selected for synthesis and investigation.

However, a complete space filling of the bulge, as observed for the sterically demanding *sec*-butyl phenol moiety in KP-CF39 **22**, was not expected to be realised by these derivatives. An overlay of the docking pose of indole derivative **94i** (orange) with the

cocrystallised pose of KP-CF39 **22** (pink) is also shown in figure 5.58B, viewing from the direction of the binding pocket opening. It demonstrates that the flexible alkyl linker in KP-CF39 **22** allows the phenoxy arene to take a deeper positioning in the binding pocket bulge, resulting in a larger area of lipophilic interactions and thus, presumably, higher binding affinity.

Thus, a second task for cycle 2 was to design a ligand in which a newly introduced phenyl moiety would occupy the binding site of the *sec*-butylphenoxy substituent in KP-CF39 **22**. Although, for this purpose, many different linkers were coupled in various substitution patterns to both initial lead structures **94c** and **e**, *in silico*, the desired positioning of the phenyl substituent in the binding pocket was unique to structure **34** (see chapter 5.3). Associated difficulties emanated from a kink in the binding pocket that complicated the design of rigid ligands, as discussed in chapter 5.3.

However, introducing an ether substituent at 3-position of the pyrrole ring, which would have been required for the synthesis of design **34**, was considered to be synthetically hardly feasible and corresponding derivatives or precursors were commercially not available. Contrarily, 3-substituted pyrazole derivatives were commercially available and consequently, a pyrazole fragment was expected to be a more convenient ligand scaffold. Therefore, it was initially investigated in a docking experiment, whether replacing the pyrrole substituent in lead structure **94c** against a pyrazole substituent (compound **94j**) would preserve its inhibition potency.

For the compounds of cycle 2, higher binding affinities were expected than for those of cycle 1. In order to obtain demonstrative inhibition values, therefore, these compounds were added in final concentrations of 1 µM to the enzyme and the percentual amount of enzymatic activity was determined. The plotted results are shown in figure 5.59. For comparison reasons, lead compounds **94e** and **c** of cycle 1 were also tested at this concentration.

Expanding phenylureido derivative **94e** by an annulated benzene to naphthalenylureido derivative **94h** resulted in a strong increase of hDHODH inhibition from 33 % to 82 % at an inhibitor concentration of 1 µM. Indole derivative **94i** also showed a significantly higher inhibition potency, compared to the non-annulated pyrrole derivative **94c**, that only inhibited hDHODH activity by 1 % at 1 µM concentration. However, with 26 % inhibition, indole derivative **94i** was much less potent than naphthyl derivative **94h** and even slightly worse than its lead structure **94e**. Compared to the latter, it moreover has a higher molecular weight and a higher lipophilicity, neither of which would be
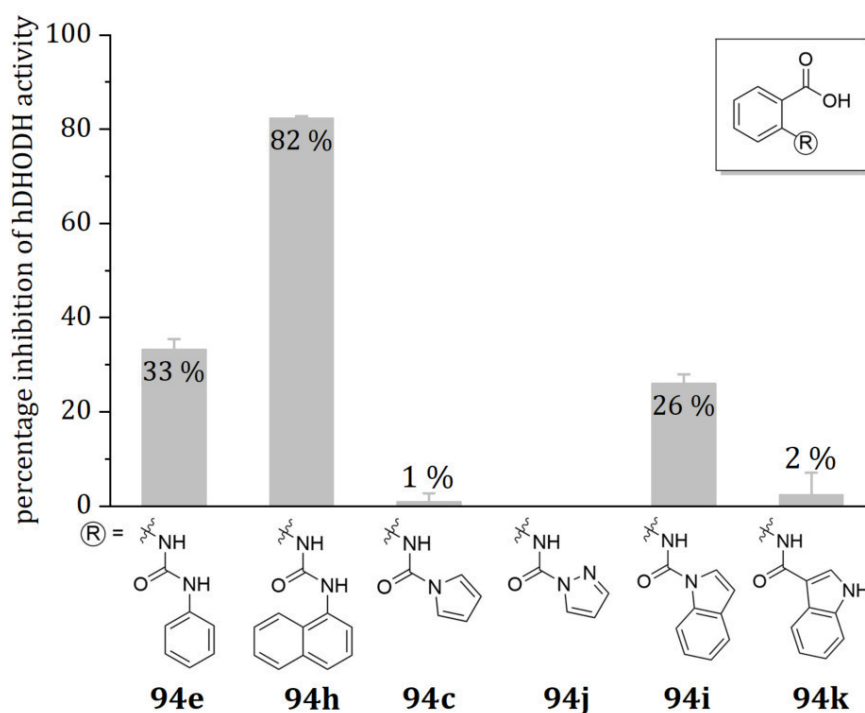
Figure 5.59: Percentage inhibition of hDHODH activity in presence of all compounds designed in cycle 2. 50 mM Tris-HCl, pH 8.0, 0.1 % Triton X-100, 100 nM L-DHO, 25 nM CoQ1, 60 nM DCPIP, 1 µM test compounds, 25 °C.

advantageous for future inhibitor design. Therefore, lead development based on indole derivative **94i** was not further pursued, here.

Moreover, a constitutional isomer of indole derivative **94i** was examined, in which the indole fragment was coupled to the amido function via its 3-position (**94k**). This modification resulted in a strong loss in activity, probably due to an interruption of the hydophobic interaction area, induced by the accessible amino function.

For pyrazole derivative **94j**, unfortunately, no enzymatic inhibition was observed at all, neither at a concentration of 1 µM, nor at 10 µM (not shown). Therefore, this approach was not further pursued, here.

Consequently, from cycle 2, ligand **94h** emerged as most potent inhibitor and novel lead structure.

5.4.3 X-ray crystallographic investigation of the binding pose of novel lead structure 94h

In order to develop a solid basis for the rational design of cycle 3, the novel lead structure **94h** was co-crystallised with the enzyme and the structure of the resulting complex was determined via X-ray crystallography.

For this purpose, initially, the previously prepared His$_6$-tagged hDHODH (see chapter 5.2.1) was treated with the detergents Zwittergent 3-10 and HEGA-8, which were shown to improve crystallisation by DAS *et al.*.[149] Subsequently, inhibitor **94h** and natural substrate DHO **2** were added in twofold excess and the resulting enzyme mixture was treated with a reservoir solution in 1:1 v/v ratio. This ratio was investigated to be optimal for crystallisation of the used enzyme batch, in prior studies.[187] In order to discover optimal crystallisation conditions for this specific enzyme-ligand complex, reservoir solutions with varying concentrations of sodium acetate, ammoniumsulfate, sodium chloride and glycerol were added to the enzyme-ligand mix in each well of a 96-well plate. The formation of crystals was observed after three day incubation with 0.1 M sodium acetate, 2.9 M ammonium sulfate and 10 % glycerol. After 40 days incubation the fully grown crystals were harvested, cryo-protected and irradiated at X-ray beamline P14 at DESY Hamburg, kindly supported by G. BOURENKOV. An image of the fully grown crystals is shown in figure 5.60A.

A   B
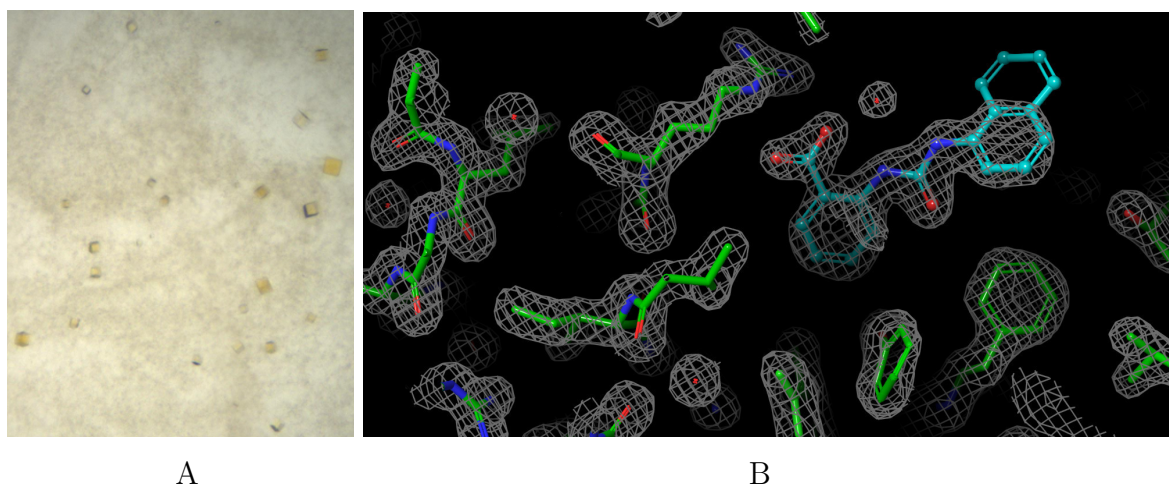
Figure 5.60: A: Crystals of hDHODH-ligand **94h**-complex, grown for 40 days at 0.1 M NaOAc, 2.9 M NH$_4$SO$_4$, 10 % glycerol, 20 °C. B: Electron density map (2Fo-Fc) and refined molecular structure of the cocrystallised complex (hDHODH-**94h**), determined by X-ray crystallography.

The protein was observed to crystallise in $P3_121$ space group. An electron density map with a resolution of 1.9 Å was calculated from the obtained diffraction data set and refined with the fitted atomic model of PDB-entry 1D3G[87]. As expected, inhibitor **94h** bound to the hydrophobic access tunnel for ubiquinone **8** and, thus, occupied the binding site of a panel of other known inhibitors (see chapter 3.4), including KP-CF39 **22** (see chapter 5.3). An excerpt of the determined structure with overlaid electron density map is visualised in figure 5.60B, which shows the novel lead structure's binding pose (turquoise). The high resolution diffraction data enabled a precise positioning of the ligand as well as the surrounding protein side chains (green). However, the electron density map did not reveal the exact conformation of the ligand's naphthyl substituent. Apparently, its distance to surrounding protein side chains allowed its rotation to a certain degree, which resulted in various ligand conformations present within the irradiated crystal and thus a blurred electron density. A selection of ligand conformations, that were obtained by manually rotating the naphthyl substituent within limits tolerated by the enzyme, is shown in figure 5.61A, viewing from the direction of the binding pocket opening.
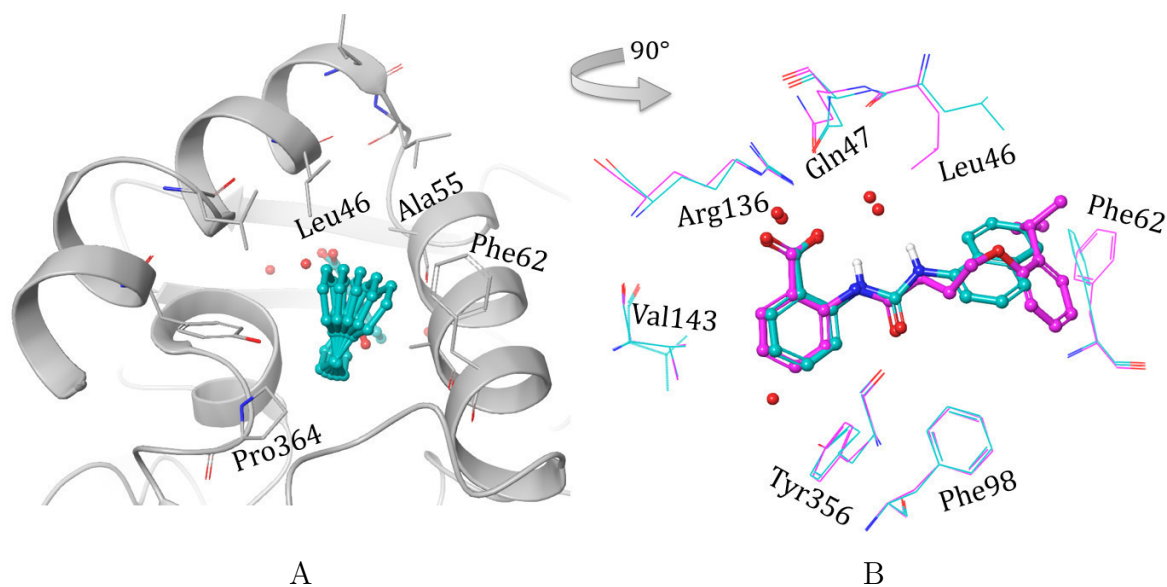
Figure 5.61: A: Tolerated conformations of the naphthyl substituent of ligand **94h** in the enzyme's crystallised binding pocket. B: Overlaid binding poses of KP-CF39 **22** and ligand **94h**.

Figure 5.61B shows the overlaid binding poses of KP-CF39 **22** (pink) and novel lead compound **94h** (turquoise). The 2-amidobenzoic acid fragment of both ligands arranged almost congruently. Regarding the protein side chains, a strong conformational change of Leu46 can be observed, as well as a slight rotation of Phe62. The flipping of Leu46

probably enabled a more relaxed fit of naphthyl derivative **94h** in the binding pocket and thus preserved the ionic interaction of the carboxy function. The rotation of Phe62 probably enhanced lipophilic interactions with the naphthyl moiety. Similar to the X-ray structure of KP-CF39 **22**, two water molecules crystallised in close proximity to the carboxy moiety of the ligand. Furthermore, another water molecule crystallised below the anthranilic acid arene of compound **94h**, probably due to a minimal shift of the arene in the pocket, which provided the water molecule with its required space.
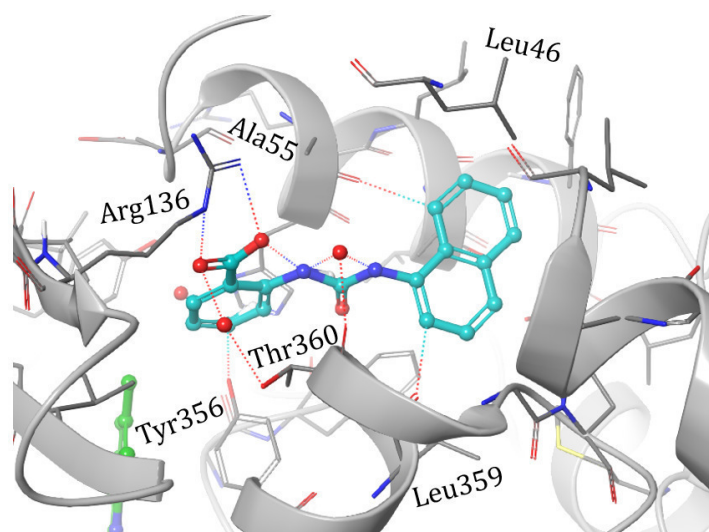
Figure 5.62: Inspection of the formed interactions of bound ligand **94h** in its binding site of hDHODH.

Figure 5.62 shows interactions, that were formed between protein and ligand. Besides the hydrogen bonding interactions, that were already observed for KP-CF39 **22** (see chapter 5.3), the second amino functionality of the ureido moiety additionally interacts with one of the water molecules, as suspected (see chapter 5.3). Moreover, three aromatic hydrogen bonds to Tyr356, Ala55 and Leu359 contribute to binding and confirm the suitability of the naphthyl substituent.

5.4.4 Cycle 3 of lead structure development

After having explored the size and nature of tolerated ring substituents at the amido or ureido function in cycle 1 and 2, the anthranilate scaffold was modified in cycle 3, intending to further improve binding affinity. The determined binding pose of cocrystallised ligand **94h** (see fig. 5.61B) served as model for the rational design.

Its closer inspection revealed the spatial proximity of the polar side chain of Tyr356 to the non-substituted, rather lipophilic part of the anthranilate ring. Modifying the ligand structure with a suitable polar functionality at this position was considered to not only increase binding affinity by introducing an additional intermolecular interaction, but also to benefit the ligand's specificity to its target enzyme. Moreover, the lead structure's overall hydrophilicity would increase by such modification and thus compensate the introduction of lipophilic moieties in the course of future lead optimisation.
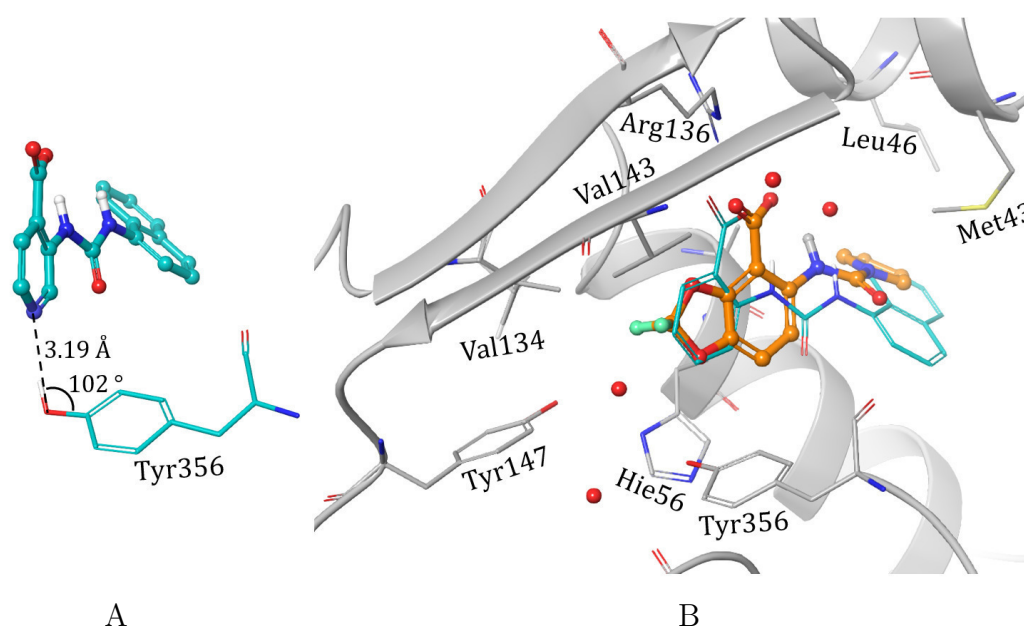
Figure 5.63: A: Geometric inspection of a hypothetically formed interaction between Tyr356 and a pyridine nitrogen atom, which was introduced into the structure of cocrystallised ligand **94h**, *in silico*. B: Docking pose of structure **96** (orange), overlaid to the crystallised binding pose of lead structure **94h** (turquoise, thin tubes).

The most evident modification was to replace the C-4 carbon atom, whose proton points towards the target hydroxy function of Tyr356, by a pyrimidine nitrogen atom, which was introduced into the structure of cocrystallised ligand **94h**, *in silico*, as shown in figure 5.63A. The distance between the newly introduced nitrogen atom and the oxygen atom of Tyr356 was determined to 3.19 Å. This distance is longer than the optimal distance of about 2.8 Å[50] which would be required for the formation of such hydrogen bond. Moreover, the measured angle of 102° is smaller than the required angular preference of about 150°[50] for hydrogen bonding. However, it must be considered that an X-ray structure is merely a snapshot of the enzyme in its crystallised state and does not at all fully represent its solvated, moving state. Even a slight movement

of the enzyme may lead to the formation of this desired hydrogen bond interaction. Considering this, structure **97** (figure 5.64) emerged as first design of this cycle.
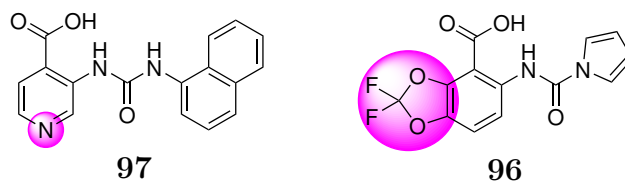
Figure 5.64: Structures of the two designs of cycle 3.

From the *in silico*-exploration of further modifications at the anthranilate ring, a promising scaffold emerged, that bears a fluorinated benzodioxole moiety. The docking pose of a corresponding derivative is shown in figure 5.63B and its structure **96** in figure 5.64. In its docking pose, one benzodioxole oxygen atom exactly occupies the site of the C-4 atom of the binding pose of ligand **94h**. Thus, the formation of a hydrogen bond is conceivable here, too. Moreover, the dioxole substituent seems to adapt well to the hydrophilic site of the binding pocket with its hydrophobic cap, which was predicted to be occupied by the fluorine substituents (see chapter 3.4). The introduction of the two fluorine substituents will presumably prevent chemical or enzymatic decomposition of the dioxole substituent. The docking pose moreover suggests that the arrangement of the original anthranilate fragment in the binding site will be strongly distorted by this modification. However, favourable interactions are still conceivable.

In order to evaluate the effect of the introduced dioxole fragment on the ligand's inhibition strength, pyrrole was chosen as amido substituent, although an indole substituent would have promised stronger inhibition (see fig. 5.59). It was assumed that by using the smaller pyrrole substituent, the effect of the described distortion on binding affinity could be reduced and thus, an approximately isolated evaluation of the effect of the benzodioxole unit would be more feasible.

For benzodioxole derivative **96** no inhibition of hDHODH activity was found at a concentration of 1 µM. Thus, at least for the specific example of a pyrrole-based ligand, the benzodioxole modification did not induce an improvement of inhibition strength. Nevertheless, it is still conceivable that such improvement may be realised when using a more flexible ureido substituent. However, this was not tried, here.
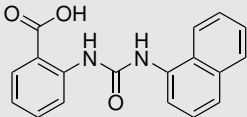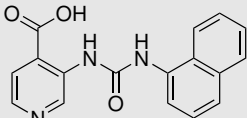
The hDHODH inhibition potency of isonicotinic acid derivative **97** was determined to 91 % at a concentration of 1 µM. Thus, it is a strong inhibitor and even more potent than its analogue and lead structure **94h** without aromatic nitrogen atom (table 5.14).

5 Results and discussion

In a seperate experiment, its IC_{50} value was calculated to 89 ± 8 nM.

Overall, the lead structure development procedure resulted in two potent hDHODH inhibitors **94h** and **97**. Their pharmacokinetic properties were investigated as described in chapter 5.1 and the results are listed in table 5.14.

Table 5.14: hDHODH inhibition potencies, metabolic stabilities (S_{S9}), percentage compound amount remaining within 1 h incubation in rat S9 mix), lipophilicities (logD) and PAMPA-permeabilities (P_{PAMPA}) of the two novel lead compounds **94h** and **97**

Compound	hDHODH inhibition at 1 μM [%]	S_{S9} [%]	logD	P_{PAMPA} [$\cdot 10^{-5}$ cm/s]
94h	82 ± 0	84.4 ± 1.6	1.019 ± 0.004	1.15 ± 0.14
97	91 ± 2	89.6 ± 1.5	0.323 ± 0.002	0.684 ± 0.037

For compound **94h**, a metabolic stability of 84.4 % was determined after one hour incubation in S9 mix. The formation of one metabolite, presumably a hydroxylation product, was observed. The higher metabolic stability of 89.6 % of isonicotinic acid derivative **97** is probably related to its lower overall lipophilicity.

LogD values of 0.323 and 1.019 rate the two compounds as rather hydrophilic, but still in the range of suitable druggability (see chapter 5.1). Despite these low logD values, good membrane permeation was observed, especially when compared to the inhibitors investigated in chapter 5.3 and in particular for compound **94h**.

Consequently, both compounds are not only potent hDHODH inhibitors but also have suitable pharmacokinetic *in vitro* properties, rendering them promising novel lead structures with high potential.

For future lead optimisations, the naphthyl carbon atoms C-5 and particularly C-7 and

C-8 are considered suitable for functionalisation. Lipophilic, electron-withdrawing moieties are recommended as substituents. This will presumably increase the permeability on the one hand and the stability against metabolic hydroxylation on the other.

5.4.5 Synthesis

Reference compound **18** was successfully obtained in a two step synthesis procedure which is shown in figure 5.65.
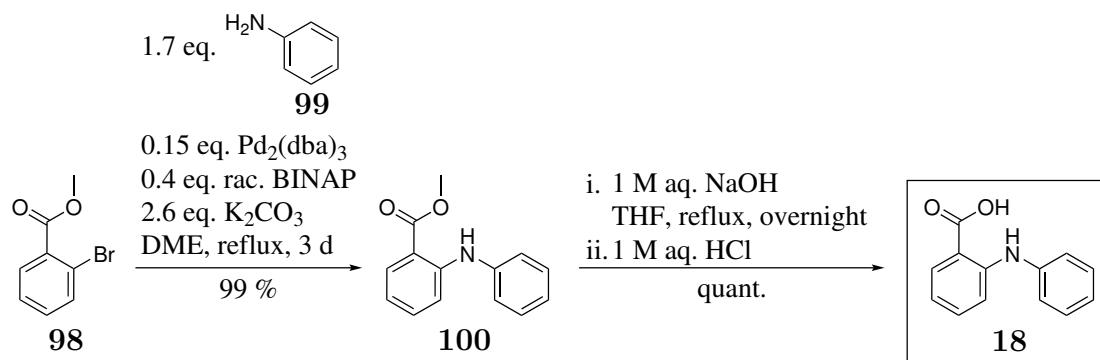
Figure 5.65: Synthesis of fenamic acid based reference inhibitor **18**.

In the first step, bromide **98** and aniline **99** were coupled via Buchwald-Hartwig[188, 189] amination, following a general protocol[190] of LAUBACH. Tris(dibenzylideneacetone)dipalladium (Pd$_2$(dba)$_3$) was used as precatalyst, (*rac*)-2,2'–bis(diphenylphosphino)–1,1'–binaphthyl (BINAP) as ligand, potassium carbonate as base and dimethoxyethane (DME) as high-boiling solvent to enable reaction temperatures up to 85 °C. Methylester **100** was obtained in 99 % yield after three day stirring, aqueous workup and column chromatographic purification.

The reaction mechanism which was postulated by BUCHWALD *et al.*[191] is shown in figure 5.66. First, the catalytically active Pd^0 species was generated via ligand exchange of the dibenzylideneacetone ligands against a BINAP ligand. In a process called oxidative addition, the metal atom inserted into the C-Br bond of aryl bromide **98** (deprotonation). Subsequently, amine **99** bound to the metal ion (amination) and potassium carbonate eliminated hydrogen bromide from the complex. Finally, biarylamine **100** was reductively eliminated from the complex under regeneration of the catalyst.
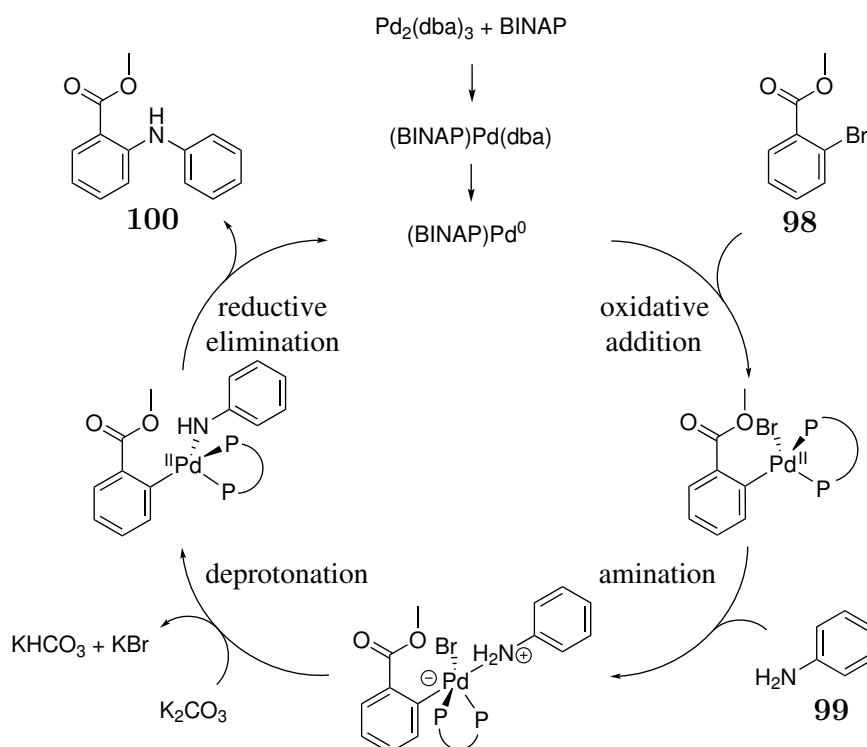
Figure 5.66: Mechanism of the Buchwald-Hartwig cross coupling between bromide **98** and aniline **99**.

After successful synthesis of methyl ester **100**, the protecting methyl group was finally cleaved under common saponification conditions to yield target compound **18** quantitatively and in high purity after recrystallisation. Thus, reference compound **18** was obtained in an overall yield of 99 % over two steps.

The synthesis of all other anthranilate-based target compounds **94a-k** of this chapter was carried out via one of the three routes shown in figure 5.67.
On routes A and B, a methyl group was chosen to protect the free anthranilate carboxy function during coupling reactions. Thus, target compounds **94a-d** and **g-j** were retrosynthetically derived from the respective methylated precursors **101a-d** and **g-j**. Amido-based esters **101a,b,g** and **h** might be synthesised by amide coupling reactions of methyl anthranilate **62** and carboxylic acids **102a,b,g** and **h** (route A). The ureido moiety in esters **101c,d,i** and **j** (route B) might be established by coupling reactions of methyl anthranilate **62**, triphosgene **63** and the respective secondary amines **103c,d,i** and **j**.
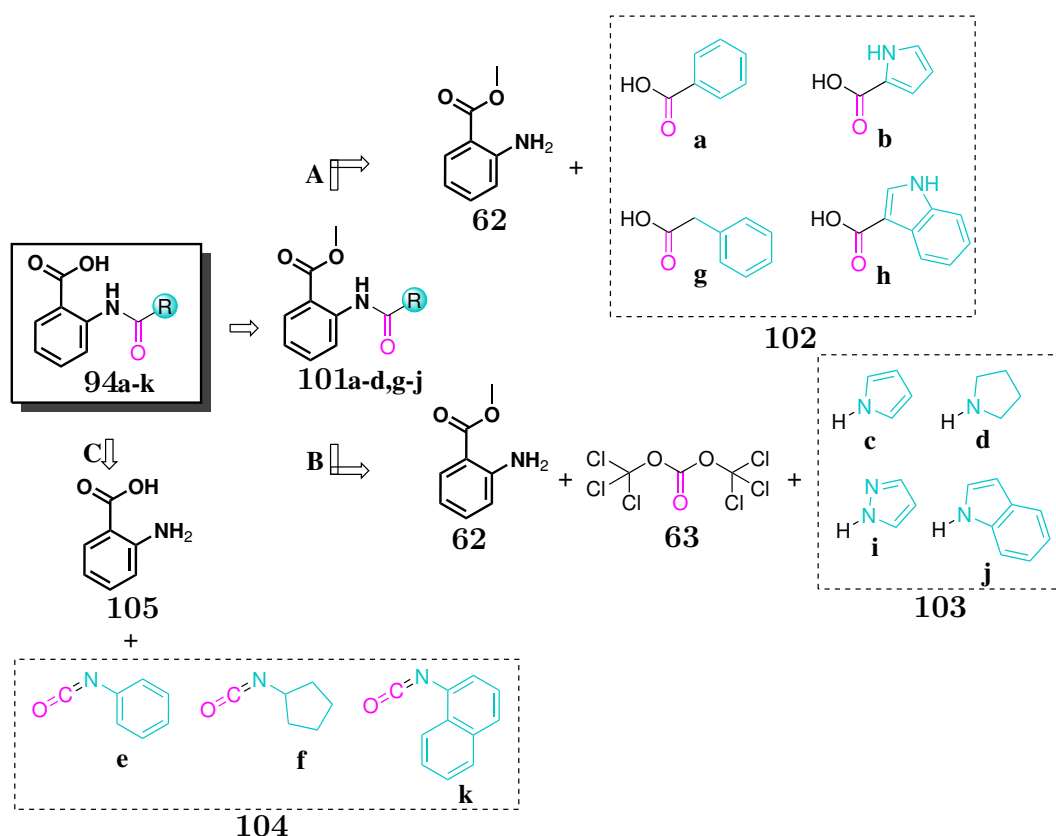
Figure 5.67: Retrosynthesis scheme to amides **94a**,**b**,**g** and **h** (route A) and ureides **94c**,**d**,**i**,**j** (route B) and **94e**,**f**,**k** (route C).

It was previously observed that 2-ureido benzoates cyclise to quinazolinediones under basic conditions, due to deprotonation of the ureido nitrogen atom that afterwards nucleophilically adds to the carboxy carbon atom to form a six-membered ring (see chapter 5.3.6). Since this nitrogen atom is doubly substituted in compounds **94c**,**d**,**i** and **j** as well as their precursors **101c**,**d**,**i** and **j**, deprotonation was impossible and thus, deprotection under basic conditions was regarded realisable. Contrarily, for the same reason methylanthranilate **62** was regarded unsuitable as starting material for the synthesis of inhibitors **94e**,**f** and **k** (route C) with doubly protonated ureido functions. Instead, it would have been conceivable to apply the already proven approach of using a benzyl protecting group (see chapter 5.3.6) for their synthesis. However, a simpler and faster approach was offered by route C, in which a coupling reaction of commercially available isocyanates **104e**,**f** and **k** with unprotected anthranilic acid **105** was intended to give target compounds **94e**,**f** and **k** in a single step. However, this approach was not only assumed to offer a simple access to these target compounds, but moreover to isonicotinic acid derivative **97** (not shown), whose benzyl-protected precursor was commercially not available.

Route A

Amides **94a**,**b**,**g** and **h** were synthesised via route A, following the established, general protocol[122, 124, 125] which was already used in chapter 5.3.6 for the preparation of amide **29**. The according reaction conditions are shown in figure 5.68 and the achieved yields are listed in table 5.15.
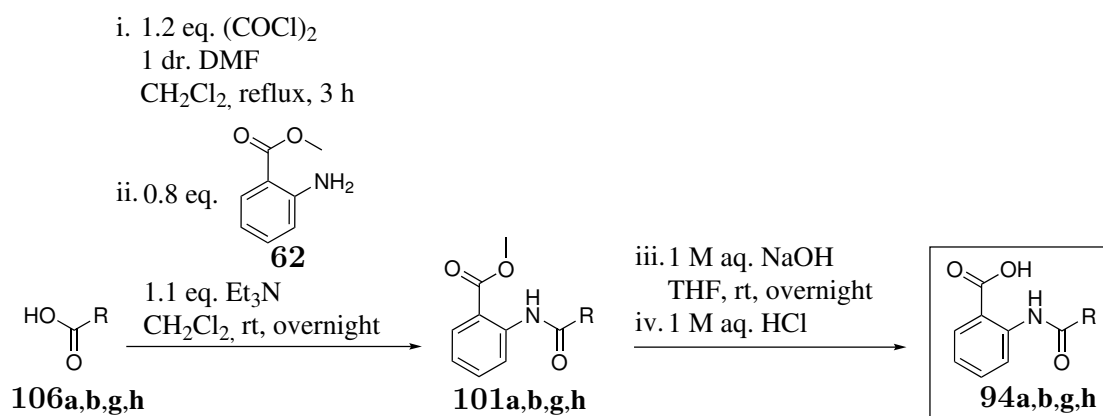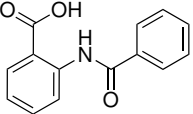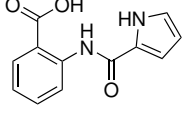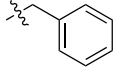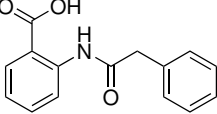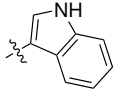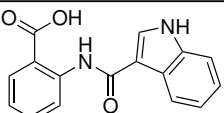
Figure 5.68: Syntheses of 2-amidobenzoic acid based inhibitors **94a**,**b**,**g** and **h**.

All coupling reactions (steps i. and ii.) succeeded in good to quantitative yields. Compared to the previously described, analogous coupling reaction with alkyl alcohol **39** (see chapter 5.3.6, fig. 5.25), higher yields were achieved, here. One possible reason for this discrepancy is the electron-withdrawing effect of the aromatic α-substituents R, which apparently increased the reactivity of the carbonyl carbon atom towards initial chlorination (i.) and subsequent coupling (ii.). However, the comparably lower yield for indole derivative **101h** probably resulted from the bad solubility of its starting material $1H$-indole-3-carboxylic acid **106h** in the reaction medium.

Target compounds **94a**,**b**,**g** and **h** were subsequently obtained under common ester hydrolysis conditions (steps iii. and iv.) and final recrystallisation in good to very good yields of 70-97 %.

Table 5.15: Yields obtained for the syntheses of 2-amidobenzoic acid derivatives **101** and **94a**,**b**,**g** and **h** (fig. 5.68).

R	Starting material	Yield steps i./ii.	Product steps i./ii.	Yield steps iii./iv.	target compound
	106a	99 %	**101a**	70 %	 **94a**
	106b	93 %	**101b**	97 %	 **94b**
	106g	quant.	**101g**	76 %	 **94g**
	106h	70 %	**101h**	85 %	 **94h**

Route B

Ureides **94c**, **d**, **i** and **j** were synthesised in two steps following route B. In the first step, the ureido functions were established by triphosgene-mediated coupling. For this purpose, the protocol, that was successfully used for the synthesis of ureido-based precursor compounds **88a-f** and **89a-c** (chapter 5.3.6), was slightly adjusted. Here, methyl anthranilate **62** was used as starting material instead of benzyl anthranilate **87**, as the resulting methyl esters **101c,d,i** and **j** were considered not to cyclise under basic deprotection conditions in the final step. After the formation of 2-isocyanatobenzoic acid **64** and the removal of volatile components in the mixture, the residue was treated with the respective amine, either in its original or its deprotonated and thus activated form.

Aliphatic pyrrolidine **103d** was added without prior activation, as its nucleophilicity was considered sufficient for a reaction with 2-isocyanatobenzoic acid **64** (figure 5.69). After stirring at room temperature for 15 h, aqueous work-up and column chromatographic purification, methyl ester **101d** was obtained in a very good yield of 88 %, calculated in relation to the amount of added amine. Compared with the yields that were obtained for analogous coupling reactions with benzyl anthranilate as starting material (see chapter 5.3.6), this yield was higher, especially considering the short reaction time of step i.. Apparently, the lower steric demand of the methyl protecting moiety resulted in a faster conversion of methyl anthranilate.
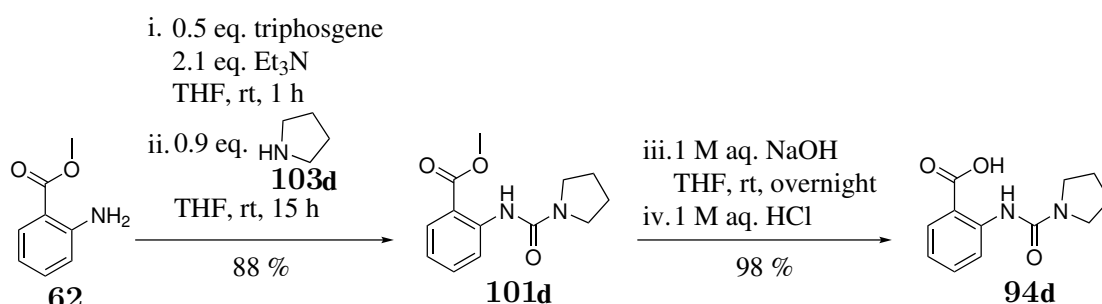
Figure 5.69: Synthesis of pyrrolidine-based target compound **94d**.
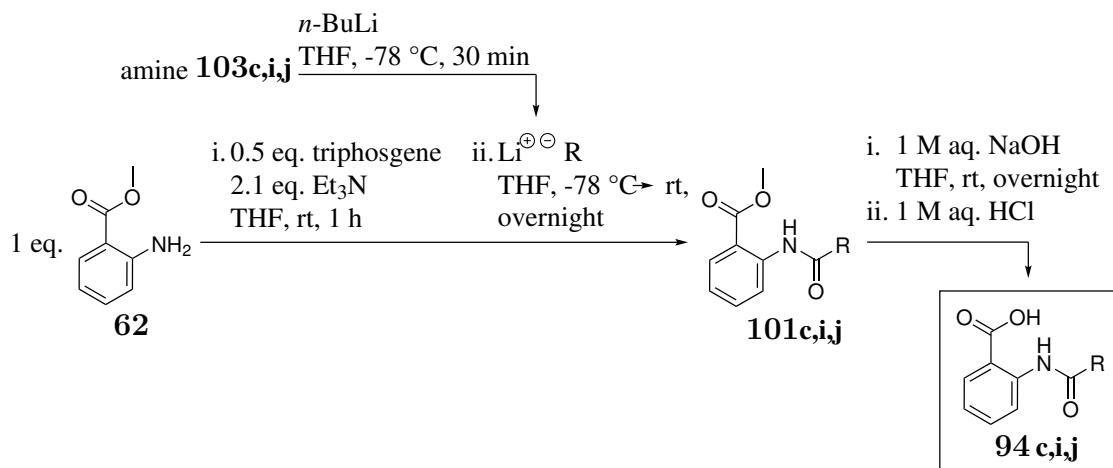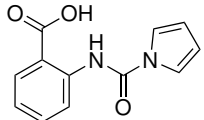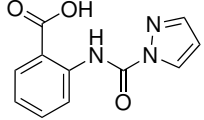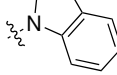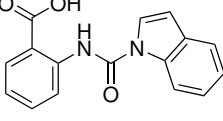
Figure 5.70: Synthesis of 2-ureidobenzoic acid based inhibitors **94c,i** and **j**.

In the structures of the other amines pyrrole **103c**, pyrazole **103i** and indole **103j** electrons of the nitrogen atom are delocalised in the aromatic system. Therefore, they were not available for a nucleophilic addition to isocyanate **64**. Consequently, their previous deprotonation using *n*-butyllithium (*n*-BuLi) was intended to provide them with sufficient nucleophilicity for this reaction. The corresponding reaction scheme is shown in figure 5.70. Due to the good conversion of methyl anthranilate **62** in

the previous reaction (see fig. 5.69), methyl anthranilate **62** was used as limiting reactant, here. 1.5 equivalents of *n*-butyllithium were used, aiming to achieve a complete deprotonation of the added 1.4 equivalents of pyrrole **103c** or indole **103j**.

Table 5.16: Yields obtained for the syntheses of 2-ureidobenzoic acid derivatives **101** and **94c,i** and **j** (fig. 5.70).

R	Amine	Yield step 1	Product step 1	Yield step 2	target compound
	103c	44 %	**101c**	99 %	**94c**
	103i	87 %	**101i**	33 %	**94i**
	103j	66 %	**101j**	quant.	**94j**

Unfortunately, this excess of *n*-butyllithium lowered the yield of desired products **101c** and **j** to 44 % and 66 %, due to the formation of a by-product, which was identified as methyl pentanamidobenzoate **107** (see fig. 5.71) by NMR-spectroscopic and mass-spectrometric analysis. It was formed through a nucleophilic addition of excess *n*-butyllithium **108** at 2-isocyanatobenzoic acid **64**, followed by protonation of salt **109** during aqueous workup (figure 5.71).
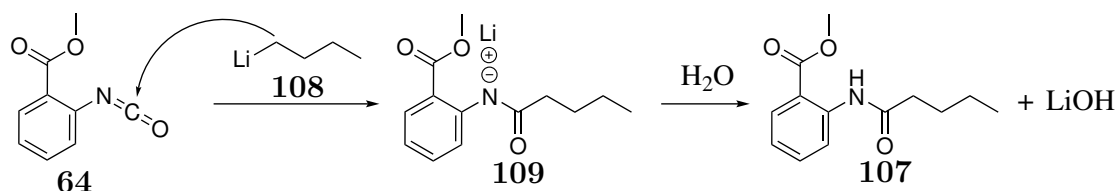
Figure 5.71: Mechanism for the formation of by-product **107**.

Consequently, pyrazole **103i** was used in excess (1.5 equivalents) over *n*-butyllithium (1.4 equivalents) for its coupling reaction (see fig. 5.70). With this approach, methyl

ester **101i** was achieved in a very good yield of 87 % (see tab. 5.16).

Final deprotection under basic condition, followed by acidification, resulted in the quantitative formation of target compounds **94c**,**i** and **j** (see fig. 5.70 and tab. 5.16), which were all achieved in high purity after aqueous workup and recrystallisation. However, the ester hydrolysis of pyrazole derivative **101** resulted in the formation of two by-products besides desired product **94i**, which was obtained in a moderate yield of 33 %, only. The by-products were identified as methyl anthranilate **62** and anthranilic acid **105**. Presumably, besides the desired methylester hydrolysis, the hydroxy anion nucleophilically added to the ureido-carbon atom under elimination of a pyrazolid anion, followed by spontaneous decarboxylation of both products **110** and **111**. In contrast to pyrrole, the additional heteroatom in pyrazole improves charge stabilisation, thus making it a better leaving group.
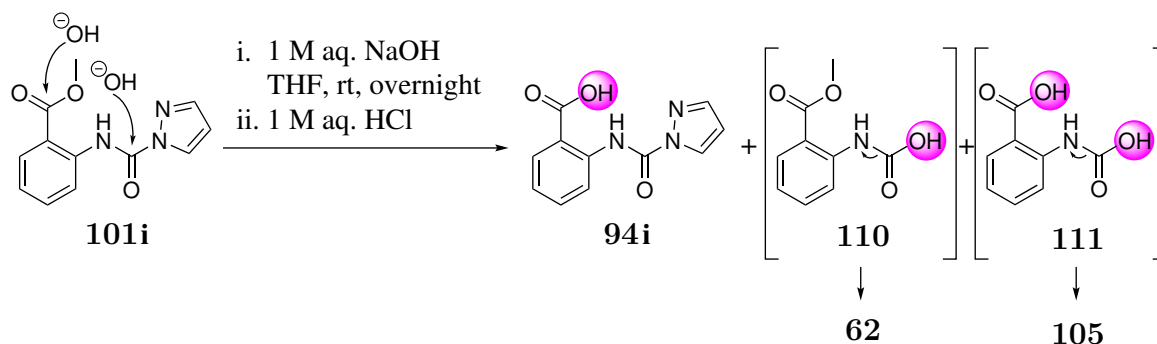
Figure 5.72: Structures of desired product **94i** and assumed intermediates **110** and **111** that formed during the hydrolysis of compound **101i**.

The synthesis of benzodioxole derivative **96** also followed route B, using 5-aminobenzodioxole-4-carboxylic acid **112** as amine. This compound was previously prepared from commercially available 2,2-difluorobenzo-1,3-dioxole **113** as part of M. HOFMANN's bachelor thesis [P8].[192] Its synthesis planning is summarised in figure 5.73.

The carbonyl function may be introduced by a formylation reaction at the 4-position. Subsequent oxidation followed by esterification was intended to lead to the desired methyl ester moiety. The amino function at 5-position may be obtained via hydrogenation of a nitro moiety, which may be previously introduced via nitration.
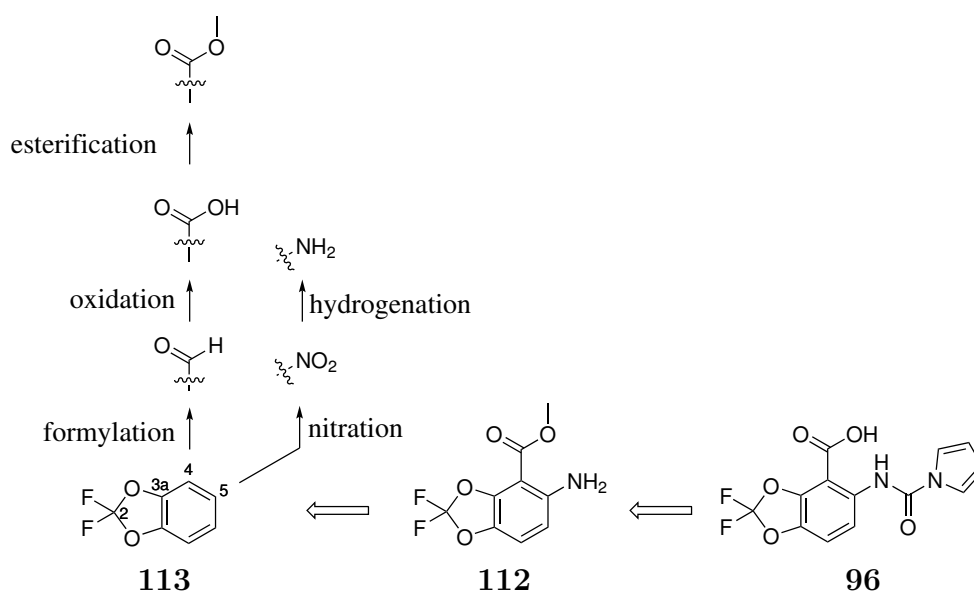
Figure 5.73: Retrosynthesis scheme of benzodioxole derivative **96**.

Figure 5.74 shows the established route as well as reaction conditions and yields of the single synthesis steps that successfully lead to amine **112**. The nitration reaction and subsequent separation of its formed regioisomers emerged as key step of the synthesis procedure. For this reaction, formylated benzodioxole derivative **114** proved to be a
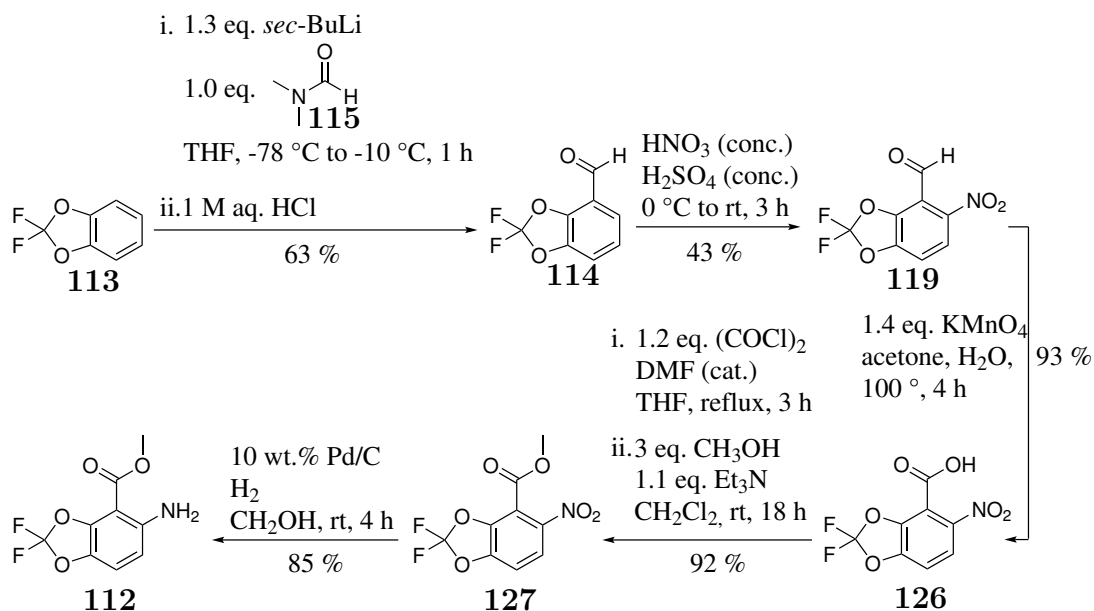

Figure 5.74: Procedure, conditions and yields for the synthesis of aminobenzo-1,3-dioxole-4-carboxylic acid **112**.

suitable starting material as its nitration products were separable via column chromatography, which could not be realised after ester formation.[192] The amino function was introduced in the last step, in order to prevent side reactions.

The regioselective *ortho*-formylation of fluorinated benzodioxole **113** has been established and published by Schlosser *et al.*.[193] Following this protocol, the *ortho*-position of benzodioxole derivative **113** was initially deprotonated and lithiated with *sec*-butyllithium at -78 °C and subsequently formylated through the addition of *N,N*-dimethylformamide **115** and hydrochloric acid. In deviation of the published protocol, *sec*-butyllithium was used in a slight excess of 1.3 equivalents.

The detailed reaction mechanism is shown in figure 5.75. Immediately after its addition to the reaction mixture, *sec*-butyllithium **116** coordinated to one of the dioxole oxygen atoms and selectively deprotonated the adjacent carbon atom. Thereby, *n*-butane was formed as well as lithiated arene **117** in which the metal ion still was coordinated to the dioxole oxygen atom. Through a nucleophilic addition of the negatively charged carbon atom to the carbonyl carbon atom of added *N,N*-dimethylformamide **115**, tetrahedral intermediate **118** was formed. Final treatment with hydrochloric acid solution resulted in the elimination of dimethylammonium chloride under formation of aldehyde **114**.
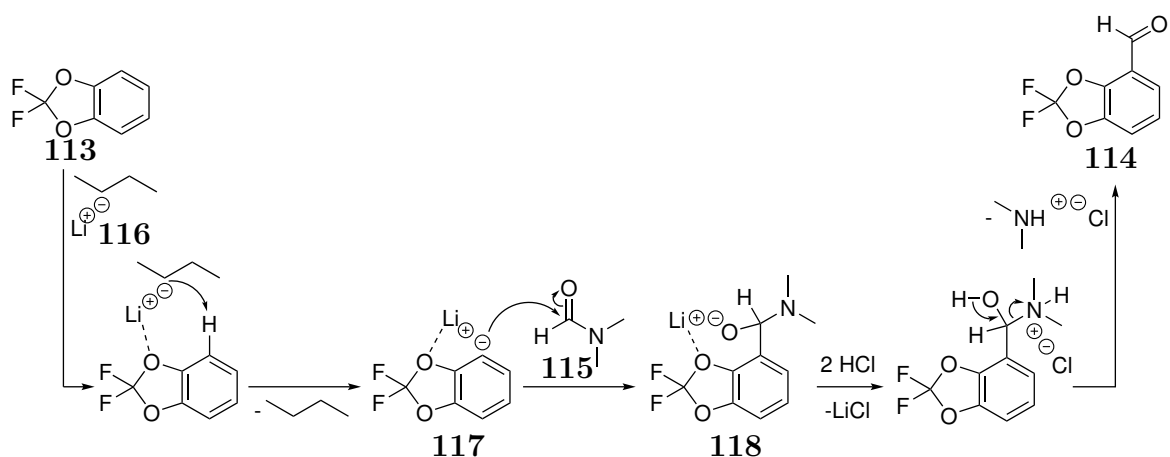
Figure 5.75: Mechanism for the *ortho*-formylation of 2,2-difluorobenzo-1,3-dioxole **113**.

The product was obtained in a yield of 63 % after column chromatographic purification and the published yield of 88 %[193] could not be achieved. Due to the low boiling point of aldehyde **114** (73 °C)[193] compound losses during final solvent evoparation could not be prevented. Moreover, aldehyde **114** was found to be strongly sensitive to oxidation by atmospheric oxygen. Even at 4 °C, the precipitation of a colorless solid was observed,

which was identified as the respective carboxylic acid derivative. In further synthesis attempts, it was observed that an excessive addition of *sec*-butyllithium lead to a twofold formylation of the starting material **113** and thus should be avoided.

The nitration of aldehyde **114** succeeded under *in situ* generation of nitrating acid by successive addition of concentrated nitric acid and concentrated sulphuric acid to the starting material at 0 °C. In contrast, treatment with nitric acid or a mixture of nitric acid and acetic anhydride did not result in the formation of desired product **119**.[192] Two nitration isomers were formed which were isolated by column chromatographic purification on silica gel. *Ortho*-nitrated product **119** was obtained in a yield of 43 %. Its identification was supported by 2D-NMR spectroscopy and single-crystal X-ray analysis (figure 5.76A). The second isomer was identified as *meta*-nitrated product **120** and obtained in a yield of 53 %. Compared to the vicinal aromatic protons of *ortho* product **119**, smaller coupling constants were observed for the two aromatic proton signals, thus supporting their relative meta-positioning. Figure 5.76B shows the ^{1}H-NMR spectrum of the crude product mixture measured before column chromatographic purification. Besides the difference in coupling constants, it can be observed that no *para*-nitrated product was formed during the reaction.
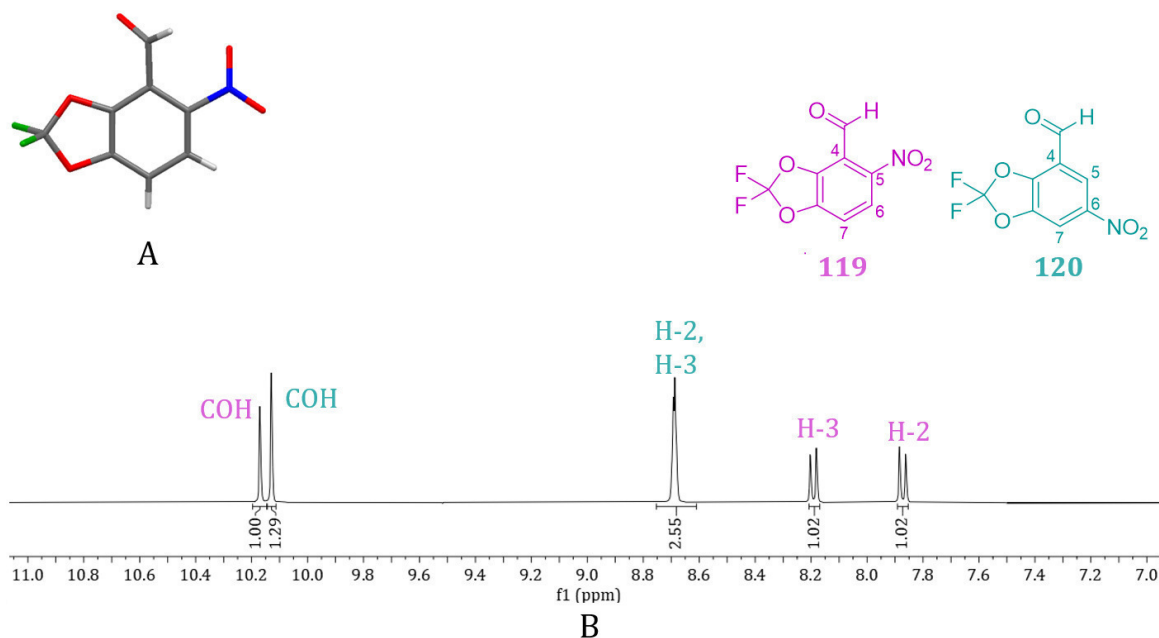
Figure 5.76: A: Three-dimensional structure of the desired nitration product **119**, determined by X-ray crystallography. B: ^{1}H-NMR spectrum of the crude product mixture of the nitration reaction before purification and structures of the later isolated isomers **119** and **120** (400 MHz, 25 °C, DMSO-d_6).

When considering the electronic properties and the steric hindrance of the aromatic carbon atoms, only, the yield of the obtained 5-nitro (*ortho*) product appears unusually high. The difluorodioxol substituent only has a minor influence on the nitration position, whereas aldehyde moieties direct nucleophilic aromatic substitutions to their *meta*-position by lowering electron density at *ortho*- and *para*-position. Moreover, the 5- and 7-positions are sterically shielded by the adjacent substituents and thus their reactivity is additionally reduced. Nitration of the 6-position thus would be strongly preferred. However, the aldehyde moiety even had a beneficial effect on C-5 nitration, as shown in figure 5.77, in which the mechanism of the *ortho*-favoured nitration is shown which was postulated by SAINZ-DÍAZ *et al.*.[194]

Initially, the reactive nitrating acid **121** was formed *in situ* by protonation and subsequent dehydratisation of nitric acid **122** by sulfuric acid. Subsequently, its positively charged nitrogen atom was electrophilically added to the carbonyl oxygen of aldehyde **114**. In the next step, the C-5 atom was nucleophilically added to the adjacent nitrogen atom under recovery of the aldehyde function. This reaction mechanism apparently proceeded in competition to the classical nucleophilic aromatic nitration at 6-position, which still slightly dominates. Thus, the addition of nitric acid in smaller quantity might favour *ortho*-nitration.
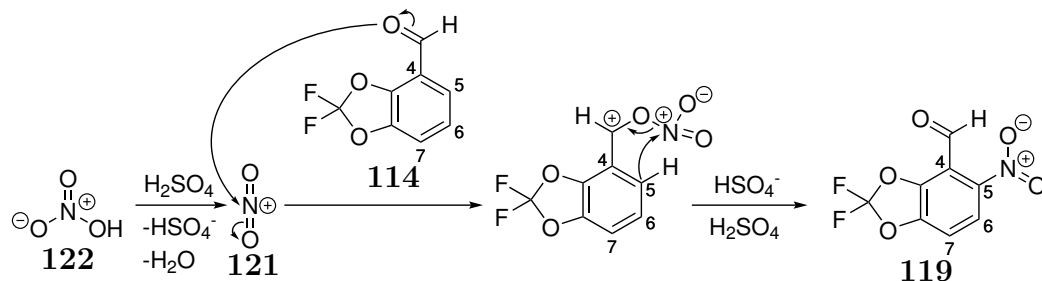
Figure 5.77: 5-Nitration mechanism of aldehyde **114**.

The subsequent oxidation of the aldehyde function to a carboxy moiety (see fig. 5.74) was carried out following a general protocol[195] of SAMANT *et al.*. Accordingly, aldehyde **119** was added to an aqueous solution of potassium permanganate and the mixture was stirred under reflux for four hours. Figure 5.78 shows the oxidation mechanism, which was derived from the literature.[198]

In aqueous solution, aldehydes are partly converted to their geminal diols by the nucleophilic addition of water, even though the equilibrium of this reaction lies far to the site of starting material.[168] One hydroxy function of this geminal diol **124** nucleophilically added to the metal ion of potassium permanganate **123** under elimination
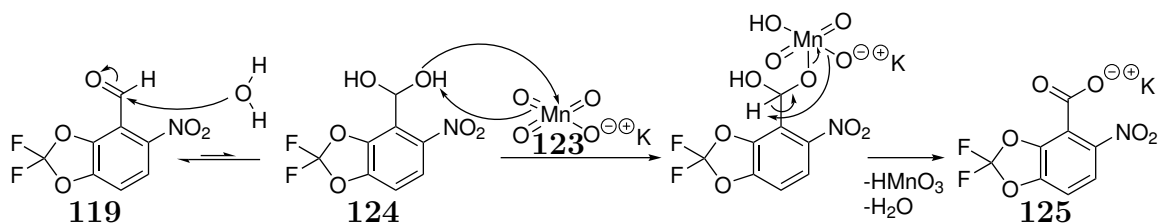
Figure 5.78: Mechanism of the KMnO$_4$-catalysed oxidation of aldehyde **119**.

of potassium hydroxide. Carboxylate **125** was subsequently formed under elimination of manganite **128** and water, spontaneously.[198] As the starting material was converted, the characteristical purple color of the reaction solution disappeared under precipitation of black, insoluble manganite. The solid was separated from the dissolved product by filtration after complete conversion of aldehyde **119**. Finally, the filtrate was acidified with hydrogen chloride to give carboxylic acid **126** in a very good yield of 93 %.

Before hydrogenation of the nitro group to an amino function, the carboxy function was protected by a methyl group (see fig. 5.74). For this purpose, carboxylic acid **126** was first converted to the corresponding acid chloride, following the known protocol of amide synthesis. Subsequent addition of an excess of methanol and triethylamine gave methyl ester **127** in a very good yield of 92 %.

Final reduction of the nitro group was carried out under catalysis of palladium on activated carbon in an atmosphere of elemental hydrogen, following the established protocol. Thus, amine **112** was obtained in a good yield of 85 %.
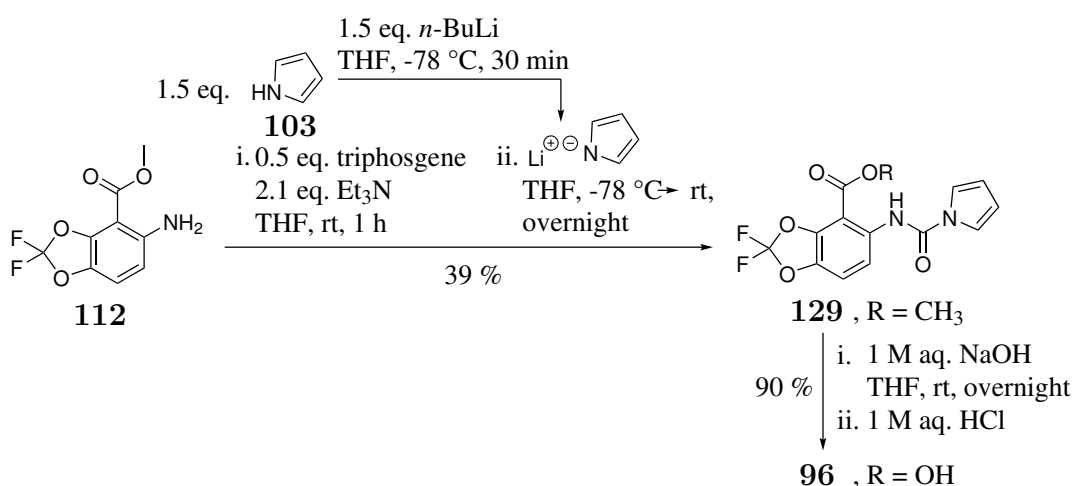
Figure 5.79: Synthesis of target compound **96**, bearing a fluorinated benzodioxole scaffold.

5 Results and discussion

After the successful synthesis of amine **112**, target compound **96** was synthesised in two steps following the established synthesis route B as shown in figure 5.79. The obtained yields of 39 % (methyl ester **129**) and 90 % both are in line with the yields of previously discussed, analogous reactions that followed route B (see tab. 5.16).

Route C
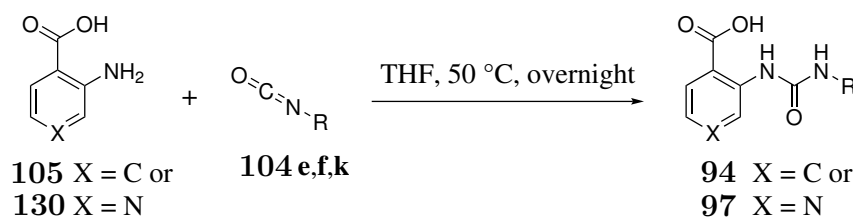
Figure 5.80: Synthesis conditions of route C for the synthesis of target compounds **94e,k** and **97**.

Table 5.17: Yields obtained for the synthesis of 2-ureidobenzoic acid derivatives **94e,f,k** and **97** via route C.

Amine	Isocyanate	R	Yield	Target compound	
105	**104e**		quant.		**94e**
105	**104f**		10 %		**94f**
105	**104k**		quant.		**94k**
130	**104k**		24 %		**97**

The syntheses of anthranilic acid-based target compounds **94e,f** and **k** as well as isonicotinic acid-based target compound **97** succeeded by a direct coupling of the respective, unprotected carboxylic acid **105** or **130** with isocyanate **104e**, **f** or **k** under the conditions shown in figure 5.80. The according yields are listed in table 5.17. Aromatic isocyanates **104e** and **k** were successfully converted with anthranilic acid **105**

to the corresponding target compounds **94e** and **k** in quantitative yields. However, 2-aminoisonicotinic acid **130** was not fully converted under the same reaction conditions, probably due to its reduced nucleophilicity. Even under DMAP-catalysis, the conversion was not significantly increased. The conversion of anthranilic acid **105** with cyclopentylisocyanate **104f** was even worse. Compared to aryl isocyanates **104e** and **k**, alkyl isocyanate **104f** is less reactive due to the electron donating alkyl moiety. In order to enhance the conversion, two more equivalents of isocyanate **104f** were added to the reaction mixture, which was stirred for three more days. Unfortunately, this even decreased the amount of product under the formation of a second product, which was identified by single-crystal X-ray crystallographic analysis as oxazinone derivative **131** (see figure 5.81). After column chromatographic purification, the desired target compound **94f** was obtained in a low yield of 10 %, which however was sufficient for subsequent hDHODH inhibition experiments. Oxazinone derivative **131** was obtained in a yield of 26 %, besides reisolated anthranilic acid **23**.

The condensation reaction of anthranilic acid **105** with isocyanates to form 3-substituted quinazoline-2,4-dione derivatives is well known in the literature, occurs under the presence of an excess of the respective isocyanate and has been mechanistically elucidated by FRY *et al.*[196] and SHEEHAN *et al.*[197]. It is shown in figure 5.81 for the formation of compound **131**.
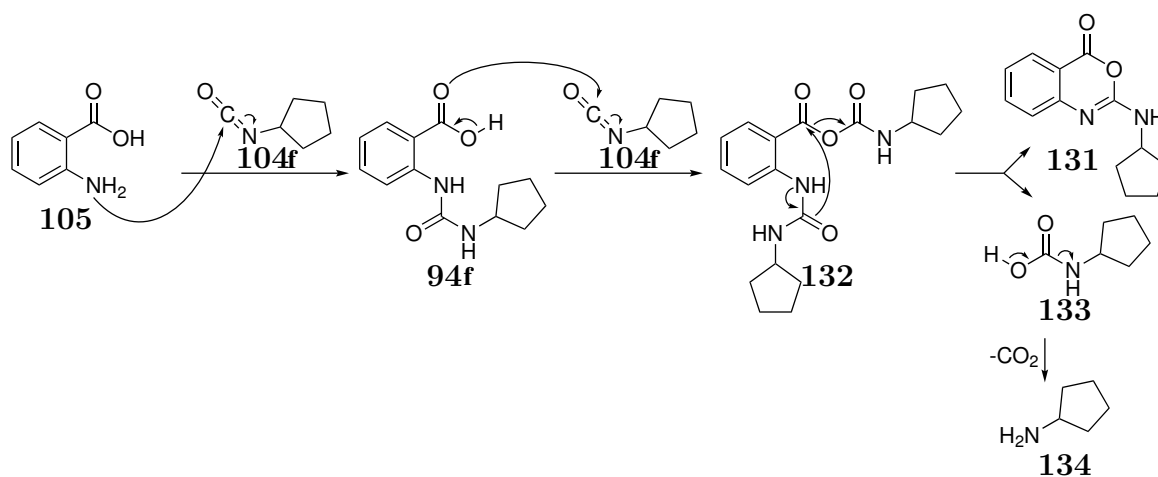
Figure 5.81: Mechanism for the undesired formation of oxazinone derivative **131** in presence of cyclopentylisocyanate **104f** in excess.

In the first step, the desired target compound **94f** was formed by a nucleophilic addition of the amino function of anthranilic acid **105** to the electrophilic carbon atom of cyclopentyl isocyanate **104f**. Subsequently, a second isocyanate molecule reacted with

the less nucleophilic carbonyl oxygen atom, resulting in the formation of carbamoyl anhydride **132**. Subsequently, a nucleophilic addition of the ureido oxygen atom to the activated ester function resulted in the formation of a six-membered quinazolinedione cycle. The eliminated carbamic acid **133** finally decomposed to cyclopentylamine **134** and CO_2.

Overall, Route C proved to be well suited for the synthesis of 2-ureidobenzoic acid derivatives with aromatic substituents. For the coupling of isonicotinic acid **130** or the introduction of aliphatic amines, the previously proven method of triphosgene-mediated coupling using a benzyl protecting group (see chapter 5.3.6) should be used, instead.

All target compounds of this chapter were obtained in sufficient quantities for the performed pharmacologic investigations.

6 Experimental section

6.1 General

6.1.1 Reagents, solvents and buffers

The inhibitor KP-CF39 **22** was gratefully provided by K. Pfaff[125] and starting
material **98** was gratefully provided by A. Laubach[190].
Sodium hydride (Sigma Aldrich, 60 % dispersion in mineral oil) was washed with dry
hexanes and stored under anhydrous conditions under nitrogen atmosphere. All other
used reagents were used as purchased from commercial suppliers in synthesis quality
(abcr, Acros, Activate Scientific, Alfa Aesar, Carbosynth, Carl Roth, Fisher Scientific,
Fluorochem, Fluka, Grüssing, Merck, Sigma-Aldrich, TCI).

Solvents for extraction and column chromatography (Dichloromethane, ethyl acetate
(EA), methanol, and petroleum ether (PE, 50-70)) were purchased in technical quality
and distilled under atmospheric pressure. All other solvents were used as purchased
from commercial suppliers in analytical quality (Merck, VWR).
The **anhydrous solvents** dichloromethane (Sigma-Aldrich, Chromasolv®, amylene-
stabilised), tetrahydrofurane (Sigma-Aldrich Chromasolv® Plus), acetonitrile (Sig-
ma-Aldrich Chromasolv®, amylene-stabilised) and diethyl ether (Sigma-Aldrich,
ACS reagent) were purified and dried using a solvent purification system (MB SPS-800
from Braun) and subsequently stored over appropriate molecular sieves until use. All
other anhydrous solvents were used as purchased from commercial suppliers (Acros
Organics, Sigma-Aldrich, VWR).
The **deuterated solvents** dimethyl sulfoxide-d_6 (DMSO-d_6) and acetonitrile-d_3
(CD$_3$CN) were purchased from Euriso-Top.
Ultrapure water was generated under UV-irradiation by a Sartorius Arium® pro
unit (Sartopore 0.2 µM).

All **buffers** were prepared in ultrapure water and the pH values were set by using
phosphoric acid or hydrochloric acid and aqueous sodium hydroxide solution, followed
by degassing under reduced pressure.

Phosphate Buffer:	pH 7.3
	sodium chloride (38.5 mM)
	potassium dihydrogen phosphate (11.5 mM)

Phosphate buffered saline (PBS)   pH 7.4

                                      sodium chloride (137 mM)

                                      potassium chloride (2.7 mM)

                                      disodium hydrogen phosphate (10 mM)

                                      potassium dihydrogen phosphate (2.0 mM)

Enzyme Assay Buffer: pH 8.0

                              2-amino-2-(hydroxymethyl)-1,3-propanediol hydro-
                                chloride (Tris-HCl, 50 mM)

                              2-[4-(2,4,4-trimethylpentan-2-yl)phenoxy]ethanol (Triton
                                X-100, 0.1 v%)

HisTrap-Binding Buffer: pH 7.8

                              (4-(2-hydroxyethyl)-1-piperazineethanesulfonic acid
                              (HEPES, 50 mM)

                              sodium chloride (300 mM)

                              imidazole (10 mM)

                              glycerol (10 v%)

Elution Buffer: pH 7.8

                          HEPES (50 mM)

                          sodium chloride (300 mM)

                          imidazole (500 mM)

                          glycerol (10 v%)

                          Triton X-100 (0.01 v%)

Gel Filtration Buffer: pH 7.8

                          HEPES (20 mM)

                          sodium chloride (300 mM)

                          glycerol (10 v%)

6.1.2 Purification

Column chromatography was carried out on silica gel 60 (Macherey-Nagel, 0.040-0.063 mm, 230-400 mesh).

Nickel affinity chromatography was performed using a GE Healthcare HisTrap column (1 mL).

Size exclusion chromatography was performed on ÄKTA pure system, using a GE Healthcare Superdex 200 10/300 GL column.

Recrystallisation was performed by solvent diffusion in a slanted 1 L flask. For this purpose, the crude product was suspended in a small volume of dichloromethane and methanol was added dropwise until complete dissolution. The solution was carefully overlaid with 500 mL petroleum ether. After the formation of crystallisation seeds at room temperature, crystallisation was continued at 25 °C.

6.1.3 Analytics

Nuclear magnetic resonance spectroscopy (NMR) was performed at the NMR division at the Department of Chemistry of the University (head: T. HACKL, Y.-J. LEE) of Hamburg at 25 °C on the following devices:

Bruker Fourier 300   (^{1}H spectra: 300 MHz, ^{13}C spectra: 75 MHz),
Bruker Avance I 400   (^{1}H spectra: 400 MHz, ^{13}C spectra: 101 MHz),
Bruker Avance I 500   (^{1}H spectra: 500 MHz, ^{13}C spectra: 126 MHz) or
Bruker Avance III HD 600   (^{1}H spectra: 600 MHz, ^{13}C spectra: 151 MHz, ^{19}F spectra: 565 MHz).

The spectra were analysed with MestReNova software. The solvent resonance of DMSO-d_6 ($\delta = 2.50$ or 35.52 ppm), CD_3CN ($\delta = 1.94$ or 1.32 ppm) or $CDCl_3$ (7.26 or 77.16) was used as internal standard. Two-dimensional NMR experiments (COSY, NOESY, HSQC and HMBC) were used for signal assignments.

Infrared Spectroscopy (IR) was carried out on a Bruker Alpha P FT-IR (software: OPUS), using the attenuated total reflection (ATR) mode at room temperature.

Mass spectra (MS) and high resolution mass spectra (HRMS) were recorded by the MS service at the Department of Chemistry of the University of Hamburg (head: M. RIEDNER) at 25 °C on the following devices:

HRMS: Agilent 6224 ESI-TOF (positive and negative mode, electrospray ionisation (ESI)) or

MS: Thermo ISQ LT EI/ Thermo Trace 1300 (electron ionisation (EI)).
The spectra were analysed using MestReNova software.

Melting points were determined with a Büchi M-565 automatic melting point apparatus.

Thin layer chromatography (TLC) was carried out on aluminium plates precoated with silica gel and fluorescent indicator (Macherey-Nagel, Alugram® Xtra SIL G/UV254, no. 818333, 0.2 mm). All R_f values were determined under chamber saturation. Compounds were UV-detected (254 nm) or stained by heating with one of the following reagents:

vanillin   (5 g vanillin, 900 mL methanol, 100 mL acetic acid, 35 mL conc. sulfuric acid) or

permanganate   (2.4 g $KMnO_4$, 16 g K_2CO_3, 4 mL NaOH (5 % in H_2O), 240 mL demin. water).

Ultraviolet/ visible spectrophotometry (UV/Vis) was performed on a Berthold TriStar² LB 942 Microplate Reader (software: ICE) at $\lambda_{em} = 600$ nm and 25 °C with one data point per 10 seconds for 3600 sec in total, using ThermoFisher Nunc UV-transparend 96-well Plates (8404).
Protein concentrations were determined on a peqlab NanoDrop 2000c Spectrophotometer at room temperature.

Fluorescence spectrophotometry was performed on a Berthold TriStar² LB 942 Microplate Reader (software: ICE) at $\lambda_{exc} = 300$ nm and $\lambda_{em} = 407$ nm, using ThermoFisher 96-well Microplates for Fluorescence-based Assays (M33089).

Analytical **high performance liquid chromatography** (HPLC) was carried out on a Agilent 1260 Infinity II system (software: OpenLAB CDS) with multicolumn thermostat (20 °C), using a C_{18} column (Macherey-Nagel, EC 125/3 Nucleodur 100-5). Compound elution was monitored via diode array detection (DAD, $\lambda_{em} = 300$ nm) and fluorescence detection (FLD, $\lambda_{exc} = 300$ nm, $\lambda_{em} = 407$ nm). Gradient elution (A: 0.1 v% formic acid in acetonitrile; B: 0.1 v% formic acid in ultrapure water) was performed according to one of the following methods:

Method 1 (Flow: 0.3 mL/min)		Method 2 (Flow: 0.5 mL/min)		Method 3 (Flow: 0.5 mL/min)	
0-7 min:	5-42 % A	0-6 min:	5-42 % A	0-6 min:	5-90 % A
7-30 min:	42-58 % A	6-15 min:	42-58 % A	6-8 min:	90 % A isocr.
30-36 min:	58-90 % A	15-21 min:	58-90 % A		
36-41 min:	90 % A isocr.	21-26 min:	90 % A isocr.		

Analytical **mass spectrometry-coupled liquid chromatography** (LC/MS) was carried out under the kind assistance of D. GELLERT at the MS division at the

Department of Chemistry of the University of Hamburg (head: M. RIEDNER) on a Agilent 1200 system with coupled 6224 ESI-TOF, using elution method 1 and the same column as for HPLC runs.

Sodium dodecyl sulfate polyacrylamide gel electrophoresis (SDS-PAGE) was performed on previously prepared 15-well SDS-PAGE gels (10 % Bis-Tris). 10 µL samples were prepared by adding 2.5 µL SDS-PAGE Sample Loading Buffer to 7.5 µL of the respective analyte-suspension and heating at 95 °C for 5 min and were subsequently loaded to the gel. ROTI®Mark Standard was loaded in each gel run. Electrophoresis was performed at 200 V, 150-200 mM and 25 W in MES SDS Running Buffer. The gels were stained with Coomassie Brilliant Blue.

Nano differential scanning fluorimetry (NanoDSF) was performed under the friendly instruction of I. PFEFFER (group of M. WILMANNS at EMBL Hamburg) on a NanoTemper Prometheus NT.48 with backscattering optics (software: PR. ThermControl) using NanoTemper 11 µL nanoDSF grade standard capillaries. The capillaries were loaded with samples containing recombinant His_6-$hDHODH_{29\text{-}396}$ (20 µM), L-dihydroorotate (40 µM) and optionally the inhibitor KP-CF39 **22** (40 µM) in Gel Filtration Buffer and were exposed to thermal stress from 20 °C to 85 °C by applying a thermal ramping rate of 1 °C/min. Protein unfolding was followed by fluorescence detection at $\lambda_{exc} = 280$ nm and $\lambda_{em} = 330$ nm.

6.2 X-ray crystallography

6.2.1 Small molecule X-ray crystallography

Small molecule single-crystal X-ray diffraction *was performed at the X-Ray division at the Department of Chemistry of the University (*I. NEVOIGT*, head:* F. HOFFMANN*) on a Agilent (Oxford Diffraction) SuperNova four-circle single crystal diffractometer, which was operated with microfocus tubes and a molybdenum source.*

Crystallographic sructure determination was performed using Bruker SHELXTL software (XPREP for space group determination, ShelXS for phase problem solvation via direct methods and ShelXL for structure refinement). All hydrogen atoms were refined with isotropic temperature factors, whereas anisotropic temperature factors were applied for the refinement of all other atoms.

6.2.2 Protein X-ray crystallography

Protein X-ray diffraction *measurements were operated by* G. BOURENKOV *(coordinator:* T. R. SCHNEIDER*) at EMBL Hamburg. The hDHODH-ligand* **94h**-*complex crystals were mounted in nylon loops, cryoprotected in silicon oil (Hampton Research) and flash-cooled in liquid nitrogen. The synchrotron data set was collected at 100 K at beamline P14 operated by EMBL Hamburg at the PETRA III storage ring (DESY, Hamburg, Germany).*

Indexing and integration of the collected data was performed using the program XDS. Anisotropic scaling was performed with ccp4 software (POINTLESS for intensity data preparation, AIMLESS for data reduction in the resolution range of 1.9-30 Å). Phenix software was used for molecular replacement (Phaser-MR) on basis of the PDB 1D3G[87] atomic model and for refinement (phenix.refine) under optimisation of Xray/stereochemistry weight and X-ray/ADP weight. 21x3 cycles of phenix refinement were each followed by manual real space refinement using WinCoot software to finally give the complex structure. Crystallography results are shown in table 6.2.

Table 6.2: Results of the crystallographic structure determination of the cocrystallised hDHODH-ligand **94h**-complex

Space group	Resolution	R_{free}	R_{work}	Ramachandran outliers	Rotamer outliers
$P3_121$	1.90 Å	0.184	0.158	<1 %	<1 %

6.3 Protein preparation and crystallisation

The **expression and purification** of His_6-hDHODH$_{29\text{-}396}$ was performed under the friendly instruction of I. PFEFFER (group of M. WILMANNS at EMBL Hamburg) from a His_6-HsDHODH29-396-pET-28a DNA plasmid, which was kindly provided by H. MUNIER-LEHMANN *et al.*.[150]

All expression steps were performed under sterile conditions. Plasmids (1 µL) were transferred to *E. coli* BL21(DE3) cells by incubation at 40 °C for 30 s. The immediately ice-cooled heat-shock transformation mix was treated with SOC medium (500 µL) and incubated at 37 °C and 200 rpm for 1 h. 100 µL of the resulting mixture were inoculated into kanamycin-treated agar plates, followed by incubation at 37 °C for 16 h. One of

the colonies was grown in Lysogeny Broth medium (100 mL) containing kanamycin (30 µg/ml) for 16 h at 37 °C and 142 rpm. A mixture of kanamycin (30 µg/ml) and flavin mononucleotide (0.01 mM) in Terrific Broth medium (6 L) was inoculated with 7 mL of the cell-containing starter culture. After 2 h incubation at 37 °C, $OD_{600} = 0.8$ was reached and *iso*-propyl-β-D-thiogalactoside (IPTG) (0.2 mM) was added to the mixture, that was subsequently incubated at 16 °C for another 20 h. Finally, the cells were harvested by centrifugation at 7000 g and 18 °C for 15 min to give 37 g cell pellet. The cell pellet (10 g) was suspended in His-binding buffer (40 mL), treated with DNAse I (1 mL) and protease inhibitor mix I (1 mL) and sonicated three times for three minutes under pulsation at 0 °C. The resulting lysate was incubated with Triton X-100 (1 v%) for 1 h and ultracentrifugated at 30000 rpm for 20 min, both at 4 °C. After the supernatant was filtered (0.45 µm), the protein was purified via Nickel affinity chromatography (washing with HisTrap-binding Buffer, gradient elution with Elution Buffer). Protein-containing fractions were combined and concentrated with a Corning® Spin-X® UF protein concentrator (30000 MECO), while exchanging the buffer to Gel Filtration Buffer. Aggregates were removed by centrifugation at 4 °C and 14000 rpm for 10 min. Size-exclusion chromatography (Gel Filtration Buffer) afforded the pure protein. Protein-containing fractions were combined in two fractions and the fraction for crystallisation was incubated with Zwittergent3-10 (40 mM, abcr) and HEGA-8 (200 mM, Anatrace) for 1 h, before both fractions were finally concentrated to give 350 µL of a 28.6 mg/mL protein solution, in total (for 37 g cell pellet). The protein purity was evaluated via SDS-PAGE.

Prior to protein crystallisation, the detergent-containing protein (20 mg/mL) was diluted with Gel Filtration Buffer (20 µL), followed by the addition of L-dihydroorotate (2 mM) and ligand **94h** (2 mM).
Protein crystallisation was performed under the technical support of the HTX facility at EMBL Hamburg (C. Günther, head: M. G. Alai). Crystals were grown by vapor diffusion from sitting drops of a mixture containing protein solution (150 µL) and reservoir solution (150 µL) at 20 °C. The crystals started to appear after three day incubation with a reservoir solution containing sodium acetate (0.10 mM, pH 4.8), ammonium sulfate (2.9 M) and glycerol (10 v%) and were grown for 40 days in total.

6.4 Biochemical assays

6.4.1 hDHODH inhibition assay

Prior to the hDHODH inhibition assay, His_6-hDHODH$_{29\text{-}396}$ (325 µM) was thawed to 0 °C and carefully diluted to 87.5 nM with ice-cooled Enzyme Assay Buffer. Stock solutions of all test compounds (100 mM), L-dihydroorotate (250 mM) and ubiquinone-1 (250 mM) were prepared in DMSO, stored at -20 °C and thawed to room temperature before use.

The reaction was performed in triplicates in a 96 well plate with total volumes of 200 µL containing L-dihydroorotate (0.10 mM), ubiquinone-1 (CoQ1; 25 µM), 2,6-dichlorophenolindophenol (DCPIP; 60 µM), HsDHODH$_{29\text{-}396}$ (35 nM) and the test compound (varying concentrations) in Enzyme Assay Buffer.

The compound stock solutions were diluted in Enzyme Assay Buffer to give nine different concentrations and each sample was treated with a freshly prepared substrate mixture containing L-dihydroorotate, ubiquinone-1 and DCPIP. A reference solution without inhibitor but the equivalent amount of buffer added instead was run for each test compound. By simultaneous addition of 80 µL of the prepared, ice-cooled enzyme solution (87.5 µM) per well and immediate mixing by thorough pipetting, the reaction was started. The absorption of the mixture was monitored at via UV/Vis spectrophotometry at 600 nm. During the first 200 s from enzyme addition, constant initial enzyme velocities were observed, from which the IC$_{50}$ values were calculated by non-linear fitting (Origin software) to the following equation:

$$v_{\mathrm{c}} = \frac{v_0}{1 + \dfrac{\mathrm{c}}{\mathrm{IC}_{50}}} \tag{1}$$

where v_{c} is the determined initial, linear enzyme velocity at concentration c

$\quad\quad\ v_0$ is the determined enzyme velocity without added inhibitor and

$\quad\quad\ c$ is the concentration of added test compound.

Brequinar was assessed as reference inhibitor.

6.4.2 Determination of octanol-water distribution

Octanol and PBS were saturated with each other prior to the experiment. Stock solutions of all test compounds (100 mM) were prepared in DMSO, stored at -20 °C and diluted with the saturated PBS to 100 µM prior to the experiment. The experiment was performed in duplicates in 2.5 mL Eppendorf tubes.

300 µL of the test compound solution (100 µM) was overlaid with 300 µL saturated octanol. The emulsions were vortexed for 1 min and rotated for 1 h at 180 rpm and 25 °C. After phase separation, the compound concentrations in the aqueous phase and the initial 100 µM compound solution were determined via HPLC-analysis (eluation method 3).

Distribution coefficients logD were calculated by the following equation:

$$\text{logD} = \log(\frac{AUC_{\text{ref}} - AUC_{\text{aq}}}{AUC_{\text{aq}}}) \tag{2}$$

where AUC_{ref} is the area under the compound peak curve in the chromatogram obtained for the 100 µM reference compound solution and

AUC_{aq} is the area under the compound peak curve in the chromatogram obtained for the aqueous phase, separated after one experiment.

6.4.3 Permeability assay (PAMPA)

Stock solutions of all test compounds (100 mM) were prepared in DMSO, stored at -20 °C and diluted with PBS to 200 µM prior to the experiment. The assay was performed in triplicates in a 96 well Corning Gentest Pre-coated PAMPA Plate System, which was stored at -20 °C and thawed to room temperature for 1 h prior to the assay. Wells of the donor plate were filled with 300 µL of the compound solutions (200 µM) and 200 µL PBS were added to the wells of the receiver plate. Two controls without inhibitor but an equivalent amount of buffer instead was run. Bubble-free assembling of the two plates was followed by 5 h incubation at 25 °C. Finally, the plates were carefully seperated from each other. 150 µL of each well of both plates as well as 150 µL of the initial 200 µM compound solutions in triplicates were quantified by fluorescence spectrophotometry.

Membrane Permeabilities P_{PAMPA} were calculated by the following equation:[199]

$$P_{\text{PAMPA}} = \frac{-\ln(1 - \dfrac{c_{\text{acc}}(t)}{c_{\text{eq}}})}{A_{\text{perm}} \cdot (\dfrac{1}{V_{\text{don}}} + \dfrac{1}{V_{\text{acc}}}) \cdot t} \tag{3}$$

where $c_{\text{acc}}(t)$ is the emitted fluorescence intensity of an 150 µL aliquot, taken from the acceptor well at time t,

A_{perm} is the area of the membrane filter (0.3 cm^2),

V_{don} is the donor well volume (0.3 mL),

V_{acc} is the acceptor well volume (0.2 mL) and

c_{eq} is the equilibrium concentration,

with $c_{\text{eq}} = \dfrac{c_{\text{don}}(t) \cdot V_{\text{don}} + c_{\text{acc}}(t) \cdot V_{\text{acc}}}{V_{\text{don}} + V_{\text{acc}}}$,

where $c_{\text{don}}(t)$ is the emitted fluorescence intensity of an 150 µL aliquot, taken from the donor well at time t.

Caffeine was assessed as reference compound.

6.4.4 Metabolism assay

Stock solutions of all test compounds (100 mM) were prepared in DMSO, stored at -20 °C and diluted in Phosphate Buffer to 600 µM prior to the assay. Rat liver S9 fractions (Sigma Aldrich, Lot # SLCC9026 and # SLCB2232) were combined, aliquoted (200 µL), stored at -80 °C and thawed to 0 °C before use.

The reaction was performed in triplicates in eppendorf tubes with total volumes of 300 µL containing $MgCl_2$ (5 mM), NADPH (5 mM), rat S9 fraction (1 mg) and the test compound (100 µM) in Phosphate Buffer. (For phase II investigation, gluthatione (5 mM) and UDP glucuronic acid (2.5 mM) were added.)
The ice cooled S9 fraction was added to a solution of $MgCl_2$ and NADPH in phosphate buffer and the resulting mixture was preincubated for 10 minutes at 37 °C in a shaker. Subsequently the reaction was started by addition of the test compound (50 µL), followed by threefold pipetting. After 0 h, 1 h and 3 h, samples of 50 µL were taken from the reaction, mixed with 150 µL ice-cooled methanol and centrifuged at 14000 rpm

and 4 °C for 15 minutes. The supernatant was filtered with a syringe filter, immediately quantified on HPLC (Methods 2 and 3) and stored at -20 °C until LC/MS analysis.

The compounds' metabolic stabilities S_{S9} were calculated by the following equation:

$$S_{\text{S9}} = \frac{AUC_{\text{cmp,1h}}}{AUC_{\text{cmp,0h}}} \cdot 100 \tag{4}$$

where $AUC_{\text{cmp,1h}}$ is the area under the compound peak curve in the chromatogram obtained after 1 h incubation and

$AUC_{\text{cmp,0h}}$ is the area under the compound peak curve in the chromatogram obtained for the aliquot which was sampled directly after compound addition.

The experiment was repeated for each test compound with heat-inactivated S9-mix. For this purpose, the S9-mix was previously incubated at 37 °C for 22 h.

7-Ethoxycoumarin (or 7-hydroxycoumarin for phase II investigation) was assessed as reference inhibitor and a control without inhibitor but an equivalent amount of buffer instead was run.

6.4.5 Lymphocyte inhibition assay

CD4- and CD8-lymphocyte inhibition experiments were carried out by Antonia Lehmann (group of Friedrich Haag) in the Department for Clinical Immunology of the University Medical Center Hamburg-Eppendorf (BNITM) in Hamburg.

Lymphocyte inhibition was determined by using human PBMCs (pe-ripheral blood mononuclear cells) as cell culture. The inhibitor compound was added at 8 different concentrations with each de-termination in triplicate and one control without inhibitor. T-cell stimulation was done by Cytostim. Quantification was achieved by a flow cytometry-based method (Facs analysis) with staining of PBMCs with eFluor670 (eBiosci-ence(TM)). The PBMCs are assigned to their populations (CD4/CD8 T cells) by use of other markers.

6.4.6 Antiviral assays (CCHFV, LASV, EBOV)

The assays in cells infected with Crimean Congo hemorrhagic fever virus (CCHFV), Lassa virus (LASV) and Ebola virus (EBOV) were carried out by Lisa Oestereich in the Department of Virology of the Bernhard Nocht Institute for Tropical Medicine (BNITM) in Hamburg.

CCHFV strain Afg-09 2990[200] had been isolated at BNITM laboratory and passaged ≤ 3 times before it has been used in this study. LASV strain Ba366[201] has been produced recombinantly and has been passaged at BNITM laboratory ≤ 3 times. EBOV strain Mayinga 1976 has been provided around 1980 by the Center for Disease Control, Atlanta, Georgia. The passage history since 1976 is not documented. All virus stocks have been grown on Vero 81 cells, quantified by immunofocus assay (see below) and stored at -80 °C until use.

All test compounds were dissolved in DMSO at a concentration of 100 mM and stored at –20 °C. Vero 81 cells were grown in Dulbecco's Modified Eagle's Medium (DMEM) supplemented with 3 % fetal calf serum (FCS) and streptomycin/penicillin and seeded at a density of 1 x 104 cells per well of a 96-well plate one day before infection. Cells were inoculated with LASV Ba366, CCHFV Afg 09-2990 or EBOV Mayinga at a multiplicity of infection (MOI) of 0.01 in the BSL-4 laboratory. The inoculum was removed after 1 h and replaced by fresh medium complemented with different concentrations of compound. Concentration of infectious virus particles in cell culture supernatant was measured three days (LASV and CCHFV) or four days (EBOV) post infection (p.i.) by immunofocus assay. Cell growth and viability under compound treatment was determined by the 3-(4,5-dimethylthiazol-2-yl)-2,5-diphenyl-2H-tetrazoliumbromide (MTT) method as described previously[202]. A sigmoidal dose–response curve was fitted to the data using Prism GraphPad 6.0 (GraphPad Software). The inhibitory concentrations that reduced the virus titer by 50 % (IC_{50}) were calculated from the sigmoidal functions.

Infectious virus particles were determined by immunofocus assay as previously described[202]. Briefly, 1x106 Vero cells per 96-well plates were inoculated with 50 µl of serial 10-fold dilutions of sample. The inoculum was removed after 1 h and replaced by a 1 %-methylcellulose - medium overlay. After three days of incubation, cells were fixed with 4 % formaldehyde, washed with PBS, and permeabilised with 0.5 % Triton X-100 in PBS. After washing with PBS and blocking with 2 % FCS in PBS, cell foci infected with EBOV, CCHFV or LASV were detected with nucleoprotein (NP)-specific monoclonal antibodies (LASV and CCHFV) or polyclonal antiserum (EBOV) against the whole virus. After washing, cells were incubated with peroxidase-labeled anti-mouse IgG. Foci were visualised with tetramethylbenzidine and counted.

6.4.7 Pharmacokinetic *in vivo* studies

The pharmacokinetic in vivo experiments were performed by K. Rox *at Helmholtz Centre for Infection Research (Braunschweig).*

Outbred male CD-1 mice (Charles River, Netherlands), 4 weeks old, were used. The animal studies were conducted in accordance with the recommendations of the European Community (Directive 86/609/EEC, 24 November 1986). All animal procedures were performed in strict accordance with the German regulations of the Society for Laboratory Animal Science (GV- SOLAS) and the European Health Law of the Federation of Laboratory Animal Science Associations (FELASA). Animals were excluded from further analysis if sacrifice was necessary according to the human endpoints established by the ethical board. All experiments were approved by the ethical board of the Niedersächsisches Landesamt für Verbraucherschutz und Lebensmittelsicherheit, Oldenburg, Germany.

CF278 **33c** *was dissolved in 20 % DMSO, 30 % PEG400, 30 % Tris 1 % pH 9.0, 20 % water. Mice were administered CF278* **33c** *at 5 mg/kg (i.v.), 30 mg/kg (p.o.) and 30 mg/kg (s.c.). About 20 µl of whole blood was collected serially from the lateral tail vein at time points 0.25, 0.5, 1, 2, 4, and 8 h post administration. After 24 h mice were sacrificed and blood was collected from the heart. Whole blood was collected into Eppendorf tubes coated with 0.5 M EDTA and immediately spun down at 13000 rpm for 10 min at 4 °C. The plasma was transferred into a new Eppendorf tube and then stored at -80 °C until analysis. Moreover, spontaneous urine was collected at the same time points.*

*All PK plasma samples were analyzed via HPLC-MS/MS using an Agilent 1290 Infinity II HPLC system and coupled to an AB Sciex QTrap6500+ mass spectrometer. First, a calibration curve was prepared by spiking different concentrations of CF278 **33c** into mouse plasma (pooled, from CD-1 mice) for plasma samples or into urine for urine samples. Caffeine was used as an internal standard. In addition, quality control samples (QCs) were prepared in the same way.*

The following extraction procedure was used: 7.5 µl of a plasma sample (calibration samples, QCs or PK samples) was extracted with 37.5 µl of a 1:1 mixture of acetonitrile/methanol containing 12.5 ng/ml of caffeine as internal standard for 5 min at 2000 rpm on an Eppendorf MixMate® vortex mixer. 15 µl of a urine sample (calibration samples, QCs or PK samples) was extracted with 25 µl of a 1:1 mixture of acetonitrile/methanol containing 12.5 ng/ml of caffeine as internal standard for 5 min at 2000 rpm on an Eppendorf MixMate® vortex mixer. Then samples were spun down at 13.000 rpm for 5 min. Supernatants were transferred to standard HPLC-glass vials.

HPLC conditions were as follows: column: Agilent Zorbax Eclipse Plus C18, 50x2.1 mm, 1.8 µm; temperature: 30 °C; injection volume: 10 µl; flow rate: 700 µl/min; solvent A: water + 0.1 % formic acid; solvent B: acetonitrile + 0.1 % formic acid; gradient: 99 % A at 0 min and until 1 min, 99 % 0 % A from 1.0 min to 4.0 min, 0 % A until 4.5 min.

*Mass spectrometric conditions were as follows: Scan type: MRM, negative and positive mode; Q1 and Q3 masses for caffeine and CF278 **33c** can be found in table 6.6; peak areas of each sample and of the corresponding internal standard were analyzed using MultiQuant 3.0 software (AB Sciex). Peak areas of the respective sample were normalised to the internal standard peak area. MS/MS pairs used for quantification are marked with a Q in the table (tab. 6.6), the other MS/MS pairs of the respective compound were used for qualification. Peaks of PK samples were quantified using the calibration curve. The accuracy of the calibration curve was determined using QCs independently prepared on different days.*

PK parameters were determined using a non-compartmental analysis with PKSolver1[203].

Table 6.6: Results from PHLC-MS/MS analysis of PK plasma samples.

ID	Q1 Mass [Da]	Q3 Mass [Da]	time [msec]	DP [volts]	CE [volts]	CXP [volts]
CF278 33c	379.016	135.9 (Q)	50.0	-45.0	-22.0	-15.0
		92.0	50.0	-45.0	-58.0	-9.0
		325.1	50.0	-45.0	-24.0	-17.0
caffeine	195.024	138.0 (Q)	30.0	130.0	25.0	14.0
		110.0	30.0	130.0	31.0	18.0

6.5 Molecular modeling and docking

Molecular Modeling was performed with the software MAESTRO (Version 11.1 (2017), 12.4 (2020), Schrödinger, LLC, New York). The protein structure was prepared with the Structure Preparation Module of MAESTRO. The binding pocket was defined according to the position of the cocrystallised ligand **22** or **94h** under standard settings. Prior to docking, ligands were generated and processed with the LigPrep Module of MAESTRO. Docking was performed using Glide in MAESTRO (extra precision docking, flexible ligand sampling, Scaling factor: 0.8, partial charge cutuff: 0.15, post-docking minimisation). Each best five docking poses were considered.

6.6 Syntheses

6.6.1 General procedures

General procedure 1: Amide synthesis

In an inert atmosphere, a solution of the respective carboxylic acid (1 eq.) in dry dichloromethane (5 mL/mmol) was cooled to 0 °C. After addition of oxalyl chloride (1.2 eq.) and one drop of dry *N,N*-dimethylformamide, the reaction mixture was stirred for three hours under reflux. Volatile components of the mixture were removed under reduced pressure. The residue was dissolved in a minimal amount of dry dichloromethane and added to a solution of methyl anthranilate (0.8 eq.) and dry triethylamine (1.1 eq.) in dry dichloromethane (4.5 mL/mmol). After the reaction mixture was stirred

for 15 hours at room temperature, it was treated with saturated sodium bicarbonate solution and extracted three times with dichloromethane. The combined organic phases were dried over sodium sulphate and the solvent was removed under reduced pressure. Finally, the crude product was purified via column chromatography.

General procedure 2: Synthesis of phenol ethers

Unter inert conditions, a solution of the respective phenol (1 eq.) in dry *N*,*N*-dimethylformamide (1 mL/mmol) was added to dried potassium carbonate (2.5 eq.). After the mixture was stirred at room temperature for 15 min, a catalytic amount of tetra-*N*-butylammonium iodide was added. At 110 °C, the reaction mixture was treated with a solution of 2-bromoethanol (2-2.5 eq.) in dry tetra-*N*,*N*-dimethylformamide (2 mL/mmol) over a period of 2 h and stirred for further 15 h. After cooling to room temperature, the mixture was diluted with water and extracted with ethyl acetate three times. The combined organic extracts were washed with brine, dried over sodium sulfate and the solvents were evaporated. Finally, the crude product was purified via column chromatography (PE/CH$_2$Cl$_2$ 2:1 v/v, unless otherwise indicated).

General procedure 3: Mesylation of alcohols

Under nitrogen atmosphere, a solution of the alcohol (1 eq.) in dry dichloromethane (3 mL/mmol) was treated with dry triethylamine (2 eq.) and cooled to 0 °C whereupon methanesulfonyl chloride (1.15 eq.) was added dropwise. After 3 h stirring at room temperature, dichloromethane and water were added, the phases were seperated and the aqueous phase was extracted with dichloromethane three times. The combined organic phases were washed with brine, dried over sodium sulfate and volatile components were removed in vacuo.

General procedure 4: Azidation

Under inert conditions, the mesylated or chlorinated compound (1 eq.) was dissolved in dry *N*,*N*-dimethylformamide (3 mL/mmol) and treated with sodium azide (1.1-3 eq.). The suspension was stirred at 50 °C overnight, subsequently diluted with water and extracted with diethyl ether twice. The combined organic phases were dried over sodium sulfate and freed from solvent under reduced pressure.

General procedure 5: Palladium-catalyzed hydrogenation

The azide or benzyl ester was mixed with dry tetrahydrofurane (10 mL/mmol) and palladium on carbon (Pd/C, 10 w%) and stirred under hydrogen atmosphere until TLC analysis revealed a complete conversion of the starting material (2-20 h). After dilution with dichloromethane, the catalyst was removed by filtration and the solution

was concentrated under reduced pressure. The obtained crude product was purified via filtration through celite or column chromatography.

General procedure 6: Urea formation using triphosgene

All reaction steps were performed under nitrogen atmosphere. Methyl anthranilate or benzyl anthranilate (1 eq.) was dissolved in dry tetrahydrofurane (8 mL/mmol) and added slowly to a solution of triphosgene (0.5 eq.) in dry tetrahydrofurane (1 mL/mmol). After careful, dropwise addition of dry triethylamine (2 eq.), the milky reaction mixture was stirred for 45-180 min at room temperature. Subsequently, excess phosgene was removed by degassing and volatile reaction components were evaporated. The solid residue was suspended in dry tetrahydrofurane (8 mL/mmol) and treated with the respective amine (0.8-0.9 eq.). The reaction mixture was stirred overnight, diluted with water and extracted with dichloromethane three times. Dehydration of the combined organic phases over sodium sulfate and subsequent evaporation of the solvents afforded the crude product that was finally purified via column chromatography (PE/CH_2Cl_2 1:3 v/v, unless otherwise indicated).

General procedure 7 Synthesis of *O*-aryl-*N*-cyclopentylcarbamates

Under nitrogen atmosphere, a 0 °C cooled solution of the phenol (1 eq.) and 4-(dimethylamino)pyridine (DMAP; 0.1 eq.) in dry tetrahydrofurane (0.5 mL/mmol) was treated with cyclopentyl isocyanate (2 eq.). After stirring at 70 °C for 30 h the mixture was cooled to room temperature, treated with 1 M hydrochloric acid (2 mL/mmol) and extracted three times with diethyl ether. The combined organic extracts were washed with sat. sodium bicarbonate solution and the separated aqueous phase was reextracted with diethyl ether. Next, the organic phases were combined, dried over sodium sulfate and the solvents were removed in vacuo. Purification of the crude products was performed by column chromatography (PE/CH_2Cl_2 1:4 v/v).

General procedure 8: Hydrolysis of esters and carbamates

The carbonyl compound (1 eq.) was dissolved in tetrahydrofurane (4 mL/mmol) and treated with aqueous sodium hydroxide solution (1M; 3 mL/mmol). After vigorous stirring for 3-20 h the resulting mixture was acidified to pH 1 by addition of hydrochloric acid (1M) and subsequently extracted with dichloromethane until no product was detected in the aqueous phase via thin layer chromatography using dichloromethane/ methanol 9:1 v/v. The combined organic extracts were dried over sodium sulfate and concentrated under reduced pressure. Finally, the crude product was purified.

General procedure 9: Synthesis of benzofuran-2-ylmethanols via tandem Sonogashira coupling/cyclisation

The reaction was performed under inert conditions. To a solution of the substituted 2-iodophenol derivative (1 eq.) in dry *N,N*-dimethylformamide (1 mL/mmol) were successively added 1,1,3,3-tetramethylguanidine (TMG, 3 eq.), bis(triphenylphosphine)-palladium dichloride (0.05 eq.) and copper(I) iodide (0.1 eq.). After 5 min stirring at room temperature, the reaction mixture was treated dropwise with a solution of 2-propin-1-ol (1.1 eq.) in dry *N,N*-dimethylformamide (2 mL/mmol) and then stirred at 40 °C overnight. The resulting mixture was diluted with diethyl ether and washed with water and brine once each. The aqueous phases were reextracted with diethyl ether until no product was detected in the aqueous phase via thin layer chromatography using dichloromethane as eluent. Finally, after the combined organic phases were dried over sodium sulfate and the solvent was evaporated, the obtained crude product was purified via column chromatography (CH_2Cl_2, unless otherwise indicated).

General procedure 10: Urea formation with heteroarenes

All reaction steps were performed under nitrogen atmosphere. The respective methyl carboxylate **62** or **112** (1 eq.) was dissolved in dry tetrahydrofurane (8 mL/mmol) and added slowly to a solution of triphosgene (0.5 eq.) in dry tetrahydrofurane (1 mL/mmol). After careful, dropwise addition of dry triethylamine (2 eq.), the milky reaction mixture was stirred for 45-90 min at room temperature. Subsequently, excess phosgene was removed by degassing and volatile reaction components were evaporated. The solid residue was suspended in dry tetrahydrofurane (8 mL/mmol). A solution of the respective heteroarene (1.4-1.5 eq.) in dry tetrahydrofurane (2.5 mL/mmol) was treated with *n*-butyllithium solution (1.6 M in hexane; 1.4-1.5 eq.) at -78 °C, stirred for 15 min and added to the prepared isocyanate suspension at -78 °C. The reaction mixture was stirred overnight while thawing to room temperature, diluted with water and extracted with dichloromethane three times. Dehydration of the combined organic phases over sodium sulfate and subsequent evaporation of the solvents afforded the crude product that was finally purified via column chromatography.

General procedure 11: Urea formation from isocyanates

Under nitrogen atmosphere, a solution of the isocyanate (1 eq.) in dry tetrahydrofurane (8 mL/mmol) was treated with 2-aminobenzoic acid **105** (0.2-0.9 eq.). After stirring at 50 °C overnight, the mixture was treated with methanol and extracted three times with dichloromethane. The combined organic extracts were dried over sodium sulfate and the solvent was removed in vacuo. Purification of the crude products was performed

by column chromatography or recrystallisation via solvent diffusion.

6.6.2 Synthesis of 3-methylanthranilic acid derivative 29

4-(2-(*sec*-butyl)phenoxy)butanoic acid 39

The synthesis procedure and analytical data agree with the literature.[124]

Methyl 2-(*O*-4-(2-*sec*-butylphenoxy)butanoylamino)-3-methylbenzoate 41

According to general procedure **1**, the compound was prepared using 4-(2-(*sec*-butyl)phenoxy)butanoic acid **39** (237 mg, 1.00 mmol), oxalyl chloride (0.10 mL, 0.15 g, 1.2 mmol), methyl 2-amino-3-methylbenzoate (133 mg, 805 µmol) and dry triethyl amine (0.15 mL, 0.11 g, 1.1 mmol). Column-chromatographic purification (CH₂Cl₂) finally yielded methyl ester **41** (248 mg, 647 µmol, 80 %) as colorless solid.

$C_{23}H_{29}NO_4$

383.4880 g/mol
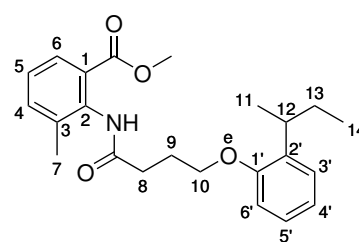
¹H NMR (600 MHz, DMSO-d_6): δ [ppm] = 9.54 (s, 1H, CONH), 7.55 (dd, $^3J_{HH}$ = 7.8 Hz, $^4J_{HH}$ = 1.6 Hz, 1H, H-6), 7.45 (d, $^3J_{HH}$ = 7.3 Hz, 1H, H-4), 7.23 (t, $^3J_{HH}$ = 7.6 Hz, 1H, H-5), 7.17-7.08 (m, 2H, H-3', H-5'), 6.94 (dd, $^3J_{HH}$ = 8.1 Hz, $^4J_{HH}$ = 1.2 Hz, 2H, H-6'), 6.89 (td, $^3J_{HH}$ = 7.4 Hz, $^4J_{HH}$ = 1.2 Hz, 1H, H-4'), 4.02 (t, $^3J_{HH}$ = 6.4 Hz, 2H, H-10), 3.72 (s, 3H, COOCH₃), 3.08 (sext, $^3J_{HH}$ = 7.0 Hz, 1H, H-12), 2.54-2.48 (m, 2H, H-8), 2.20 (s, 3H, H-7), 2.04 (p, $^3J_{HH}$ = 6.8 Hz, 2H, H-9), 1.64-1.48 (m, 2H, H-13), 1.16 (d, $^3J_{HH}$ = 7.0 Hz, 3H, H-11), 0.77 (t, $^3J_{HH}$ = 7.4 Hz, 3H, H-14). **¹³C NMR** (151 MHz, DMSO-d_6): δ[ppm] = 170.7 (CONH), 166.9 (COO), 156.0 (C-1'), 135.3 (C-3), 135.1 (C-2'), 134.9 (C-2), 133.7 (C-4), 128.3 (C-1), 127.4 (C-6), 126.6 (C-3'/C-5), 126.5 (C-5'/C-3'), 125.6 (C-5), 120.4 (C-4'), 111.7 (C-6'), 67.0 (C-10), 51.8 (OCH₃), 33.1 (C-12), 32.0 (C-8) 29.3 (C-13), 24.9 (C-9), 20.4 (C-11), 17.9 (C-7), 12.1 (C-14). **ATR-IR**: $\tilde{\nu}$ [cm⁻¹] = 3289, 2958, 2928, 2872, 1724, 1702, 1661, 1598, 1492, 1449, 1377, 1273, 1235, 1193, 1143, 1093, 1048, 1019. **HRMS** (ESI⁺): m/z = 384.2062 (384.2169 calculated for [M+H]⁺). **R$_f$** = 0.63 (CH₂Cl₂/CH₃OH 99:1 v/v).

2-(*O*-4-(2-*sec*-butylphenoxy)butanoylamino)-3-methylbenzoic acid 29

The compound was prepared according to general procedure **8** using methyl ester **41** (216 mg, 563 µmol). After 13 h stirring and purification via recrystallisation by solvent diffusion, carboxylic acid **29** (133 mg, 360 mmol, 64 %) was obtained as colorless crystals.
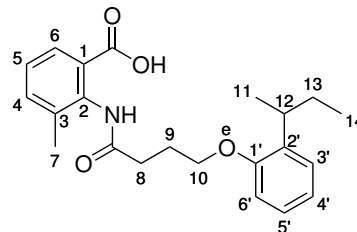
C$_{22}$H$_{27}$NO$_4$
369.4610 g/mol

^{1}H NMR (400 MHz, DMSO-d_6): δ [ppm] = 12.70 (brs, 1H, COOH), 9.53 (s, 1H, CONH), 7.59 (dd, $^3J_{HH}$ = 7.8 Hz, $^4J_{HH}$ = 1.6 Hz, 1H, H-6), 7.42 (dd, $^3J_{HH}$ = 7.8 Hz, $^4J_{HH}$ = 1.7 Hz, 1H, H-4), 7.22 (t, $^3J_{HH}$ = 7.6 Hz, 1H, H-5), 7.18-7.08 (m, 2H, H-3', H-5'), 6.94 (dd, $^3J_{HH}$ = 8.0 Hz, 1H, H-6'), 6.86 (td, $^3J_{HH}$ = 7.4 Hz, $^4J_{HH}$ = 1.2 Hz, 1H, H-4'), 4.01 (t, $^3J_{HH}$ = 6.4 Hz, 2H, H-10), 3.07 (sext, $^3J_{HH}$ = 7.0 Hz, 1H, H-12), 2.53-2.45 (m, 2H, H-8), 2.18 (s, 3H, H-7), 2.05 (p, $^3J_{HH}$ = 6.7 Hz, 2H, H-9), 1.66-1.47 (m, 2H, H-13), 1.16 (d, $^3J_{HH}$ = 7.0 Hz, 3H, H-11), 0.79 (t, $^3J_{HH}$ = 7.4 Hz, 3H, H-14). **^{13}C NMR** (101 MHz, DMSO-d_6): δ[ppm] = 170.7 (CONH), 168.0 (COO), 156.0 (C-1'), 135.5 (C-2', C-3), 134.9 (C-2), 133.5 (C-4), 129.0 (C-1), 127.6 (C-6), 126.6 (C-3'/C-5'), 126.5 (C-5'/C-3'), 125.6 (C-5), 120.4 (C-4'), 111.7 (C-6'), 67.1 (OCH$_3$), 33.1 (C-12), 32.2 (C-8), 29.3 (C-13), 25.0 (C-9), 20.5 (C-11), 18.0 (C-7), 12.1 (C-14). **ATR-IR**: $\tilde{\nu}$ [cm^{-1}] = 3292, 3032, 2960, 2929, 2872, 1693, 1655, 1599, 1521, 1492, 1463, 1449, 1402, 1265, 1237, 1181, 1155, 1092, 1037, 923, 743, 654, 586, 441. **HRMS** (ESI$^-$): m/z = 368.1845 (368.1867 calculated for [M-H]$^-$). **Mp** = 108.7 °C. **R$_f$** = 0.34 (CH$_2$Cl$_2$/CH$_3$OH 9:1 v/v).

6.6.3 Synthesis of carbamate 30

2-(2-(Butan-2-yl)phenoxy)ethan-1-ol 44a

According to general procedure **2**, 2-(butan-2-yl)phenol **37a** (3.1 mL, 3.0 g, 20 mmol), K$_2$CO$_3$ (6.9 g, 50 mmol) and 2-bromoethanol (3.5 mL, 6.2 g, 50 µmol) were used to obtain phenyl ether **44a** (3.9 g, 20 mmol, 98 %) as colorless liquid.
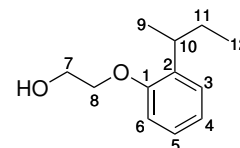
C$_{12}$H$_{18}$O$_2$
194.2740 g/mol

^{1}H NMR (600 MHz, DMSO-d_6): δ [ppm] = 7.16-7.09 (m, 2H, H-3, H-5), 6.93 (d, $^3J_{HH}$ = 7.9 Hz, 1H, H-6), 6.88 (dt, $^3J_{HH}$ = 7.4 Hz, $^4J_{HH}$ = 0.9 Hz, 1H, H-4), 4.78 (t, $^3J_{HH}$ = 5.5 Hz, 1H, OH), 3.96 (hept, $^3J_{HH}$ = 5.0 Hz, 2H, H-8), 3.72 (q, $^3J_{HH}$ = 5.3 Hz, 2H,

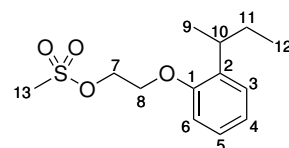H-7), 1.84 (sext, $^3J_{HH}$ = 7.0 Hz, 1H, H-10), 1.62-1.47 (m, 2H, H-11), 1.13 (d, $^3J_{HH}$ = 7.0 Hz, 3H, H-9), 0.77 (t, $^3J_{HH}$ = 7.4 Hz, 3H, H-12). **^{13}C NMR** (151 MHz, DMSO-d_6): δ[ppm] = 156.1 (C-1), 135.1 (C-2), 126.5 (C-5), 126.5 (C-3), 120.4 (C-4), 111.9 (C-6), 69.8 (C-8), 59.8 (C-7), 33.0 (C-10), 29.2 (C-11), 20.4 (C-9), 12.0 (C-12). **ATR-IR**: $\tilde{\nu}$ [cm^{-1}] = 3360, 2960, 2928, 2872, 1599, 1585, 1490, 1448, 1377, 1356, 1289, 1237, 1189, 1152, 1094, 1077, 1048, 920, 897, 801, 749. **HRMS** (ESI$^+$): m/z = 195.1353 (195.1380 calculated for [M+H]$^+$). **R_f** = 0.36 (CH$_2$Cl$_2$).

Methyl 2-((methoxycarbonyl)amino)benzoate 61

The compound was prepared under nitrogen atmosphere. Methyl 2-aminobenzoate **62** (0.66 mL, 0.77 g, 5.1 mmol) was dissolved in dry toluene and methylchloroformiate (1.2 mL, 1.4 g, 15 mmol, 3.0 eq.) was slowly added, before the reaction mixture was stirred at 111 °C for 8 h. After evaporation of solvent and volatile components, carbamate **61** (1.1 g, 5.1 mmol, 100 %) was obtained as colorless liquid.
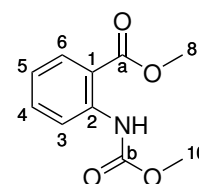
C$_{10}$H$_{11}$NO$_4$
209.2010 g/mol

^{1}H NMR (400 MHz, DMSO-d_6): δ [ppm] = 10.25 (s, 1H, NH), 8.16 (dd, $^3J_{HH}$ = 8.5 Hz, $^4J_{HH}$ = 1.2 Hz, 1H, H-3), 7.93 (dd, $^3J_{HH}$ = 8.0 Hz, $^4J_{HH}$ = 1.7 Hz, 1H, H-6), 7.62 (ddd, $^3J_{HH}$ = 8.7 Hz, $^3J_{HH}$ = 7.3 Hz, $^4J_{HH}$ = 1.7 Hz, 1H, H-4), 7.19-7.10 (m, 1H, H-5), 3.86 (s, 3H, H-8), 3.70 (s, 3H, H-10). **^{13}C NMR** (101 MHz, DMSO-d_6): δ[ppm] = 167.8 (CO-a), 153.4 (CO-b), 140.3 (C-2), 134.4 (C-4), 130.7 (C-6), 122.3 (C-5), 119.1 (C-3), 116.0 (C-1), 52.5 (C-8), 52.2 (C-10). **ATR-IR**: $\tilde{\nu}$ [cm^{-1}] = 3296, 3011, 2959, 1735, 1686, 1593, 1530, 1456, 1430, 1320, 1266, 1225, 1185, 1173, 1148, 1099, 1062, 1044, 965, 850, 822, 757, 734, 698, 677, 618, 527, 510, 419, 389. **MS** (EI): m/z = 209.14 (209.07 calculated for [M]$^{+\cdot}$). **R_f** = 0.65 (CH$_2$Cl$_2$).

2-(2-(*sec*-butyl)phenoxy)ethyl 2-(((2-(2-(*sec*-butyl)phenoxy)ethoxy)carbonyl)amino) benzoate 69

The reaction was performed in a nitrogen atmosphere in presence of activated molecular sieves (4 Å). Carbamate **61** (63 mg, 0.30 mmol) was dissolved in dry toluene (2 mL) and potassium *tert*-butoxide (81 mg, 0.72 mmol) was added. The reaction mixture was stirred at 100 °C for 23 h, poured into ice and extracted with ethyl acetate three times. After the organic phases were combined, they were washed with brine, dried

over sodium sulfate. Finally, the solvent was evaporated and the crude product was purified by column chromatography (PE/CHCl$_2$ 20:1 v/v) to afford product **69** (77 mg, 0.14 mmol, 48 %).

C$_{32}$H$_{39}$NO$_6$

533.6650 g/mol

^{1}H NMR (400 MHz, DMSO-d_6): δ [ppm] = 10.39 (s, 1H, NH-a), 8.25 (dd, $^3J_{HH}$ = 8.6 Hz, $^4J_{HH}$ = 1.1 Hz, 1H, H-3), 7.94 (dd, $^3J_{HH}$ = 8.0 Hz, $^4J_{HH}$ = 1.7 Hz, 1H, H-6), 7.63 (ddd, $^3J_{HH}$ = 8.7 Hz, 7.3 Hz, $^4J_{HH}$ = 1.7 Hz, 1H, H-4), 7.18-7.08 (m, 5H, H-3', H-3", H-5, H-5', H-5"), 6.96 (m, 2H, H-6', H-6"), 6.90 (m, 2H, H-4', H-4"), 4.64 (dd, $^3J_{HH}$ = 5.4 Hz, 3.5 Hz, 2H, H-7"), 4.48 (dd, $^3J_{HH}$ = 5.7 Hz, 3.2 Hz, 2H, H-7'), 4.30 (dd, $^3J_{HH}$ = 5.5 Hz, 3.3 Hz, 2H, H-8"), 4.20 (dd, $^3J_{HH}$ = 5.6 Hz, 3.3 Hz, 2H, H-8'), 3.01 (sext, $^3J_{HH}$ = 7.1 Hz, 1H, H-10"), 2.95 (sext, $^3J_{HH}$ = 7.1 Hz, 1H, H-10'), 1.60-1.32 (m, 4H, H-11', H-11"), 1.10-1.05 (m, 3H, H-9"), 1.05-1.01 (m, 3H, H-9'), 0.68 (t, $^3J_{HH}$ = 7.4 Hz, 3H, H-12"), 0.62 (t, $^3J_{HH}$ = 7.4 Hz, 3H, H-12'). **^{13}C NMR** (100 MHz, CD$_3$CN): δ[ppm] = 167.3.3 (C-a), 155.6 (C-1"), 152.8 (C-b), 140.7 (C-2), 135.1 (C-2', C-2"), 134.7 (C-4), 130.7 (C-6), 126.7 (C-3', C-3", C-5', C-5"), 122.1 (C-5), 120.9 (C-4', C-4"), 118.8 (C-3), 115.1 (C-1), 112.0 (C-6', C-6"), 66.2 (C-8), 65.9 (C-8') 63.6 (C-7'), 63.3 (C-7), 33.3 (C-10, C-10'), 29.1 (C-11, C-11'), 20.2 (C-9, C-9'), 11.9 (C-12, C-12'). **R$_f$** = 0.63 (CH$_2$Cl$_2$).
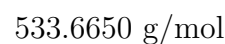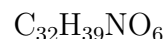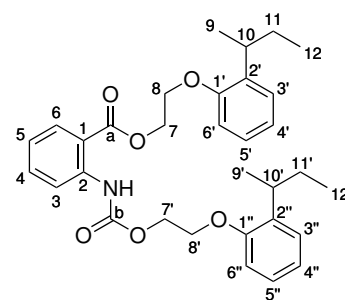
Methyl 2-(((2-(2-(*sec*-butyl)phenoxy)ethoxy)carbonyl)amino)benzoate 68

All reaction steps were performed under nitrogen atmosphere. Methyl anthranilate **62** (0.26 mL, 0.30 g, 2.0 mmol) was dissolved in dry tetrahydrofurane (16 mL) and added slowly to a solution of triphosgene (593 mg, 2.00 mmol) in dry tetrahydrofurane (2 mL). After careful, dropwise addition of dry triethylamine (0.58 mL, 0.43 g, 4.2 mmol), the reaction mixture was stirred for 1 h at room temperature. Subsequently, excess phosgene was removed by degassing and volatile reaction components were evaporated. The

C$_{21}$H$_{25}$NO$_5$

371.4330 g/mol

solid residue was suspended in dry tetrahydrofurane (16 mL). Alcohol **44a** (583 mg, 3.0 mmol) was added to a suspension of sodium hydride (77 mg, 3.2 mmol) in dry tetrahydrofurane (16 mL), stirred for 15 min at room temperature and the supernatant was added to the prepared isocyanate suspension. The reaction mixture was stirred for 15 h, diluted with water and extracted with dichloromethane three times. Dehydration
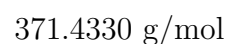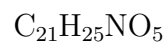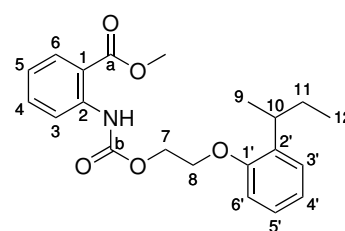
of the combined organic phases over sodium sulfate and subsequent evaporation of the solvents afforded the crude product that was finally purified twice via column chromatography (toluene, PE/CH$_2$Cl$_2$ gradient 1:1 to 0:1 v/v). Methylester **68** (0.65 g, 1.8 mmol, 88%) was finally obtained as colorless crystals.

^{1}H NMR (400 MHz, DMSO-d_6): δ [ppm] = 10.34 (s, 1H, NH-a), 8.21 (dd, $^3J_{HH}$ = 8.5 Hz, $^4J_{HH}$ = 1.2 Hz, 1H, H-3), 7.94 (dd, $^3J_{HH}$ = 8.0 Hz, $^4J_{HH}$ = 1.7 Hz, 1H, H-6), 7.63 (ddd, $^3J_{HH}$ = 8.6 Hz, 7.3 Hz, $^4J_{HH}$ = 1.7 Hz, 1H, H-4), 7.18-7.13 (m, 3H, H-3', H-5, H-5'), 6.96 (dd, $^3J_{HH}$ = 8.2 Hz, $^4J_{HH}$ = 1.2 Hz, 1H, H-6'), 6.93-6.88 (m, 1H, H-4'), 4.51-4.47 (m, 2H, H-7), 4.24-4.19 (m, 2H, H-8), 3.84 (s, 3H, COOCH$_3$), 3.02 (h, $^3J_{HH}$ = 7.0 Hz, 1H, H-10), 1.59-1.40 (m, 2H, H-11), 1.09 (d, $^3J_{HH}$ = 7.0 Hz, 3H, H-9), 0.70 (t, $^3J_{HH}$ = 7.4 Hz, 3H, H-12). **^{13}C NMR** (101 MHz, CD$_3$CN): δ[ppm] = 168.3 (C-a), 156.1 (C-1'), 153.3 (C-b), 140.8 (C-2), 135.7 (C-2'), 134.9 (C-4), 131.2 (C-6), 127.2 (C-3'), 127.1 (C-5'), 122.8 (C-4), 121.3 (C-5), 119.4 (C-3), 116.2 (C-1), 112.5 (C-6'), 66.7 (C-8), 63.8 (C-7), 52.9 (OCH$_3$) 33.8 (C-10), 29.6 (C-11), 20.7 (C-9), 12.4 (C-12). **ATR-IR**: $\tilde{\nu}$ [cm^{-1}] = 3258, 2956, 2928, 2873, 1737, 1690, 1590, 1528, 1490, 1447, 1435, 1378, 1359, 1315, 1302, 1275, 1236, 1209, 1167, 1154, 1144, 1098, 1089, 1072, 1058, 996, 959, 921, 907, 878, 843, 818, 797, 753, 727, 698, 674, 620, 608, 523, 470, 418, 396. **HRMS** (ESI$^+$): m/z = 372.1804 (372.1805 calculated for [M+H]$^+$). **R$_f$** = 0.29 (toluene).

2-(((2-(2-(*sec*-butyl)phenoxy)ethoxy)carbonyl)amino)benzoic acid 30

The compound was prepared according to general procedure **8**, using methyl ester **68** (189 mg, 5.09 mmol). The reaction mixture was stirred for 20 h at room temperature and for 2 h under reflux. The crude product was purified by column chromatography (PE/CH$_2$Cl$_2$ 35:1 v/v) and recrystallisation by solvent diffusion. Carboxylic acid **30** (182 mg, 359 µmol mmol, 71 %) was furnished as colorless crystals.

C$_{20}$H$_{23}$NO$_5$
357.4060 g/mol

^{1}H NMR (400 MHz, DMSO-d_6): δ [ppm] = 13.71 (brs, 1H, COOH), 10.84 (s, 1H, NH-a), 8.31 (dd, $^3J_{HH}$ = 8.6 Hz, $^4J_{HH}$ = 1.1 Hz, 1H, H-3), 7.98 (dd, $^3J_{HH}$ = 8.0 Hz, $^4J_{HH}$ = 1.7 Hz, 1H, H-6), 7.61 (ddd, $^3J_{HH}$ = 8.7 Hz, 7.3 Hz, $^4J_{HH}$ = 1.8 Hz, 1H, H-4), 7.18-7.06 (m, 3H, H-3', H-5, H-5'), 6.97 (m, 1H, H-6'), 6.90 (td, $^3J_{HH}$ = 7.5 Hz, $^4J_{HH}$ = 1.2 Hz, 1H, H-4'), 4.49 (dd, $^3J_{HH}$ = 5.7 Hz, 3.3 Hz, 2H, H-7), 4.22 (dd, $^3J_{HH}$ = 5.4 Hz, 3.6 Hz, 2H, H-8), 3.00 (sext, $^3J_{HH}$ = 7.0 Hz, 1H, H-10),
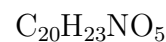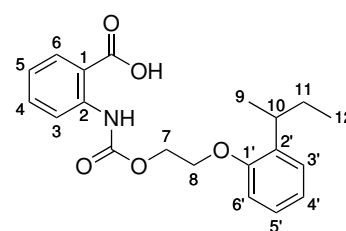
1.61-1.37 (m, 2H, H-11), 1.08 (d, $^3J_{HH}$ = 7.0 Hz, 3H, H-9), 0.69 (t, $^3J_{HH}$ = 7.4 Hz, 3H, H-12). **^{13}C NMR** (101 MHz, CD$_3$CN): δ[ppm] = 169.7 (COOH), 155.6 (C-1'), 152.7 (CONH), 141.1 (C-2), 135.2 (C-2'), 134.4 (C-4), 131.3 (C-6), 126.7 (C-3', C-5'), 121.9 (C-5), 120.9 (C-4), 118.1 (C-3), 115.3 (C-1), 112.1 (C-6'), 66.2 (C-8), 63.2 (C-7), 33.4 (C-10), 29.1 (C-11), 20.2 (C-9), 12.0 (C-12). **HRMS** (ESI$^-$): m/z = 356.1504 (356.1503 calculated for [M-H]$^-$). **R$_f$** = 0.43 (CH$_2$Cl$_2$/CH$_3$OH 9:1 v/v) Mp = 128.7 °C.

6.6.4 Synthesis of ureide 31a

2-(2-(Butan-2-yl)phenoxy)ethyl methanesulfonate 75a

The compound was prepared according to general procedure **3**.
Alcohol **44a** (1.6 g, 8.0 mmol), triethylamine (2.2 mL, 1.6 g, 16 mmol) and methanesulfonyl chloride (0.68 mL, 1.0 g, 8.8 mmol) were used to obtain mesylate **75a** (2.2 g, 8.0 mmol, 100 %) as yellow crystals.

C$_{13}$H$_{20}$O$_4$S
272.3590 g/mol

^{1}H NMR (400 MHz, DMSO-d_6): δ [ppm] = 7.20-7.10 (m, 2H, H-3, H-5), 6.98-6.88 (m, 2H, H-4, C-6), 4.56-4.50 (m, 2H, H-8), 4.26-4.20 (m, 2H, H-7), 3.21 (s, 3H, H-13), 3.06 (sext, $^3J_{HH}$ = 7.0 Hz, 1H, H-10), 1.64-1.44 (m, 2H, H-11), 1.14 (d, $^3J_{HH}$ = 7.0 Hz, 3H, H-9), 0.77 (t, $^3J_{HH}$ = 7.4 Hz, 3H, H-12). **^{13}C NMR** (101 MHz, DMSO-d_6): δ[ppm] = 155.5 (C-1), 135.2 (C-2), 126.8 (C-5), 126.7 (C-3), 121.1 (C-4), 112.1 (C-6), 68.9 (C-8), 66.0 (C-7), 36.8 (C-13), 33.2 (C-10) 29.2 (C-11), 20.4 (C-9), 12.1 (C-12). **ATR-IR**: $\tilde{\nu}$ [cm^{-1}] = 3037, 2961, 2925, 2868, 1492, 1446, 1333, 1303, 1284, 1234, 1171, 1103, 1013, 982, 932, 901, 815, 786, 746, 714, 609, 528, 505, 480, 440. **HRMS** (ESI$^+$): m/z = 295.0979 (295.0975 calculated for [M+Na]$^+$). **R$_f$** = 0.52 (PE/CH$_2$Cl$_2$ 1:2 v/v).

1-(2-Azidoethoxy)-2-(Butan-2-yl)benzene 72a

According to general procedure **4**, mesylate **75a** (2.18 g, 8.00 mmol) and sodium azide (1.51 g, 23.2 mmol) were used, followed by purification via column chromatography (PE/CH$_2$Cl$_2$ 6:1 v/v), to prepare azide **72a** (1.47 g, 6.71 mmol, 84 %) as colorless liquid.

¹H NMR (400 MHz, DMSO-d_6): δ [ppm] = 7.20-7.10 (m, 2H, H-3, H-5), 6.99-6.89 (m, 2H, H-4, H-6), 4.17-4.10 (m, 2H, H-8), 3.68-3.61 (m, 2H, H-7), 3.10 (sext, $^3J_{HH}$ = 7.1 Hz, 1H, H-10), 1.65-1.44 (m, 2H, H-11), 1.14 (d, $^3J_{HH}$ = 7.0 Hz, 3H, H-9), 0.78 (t, $^3J_{HH}$ = 7.4 Hz, 3H, H-12). **¹³C NMR** (101 MHz, DMSO-d_6): δ[ppm] = 155.5 (C-1), 135.1 (C-2), 126.7 (C-5), 126.6 (C-3), 121.0 (C-4), 111.8 (C-6), 66.9 (C-8), 50.2 (C-7), 36.8 (C-13), 32.8 (C-10) 29.3 (C-11), 20.5 (C-9), 12.0 (C-12). **ATR-IR**: $\tilde{\nu}$ [cm^{-1}] = 3033, 2962, 2930, 2872, 2105, 1600, 1585, 1491, 1448, 1378, 1351, 1286, 1231, 1189, 1153, 1127, 1096, 1059, 1016, 999, 922, 852, 793, 748, 646, 608, 555, 488, 453. **MS** (EI): m/z = 219.16 (219.14 calculated for [M]$^{+\cdot}$). **R$_f$** = 0.40 (PE/CH$_2$Cl$_2$ 6:1 v/v).
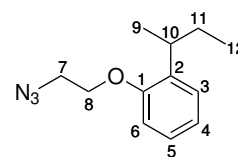
$C_{12}H_{17}N_3O$

219.2880 g/mol

2-(2-(Butan-2-yl)phenoxy)ethan-1-amine 42a

According to general procedure **5**, the compound was prepared using azide **72a** (1.48 g, 6.75 mmol) and Pd/C (148 mg). After 3 h stirring, purification was performed via column chromatography (EA/CH$_3$OH gradient 50:1 to 9:1 v/v) to obtain amine **42a** (1.17 mg, 6.06 mmol, 90 %) as colorless liquid.
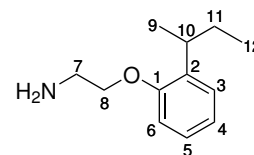
$C_{12}H_{19}NO$

193.2900 g/mol

¹H NMR (600 MHz, DMSO-d_6): δ [ppm] = 7.15-7.09 (m, 2H, H-3, H-5), 6.91 (dd, $^3J_{HH}$ = 8.2 Hz, $^4J_{HH}$ = 1.2 Hz, 1H, H-6), 6.88 (dt, $^3J_{HH}$ = 7.4 Hz, $^4J_{HH}$ = 1.1 Hz, 1H, H-4), 3.90 (dt, $^3J_{HH}$ = 5.8 Hz, $^4J_{HH}$ = 1.8 Hz, 2H, H-8), 3.05 (sext, $^3J_{HH}$ = 7.0 Hz, 1H, H-10), 2.88 (t, $^3J_{HH}$ = 5.7 Hz, 2H, H-7), 1.61-1.47 (m, 2H, H-11), 1.14 (d, $^3J_{HH}$ = 7.0 Hz, 3H, H-9), 0.77 (t, $^3J_{HH}$ = 7.4 Hz, 3H, H-12). **¹³C NMR** (151 MHz, DMSO-d_6): δ[ppm] = 156.1 (C-1), 134.9 (C-2), 126.6 (C-5), 126.5 (C-3), 120.4 (C-4), 111.7 (C-6), 70.4 (C-8), 41.2 (C-7), 33.1 (C-10), 29.3 (C-11), 20.4 (C-9), 12.1 (C-12). **ATR-IR**: $\tilde{\nu}$ [cm^{-1}] = 3382, 3303, 2959, 2929, 2871, 1599, 1584, 1490, 1448, 1377, 1355, 1288, 1234, 1188, 1512, 1126, 1094, 1046, 1016, 959, 888, 821, 746, 608, 496, 45. **HRMS** (ESI$^+$): m/z = 194.1536 (194.1539 calculated for [M+H]$^+$). **R$_f$** = 0.14 (EA/CH$_3$OH 50:1 v/v).

Benzyl 2-(3-(2-((butan-2-yl)phenoxy)ethyl)ureido)benzoate 88a

The compound was prepared according to general procedure **6** using triphosgene (0.23 g, 0.75 mmol), benzyl anthranilate (0.18 g, 0.80 mmol), triethylamine (0.22 mL, 0.16 g,

1.6 mmol) and amine **42a** (0.13 g, 0.67 mmol). Ureide **88a** (0.23 g, 0.51 mmol, 76 %) was obtained as colorless solid. **¹H NMR** (500 MHz, CD₃CN): δ [ppm] = 10.05 (s, 1H, NH-a), 8.46 (dd, $^3J_{HH}$ = 8.6 Hz, $^4J_{HH}$ = 0.8 Hz, 1H, H-3), 8.01 (dd, $^3J_{HH}$ = 8.0 Hz, $^4J_{HH}$ = 1.6 Hz, 1H, H-6), 7.51 (ddd, $^3J_{HH}$ = 8.8 Hz, 7.3 Hz, $^4J_{HH}$ = 1.7 Hz, 1H, H-4), 7.48-7.44 (m, 2H, H-2"), 7.43-7.38 (m, 2H, H-3"), 7.38-7.33 (m, 1H, H-4"), 7.17 (dd, $^3J_{HH}$ = 7.8 Hz, $^4J_{HH}$ = 1.7 Hz, 1H, H-3'), 7.15-7.11 (m, 1H, H-5'), 6.99 (ddd, $^3J_{HH}$ = 8.2 Hz, 7.4 Hz, $^4J_{HH}$ = 1.7 Hz, 1H, H-5), 6.94-6.89

$C_{27}H_{30}N_2O_4$
446.5470 g/mol

(m, 2H, H-4', H-6'), 6.04 (brs, 1H, NH-b), 5.33 (s, 2H, H-13), 4.04 (t, $^3J_{HH}$ = 5.4 Hz, 2H, H-8), 3.58 (q, $^3J_{HH}$ = 5.6 Hz, 2H, H-7), 3.16 (sext, $^3J_{HH}$ = 7.1 Hz, 1H, H-10), 1.67-1.50 (m, 2H, H-11), 1.15 (d, $^3J_{HH}$ = 7.0 Hz, 3H, H-9), 0.77 (t, $^3J_{HH}$ = 7.0 Hz, 3H, H-12). **¹³C NMR** (126 MHz, CD₃CN): δ[ppm] = 168.9 (COOH), 157.4 (C-1'), 155.9 (CONH), 144.4 (C-2), 137.2 (C-1"), 136.9 (C-2'), 135.2 (C-4), 131.7 (C-6), 129.6 (C-3"), 129.3 (C-4"), 129.0 (C-2"), 127.7 (C-3'), 127.6 (C-5'), 121.8 (C-4), 121.5 (C-5), 120.6 (C-3), 115.1 (C-1), 112.9 (C-6'), 68.2 (C-8), 67.6 (C-13), 40.5 (C-7), 34.3 (C-10), 30.6 (C-11), 21.0 (C-9), 12.5 (C-12). **ATR-IR**: $\tilde{\nu}$ [cm⁻¹] = 3293, 3070, 3034, 2960, 2929, 2872, 1683, 1655, 1589, 1548, 1531, 1486, 1447, 1377, 1238, 1217, 1158, 1143, 1096, 1075, 1046, 1029, 912, 750, 697, 635, 588, 532. **HRMS** (ESI⁺): m/z = 447.2294 (447.2278 calculated for [M+H]⁺). **R_f** = 0.25 (CH₂Cl₂).
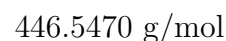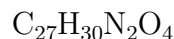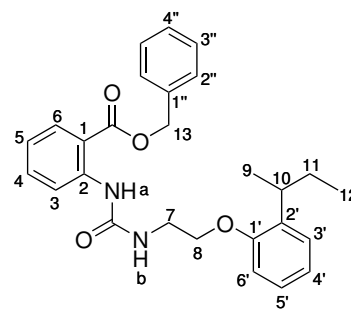
2-(3-(2-((Butan-2-yl)phenoxy)ethyl)ureido)benzoic acid 31a

The compound was prepared according to general procedure **5** using benzoate **88a** (186 mg, 417 µmol) and Pd/C (20 mg). The reaction mixture was stirred for 15 h and the crude product was purified via recrystallisation by solvent diffusion to obtain carboxylic acid **31a** (136 mg, 382 µmol, 92 %) as colorless crystals.
¹H NMR (600 MHz, DMSO-d_6): δ [ppm] = 10.22 (s, 1H, NH-a), 9.72 (brs, 1H, COOH), 8.48 (d, $^3J_{HH}$ = 8.4 Hz, 1H, H-3), 7.97 (dd, $^3J_{HH}$ = 8.0 Hz, $^4J_{HH}$ = 1.6 Hz, 1H, H-6), 7.51 (ddd, $^3J_{HH}$ = 8.7 Hz, 7.3 Hz, $^4J_{HH}$ = 1.7 Hz, 1H, H-4), 7.16 (dd, $^3J_{HH}$

$C_{20}H_{24}N_2O_4$
356.4220 g/mol

= 7.8 Hz, $^4J_{HH}$ = 1.6 Hz, 1H, H-3'), 7.15-7.10 (dt, $^3J_{HH}$ = 7.8 Hz, $^4J_{HH}$ = 1.6 Hz, 1H, H-5'), 6.98 (ddd, $^3J_{HH}$ = 8.2 Hz, 7.2 Hz, $^4J_{HH}$ = 1.2 Hz, 1H, H-5), 6.91 (m, 2H,
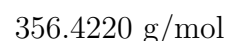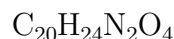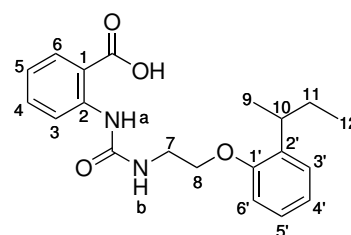
H-4', H-6'), 6.03 (brs, 1H, NH-b), 4.03 (t, $^3J_{HH}$ = 5.4 Hz, 2H, H-8), 3.57 (q, $^3J_{HH}$ = 5.6 Hz, 2H, H-7), 3.15 (sext, $^3J_{HH}$ = 7.0 Hz, 1H, H-10), 1.63-1.46 (m, 2H, H-11), 1.14 (d, $^3J_{HH}$ = 7.0 Hz, 3H, H-9), 0.77 (t, $^3J_{HH}$ = 7.4 Hz, 3H, H-12). **^{13}C NMR** (151 MHz, DMSO-d_6): δ[ppm] = 170.3 (COOH), 157.3 (C-2'), 155.9 (CONH), 144.8 (C-2), 136.8 (C-2'), 135.3 (C-4), 132.1 (C-6), 127.7 (C-3'), 127.6 (C-5'), 121.8 (C-4'), 121.3 (C-5), 120.2 (C-3), 114.5 (C-1), 112.8 (C-6'), 68.1 (C-8), 40.5 (C-7), 34.3 (C-10), 30.6 (C-11), 21.0 (C-9), 12.5 (C-12). **ATR-IR**: $\tilde{\nu}$ [cm^{-1}] = 3390, 2960, 2929, 2870, 2628, 2561, 1681, 1656, 1604, 1584, 1556, 1528, 1491, 1466, 1449, 1409, 1320, 1262, 1226, 1164, 1153, 1127, 1090, 1047, 918, 746, 667, 637, 610, 560, 524. **HRMS** (ESI$^-$): m/z = 355.1667 (355.1663 calculated for [M-H]$^-$). **R_f** = 0.33 (CH$_2$Cl$_2$/CH$_3$OH 9:1 v/v).

Methyl 2-(3-(2-((butan-2-yl)phenoxy)ethyl)ureido)benzoate 84

The compound was prepared according to general procedure **6** using triphosgene (534 mg, 1.80 mmol), methyl anthranilate **62** (0.23 mL, 0.27 g, 1.8 mmol), triethylamine (0.52 mL, 0.38 g, 3.8 mmol) and amine **42a** (335 mg, 1.53 mmol). Ureide **84** (525 mg, 1.41 mmol, 93 %) was obtained as colorless crystals.

C$_{21}$H$_{26}$N$_2$O$_4$
370.4490 g/mol
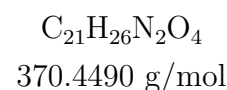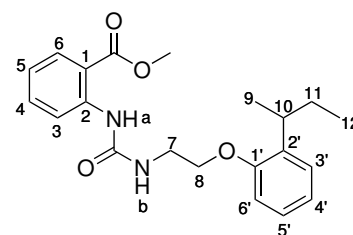
^{1}H NMR (600 MHz, DMSO-d_6): δ [ppm] = 9.80 (s, 1H, NH-a), 8.36 (d, $^3J_{HH}$ = 8.6 Hz, 1H, H-3), 7.89 (dd, $^3J_{HH}$ = 8.0 Hz, $^4J_{HH}$ = 1.7 Hz, 1H, H-6), 7.67 (brs, 1H, NH-b), 7.51 (ddd, $^3J_{HH}$ = 8.7 Hz, 7.1 Hz, $^4J_{HH}$ = 1.7 Hz, 1H, H-4), 7.15-7.10 (m, 3H, H-3', H-5'), 6.99 (ddd, $^3J_{HH}$ = 8.1 Hz, 7.3 Hz, $^4J_{HH}$ = 1.2 Hz, 1H, H-5), 6.94 (dd, $^3J_{HH}$ = 8.6 Hz, $^4J_{HH}$ = 1.2 Hz, H-6'), 6.89 (td, $^3J_{HH}$ = 7.5 Hz, $^4J_{HH}$ = 1.1 Hz, H-4'), 4.00 (t, $^3J_{HH}$ = 5.7 Hz, 2H, H-8), 3.85 (s, 3H, OCH$_3$ 3.48 (dq, $^3J_{HH}$ = 5.6 Hz, 2.5 Hz 2H, H-7), 3.09 (sext, $^3J_{HH}$ = 7.0 Hz, 1H, H-10), 1.59-1.42 (m, 2H, H-11), 1.10 (d, $^3J_{HH}$ = 6.9 Hz, 3H, H-9), 0.72 (t, $^3J_{HH}$ = 7.4 Hz, 3H, H-12). **^{13}C NMR** (151 MHz, DMSO-d_6): δ[ppm] = 167.7 (COOH), 155.9 (C-1'), 154.8 (CONH), 142.6 (C-2), 135.1 (C-2'), 134.0 (C-4), 130.4 (C-6), 126.6 (C-3', C-5'), 120.6 (C-4'), 120.4 (C-5), 119.7 (C-3), 114.3 (C-1), 111.9 (C-6'), 66.9 (C-8), 52.2 (OCH$_3$), 39.0 (C-7), 32.9 (C-10), 29.3 (C-11), 20.4 (C-9), 12.0 (C-12). **ATR-IR**: $\tilde{\nu}$ [cm^{-1}] = 3302, 3081, 2958, 2873, 1702, 1691, 1663, 1597, 1583, 1553, 1509, 1490, 1463, 1447, 1374, 1357, 1303, 1254, 1226, 1191, 1164, 1145, 1114, 1084, 1059, 1044, 1016, 960, 908, 797, 756, 738, 678, 658, 618, 604, 532, 518, 389. **HRMS** (ESI$^+$): m/z = 371.1958 (371.1965 calculated for [M+H]$^+$). **R_f** = 0.10 (CH$_2$Cl$_2$/PE 2:1 v/v).

3-(2-(2-(*sec*-butyl)phenoxy)ethyl)quinazoline-2,4(1*H*,3*H*)-dione 85

The compound was prepared according to general procedure **8**
using methyl ester **84** (238 mg, 642 µmol) and stirring for 18 h
at room temperature. The crude product was recrystallised
via solvent diffusion to finally give quinazoline derivative **85**
(194 mg, 574 µmol, 89 %) as colorless crystals.

¹H NMR (400 MHz, DMSO-d_6): δ [ppm] = 11.50 (s, 1H, NH),
7.97 (dd, $^3J_{HH}$ = 7.9 Hz, $^4J_{HH}$ = 1.5 Hz, 1H, H-6), 7.65 (ddd,
$^3J_{HH}$ = 8.5 Hz, 7.2 Hz, $^4J_{HH}$ = 1.5 Hz, 1H, H-4), 7.25-7.15 (m,
2H, H-3, H-5), 7.13-7.04 (m, 2H, H-4', H-6'), 6.93 (dd, $^3J_{HH}$
= 8.3 Hz, $^4J_{HH}$ = 1.2 Hz, 1H, H-3'), 6.86 (td, $^3J_{HH}$ = 7.4 Hz,

$C_{20}H_{22}N_2O_3$
338.1630 g/mol

$^4J_{HH}$ = 1.. Hz, 1H, H-5'), 4.36 (t, $^3J_{HH}$ = 5.8 Hz, 2H, H-7), 4.19 (t, $^3J_{HH}$ = 5.6 Hz, 2H,
H-8), 2.89 (sext, $^3J_{HH}$ = 7.1 Hz, 1H, H-10), 1.48-1.24 (m, 2H, H-11), 0.95 (d, $^3J_{HH}$ =
6.9 Hz, 3H, H-9), 0.59 (t, $^3J_{HH}$ = 7.3 Hz, 3H, H-12). **¹³C NMR** (101 MHz, DMSO-d_6):
δ[ppm] = 162.1 (C-a), 155.6 (C-1'), 150.2 (C-b), 139.5 (C-2), 135.1 (C-2', C-4'), 127.4
(C-6), 126.6 (C-4', C-6'), 122.5 (C-5), 120.7 (C-5'), 115.1 (C-3), 113.8 (C-1), 111.6 (C-
3'), 64.3 (C-8), 39.0 (C-7), 32.8 (C-10), 29.0 (C-11), 20.2 (C-9), 11.8 (C-12). **ATR-IR**:
$\tilde{\nu}$ [cm⁻¹] = 3233, 3196, 3136, 3067, 2958, 2931, 2873, 1726, 1636, 1598, 1584, 1491, 1472,
1441, 1411, 1335, 1278, 1263, 1232, 1181, 1153, 1095, 1051, 1031 826, 758, 749, 733,
691, 680, 657, 573, 461, 416. **HRMS** (ESI⁺): m/z = 339.1701 (339.1703 calculated for
[M+H]⁺). **R$_f$** = 0.76 (CH$_2$Cl$_2$/CH$_3$OH$_{9:1}$v/v).

6.6.5 Synthesis of phenoxy-based target compound 31b

2-(2-(2-Methylbutan-2-yl)phenoxy)ethan-1-ol 44b

According to general procedure **2**, 2-(2-methylbutan-2-yl)-
phenol **37b** (6.7 mL, 6.6 g, 40 mmol), K$_2$CO$_3$ (14 g, 0.10 mol)
and 2-bromoethanol (7.1 mL, 12 g, 0.10 mol) were used to obtain
phenyl ether **44b** (4.4 g, 21 mmol, 52 %) as colorless liquid.

¹H NMR (400 MHz, DMSO-d_6): δ [ppm] = 7.18-7.11 (m, 2H,
H-3, H-5), 6.93 (dd, $^3J_{HH}$ = 8.8 Hz, $^4J_{HH}$ = 1.1 Hz, 1H, H-6), 6.85

$C_{13}H_{20}O_2$
208.3010 g/mol

(dt, $^3J_{HH}$ = 7.5 Hz, $^4J_{HH}$ = 1.1 Hz, 1H, H-4), 4.80 (t, $^3J_{HH}$ =
5.2 Hz, 1H, OH), 3.97 (t, $^3J_{HH}$ = 5.2 Hz, 2H, H-8), 3.76 (q, $^3J_{HH}$
= 5.2 Hz, 2H, H-7), 1.84 (q, $^3J_{HH}$ = 7.5 Hz, 2H, H-11), 1.30 (s, 6H, H-9), 0.54 (t,
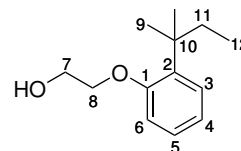
$^3J_{HH}$ = 7.5 Hz, 3H, H-12). **^{13}C NMR** (101 MHz, DMSO-d_6): δ[ppm] = 157.5 (C-1), 135.4 (C-2), 127.5 (C-5), 127.1 (C-3), 120.0 (C-4), 112.3 (C-6), 69.5 (C-8), 59.8 (C-7), 38.0 (C-10), 32.6 (C-11), 27.9 (C-9), 9.6 (C-12). **ATR-IR**: $\tilde{\nu}$ [cm^{-1}] = 3396, 2961, 2874, 1805, 1776, 1597, 1580, 1488, 1461, 1442, 1384, 1291, 1235, 1167, 1134, 1096, 1075, 1052, 920, 908, 897, 776, 744, 718, 686, 613, 576, 542, 506, 489. **HRMS** (ESI$^+$): m/z = 209.1513 (209.1536 calculated for [M+H]$^+$). **MS** (EI): m/z = 208.17 (208.15 calculated for [M]$^{+\cdot}$). **Mp** = 126.3 °C. **R$_f$** = 0.26 (PE/CH$_2$Cl$_2$ 2:1 v/v).

2-(2-(2-Methylbutan-2-yl)phenoxy)ethyl methanesulfonate 75b

The compound was prepared according to general procedure **3**. Alcohol **44b** (3.1 g, 15 mmol), triethylamine (3.1 mL, 2.3 g, 22 mmol) and methanesulfonyl chloride (1.3 mL, 1.9 g, 17 mmol) were used to obtain mesylate **75b** (2.9 g, 10 mmol, 70 %) as yellowish solid.
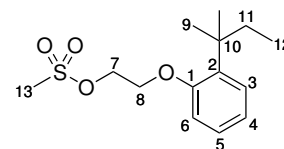
C$_{14}$H$_{22}$O$_4$S
286.3860 g/mol

^{1}H NMR (400 MHz, DMSO-d_6): δ [ppm] = 7.22-7.14 (m, 2H, H-3, H-5), 6.95 (dd, $^3J_{HH}$ = 8.7 Hz, $^4J_{HH}$ = 1.1 Hz, 1H, H-6), 6.90 (dt, $^3J_{HH}$ = 7.6 Hz, $^4J_{HH}$ = 1.0 Hz, 1H, H-4), 4.60-4.51 (m, 2H, H-7), 4.29-4.21 (m, 2H, H-8), 3.22 (s, 3H, H-13), 1.83 (q, $^3J_{HH}$ = 7.5 Hz, 2H, H-11), 1.30 (s, 6H, H-9), 0.55 (t, $^3J_{HH}$ = 7.5 Hz, 3H, H-12). **^{13}C NMR** (101 MHz, DMSO-d_6): δ[ppm] = 156.7 (C-1), 135.5 (C-2), 127.7 (C-5), 127.1 (C-3), 120.6 (C-4), 112.2 (C-6), 68.8 (C-7), 65.7 (C-8), 38.0 (C-10), 36.7 (C-13), 32.6 (C-11), 27.8 (C-9), 9.5 (C-12). **ATR-IR**: $\tilde{\nu}$ [cm^{-1}] = 2965, 2931, 2875, 1598, 1580, 1491, 1462, 1440, 1343, 1235, 1172, 1139, 1100, 1019, 975, 931, 922, 816, 796, 781, 749, 737, 552, 529, 507, 464, 432. **MS** (EI): m/z = 286.18 (286.12 calculated for [M]$^{+\cdot}$). **R$_f$** = 0.27 (PE/CH$_2$Cl$_2$ 2:1 v/v).

1-(2-Azidoethoxy)-2-(2-Methylbutan-2-yl)benzene 72b

According to general procedure **4**, mesylate **75b** (2.80 g, 9.78 mmol) and sodium azide (1.90 g, 29.2 mmol) were used, followed by purification via column chromatography (PE/CH$_2$Cl$_2$ 6:1 v/v), to prepare azide **72b** (1.36 g, 5.83 mmol, 60 %) as colorless liquid.

¹H NMR (400 MHz, DMSO-d_6): δ [ppm] = 7.20-7.14 (m, 2H, H-3, H-5), 6.96 (dd, $^3J_{HH}$ = 8.6 Hz, $^4J_{HH}$ = 1.3 Hz, 1H, H-6), 6.89 (dt, $^3J_{HH}$ = 7.4 Hz, $^4J_{HH}$ = 1.3 Hz, 1H, H-4), 4.15-4.07 (m, 2H, H-8), 3.76-3.69 (m, 2H, H-7), 1.84 (q, $^3J_{HH}$ = 7.5 Hz, 2H, H-11), 1.31 (s, 6H, H-9), 0.56 (t, $^3J_{HH}$ = 7.5 Hz, 3H, H-12). **¹³C NMR** (101 MHz, DMSO-d_6): δ[ppm] = 156.8 (C-1), 135.5 (C-2), 127.7 (C-5), 127.2 (C-3), 120.6 (C-4), 112.4 (C-6), 66.0 (C-8), 50.3 (C-7), 38.0 (C-10), 32.6 (C-11), 27.8 (C-9), 9.6 (C-12). **ATR-IR**: $\tilde{\nu}$ [cm⁻¹] = 2962, 2931, 2873, 2094, 1597, 1579, 1488, 1461, 1442, 1228, 1053, 919, 781. **MS** (EI): m/z = 233.20 (233.15 calculated for [M]⁺·). **R$_f$** = 0.14 (PE/CH$_2$Cl$_2$ 6:1 v/v).
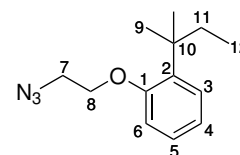
$C_{13}H_{19}N_3O$

233.3150 g/mol

2-(2-(2-Methylbutan-2-yl)phenoxy)ethan-1-amine 42b

The compound was prepared according to general procedure **5**, using azide **72b** (1.29 g, 5.53 mmol) and Pd/C (129 mg). After 2 h stirring, purification was performed via column chromatography (CH$_2$Cl$_2$/CH$_3$OH 19:1 v/v) to obtain amine **42b** (948 mg, 4.57 mmol, 83 %) as colorless liquid.
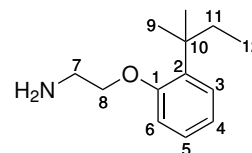
$C_{13}H_{21}NO$

207.3170 g/mol

¹H NMR (400 MHz, DMSO-d_6): δ [ppm] = 7.19-7.11 (m, 2H, H-3, H-5), 6.96-6.89 (m, 1H, H-6), 6.85 (dt, $^3J_{HH}$ = 7.6 Hz, $^4J_{HH}$ = 1.1 Hz, 1H, H-4), 3.91 (t, $^3J_{HH}$ = 5.8 Hz, 1H, H-8), 2.92 (t, $^3J_{HH}$ = 5.8 Hz, 1H, H-7), 1.81 (q, $^3J_{HH}$ = 7.5 Hz, 2H, H-11), 1.29 (s, 6H, H-9), 0.55 (t, $^3J_{HH}$ = 7.5 Hz, 3H, H-12). **¹³C NMR** (101 MHz, DMSO-d_6): δ[ppm] = 157.3 (C-1), 135.1 (C-2), 127.5 (C-5), 127.1 (C-3), 120.0 (C-4), 112.0 (C-6), 70.2 (C-8), 41.2 (C-7), 38.0 (C-10), 32.8 (C-11), 27.9 (C-9), 9.5 (C-12). **ATR-IR**: $\tilde{\nu}$ [cm⁻¹] = 3382, 3057, 2961, 2931, 2863, 1597, 1579, 1489, 1462, 1442, 1376, 1290, 1232, 1197, 1168, 1133, 1095, 1052, 1009, 886, 812, 780, 744. **HRMS** (ESI⁺): m/z = 208.1696 (208.1696 calculated for [M+H]⁺). **R$_f$** = 0.14 (CH$_2$Cl$_2$/CH$_3$OH 19:1 v/v).

Benzyl 2-(3-(2-((2-Methylbutan-2-yl)phenoxy)ethyl)ureido)benzoate 88b

The compound was prepared according to general procedure **6** using triphosgene (0.30 g, 1.0 mmol), benzyl anthranilate **87** (0.23 g, 1.0 mmol), triethylamine (0.29 mL, 0.21 g, 2.1 mmol) and amine **42b** (0.18 g, 0.88 mmol). Ureide **88a** (0.40 g, 0.87 mmol, 99 %) was obtained as colorless solid.

¹H NMR (600 MHz, CD₃CN): δ [ppm] = 10.05 (brs, 1H, NH-a), 8.45 (dd, $^3J_{HH}$ = 8.6 Hz, $^4J_{HH}$ = 1.2 Hz, 1H, H-3), 8.00 (dd, $^3J_{HH}$ = 8.0 Hz, $^4J_{HH}$ = 1.7 Hz, 1H, H-6), 7.51 (ddd, $^3J_{HH}$ = 8.7 Hz, 7.2 Hz, $^4J_{HH}$ = 1.7 Hz, 1H, H-4), 7.48-7.44 (m, 2H, H-2"), 7.43-7.39 (m, 2H, H-3"), 7.38-7.33 (m, 1H, H-4"), 7.22 (dd, $^3J_{HH}$ = 8.0 Hz, $^4J_{HH}$ = 1.7 Hz, 1H, H-3'), 7.16 (ddd, $^3J_{HH}$ = 8.2 Hz, 7.3, $^4J_{HH}$ = 1.7 Hz, 1H, H-5'), 6.98 (ddd, $^3J_{HH}$ = 8.2 Hz, 7.2, $^4J_{HH}$ = 1.2 Hz, 1H, H-5), 6.93 (dd, $^3J_{HH}$ = 8.2 Hz, $^4J_{HH}$ = 1.2 Hz, 1H, H-5'), 6.88 (dt, $^3J_{HH}$ = 7.5 Hz, $^4J_{HH}$ = 1.3 Hz, 1H,

C₂₈H₃₂N₂O₄
460.5740 g/mol

H-4'), 6.03 (brs, NH-b), 5.33 (s, 2H, H-13), 4.07 (t, $^3J_{HH}$ = 5.6 Hz, 2H, H-8), 3.61 (q, $^3J_{HH}$ = 5.6 Hz, 2H, H-7), 1.87 (q, $^3J_{HH}$ = 7.5 Hz, 2H, H-11), 1.32 (s, 6H, H-9), 0.56 (t, $^3J_{HH}$ = 7.5 Hz, 3H, H-12). **¹³C NMR** (125 MHz, DMSO-d_6): δ[ppm] = 168.9 (COOH), 158.5 (C-1'), 155.8 (CONH), 144.4 (C-2), 137.1 (C-1", C-2'), 135.2 (C-4), 131.6 (C-6), 129.6 (C-3"), 129.2 (C-4"), 128.9 (C-2", C-3'), 128.1 (C-5') 121.5 (C-4'), 121.3 (C-5), 120.5 (C-3), 115.0 (C-1), 113.1 (C-6'), 67.6 (C-8), 67.5 (C-13), 40.4 (C-7), 39.1 (C-10), 33.9 (C-11), 28.4 (C-9), 9.9 (C-12). **ATR-IR**: $\tilde{\nu}$ [cm⁻¹] = 3254, 3089, 2959, 2919, 2871, 1679, 1662, 1606, 1593, 1566, 1537, 1523, 1491, 1462, 1441, 1385, 1314, 1283, 1254, 1230, 1161, 1142, 1132, 1123, 1096, 1077, 1055, 960, 910, 900, 802, 748, 740, 714, 695, 632, 612, 590, 538, 627, 418. **HRMS** (ESI⁺): m/z = 461.2438 (2435 calculated for [M+H]⁻). **R$_f$** = 0.33 (CH₂Cl₂).

2-(3-(2-((2-Methylbutan-2-yl)phenoxy)ethyl)ureido)benzoic acid 31b

The compound was prepared according to general procedure **5** using benzoate **88b** (200 mg, 434 µmol) and Pd/C (20 mg). The reaction mixture was stirred for 2 h and the crude product was purified by column chromatography (CH₂Cl₂/CH₃OH 10:1 v/v) and subsequent recrystallisation by solvent diffusion (CH₂Cl₂/CH₃OH/petroleum ether) to obtain carboxylic acid **88b** (308 mg, 814 µmol, 100 %) as colorless crystals.

C₂₁H₂₆N₂O₄
370.4490 g/mol

¹H NMR (500 MHz, DMSO-d_6): δ [ppm] = 10.29 (brs, 1H, NH-a), 8.37 (dd, $^3J_{HH}$ = 8.5 Hz, $^4J_{HH}$ = 0.6 Hz, 1H, H-3), 7.90 (dd, $^3J_{HH}$ = 8.5 Hz, $^4J_{HH}$ = 0.6 Hz, 1H, H-6), 7.58 (brs, 1H, NH-b), 7.46 (ddd, $^3J_{HH}$ = 8.7 Hz, 7.3 Hz, $^4J_{HH}$ = 1.7 Hz, 1H, H-4), 7.20-7.10 (m, 2H, H-3', H-5'), 6.99-6.90 (m, 2H, H-5, H-6'), 6.86
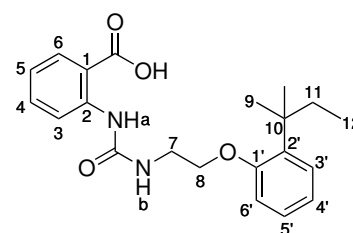
(dt, $^3J_{HH}$ = 7.5 Hz, $^4J_{HH}$ = 0.9 Hz, 1H, H-4'), 4.03 (t, $^3J_{HH}$ = 5.9 Hz, 2H, H-8), 3.51 (q, $^3J_{HH}$ = 5.7 Hz, 2H, H-7), 1.81 (q, $^3J_{HH}$ = 7.5 Hz, 2H, H-11), 1.27 (s, 6H, H-9), 0.52 (t, $^3J_{HH}$ = 7.5 Hz, 3H, H-12). **^{13}C NMR** (126 MHz, DMSO-d_6): δ[ppm] = 169.6 (COOH), 157.2 (C-1'), 154.8 (CONH), 143.1 (C-2), 135.5 (C-2'), 133.5 (C-4), 130.9 (C-6), 127.5 (C-3'/5'), 127.1 (C-3'/5'), 120.2 (C-4'), 120.0 (C-5), 119.1 (C-3), 114.8 (C-1), 112.2 (C-6'), 66.4 (C-8), 38.0 (C-7), 33.0 (C-11), 27.9 (C-9), 9.5 (C-12). **ATR-IR**: $\tilde{\nu}$ [cm^{-1}] = 3291, 3056, 2959, 2862, 1681, 1660, 1605, 1584, 1559, 1542, 1523, 1508, 1489, 1472, 1442, 1405, 1306, 1262, 1214, 1166, 1130, 1092, 1060, 1022, 916, 755, 748, 668, 644, 612, 560, 522, 473, 420, 397, 385. **HRMS** (ESI$^-$): m/z = 369.1809 (369.1820 calculated for [M-H]$^-$). **R_f** = 0.27 (CH$_2$Cl$_2$/CH$_3$OH 10:1 v/v).

6.6.6 Synthesis of phenoxy-based target compound 31c

2-(2-Morpholinophenoxy)ethan-1-ol 44c

According to general procedure **2**, 2-(4-morpholino)phenol **37c** (0.54 g, 3.0 mmol), K$_2$CO$_3$ (1.0 g, 7.5 mmol) and 2-bromoethanol (0.43 mL, 0.75 g, 6.0 mmol) were used to obtain phenyl ether **44c** (0.67 g, 3.0 mmol, 100 %) as colorless crystals.

C$_{12}$H$_{17}$NO$_3$
223.2720 g/mol

^{1}H NMR (500 MHz, CH$_3$CN): δ [ppm] = 7.02-6.94 (m, 4H, H-3, H-3, H-4, H-5, H-6), 4.09-4.04 (m, 2H, H-8), 3.79-3.76 (m, 4H, H-10), 3.74 (dt, $^3J_{HH}$ = 5.7 Hz, 4.5 Hz, 2H, H-7), 3.46 (t, $^3J_{HH}$ = 5.9 Hz, 1H, OH), 3.05-3.01 (m, 4H, H-9). **^{13}C NMR** (151 MHz, CH$_3$CN): δ[ppm] = 152.9 (C-2), 143.7 (C-1), 124.2 (C-5), 123.1 (C-4), 119.2 (C-6), 116.7 (C-3), 72.7 (C-8), 67.2 (C-10), 60.9 (C-7), 52.2 (C-9). **ATR-IR**: $\tilde{\nu}$ [cm^{-1}] = 3391, 2953, 2854, 1666, 1595, 1497, 1448, 1410, 1376, 1333, 1298, 1237, 1208, 1170, 1114, 1068, 1043, 933, 850, 788, 747, 661, 637, 607, 539, 494, 475. **HRMS** (ESI$^+$): m/z = 224.1281 (224.1281 calculated for [M+H]$^+$). **R_f** = 0.26 (CH$_2$Cl$_2$/CH$_3$OH 50:1 v/v).

1-(2-Azidoethoxy)-2-morpholinobenzene 72c

The mesylate was prepared previously, according to general procedure **3**. Alcohol **44c** (0.56 g, 2.5 mmol), triethylamine (0.70 mL, 0.51 g, 5.0 mmol) and methanesulfonyl chloride (0.22 mL, 0.33 g, 2.8 mmol) were used to obtain mesylate **75c** (0.72 g,

2.4 mmol, 95 %) as yellowish oil. Subsequently, the azide was prepared according to general procedure **4**. Mesylate **75c** (719 mg, 2.38 mmol) and sodium azide (310 mg, 4.77 mmol) were used to prepare azide **72c** (524 mg, 2.11 mmol, 89 %) as colorless liquid without purification.

$C_{12}H_{16}N_4O_2$
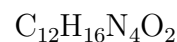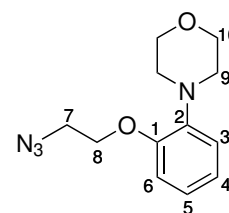
248.2860 g/mol

¹H NMR (600 MHz, DMSO-d_6): δ [ppm] = 6.97-6.89 (m, 4H, H-3, H-4, H-5, H-6), 4.12 (dd, $^3J_{HH}$ = 5.3 Hz, 4.2 Hz, 2H, H-8), 3.73 (t, $^3J_{HH}$ = 4.6 Hz, 4H, H-10), 3.68 (dd, $^3J_{HH}$ = 5.3 Hz, 4.2 Hz, 2H, H-7), 3.01-2.94 (m, 4H, H-9). **¹³C NMR** (151 MHz, DMSO-d_6): δ[ppm] = 150.8 (C-2), 141.4 (C-1), 122.6 (C-5), 121.6 (C-4), 118.1 (C-6), 113.5 (C-3), 66.9 (C-8), 66.4 (C-10), 50.7 (C-9), 50.4 (C-7). **ATR-IR**: $\tilde{\nu}$ [cm⁻¹] = 2956, 2854, 2817, 2101, 1498, 1448, 1299, 1254, 1234, 1209, 1169, 1114, 1058, 1045, 935, 925, 850, 746, 635, 537. **MS** (ESI⁺): m/z = 249.1345 (249.1346 calculated for [M+H]⁺). **R_f** = 0.69 (CH₂Cl₂/CH₃OH 99:1 v/v).

2-(2-Morpholinophenoxy)ethan-1-amine 42c

The compound was prepared according to general procedure **5**, using azide **72c** (420 mg, 1.69 mmol) and Pd/C (45 mg). After 21 h stirring amine **42c** (383 mg, 1.73 mmol, quantitative) was obtained as slightly impure, colorless oil without purification.

$C_{12}H_{18}N_2O_2$
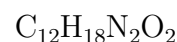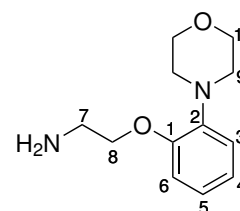
222.2880 g/mol

¹H NMR (600 MHz, DMSO-d_6): δ [ppm] = 6.95-6.91 (m, 2H, H-3, H-5), 6.89-6.85 (m, 2H, H-4, H-6), 6.92 (t, $^3J_{HH}$ = 5.7 Hz, 2H, H-8), 3.72 (t, $^3J_{HH}$ = 4.6 Hz, 4H, H-10), 3.00-2.93 (m, 4H, H-9), 2.87 (t, $^3J_{HH}$ = 5.6 Hz, 2H, H-7). **¹³C NMR** (151 MHz, DMSO-d_6): δ[ppm] = 151.3 (C-1), 141.4 (C-2), 122.5 (C-4), 121.1 (C-5), 117.8 (C-3), 113.5 (C-6), 70.8 (C-8), 66.4 (C-10), 50.7 (C-9), 41.2 (C-7). **ATR-IR**: $\tilde{\nu}$ [cm⁻¹] = 2952, 2852, 2817, 1498, 1448, 1235, 1208, 1113, 1058, 1044, 1026, 924, 849, 745, 637, 536, 493, 477. **HRMS** (ESI⁺): m/z = 223.1443 (223.1441 calculated for [M+H]). **R_f** = 0.34 (CH₂Cl₂/CH₃OH 7:1 v/v).

Benzyl 2-(3-(2-(2-morpholinophenoxy)ethyl)ureido)benzoate 88c

The compound was prepared according to general procedure **6** using triphosgene (0.27 g, 0.93 mmol), benzyl anthranilate (0.42 g, 1.8 mmol), triethylamine (0.51 mL, 0.37 g, 3.7 mmol) and amine **42c** (0.37 g, 1.7 mmol). Ureide **88c** (0.61 g, 1.3 mmol, 80 %) was obtained as colorless crystals.

¹H NMR (500 MHz, DMSO-d_6): δ [ppm] = 9.83 (s, 1H, NH-a), 8.38 (dd, $^3J_{HH}$ = 8.5 Hz, $^4J_{HH}$ = 0.8 Hz, 1H, H-3), 7.94 (dd, $^3J_{HH}$ = 8.0 Hz, $^4J_{HH}$ = 1.6 Hz, 1H, H-6), 7.72-7.64 (m, 1H, NH-b), 7.53 (ddd, $^3J_{HH}$ = 8.8 Hz, 7.2 Hz, $^4J_{HH}$ = 1.7 Hz, 1H, H-4), 7.48-7.44 (m, 2H, H-2"), 7.42-7.38 (m, 2H, H-3"), 7.37-7.33 (m, 1H, H-4"), 7.00 (ddd, $^3J_{HH}$ = 8.2 Hz, 7.1 Hz, $^4J_{HH}$ = 1.2 Hz, 1H, H-5), 6.96 (dd, $^3J_{HH}$ = 7.9 Hz, $^4J_{HH}$ = 1.7 Hz, 1H, H-6'), 6.94 (dd, $^3J_{HH}$ = 6.9 Hz, $^4J_{HH}$ = 1.8 Hz, 1H, H-3'), 6.92-6.84 (m, 2H, H-4', H-5'), 5.35 (s, 2H, NH-b), 5.33 (s, 2H, H-11), 4.03 (t, $^3J_{HH}$ = 5.6 Hz, 2H, H-8), 3.65 (t, $^3J_{HH}$ = 4.6 Hz, 4H, H-10), 3.50 (q, $^3J_{HH}$ = 5.5 Hz, 2H, H-7), 2.98-2.91 (m, 4H, H-9). **¹³C NMR** (126 MHz, DMSO-d_6): δ[ppm] = 167.1 (COO), 154.6 (CONH), 151.0 (C-1'), 142.8 (C-2), 141.3 (C-2'), 135.9 (C-1"), 134.2 (C-4), 130.5 (C-6), 128.5 (C-3"), 128.2 (C-4"), 127.9 (C-2"), 122.4 (C-3'), 121.2 (C-4'), 120.4 (C-5), 119.6 (C-3), 117.8 (C-5'), 113.9 (C-1), 113.3 (C-6'), 66.8 (C-8), 66.4 (C-10), 66.3 (C-11), 50.5 (C-9), 39.0 (C-7). **ATR-IR**: $\tilde{\nu}$ [cm⁻¹] = 3308, 2956, 2852, 2817, 1675, 1588, 1522, 1497, 1446, 1233, 1162, 1145, 1115, 1078, 1044, 1029, 934, 925, 747, 696, 525. **HRMS** (ESI⁺): m/z = 476.2180 (476.2180 calculated for [M+H]⁺). **R_f** = 0.29 (CH₂Cl₂).
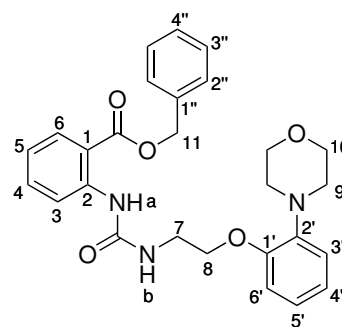
$C_{27}H_{29}N_3O_5$

475.5450 g/mol

2-(3-(2-(2-Morpholinophenoxy)ethyl)ureido)benzoic acid 31c

The compound was prepared according to general procedure **5** using benzoate **88c** (413 mg, 868 µmol) and Pd/C (45 mg). The reaction mixture was stirred for 19 h and the crude product was purified via column chromatography (CH₂Cl₂/CH₃OH 15:1 v/v) and subsequent recrystallisation by solvent diffusion (CH₂Cl₂/CH₃OH/petroleum ether) to obtain carboxylic acid **31c** (268 mg, 697 µmol, 80 %) as colorless crystals.
¹H NMR (500 MHz, DMSO-d_6): δ [ppm] = 10.33 (s, 1H, NH-a), 8.39 (dd, $^3J_{HH}$ = 8.6 Hz, $^4J_{HH}$ = 1.2 Hz, 1H, H-3), 7.91 (dd, $^3J_{HH}$ = 8.0 Hz, $^4J_{HH}$ = 1.7 Hz, 1H, H-6), 7.56 (brs, 1H, NH-b), 7.47 (ddd, $^3J_{HH}$ = 8.7 Hz, 7.2 Hz, $^4J_{HH}$ = 1.8 Hz, 1H, H-4), 6.98-6.90 (m, 3H, H-5, H-3', H-6'), 6.91-6.84 (m, 2H, H-4', H-5'), 4.03 (t, $^3J_{HH}$ = 5.6 Hz, 2H, H-8), 3.68-3.63 (m, 4H, H-10), 3.549 (q, $^3J_{HH}$ = 5.5 Hz, 2H, H-7), 2.98-2.93 (m, 4H, H-9). **¹³C NMR**
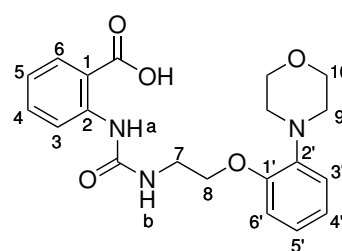
$C_{20}H_{23}N_3O_5$

385.4200 g/mol

(126 MHz, DMSO-d_6): δ[ppm] = 169.6 (COOH), 154.8 (CONH), 151.0 (C-1'), 143.1 (C-2), 141.3 (C-2'), 133.5 (C-4), 130.9 (C-6), 122.4 (C-3'), 121.2 (C-4'), 120.0 (C-5), 119.0 (C-3), 117.7 (C-5'), 115.0 (C-1), 113.3 (C-6'), 66.8 (C-8), 66.4 (C-10), 50.5 (C-9), 39.0 (C-7). **ATR-IR**: $\tilde{\nu}$ [cm^{-1}] = 3310, 2956, 2860, 1681, 1644, 1583, 1538, 1499, 1471, 1448, 1411, 1393, 1268, 1228, 1165, 1117, 1063, 1046, 924, 853, 796, 742, 695, 667, 619, 591, 561, 522, 495, 478, 432, 379. **HRMS** (ESI$^-$): m/z = 384.1568 (384.1565 calculated for [M-H]$^-$)). Decomposes at 127.0 °C. $\mathbf{R_f}$ = 0.24 (CH$_2$Cl$_2$/CH$_3$OH$_{15:1}$v/v).

6.6.7 Synthesis of phenoxy-based target compound 31d

2-(2-(Trifluoromethyl)phenoxy)ethan-1-ol 44d

According to general procedure **2**, 2-(trifluoromethyl)phenol **37d** (4.9 g, 30 mmol), K$_2$CO$_3$ (10 g, 75 mmol) and 2-bromoethanol (4.3 mL, 7.6 g, 60 mmol) were used to obtain phenyl ether **44d** (5.0 g, 24 mmol, 80 %) as colorless liquid.
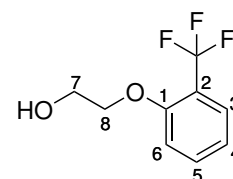
^{1}H NMR (600 MHz, DMSO-d_6): δ [ppm] = 7.64-7.58 (m, 2H, H-3, H-5), 7.27 (d, $^3J_{HH}$ = 8.3 Hz, 1H, H-6), 7.08 (t, $^3J_{HH}$ = 8.3 Hz, 1H, H-4), 4.84 (t, $^3J_{HH}$ = 5.3 Hz, 1H, OH), 4.12 (t, $^3J_{HH}$ = 5.2 Hz, 2H, H-8), 3.73 (q, $^3J_{HH}$ = 5.2 Hz, 2H, H-7). **^{13}C NMR** (151 MHz, DMSO-d_6): δ[ppm] = 156.7 (C-1), 134.2 (C-5), 126.7 (q, $^3J_{CF}$ = 5.7 Hz, C-3), 123.8 (q, $^1J_{CF}$ = 272.1 Hz, CF$_3$), 120.2 (C-4), 117.2 (q, $^2J_{CF}$ = 30.2 Hz, C-2), 113.9 (C-6), 70.4 (C-8), 59.4 (C-7). **^{19}F NMR** (565 MHz, DMSO-d_6): δ[ppm] = -60.71 (CF$_3$). **ATR-IR**: $\tilde{\nu}$ [cm^{-1}] = 3212, 2980, 2930, 1798, 1773, 1608, 1589, 1496, 1482, 1450, 1391, 1371, 1322, 1271, 1255, 1226, 1156, 1113, 1069, 1057, 1036, 972, 943, 918, 891, 857, 805, 773, 751, 716, 651, 614, 600, 582, 534, 499, 471 . **HRMS** (ESI$^+$): m/z = 207.0363 (207.0627 calculated for [M+H]$^+$). $\mathbf{R_f}$ = 0.23 (PE/CH$_2$Cl$_2$ 1:2 v/v).

2-(Trifluoromethyl)phenoxy)ethyl methanesulfonate 75d

The compound was prepared according to general procedure **3**. Alcohol **44d** (4.0 g, 19 mmol), triethylamine (5.4 mL, 3.9 g, 39 mmol) and methanesulfonyl chloride (1.7 mL, 2.5 g, 22 mmol) were used to obtain mesylate **75d** (5.3 g, 19 mmol, 97 %) as yellowish oil.

¹H NMR (600 MHz, DMSO-d_6): δ [ppm] = 7.67-7.61 (m, 2H, H-3, H-5), 7.29 (d, $^3J_{HH}$ = 8.2 Hz, 1H, H-6), 7.13 (t, $^3J_{HH}$ = 7.6 Hz, 1H, H-4), 4.55-4.51 (m, 2H, H-7), 4.48 (s, 3H, H-9) 4.42-4.38 (m, 2H, H-8). **¹³C NMR** (151 MHz, DMSO-d_6): δ[ppm] = 155.8 (C-1), 134.3 (C-5), 126.8 (q, $^3J_{CF}$ = 5.1 Hz, C-3), 123.7 (q, $^1J_{CF}$ = 272.5 Hz, CF$_3$), 120.9 (C-4), 117.3 (q, $^2J_{CF}$ = 29.9 Hz, C-2), 113.9 (C-6), 68.5 (C-7), 66.7 (C-8), 65.0 (C-9). **¹⁹F NMR** (565 MHz, DMSO-d_6): δ[ppm] = -60.71 (CF$_3$).
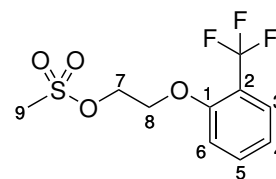
$C_{10}H_{11}F_3O_4S$
284.2492 g/mol

ATR-IR: $\tilde{\nu}$ [cm⁻¹] = 1802, 1775, 1608, 1592, 1497, 1454, 1390, 1353, 1321, 1274, 1257, 1165, 1114, 1068, 1036, 971, 927, 812, 757, 716, 651, 526, 463, 447. **R$_f$** = 0.67 (CH$_2$Cl$_2$).

1-(2-Azidoethoxy)-2-(trifluoromethyl)benzene 72d

The compound was prepared according to general procedure **4**. Mesylate **75d** (5.27 g, 18.6 mmol) and sodium azide (1.38 g, 21.3 mmol) were used, followed by purification via column chromatography (PE/CH$_2$Cl$_2$ 5:1 v/v), to prepare azide **72d** (2.77 g, 12.0 mmol, 65 %) as colorless liquid.

$C_9H_8F_3N_3O$
231.1782 g/mol
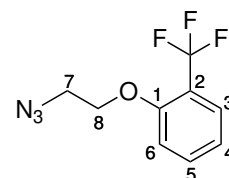
¹H NMR (600 MHz, DMSO-d_6): δ [ppm] = 7.66-7.61 (m, 2H, H-3, H-5), 7.29 (d, $^3J_{HH}$ = 8.4 Hz, 1H, H-6), 7.13 (t, $^3J_{HH}$ = 7.6 Hz, 1H, H-4), 4.28 (t, $^3J_{HH}$ = 4.8 Hz, 2H, H-8), 3.66 (t, $^3J_{HH}$ = 4.8 Hz, 2H, H-7), **¹³C NMR** (151 MHz, DMSO-d_6): δ[ppm] = 155.9 (C-1), 134.3 (C-5), 126.8 (q, $^3J_{CF}$ = 5.3 Hz, C-3), 123.7 (q, $^1J_{CF}$ = 272.2 Hz, CF$_3$), 120.7 (C-4), 117.3 (q, $^2J_{CF}$ = 30.2 Hz, C-2), 113.7 (C-6), 67.5 (C-7), 49.8 (C-8), 65.0 (C-9). **¹⁹F NMR** (565 MHz, DMSO-d_6): δ[ppm] = -60.92 (CF$_3$). **ATR-IR**: $\tilde{\nu}$ [cm⁻¹] = 2939, 2879, 2109, 1609, 1592, 1496, 1456, 1390, 1351, 1320, 1275, 1252, 1164, 1113, 1058, 1036, 946, 918, 846, 804, 753, 651, 614, 599, 554, 531, 468. **MS** (EI): m/z = 231.10 (231.06 calculated for [M]⁺·). **R$_f$** = 0.22 (PE/CH$_2$Cl$_2$ 5:1 v/v).

2-(2-(Trifluoromethyl)phenoxy)ethan-1-amine 42d

The compound was prepared according to general procedure **5**, using azide **72d** (2.74 g, 11.9 mmol) and Pd/C (280 mg). The reaction mixture was stirred for 15 h and the crude product was dissolved in CH$_2$Cl$_2$/CH$_3$OH 9:1 v/v and filtrated through celite to obtain amine **42d** (2.39 g, 11.6 mmol, 98 %) as colorless liquid.

^{1}H NMR (600 MHz, DMSO-d_6): δ [ppm] = 7.64-7.58 (m, 2H, H-3, H-5), 7.25 (d, $^3J_{HH}$ = 8.2 Hz, 1H, H-6), 7.08 (t, $^3J_{HH}$ = 7.6 Hz, 1H, H-4), 4.05 (t, $^3J_{HH}$ = 5.6 Hz, 2H, H-8), 2.88 (t, $^3J_{HH}$ = 5.6 Hz, 2H, H-7). **^{13}C NMR** (151 MHz, DMSO-d_6): δ[ppm] = 156.5 (C-1), 134.3 (C-5), 126.7 (q, $^3J_{CF}$ = 5.3 Hz, C-3), 123.9 (q, $^1J_{CF}$ = 272.0 Hz, CF$_3$), 120.2 (C-4), 117.0 (q, $^2J_{CF}$ = 29.8 Hz, C-2), 113.7 (C-6), 71.1 (C-8), 40.8 (C-7). **^{19}F NMR** (565 MHz, DMSO-d_6): δ[ppm] = -60.87 (CF$_3$). **ATR-IR**: $\tilde{\nu}$ [cm^{-1}] = 2939, 2872, 1608, 1591, 1496, 1457, 1320, 1275, 1256, 1163, 1109, 1056, 1035, 1012, 945, 888, 842, 793, 752, 650, 615, 599, 531, 469. **HRMS** (ESI$^+$): m/z = 206.0794 (206.0787 calculated for [M+H]$^+$). **R$_f$** = 0.10 (CH$_2$Cl$_2$/CH$_3$OH 19:1 v/v).
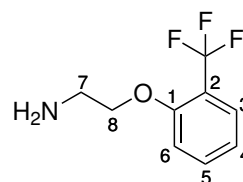
C$_9$H$_{10}$F$_3$NO

205.1802 g/mol

Benzyl 2-(3-(2-((trifluoromethyl)phenoxy)ethyl)ureido)benzoate 88d

The compound was prepared according to general procedure **6** using triphosgene (0.25 g, 0.84 mmol), benzyl anthranilate (0.39 g, 1.7 mmol), triethylamine (0.47 mL, 0.34 g, 3.4 mmol) and amine **42b** (0.31 g, 1.5 mmol). After a second purification step using column chromatography (PE/CH$_2$Cl$_2$ 4:1 v/v), ureide **88d** (0.44 g, 0.95 mmol, 62 %) was obtained as colorless crystals.

C$_{24}$H$_{21}$F$_3$N$_2$O$_4$

458.4372 g/mol

^{1}H NMR (400 MHz, DMSO-d_6): δ [ppm] = 9.83 (s, 1H, NH-a), 8.34 (dd, $^3J_{HH}$ = 8.7 Hz, $^4J_{HH}$ = 1.2 Hz, 1H, H-3), 7.94 (dd, $^3J_{HH}$ = 8.0 Hz, $^4J_{HH}$ = 1.7 Hz, 1H, H-6), 7.71 (t, $^3J_{HH}$ = 5.5 Hz, 1H, NH-b), 7.62 (m, 2H, H-3', H-5'), 7.53 (ddd $^3J_{HH}$ = 8.7 Hz, 7.2 Hz, $^4J_{HH}$ = 1.7 Hz, 1H, H-4), 7.49-7.44 (m, 2H, H-2"), 7.43-7.34 (m, 3H, H-3", H-4"), 7.30 (d, $^3J_{HH}$ = 7.6 Hz, 1H, H-6'), 7.10 (t, $^3J_{HH}$ = 7.6 Hz, 1H, H-4'), 7.01 (ddd, $^3J_{HH}$ = 8.2 Hz, 7.2 Hz, $^4J_{HH}$ = 1.2 Hz, 1H, H-5), 5.35 (s, 2H, H-9), 4.16 (t, $^3J_{HH}$ = 5.9 Hz, 2H, H-8), 4.16 (q, $^3J_{HH}$ = 5.8 Hz, 2H, H-7). **^{13}C NMR** (101 MHz, DMSO-d_6): δ[ppm] = 167.1 (COO), 156.3 (C-1'), 154.8 (CONH), 142.7 (C-2), 136.0 (C-1"), 134.3 (C-5'), 134.1 (C-4), 130.5 (C-6), 128.6 (C-3"), 128.2 (C-4"), 128.0 (C-2"), 126.7 (q, $^3J_{CF}$ = 5.2 Hz, C-3'), 123.6 (m, CF$_3$), 120.6 (C-5), 120.4 (C-4'), 119.7 (C-3), 117.2 (q, $^2J_{CF}$ = 29.6 Hz, C-2'), 114.1 (C-1), 113.8 (C-6'), 67.4 (C-8), 66.3 (C-9), 38.7 (C-7). **^{19}F NMR** (565 MHz, DMSO-d_6): δ[ppm] = -60.69 (CF$_3$). **ATR-IR**: $\tilde{\nu}$ [cm^{-1}] = 3313, 3088, 3035, 2939, 2880, 1703, 1649, 1607, 1589, 1557, 1525, 1496, 1452, 1379, 1321, 1308, 1279, 1252, 1237, 1167, 1158, 1148, 1121,

1110, 1086, 1074, 1058, 1029, 948, 832, 754, 731, 695, 679, 652, 634, 601, 581, 523, 469, 406. **HRMS** (ESI$^+$): m/z = 459.1525 (459.1526 calculated for [M+H]$^+$). **R$_f$** = 0.39 (CH$_2$Cl$_2$).

2-(3-(2-((Trifluoromethyl)phenoxy)ethyl)ureido)benzoic acid 31d

The compound was prepared according to general procedure **5** using benzoate **88d** (381 mg, 831 µmol) and Pd/C (25 mg). The reaction mixture was stirred for 2 h and the crude product was purified by recrystallisation by solvent diffusion (CH$_2$Cl$_2$/CH$_3$OH/petroleum ether) to obtain carboxylic acid **31d** (240 mg, 653 µmol, 79 %) as colorless crystals.
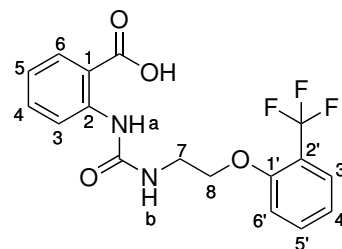
C$_{17}$H$_{15}$F$_3$N$_2$O$_4$
368.3122 g/mol

^{1}H NMR (500 MHz, DMSO-d_6): δ [ppm] = 10.17 (brs, 1H, NH-a), 8.37 (dd, $^3J_{HH}$ = 8.6 Hz, $^4J_{HH}$ = 1.1 Hz, 1H, H-3), 7.90 (dd, $^3J_{HH}$ = 8.0 Hz, $^4J_{HH}$ = 1.7 Hz, 1H, H-6), 7.62 (m, 2H, H-3', H-5', NH-b), 7.48 (ddd $^3J_{HH}$ = 8.8 Hz, 7.2 Hz, $^4J_{HH}$ = 1.8 Hz, 1H, H-4), 7.31 (d, $^3J_{HH}$ = 8.3 Hz, 1H, H-6'), 7.10 (t, $^3J_{HH}$ = 7.6 Hz, 1H, H-4'), 6.96 (ddd, $^3J_{HH}$ = 8.2 Hz, 7.2 Hz, $^4J_{HH}$ = 1.2 Hz, 1H, H-5), 4.17 (t, $^3J_{HH}$ = 6.1 Hz, 2H, H-8), 3.46 (q, $^3J_{HH}$ = 5.9 Hz, 2H, H-7). **^{13}C NMR** (126 MHz, DMSO-d_6): δ[ppm] = 169.5 (COO), 156.3 (C-1'), 154.8 (CONH), 142.7 (C-2), 134.2 (C-5'), 133.7 (C-4), 130.9 (C-6), 126.7 (q, $^3J_{CF}$ = 5.1 Hz, C-3'), 123.7 (q, $^1J_{CF}$ = 272.3 Hz, chCF3), 120.4 (C-4'), 120.1 (C-5), 119.2 (C-3), 117.3 (q, $^2J_{CF}$ = 30.0 Hz, C-2'), 114.6 (C-1), 113.8 (C-6'), 67.3 (C-8), 38.6 (C-7). **ATR-IR**: $\tilde{\nu}$ [cm^{-1}] = 3221, 3106, 2973, 2890, 2646, 2555, 1686, 1672, 1604, 1587, 1540, 1497, 1458, 1448, 1415, 1400, 1372, 1325, 1309, 1272, 1251, 1160, 1126, 1114, 1058, 1038, 943, 929, 884, 811, 755, 747, 699, 656, 620, 599, 589, 548, 525. **HRMS** (ESI$^-$): m/z = 367.0723 (367.0911 calculated for [M-H]$^-$). **Mp** = 170.8 °C. **R$_f$** = 0.28 (CH$_2$Cl$_2$/CH$_3$OH 9:1 v/v).

6.6.8 Synthesis of thiophenoxy-based target compounds 31e and 35

2-((2-(Trifluoromethyl)phenyl)thio)ethan-1-ol 44e

According to general procedure **2**, 2-(trifluoromethyl)benzene-thiol **37e** (4.6 g, 26 mmol), K_2CO_3 (10 g, 75 mmol) and 2-bromoethanol (4.3 mL, 7.6 g, 61 mmol) were used to obtain thiophenyl ether **44e** (5.1 g, 23 mmol, 90 %) as colorless liquid. **¹H NMR** (500 MHz, DMSO-d_6): δ [ppm] = 7.70 (dd , $^3J_{HH}$ = 7.9 Hz, $^4J_{HH}$ = 1.6 Hz, 1H, H-3), 7.66 (d, $^3J_{HH}$ = 8.0 Hz, 1H, H-6), 7.64-7.59 (m, 1H, H-5), 7.36 (m, 1H, H-4), 4.99 (t, $^3J_{HH}$ = 5.5 Hz, 1H, OH), 3.60 (dt, $^3J_{HH}$ = 6.7 Hz, $^3J_{HH}$ = 5.5 Hz, 2H, H-7), 3.14 (t, $^3J_{HH}$ = 6.7 Hz, 2H, H-8). **¹³C NMR** (126 MHz, DMSO-d_6): δ[ppm] = 136.3 (C-1), 132.8 (C-5), 129.3 (C-6), 127.1 (q, $^2J_{CF}$ = 29.0 Hz, C-2), 126.6 (q, $^3J_{CF}$ = 5.7 Hz, C-3), 125.5 (C-4), 123.9 (q, $^1J_{CF}$ = 273.6 Hz, CF_3), 59.5 (C-7), 35.2 (C-8). **¹⁹F NMR** (565 MHz, DMSO-d_6): δ[ppm] = -60.11 (CF_3). **ATR-IR**: $\tilde{\nu}$ [cm⁻¹] = 3340, 2932, 2882, 1594, 1572, 1471, 1440, 1309, 1257, 1167, 1110, 1096, 1045, 1032, 950, 759, 731, 703, 645, 596, 509, 444. **HRMS** (ESI⁺): m/z = 205.0298 (205.0293 calculated for [M-OH]⁺). R_f = 0.28 (PE/EA 2:1 v/v).
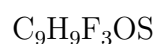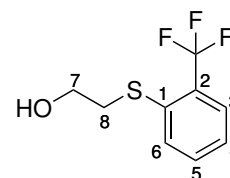
C₉H₉F₃OS
222.2252 g/mol

2-((2-(Trifluoromethyl)phenyl)thio)ethyl methanesulfonate 75e

The compound was prepared according to general procedure **3**, with the difference of using *N,N*-di*iso*propylethylamine (DI-PEA) instead of triethylamine and stirring for 15 h. Alcohol **44e** (4.0 g, 18 mmol), DIPEA (6.1 mL, 4.6 g, 36 mmol) and methanesulfonyl chloride (1.8 mL, 2.6 g, 23 mmol) were used to obtain mesylate **75e** (5.3 g, 19 mmol, 97 %) as yellowish oil. **¹H NMR** (600 MHz, DMSO-d_6): δ [ppm] = 7.78-7.71 (m, 2H, H-3, H-6), 7.66 (t, $^3J_{HH}$ = 7.7 Hz, 1H, H-5), 7.43 (t, $^3J_{HH}$ = 7.8 Hz, 1H, H-4), 4.34 (t, $^3J_{HH}$ = 6.5 Hz, 2H, H-7), 3.46 (t, $^3J_{HH}$ = 6.5 Hz, 2H, H-8), 3.17 (s, 3H, H-9). **¹³C NMR** (151 MHz, DMSO-d_6): δ[ppm] = 134.4 (C-1), 133.1 (C-5), 130.4 (C-6), 127.8 (q, $^2J_{CF}$ = 29.5 Hz, C-2), 126.9 (q, $^3J_{CF}$ = 5.8 Hz, C-3), 126.5 (C-4), 123.8 (q, $^1J_{CF}$ = 273.6 Hz, CF_3), 67.9 (C-7), 36.8 (C-9), 31.7 (C-8). **¹⁹F NMR** (565 MHz, DMSO-d_6): δ[ppm] = -59.71 (CF_3). **ATR-IR**: $\tilde{\nu}$ [cm⁻¹] = 3031, 2942, 1593,
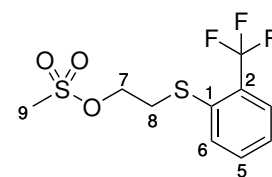
C₁₀H₁₁F₃O₃S₂
300.3102 g/mol

1472, 1441, 1354, 1310, 1260, 1167, 1111, 1097, 1046, 1033, 972, 943, 884, 843, 792, 762, 731, 703, 645, 597, 525, 489, 444, 412. **HRMS** (ESI$^+$): m/z = 205.0302 (205.0293 calculated for [M-CH$_3$O$_3$S]$^+$). **R$_f$** = 0.61 (CH$_2$Cl$_2$).

(2-Azidoethyl)(2-(trifluoromethyl)phenyl)sulfane **72e**

The compound was prepared according to general procedure **4**. Mesylate **75e** (5.36 g, 17.9 mmol) and sodium azide (1.31 g, 20.1 mmol) were used, followed by purification via column chromatography (PE/CH$_2$Cl$_2$ 9:1 v/v), to prepare azide **72e** (3.52 g, 14.3 mmol, 80 %) as colorless liquid.

C$_9$H$_8$F$_3$N$_3$S
247.2392 g/mol

¹H NMR (600 MHz, DMSO-d_6): δ [ppm] = 7.75-7.70 (m, 2H, H-3, H-6), 7.65 (t, $^3J_{HH}$ = 7.7 Hz, 1H, H-5), 7.41 (t, $^3J_{HH}$ = 7.6 Hz, 1H, H-4), 3.56 (t, $^3J_{HH}$ = 6.5 Hz, 2H, H-7), 3.33-3.29 (m, 2H, H-8). **¹³C NMR** (151 MHz, DMSO-d_6): δ[ppm] = 134.8 (C-1), 133.0 (C-5), 130.2 (C-6), 127.7 (q, $^2J_{CF}$ = 29.6 Hz, C-2), 126.8 (q, $^3J_{CF}$ = 5.7 Hz, C-3), 126.3 (C-4), 123.8 (q, $^1J_{CF}$ = 273.7 Hz, CF$_3$), 49.4 (C-7), 32.2 (C-8). **¹⁹F NMR** (565 MHz, DMSO-d_6): δ[ppm] = -59.83 (CF$_3$). **ATR-IR**: $\tilde{\nu}$ [cm^{-1}] = 3031, 2942, 1593, 1472, 1441, 1354, 1310, 1260, 1167, 1111, 1097, 1046, 1033, 972, 943, 884, 843, 792, 762, 731, 703, 645, 597, 525, 489, 444, 412. **R$_f$** = 0.23 (PE/CH$_2$Cl$_2$ 9:1 v/v).
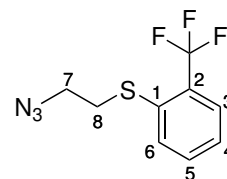
2-((2-(Trifluoromethyl)phenyl)thio)ethan-1-amine 42e

The compound was prepared according to general procedure **5**, using azide **72e** (3.49 g, 14.1 mmol) and Pd/C (350 mg). The reaction mixture was stirred for 14 h. The crude product was dissolved in CH$_2$Cl$_2$/CH$_3$OH 7:3 v/v and filtrated through celite to obtain amine **42e** (2.76 g, 12.5 mmol, 88 %) as slightly impured, yellowish liquid.

C$_9$H$_{10}$F$_3$NS
221.2412 g/mol

¹H NMR (600 MHz, CD$_3$CN): δ [ppm] = 7.69 (dd, $^3J_{HH}$ = 7.8 Hz, $^4J_{HH}$ = 1.5 Hz, 1H, H-3), 7.62 (d, $^3J_{HH}$ = 8.0 Hz, 1H, H-6), 7.56 (ddd, $^3J_{HH}$ = 8.1 Hz, 7.3 Hz, $^4J_{HH}$ = 0.8 Hz, 1H, H-5), 7.34 (t, $^3J_{HH}$ = 7.6 Hz, 1H, H-4), 3.08 (t, $^3J_{HH}$ = 6.7 Hz, 2H, H-8), 2.83 (t, $^3J_{HH}$ = 6.7 Hz, 2H, H-7). **¹³C NMR** (151 MHz, CD$_3$CN): δ[ppm] = 137.2 (C-1), 133.5 (C-5), 131.3 (C-6), 129.6 (C-2) 127.8 (q, $^3J_{CF}$ = 5.7 Hz, C-3), 126.7 (C-4), 125.2 (q, $^1J_{CF}$ = 272.6 Hz, CF$_3$), 41.8 (C-7), 38.1 (C-8). **¹⁹F NMR** (565 MHz, CD$_3$CN): δ[ppm] = -62.62 (CF$_3$). **ATR-IR**: $\tilde{\nu}$ [cm^{-1}]
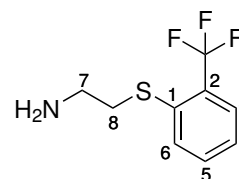
= 3288, 3067, 2927, 2864, 1664, 1593, 1572, 1440, 1309, 1256, 1168, 1110, 1096, 1045, 1032, 950, 864, 759, 731, 703, 645, 596, 510, 444. **HRMS** (ESI$^+$): m/z = 222.0580 (222.0559 calculated for [M+H]$^+$). $\mathbf{R_f}$ = 0.05 (CH$_2$Cl$_2$/CH$_3$OH 19:1 v/v).
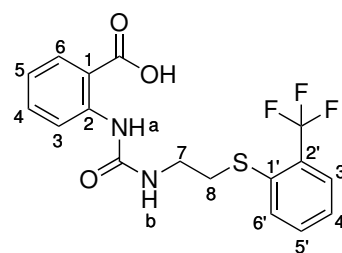
Benzyl 2-(3-(2-((2-(trifluoromethyl)phenyl)thio)ethyl)ureido)benzoate 88e

The compound was prepared according to general procedure **6** using triphosgene (0.30 g, 1.0 mmol), benzyl anthranilate (0.47 g, 2.1 mmol), triethylamine (0.60 mL, 0.44 g, 4.3 mmol) and amine **42e** (0.40 g, 1.8 mmol). Ureide **88e** (0.54 g, 1.1 mmol, 62 %) was obtained as yellowish syrup.

$C_{24}H_{21}F_3N_2O_3S$
474.4982 g/mol

^{1}H NMR (600 MHz, CD$_3$CN): δ [ppm] = 10.00 (s, 1H, NH-a), 8.43 (dd, $^3J_{HH}$ = 8.6 Hz, $^4J_{HH}$ = 1.2 Hz, 1H, H-3), 8.00 (dd, $^3J_{HH}$ = 8.0 Hz, $^4J_{HH}$ = 1.7 Hz, 1H, H-6), 7.71 (d, $^3J_{HH}$ = 8.0 Hz, 1H, H-6'), 7.68 (dd, $^3J_{HH}$ = 7.9 Hz, $^4J_{HH}$ = 1.5 Hz, 1H, H-3'), 7.55 (ddd $^3J_{HH}$ = 8.1 Hz, 7.3 Hz, $^4J_{HH}$ = 0.8 Hz, 1H, H-5'), 7.51 (ddd $^3J_{HH}$ = 8.5 Hz, 7.3 Hz, $^4J_{HH}$ = 1.6 Hz, 1H, H-4), 7.48-7.45 (m, 2H, H-2"), 7.44-7.39 (m, 2H, H-3"), 7.38-7.34 (m, 1H, H-4"), 7.32 (dt, $^3J_{HH}$ = 7.6 Hz, $^4J_{HH}$ = 1.0 Hz, 1H, H-4'), 6.99 (ddd, $^3J_{HH}$ = 8.2 Hz, 7.2 Hz, $^4J_{HH}$ = 1.2 Hz, 1H, H-5), 6.07 (brs, 1H, NH-b) 5.34 (s, 2H, H-9), 3.40 (dt, $^3J_{HH}$ = 7.0 Hz, 5.9 Hz, 2H, H-7), 3.20-3.16 (m, 2H, H-8). **^{13}C NMR** (151 MHz, CD$_3$CN): δ[ppm] = 168.9 (COO), 155.7 (CONH), 144.3 (C-2), 137.1 (C-1"), 136.8 (C-1'), 135.2 (C-4), 133.6 (C-5'), 131.7 (C-6), 131.1 (C-6'), 129.6 (C-3"), 129.4 (q, $^2J_{CF}$ = 30.0 Hz, C-2'), 129.3 (C-4"), 129.0 (C-2"), 127.8 (q, $^3J_{CF}$ = 6.0 Hz, C-3'), 126.8 (C-4'), 125.2 (q, $^1J_{CF}$ = 272.9 Hz, CF$_3$), 121.6 (C-5), 120.4 (C-3), 115.1 (C-1), 67.6 (C-9), 40.0 (C-7), 33.8 (C-8). **^{19}F NMR** (565 MHz, DMSO-d_6): δ[ppm] = -61.51 (CF$_3$). **ATR-IR**: $\tilde{\nu}$ [cm^{-1}] = 3308, 3067, 3035, 2945, 1672, 1606, 1589, 1524, 1446, 1377, 1311, 1246, 1165, 1126, 1114, 1079, 1046, 1033, 957, 752, 732, 697, 645, 597, 525. **HRMS** (ESI$^+$): m/z = 475.1298 (475.1298 calculated for [M+H]$_+$). $\mathbf{R_f}$ = 0.31 (PE/CH$_2$Cl$_2$ 1:1 v/v).

2-(3-(2-((2-(Trifluoromethyl)phenyl)thio)ethyl)ureido)benzoic acid 31e

The compound was prepared according to general procedure **5**, with the exception of using 50 w% of the catalyst instead of 10 w%. Benzoate **88e** (401 mg, 846 µmol) and

Pd/C (200 mg) were used, the reaction mixture was stirred for 2 h and the crude product was purified by recrystallisation by solvent diffusion to obtain carboxylic acid **31e** (132 mg, 343 µmol, 41 %) as colorless crystals.

$C_{17}H_{15}F_3N_2O_3S$

384.3732 g/mol

¹H NMR (600 MHz, CD$_3$CN): δ [ppm] = 13.28 (brs, 1H, COOH) 10.26 (s, 1H, NH-a), 8.38 (dd, $^3J_{HH}$ = 8.6 Hz, $^4J_{HH}$ = 1.2 Hz, 1H, H-3), 7.91 (dd, $^3J_{HH}$ = 8.0 Hz, $^4J_{HH}$ = 1.7 Hz, 1H, H-6), 7.75 (d, $^3J_{HH}$ = 8.0 Hz, 1H, H-6'), 7.73 (brs, 1H, NH-b), 7.72 (dd, $^3J_{HH}$ = 7.8 Hz, $^4J_{HH}$ = 1.5 Hz, 1H, H-3'), 7.64 (dt $^3J_{HH}$ = 7.7 Hz, $^4J_{HH}$ = 1.5 Hz, 1H, H-5'), 7.48 (ddd $^3J_{HH}$ = 8.7 Hz, 7.2 Hz, $^4J_{HH}$ = 1.8 Hz, 1H, H-4), 7.38 (t, $^3J_{HH}$ = 7.6 Hz, 1H, H-4'), 6.98-6.93 (m, 1H, H-5), 3.33-3.27 (m, 2H, H-7), 3.18 (t, $^3J_{HH}$ = 7.2 Hz, 2H, H-8). **¹³C NMR** (151 MHz, CD$_3$CN): δ[ppm] = 169.6 (COO), 154.7 (CONH), 143.0 (C-2), 135.7 (C-1'), 133.7 (C-4), 133.0 (C-5'), 131.0 (C-6), 129.2 (C-6'), 127.1 (q, $^2J_{CF}$ = 30.0 Hz, C-2'), 126.8 (q, $^3J_{CF}$ = 5.8 Hz, C-3'), 125.7 (C-4'), 123.9 (q, $^1J_{CF}$ = 274.0 Hz, CF$_3$), 120.2 (C-5), 119.0 (C-3), 114.7 (C-1), 38.6 (C-7), 32.0 (C-8). **¹⁹F NMR** (565 MHz, DMSO-d_6): δ[ppm] = -60.06 (CF$_3$). **ATR-IR**: $\tilde{\nu}$ [cm^{-1}] = 3330, 3293, 2925, 2868, 2624, 2556, 1678, 1654, 1605, 1595, 1582, 1540, 1512, 1473, 1451, 1433, 1402, 1314, 1257, 1221, 1169, 1107, 1088, 1047, 1033, 950, 918, 762, 748, 728, 694, 669, 627, 596, 559, 522, 399. **HRMS** (ESI$^+$): m/z = 383.0681 (383.0683 calculated for [M-H]$^-$). **Mp** = 141.4 °C. **R$_f$** = 0.25 (CH$_2$Cl$_2$/CH$_3$OH 9:1 v/v).

2-(3-(2-((2-(Trifluoromethyl)phenyl)sulfinyl)ethyl)ureido)benzoic acid 35

The compound was prepared under nitrogen atmosphere. Phenylthioether **31e** (38.4 mg, 99.9 µmol) was dissolved in dry dichloromethane. At 0 °C, 3-chloroperoxybenzoic acid (*m*-CPBA) was slowly added and the reaction mixture was stirred for 2 h. The crude product was freed from solvent and purified by column chromatography (CH$_2$Cl$_2$/CH$_3$OH 10:1 v/v) to obtain sulfinyl ether **35** (34.0 mg, 84.6 µmol, 85 %) as colorless solid.

$C_{17}H_{15}F_3N_2O_4S$

400.3722 g/mol

¹H NMR (600 MHz, CD$_3$CN): δ [ppm] = 10.29 (s, 1H, NH-a), 8.42 (d, $^3J_{HH}$ = 8.6 Hz, 1H, H-3), 8.22 (d, $^3J_{HH}$ = 8.0 Hz, 1H, H-6'), 7.99 (d, $^3J_{HH}$ = 7.9 Hz, 1H, H-6), 7.88 (t, $^3J_{HH}$ = 7.8 Hz, 1H, H-5'), 7.80 (d, $^3J_{HH}$ = 7.8 Hz, 1H, H-3'), 7.70 (t $^3J_{HH}$ = 7.7 Hz, 1H, H-4'), 7.49 (t $^3J_{HH}$

= 8.0 Hz, 1H, H-4), 6.98 (t, $^3J_{HH}$ = 8.0 Hz, 1H, H-5), 6.19 (brs, 1H, NH-b) 3.68-3.51 (m, 2H, H-7), 3.22-3.13 (m, 1H, H-8a), 2.87-2.79 (m, 1H, H-8b). ^{13}**C NMR** (151 MHz, CD$_3$CN): δ[ppm] = 155.8 (CONH), 144.9 (C-1'), 144.4 (C-2), 135.2 (C-4), 134.6 (C-5'), 132.4 (C-4'), 132.2 (C-6), 127.7 (q, $^3J_{CF}$ = 5.5 Hz, C-3'), 126.6 (m, C-2'), 126.3 (C-6'), 125.7 (C-5), 125.1 (m, CF$_3$), 120.0 (C-3), 114.8 (C-1), 58.5 (C-8), 35.0 (C-7). ^{19}**F NMR** (565 MHz, DMSO-d_6): δ[ppm] = -75.75 (CF$_3$). **ATR-IR**: $\tilde{\nu}$ [cm^{-1}] = 3675, 3359, 3313, 3191, 2956, 2919, 2851, 1659, 1633, 1536, 1466, 1410, 1394, 1377, 1314, 1260, 1181, 1162, 1133, 1080, 1066, 1056, 1027, 967, 889, 756, 720, 702, 645. **HRMS** (ESI$^-$): m/z = 399.0629 (399.0632 calculated for [M-H]$^-$). $\mathbf{R_f}$ = 0.09 (CH$_2$Cl$_2$/CH$_3$OH 9:1 v/v).

6.6.9 Synthesis of phenyl-based target compound 31f

Benzyl 2-(3-(2-(trifluoromethyl)phenylethyl)ureido)benzoate 88f

The compound was prepared according to general procedure **6** using triphosgene (0.16 g, 0.55 mmol), benzyl anthranilate (0.15 g, 1.1 mmol), triethylamine (0.30 mL, 0.22 g, 2.2 mmol) and 2-(2-(trifluoromethyl)phenyl) ethan-1-amine **42f** (0.19 g, 0.99 mmol). Finally, the crude product was purified by column chromatography (PE/EA 20:1 v/v) to yield ureide **88f** (0.19 g, 0.43 mmol, 44 %) as colorless crystals.
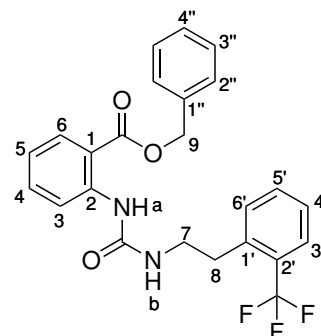
C$_{24}$H$_{21}$F$_3$N$_2$O$_3$
442.4382 g/mol

^{1}**H NMR** (600 MHz, CD$_3$CN): δ [ppm] = 9.99 (s, 1H, NH-a), 8.44 (dd, $^3J_{HH}$ = 8.5 Hz, $^4J_{HH}$ = 1.2 Hz, 1H, H-3), 8.01 (dd, $^3J_{HH}$ = 8.0 Hz, $^4J_{HH}$ = 1.7 Hz, 1H, H-6), 7.68 (d, $^3J_{HH}$ = 7.9 Hz, 1H, H-3'), 7.56 (t, $^3J_{HH}$ = 7.6 Hz, 1H, H-5'), 7.51 (ddd $^3J_{HH}$ = 8.7 Hz, 7.2 Hz, $^4J_{HH}$ = 1.7 Hz, 1H, H-4), 7.49-7.45 (m, 3H, H-6', H-2"), 7.44-7.35 (m, 4H, H-4', H-3", H-4"), 7.98 (ddd, $^3J_{HH}$ = 8.2 Hz, 7.2 Hz, $^4J_{HH}$ = 1.2 Hz, 1H, H-5), 5.96 (brs, 1H, NH-b), 5.35 (s, 2H, H-9), 3.43 (dt, $^3J_{HH}$ = 7.8 Hz, 6.2 Hz 2H, H-7), 3.01 (t, $^3J_{HH}$ = 7.3 Hz, 2H, H-8). ^{13}**C NMR** (151 MHz, CD$_3$CN): δ[ppm] = 168.9 (COO), 155.7 (CONH), 144.5 (C-2), 139.1 (C-1'), 137.2 (C-1"), 135.2 (C-4), 133.2 (C-5'), 132.9 (C-6'), 131.7 (C-6), 129.6 (C-3"), 129.3 (C-4"), 129.0 (C-2"), 127.7 (C-4'), 127.9 (q, $^2J_{CF}$ = 31.4 Hz, C-2'), 126.9 (q, $^3J_{CF}$ = 5.7 Hz, C-3'), 125.9 (q, $^1J_{CF}$ = 273.1 Hz, CF$_3$), 121.5 (C-5), 120.4 (C-3), 115.0 (C-1), 67.6 (C-9), 41.39 (C-7), 33.8 (C-8). ^{19}**F NMR** (565 MHz, DMSO-d_6): δ[ppm] = -59.84 (CF$_3$). **ATR-IR**: $\tilde{\nu}$ [cm^{-1}]

= 3297, 3063, 3034, 2972, 2911, 1694, 1682, 1654, 1607, 1590, 1545, 1509, 1451, 1382, 1370, 1314, 1276, 1251, 1164, 1145, 1129, 1104, 1078, 1060, 1034, 989, 965, 916, 891, 868, 799, 769, 751, 740, 698, 665, 650, 599, 587, 572, 540, 526, 514, 489, 450. **HRMS** (ESI$^+$): m/z = 465.1399 (465.1396 calculated for [M+Na]$^+$). **R$_f$** = 0.28 (CH$_2$Cl$_2$).

2-(3-(2-(Trifluoromethyl)phenylethyl)ureido)benzoic acid 31f

The compound was prepared according to general procedure **5** using benzoate **88f** (159 mg, 359 µmol) and Pd/C (20 mg). The reaction mixture was stirred for 19 h and the crude product was purified by column chtomatography (CH$_2$Cl$_2$/CH$_3$OH 20:1 v/v) and subsequent recrystallisation by solvent diffusion to obtain carboxylic acid **31f** (90.0 mg, 255 µmol, 71 %) as colorless, papery solid.
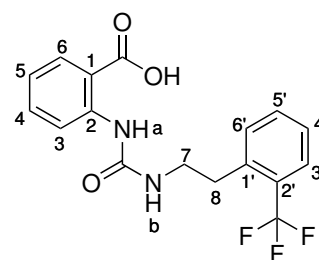
C$_{17}$H$_{15}$F$_3$N$_2$O$_3$

352.3132 g/mol

^{1}H NMR (500 MHz, DMSO-d_6): δ [ppm] = 13.27 (brs, 1H, COOH), 10.14 (brs, 1H, NH-a), 8.37 (dd, $^3J_{HH}$ = 8.5 Hz, $^4J_{HH}$ = 1.2 Hz, 1H, H-3), 7.90 (dd, $^3J_{HH}$ = 7.9 Hz, $^4J_{HH}$ = 1.7 Hz, 1H, H-6), 7.69 (dd, $^3J_{HH}$ = 8.0 Hz, $^4J_{HH}$ = 1.3 Hz, 1H, H-3'), 7.67-7.59 (m, 2H, H-5', NH-b), 7.51 (d $^3J_{HH}$ = 7.7 Hz, 1H, H-6'), 7.47 (ddd, $^3J_{HH}$ = 8.7 Hz, 7.1 Hz, $^4J_{HH}$ = 1.8 Hz, 1H, H-4), 7.43 (t, $^3J_{HH}$ = 7.6 Hz, 1H, H-4'), 6.95 (ddd, $^3J_{HH}$ = 8.2 Hz, 7.2 Hz, $^4J_{HH}$ = 1.2 Hz, 1H, H-5), 4.33 (dt, $^3J_{HH}$ = 8.1 Hz, 5.7 Hz, 2H, H-7), 2.95 (t, $^3J_{HH}$ = 7.5 Hz, 2H, H-8). **^{13}C NMR** (126 MHz, DMSO-d_6): δ[ppm] = 169.5 (COO), 154.6 (CONH), 143.1 (C-2), 137.9 (C-1'), 133.7 (C-5'), 132.5 (C-6'), 131.7 (C-4), 130.9 (C-6), 127.3 (q, $^2J_{CF}$ = 28.8 Hz, C-2'), 126.7 (C-4'), 125.7 (q, $^3J_{CF}$ = 5.5 Hz, C-3'), 124.6 (q, $^1J_{CF}$ = 274.7 Hz, CF3), 120.0 (C-5), 119.1 (C-3), 114.4 (C-1), 40.6 (C-7), 32.5 (C-8). **ATR-IR**: $\tilde{\nu}$ [cm^{-1}] = 3321, 2924, 2853, 2625, 2562, 1679, 1655, 1606, 1583, 1557, 1526, 1491, 1471, 1454, 1412, 1316, 1304, 1264, 1242, 1165, 1156, 1121, 1103, 1088, 1060, 1036, 991, 981, 959, 934, 770, 760, 740, 725, 666, 650, 622, 599, 575, 562, 515, 491, 459, 440. **HRMS** (ESI$^-$): m/z = 351.0965 (351.0962 calculated for [M-H]$^-$). **Mp** = 177.4 °C. **R$_f$** = 0.23 (CH$_2$Cl$_2$/CH$_3$OH 20:1 v/v).

6.6.10 Synthesis of benzofuranyl-based target compound 33a

4-Fluoro-2-iodo-6-(trifluoromethyl)phenol 46a

4-Fluoro-2-(trifluoromethyl)phenol **37f** (1.80 g, 10.0 mmol, 1.0 eq.) were dissolved in 5 mL methanol and treated with a suspension of 1.50 g (15.0 mmol, 1.5 eq.) calcium carbonate in 6 mL water and a solution of 1.62 g (10.0 mmol, 1.0 eq.) iodine monochloride in 4 mL methanol, successively. The reaction mixture was stirred at room temperature for 5 h before it was diluted with water and dichloromethane. After phase separation, the aqueous phase was extracted three times with dichloromethane. The combined organic phases were washed with brine and saturated sodium thiosulphate solution, once each. The organic phase was dried over sodium sulphate and the solvent was removed under reduced pressure. After purification by column chromatography (PE/CH$_2$Cl$_2$ 4:1 v/v), iodophenol derivative **46a** (2.23 g, 7.28 mmol, 73 %) was obtained as yellow oil.
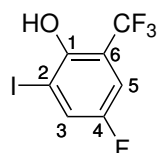
C$_7$H$_3$F$_4$IO
305.9981 g/mol

^{1}H NMR (400 MHz, DMSO-d_6): δ [ppm] = 9.80 (brs, 1H, OH), 7.95 (dd $^3J_{HH}$ = 7.7 Hz, $^4J_{HH}$ = 3.1 Hz, 1H, H-3), 7.50 (dd, $^3J_{HH}$ = 8.5 Hz, $^4J_{HH}$ = 3.1 Hz, 1H, H-5). **^{13}C NMR** (101 MHz, DMSO-d_6): δ[ppm] = 155.0 (d, $^2J_{CF}$ = 243 Hz, C-4), 151.3 (C-1), 129.6 (d, $^2J_{CF}$ = 24.3 Hz, C-3), 122.5 (q, $^2J_{CF}$ = 273 Hz, CF$_3$), 118.90 (C-6), 113.8 (dd, $^2J_{CF}$ = 25.9 Hz, $^3J_{CF}$ = 5.3 Hz, C-5), 91.6 ($^3J_{CF}$ = 8.1 Hz, C-2). **^{19}F NMR** (565 MHz, DMSO-d_6): δ[ppm] = -61.29 (CF$_3$), -121.29 (F-4). **ATR-IR**: $\tilde{\nu}$ [cm^{-1}] = 3610, 3489, 3090, 1613, 1595, 1464, 1433, 1313, 1301, 1270, 1227, 1195, 1126, 1058, 930, 872, 801, 770, 741, 690, 620, 564, 520, 500, 409. **HRMS** (ESI$^-$): m/z = 304.9099 (304.9092 calculated for [M-H]$^-$). **R$_f$** = 0.35 (PE/CH$_2$Cl$_2$ 4:1 v/v).

(5-Fluoro-7-(trifluoromethyl)benzofuran-2-yl)methanol 45a

According to general procedure **9**, iodophenol derivative **46a** (2.45 g, 8.00 mmol), TMG (3.0 mL, 2.8 g, 24 mmol), Pd(Ph$_3$)$_2$Cl$_2$ (281 mg, 0.40 mmol), CuI (152 mg, 0.80 mmol) and 2-propin-1-ol (0.55 mL, 0.47 g, 8.4 mmol) were used to obtain benzofuranyl derivative **45a** (1.40 g, 5.99 mmol, 75 %) as slightly orange solid.

¹H NMR (600 MHz, DMSO-d_6): δ [ppm] = 7.81 (dd, $^3J_{HH}$ = 8.4 Hz, $^4J_{HH}$ = 2.8 Hz, 1H, H-4) 7.56 (dd, $^3J_{HH}$ = 9.2 Hz, $^4J_{HH}$ = 2.6 Hz, 1H, H-6), 6.94 (t, $^3J_{HH}$ = 0.9 Hz, 1H, H-3), 5.64 (t, $^3J_{HH}$ = 5.9 Hz, 1H, OH), 4.62 (dd, $^3J_{HH}$ = 5.9 Hz, $^4J_{HH}$ = 0.9 Hz, 2H, H-1). **¹³C NMR** (151 MHz, DMSO-d_6): δ[ppm] = 162.4 (C-2), 157.5 (d, $^1J_{CF}$ = 238 Hz, C-5), 146.1 (C-7a), 131.4 (d, $^3J_{CF}$ = 10.6 Hz, C-3a), 122.5 (d, $^1J_{CF}$ = 270 Hz, CF$_3$), 113.2 (dd, $^2J_{CF}$ = 33.9 Hz, $^3J_{CF}$ = 9.2 Hz, C-7), 111.8 (d, $^2J_{CF}$ = 24.8 Hz, C-4), 109.0 (dd, $^2J_{CF}$ = 29.5 Hz, $^3J_{CF}$ = 4.5 Hz, C-6), 103.8 (d, $^4J_{CF}$ = 3.8 Hz, C-3), 56.0 (C-1). **¹⁹F NMR** (565 MHz, DMSO-d_6): δ[ppm] = -59.8 (CF$_3$), -119.0 (F-5). **ATR-IR**: $\tilde{\nu}$ [cm^{-1}] = 3239, 3095, 2941, 2879, 1753, 1714, 1615, 1601, 1479, 1455, 1434, 1376, 1326, 1261, 1207, 1179, 1156, 1139, 1113, 1054, 996, 951, 917, 877, 852, 825, 753, 732, 707, 694, 678, 641, 595, 551, 532, 506, 491, 407. **HRMS** (ESI$^-$): m/z = 233.0239 (233.0231 calculated for [M-H]$^-$). **R$_f$** = 0.13 (PE/EA 5:1 v/v).
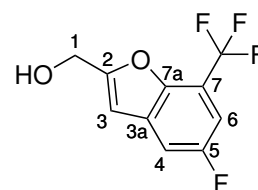
C$_{10}$H$_6$F$_4$O$_2$

234.0304 g/mol

2-(Azidomethyl)-5-fluoro-7-(trifluoromethyl)benzofuran 73a

According to general procedure **3**, using alcohol **45a** (987 mg, 4.20 mmol), triethylamine (1.2 mL, 0.85 g, 8.4 mmol) and methanesulfonyl chloride (0.37 mL, 0.55 g, 4.8 mmol) and general procedure **4**, using sodium azide (355 mg, 5.46 mmol) and purification via column chromatography (PE/CH$_2$Cl$_2$ 5:1 v/v), azide **73a** (561 mg, 2.16 mmol, 51 %) was obtained as yellowish oil.
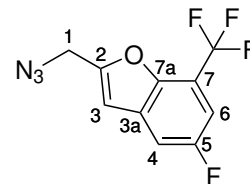
C$_{10}$H$_5$F$_4$N$_3$O

259.1636 g/mol

¹H NMR (600 MHz, DMSO-d_6): δ [ppm] = 7.88 (dd, $^3J_{HH}$ = 8.5 Hz, $^4J_{HH}$ = 2.6 Hz, 1H, H-4) 7.65 (dd, $^3J_{HH}$ = 9.1 Hz, $^4J_{HH}$ = 2.6 Hz, 1H, H-6), 7.15 (s, 1H, H-3), 4.75 (s, 2H, H-1). **¹³C NMR** (151 MHz, DMSO-d_6): δ[ppm] = 158.87 (C-2), 157.0 (d, $^1J_{CF}$ = 93.4 Hz, C-5), 146.8 (C-7a), 131.3 (d, $^3J_{CF}$ = 11.0 Hz, C-3a), 122.8 (d, $^1J_{CF}$ = 274 Hz, CF$_3$), 114.0 (dd, $^2J_{CF}$ = 35.6 Hz, $^3J_{CF}$ = 9.1 Hz, C-7), 112.8 (d, $^2J_{CF}$ = 24.9 Hz, C-4), 110.5 (dd, $^2J_{CF}$ = 29.6 Hz, $^3J_{CF}$ = 4.6 Hz, C-6), 106.9 (d, $^4J_{CF}$ = 3.9 Hz, C-3). **¹⁹F NMR** (565 MHz, DMSO-d_6): δ[ppm] = -59.8 (CF$_3$), -119.0 (F-5). **ATR-IR**: $\tilde{\nu}$ [cm^{-1}] = 3111, 3079, 2994, 2932, 2460, 2222, 2117, 2081, 1982, 1753, 1628, 1616, 1597, 1481, 1433, 1365, 1331, 1296, 1263, 1234, 1198, 1178, 1162, 1112, 997, 976, 930, 917, 872, 834, 814, 747, 721, 678, 651, 628, 604, 560, 501, 463, 397. **MS** (EI): m/z = 259.00 (259.04 calculated for [M]$^{+\cdot}$). **R$_f$** = 0.29 (PE/CH$_2$Cl$_2$ 5:1 v/v).

(5-Fluoro-7-(trifluoromethyl)benzofuran-2-yl)methanamine 43a

The compound was prepared according to general procedure **5** using azide **73a** (530 mg, 2.05 mmol) and Pd/C (53 mg). The reaction mixture was stirred for 20 h and the crude product was purified by column chromatography (CH$_2$Cl$_2$) to obtain amine **43a** (404 mg, 1.73 mmol, 85 %) as colorless liquid.

C$_{10}$H$_7$F$_4$NO
233.1656 g/mol

^{1}H NMR (600 MHz, DMSO-d_6): δ [ppm] = 7.78 (dd, $^3J_{HH}$ = 8.6 Hz, $^4J_{HH}$ = 2.6 Hz, 1H, H-4) 7.50 (dd, $^3J_{HH}$ = 9.3 Hz, $^4J_{HH}$ = 2.6 Hz, 1H, H-6), 6.87 (t, $^3J_{HH}$ = 1.2 Hz, 1H, H-3), 3.88 (d, $^3J_{HH}$ = 1.2 Hz, 1H, H-3). **^{13}C NMR** (151 MHz, DMSO-d_6): δ[ppm] = 165.7 (C-2), 157.9 (d, $^1J_{CF}$ = 237.8 Hz, C-5), 146.4 (C-7a), 132.2 (d, $^3J_{CF}$ = 10.7 Hz, C-3a), 123.0 (d, $^1J_{CF}$ = 270 Hz, CF$_3$), 113.4 (dd, $^2J_{CF}$ = 34.4 Hz, $^3J_{CF}$ = 9.6 Hz, C-7), 111.8 (d, $^2J_{CF}$ = 24.9 Hz, C-4), 108.7 (dd, $^2J_{CF}$ = 29.5 Hz, $^3J_{CF}$ = 4.7 Hz, C-6), 102.8 (d, $^4J_{CF}$ = 3.8 Hz, C-3). **^{19}F NMR** (565 MHz, DMSO-d_6): δ[ppm] = -59.8 (CF$_3$), -119.3 (F-5). **ATR-IR**: $\tilde{\nu}$ [cm^{-1}] = 3111, 3079, 2994, 2932, 2460, 2222, 2117, 2081, 1982, 1753, 1628, 1616, 1597, 1481, 1433, 1365, 1331, 1296, 1263, 1234, 1198, 1178, 1162, 1112, 997, 976, 930, 917, 872, 834, 814, 747, 721, 678, 651, 628, 604, 560, 501, 463, 397. **HRMS** (ESI$^+$): m/z = 234.0687 (234.0537 calculated for [M+H]$^+$). **R$_f$** = 0.15 (CH$_2$Cl$_2$/CH$_3$OH 19:1 v/v).
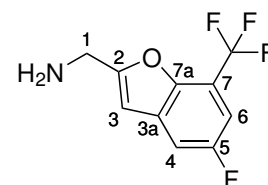
Benzyl 2-(3-((5-fluoro-7-(trifluoromethyl)benzofuran-2-yl)methyl)ureido)-benzoate 89a

The compound was prepared according to general procedure **6** using triphosgene (294 mg, 990 µmol), benzyl anthranilate (450 mg, 1.98 mmol), triethylamine (0.55 mL, 0.40 g, 4.0 mmol) and amine **43a** (369 mg, 1.58 mmol). Ureide **89a** (616 mg, 1.26 mmol, 80 %) was obtained as colorless solid.

C$_{25}$H$_{18}$F$_4$N$_2$O$_4$
486.4226 g/mol

^{1}H NMR (600 MHz, DMSO-d_6): δ [ppm] = 10.15 (brs, 1H, NH-a), 8.45 (dd, $^3J_{HH}$ = 8.6 Hz, $^4J_{HH}$ = 1.2 Hz, 1H, H-3), 8.02 (dd, $^3J_{HH}$ = 8.0 Hz, $^4J_{HH}$ = 1.7 Hz, 1H, H-6), 7.54 (dd, $^3J_{HH}$ = 8.5 Hz, $^4J_{HH}$ = 2.6 Hz, 1H, H-4'), 7.51 (ddd, $^3J_{HH}$ = 8.7 Hz, $^3J_{HH}$ = 7.2 Hz, $^4J_{HH}$ = 1.7 Hz, 1H, H-4), 7.49-7.45 (m, 2H, H-2"), 7.43-7.38 (m, 2H, H-3"), 7.38-7.34 (m, 2H, H-4", H-6')

7.01 (ddd, $^3J_{HH}$ = 8.2 Hz, $^3J_{HH}$ = 7.2 Hz, $^4J_{HH}$ = 1.2 Hz, 1H, H-5), 6.81 (t, $^4J_{HH}$ = 1.0 Hz, 1H, H-3'), 6.81 (brt, $^4J_{HH}$ = 5.7 Hz, 1H, NH-b), 5.34 (s, 2H, H-8), 4.54 (dd, $^3J_{HH}$ = 5.9 Hz, $^4J_{HH}$ = 1.1 Hz, 1H, H-7). **^{13}C NMR** (151 MHz, DMSO-d_6): δ[ppm] = 168.9 (COO), 161.1 (C-2'), 159.1 (d, $^1J_{CF}$ = 238.4 Hz, C-5'), 155.6 (CONH), 144.1 (C-7'a), 137.1 (C-2), 135.3 (C-4), 132.7 (d, $^3J_{CF}$ = 10.7 Hz, 3'a), 131.7 (C-6), 129.6 (C-3"), 129.3 (C-4"), 129.0 (C-2"), 121.9 (C-5), 120.5 (C-3), 115.3 (C-1), 112.1 (d, $^2J_{CF}$ = 25.0 Hz, C-4'), 109.9 (dq, $^2J_{CF}$ = 29.6 Hz, $^3J_{CF}$ = 4.7 Hz, C-6'), 104.7 (d, $^4J_{CF}$ = 3.9 Hz, C-3'), 67.7 (C-8), 38.0 (C-7). **^{19}F NMR** (565 MHz, DMSO-d_6): δ[ppm] = -59.75 (CF$_3$), -118.86 (C-5'-F). **ATR-IR**: $\tilde{\nu}$ [cm^{-1}] = 3284, 3095, 3069, 2936, 2873, 1702, 1644, 1606, 1589, 1543, 1497, 1481, 1470, 1454, 1434, 1366, 1332, 1310, 1299, 1260, 1208, 1182, 1167, 1147, 1123, 1090, 1049, 1031, 1012, 997, 984, 933, 918, 873, 841, 824, 760, 754, 724, 705, 692, 676, 654, 642, 608, 587, 521, 504, 458, 399. **HRMS** (ESI$^+$): m/z = 487.1276 (487.1275 calculated for [M+H]$^+$). **R$_f$** = 0.14 (PE/CH$_2$Cl$_2$ 1:2 v/v).

Benzyl 2-(3-(prop-2-yn-1-yl)ureido)benzoate 92

The compound was prepared according to general procedure **6** using triphosgene (560 mg, 1.88 mmol), benzyl anthranilate **87** (860 mg, 3.75 mmol), triethylamine (1.0 mL, 0.76 mg, 7.5 mmol) and 2-propynylamine **91** (0.19 mL, 0.16 mg, 3.0 mmol). Ureide **92** (0.63 mg, 2.0 mmol, 67 %) was obtained as colorless solid.
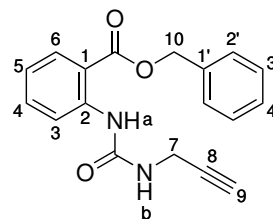
C$_{18}$H$_{16}$N$_2$O$_3$
308.1161 g/mol

^{1}H NMR (500 MHz, CDCl$_3$): δ [ppm] = 10.31 (brs, 1H, NH-a), 8.44 (d, $^3J_{HH}$ = 8.5 Hz, 1H, H-3), 7.95 (dd, $^3J_{HH}$ = 8.0 Hz, $^4J_{HH}$ = 1.7 Hz, 1H, H-6), 7.45-7.38 (m, 1H, H-4), 7.38-7.25 (m, 5H, H-2', H-3', H-4'), 6.89 (t, $^3J_{HH}$ = 7.6 Hz, 1H, H-5), 6.81 (brt, $^4J_{HH}$ = 5.7 Hz, 1H, NH-b), 5.25 (s, 2H, H-10), 4.83 (brs, 1H, NH-b) 4.00 (d, $^3J_{HH}$ = 3.1 Hz, 1H, H-7), 2.17 (t, $^3J_{HH}$ = 2.5 Hz, 1H, H-9). **^{13}C NMR** (126 MHz, CDCl$_3$): δ[ppm] = 168.6 (COO), 154.3 (CONH), 143.2 (C-2), 135.7 (C-1'), 134.9 (C-4), 131.0 (C-6), 128.9 (C-3"), 128.6 (C-4"), 128.2 (C-2"), 121.1 (C-5), 119.6 (C-3), 113.9 (C-1), 80.23 (C-8), 71.7 (C-9), 67.0 (C-10), 30.2 (C-7). **ATR-IR**: $\tilde{\nu}$ [cm^{-1}] = 3332, 3303, 3272, 3065, 3035, 2898, 2858, 1696, 1649, 1606, 1588, 1544, 1497, 1465, 1448, 1383, 1306, 1237, 1161, 1145, 1077, 1028, 964, 909, 892, 873, 854, 757, 742, 711, 695, 670, 621, 586, 521, 469, 435, 411. **HRMS** (ESI$^+$): m/z = 309.1250 (309.1234 calculated for [M+H]$^+$). **R$_f$** = 0.29 (CH$_2$Cl$_2$).

2-(3-((5-Fluoro-7-(trifluoromethyl)-2-benzofuranyl)methyl)ureido)benzoic acid 33a

The compound was prepared according to general procedure **5** using benzoate **89a** (507 mg, 1.04 mmol) and Pd/C (51 mg). The reaction mixture was stirred for 16 h and the crude product was recrystallised by solvent diffusion to obtain carboxylic acidcmpdBF-carboxylicacids**a** (404 mg, 1.02 mmol, 98 %) as colorless crystals.

$C_{18}H_{12}F_4N_2O_4$
396.2976 g/mol
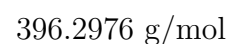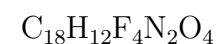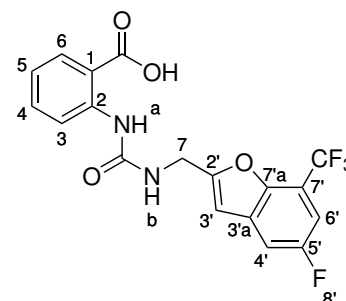
^{1}H NMR (600 MHz, DMSO-d_6): δ [ppm] = 13.35 (brs, 1H, COOH) 10.30 (brs, 1H, NH-a), 8.38 (dd, $^3J_{HH}$ = 8.6 Hz, $^4J_{HH}$ = 1.2 Hz, 1H, H-3), 8.21 (t, $^3J_{HH}$ = 5.7 Hz, 1H, NH-b), 7.92 (dd, $^3J_{HH}$ = 8.6 Hz, $^4J_{HH}$ = 1.2 Hz, 1H, H-6), 7.79 (dd, $^3J_{HH}$ = 8.5 Hz, $^4J_{HH}$ = 2.6 Hz, 1H, H-4'), 7.56 (dd, $^3J_{HH}$ = 9.2 Hz, $^4J_{HH}$ = 2.6 Hz, 1H, H-6'), 7.49 (ddd, $^3J_{HH}$ = 8.7 Hz, $^3J_{HH}$ = 7.2 Hz, $^4J_{HH}$ = 1.8 Hz, 1H, H-4), 7.98 (ddd, $^3J_{HH}$ = 8.1 Hz, $^3J_{HH}$ = 7.2 Hz, $^4J_{HH}$ = 1.2 Hz, 1H, H-5), 6.92 (s, 1H, H-3'), 4.49 (d, $^3J_{HH}$ = 5.5 Hz, 2H, H-7). **^{13}C NMR** (151 MHz, DMSO-d_6): δ[ppm] = 169.5 (COOH), 160.4 (C-2'), 157.5 (d, $^1J_{CF}$ = 238.3 Hz, C-5'), 154.6 (CONH), 145.9 (C-7'a), 142.8 (C-2), 134.2 (C-4), 131.5 (d, $^3J_{CF}$ = 10.9 Hz, 3'a), 131.0 (C-6), 122.5 (d, $^1J_{CF}$ = 269.9 Hz, CF$_3$), 120.4 (C-5), 119.2 (C-3), 114.7 (C-1), 111.6 (d, $^2J_{CF}$ = 25.0 Hz, C-4'), 108.9 (dq, $^2J_{CF}$ = 29.7 Hz, $^3J_{CF}$ = 4.9 Hz, C-6'), 103.9 (d, $^4J_{CF}$ = 4.9 Hz, C-3'), 36.8 (C-7). **^{19}F NMR** (565 MHz, DMSO-d_6): δ[ppm] = -59.75 (CF$_3$), -118.86 (C-5'-F). **ATR-IR**: $\tilde{\nu}$ [cm^{-1}] = 3333, 2913, 2648, 1686, 1655, 1607, 1586, 1561, 1474, 1437, 1428, 1410, 1370, 1328, 1318, 1267, 1183, 1162, 1130, 1114, 1085, 997, 953, 917, 866, 827, 762, 754, 729, 705, 681, 665, 629, 586, 559, 519, 492, 442, 415. **HRMS** (ESI$^+$): m/z = 395.0467 (395.0660 calculated for [M-H]$^-$). **R$_f$** = 0.23 (CH$_2$Cl$_2$/CH$_3$OH 9:1 v/v).

6.6.11 Synthesis of benzofuranyl-based target compound 33b

2-(Trifluoromethyl)phenyl cyclopentylcarbamate 50

According to general procedure **7**, 2-(trifluoromethyl)phenol **37d** (1.19 mL, 1.62 g, 9.98 mmol) and cyclopentyl isocyanate (1.24 mL, 1.22 g, 11.0 mmol) were used to obtain carbamate **50** (2.50 g, 9.16 mmol, 92 %) as colorless solid.

¹H NMR (600 MHz, CD₃CN): δ [ppm] = 7.70 (d, $^3J_{HH}$ = 7.8 Hz, 1H, H-3), 7.64 (t, $^3J_{HH}$ = 7.8 Hz, 1H, H-5), 7.38 (t, $^3J_{HH}$ = 7.7 Hz, 1H, H-4), 7.31 (d, $^3J_{HH}$ = 8.2 Hz, 1H, H-6), 6.18 (brs, $^3J_{HH}$ = 4.4 Hz, 1H, NH), 3.95 (sext, $^3J_{HH}$ = 6.9 Hz, 1H, H-7), 1.95-1.88 (m, 2H, H-8a), 1.76 -1.68 (m, 2H, H-9a), 1.63-1.55 (m, 2H, H-9b), 1.56-1.48 (m, 2H, H-8b). **¹³C NMR** (151 MHz, CD₃CN): δ[ppm] = 154.3 (C=O), 149.8 (C-1), 134.3 (C-5), 127.5 (q, $^3J_{CF}$ = 4.6 Hz, C-3), 126.5 (C-4), 126.0 (C-6), 125.5 (m, CF₃), 123.4 (m, C-2), 54.1 (C-7), 33.3 (C-8), 24.3 (C-9). **¹⁹F NMR** (565 MHz, CD₃CN): δ[ppm] = -62.16 (CF₃). **ATR-IR**: $\tilde{\nu}$ [cm⁻¹] = 3300, 2962, 2872, 1745, 1713, 1613, 1535, 1491, 1454, 1369, 1318, 1271, 1209, 1163, 1126, 1109, 1053, 1031, 987, 944, 880, 842, 791, 759, 641, 597, 538, 518, 469. **HRMS** (ESI⁺): m/z = 274.1049 (274.1049 calculated for [M+H]⁺). **R$_f$** = 0.30 (PE/EA 10:1).
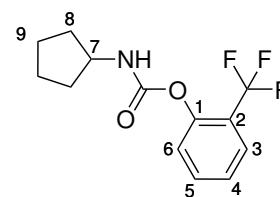
$C_{13}H_{14}F_3NO_2$

273.2552 g/mol

2-Iodo-6-(trifluoromethyl) cyclopentylcarbamate 51

In an inert atmosphere, a solution of trimethylsilyl trifluoromethanesulfonate (0.25 mL, 0.31 g, 1.4 mmol, 1.05 eq.) in diethyl ether (2 mL) was added dropwise to a solution of carbamate **50** (360 mg, 1.32 mmol, 1 eq.) and tetramethylethylenediamine (TMEDA, 0.22 mL, 0.17 g, 1.4 mmol, 1.1 eq.) in diethyl ether (8 mL). After 1 h stirring at room temperature, the reaction mixture was cooled to -78 °C and treated with TMEDA (0.40 mL, 0.31 g, 2.6 mmol, 2 eq.) and *n*-butyllithium solution (1.6 M in hexane; 1.85 mL, 2.6 mmol,

$C_{13}H_{13}F_3INO_2$

399.1517 g/mol

2 eq.) successively. At -78 °C, the mixture was stirred for 90 min, treated with a solution of iodine (0.42 g, 1.6 mmol, 1.25 eq.) in diethyl ether (1 mL) and again stirred for 90 min. Finally, the thawing reaction mixture was treated with methanol (0.2 mL) and hydrochloric acid (2M, 8 mL, 16 mmol, 12 eq.) and stirred until room temperature was reached. The phases were seperated, the aqueous phase was extracted with diethyl ether three times and the combined organic extracts were washed with sat. sodium bicarbonate solution. After reextraction of the seperated aqueous phase the combined organic phases were dried over sodium sulfate, concentrated in vacuo and purified by column chromatography (PE/EA gradient 50:1 to 10:1 v/v). Compound **51** (315 mg, 789 µmol, 60 %) was obtained as colorless solid.

¹H NMR (600 MHz, CD₃CN): δ [ppm] = 8.12 (d, $^3J_{HH}$ = 7.9 Hz, 1H, H-3), 7.72 (d,

$^3J_{HH}$ = 7.8 Hz, 1H, H-5), 7.17 (t, $^3J_{HH}$ = 7.9 Hz, 1H, H-4), 6.31 (d, $^3J_{HH}$ = 4.5 Hz, 1H, NH), 3.98-3.90 (m, 1H, H-7), 1.96-1.88 (m, 2H, H-8a), 1.77-1.68 (m, 2H, H-9a), 1.64-1.53 (m, 4H, H-8b, H-9b). **^{13}C NMR** (151 MHz, CD$_3$CN): δ[ppm] = 152.8 (C=O), 150.2 (C-1), 144.5 (C-3), 128.5 (C-4), 128.1 (q, $^3J_{CF}$ = 5.0 Hz, C-5), 125.5 (m, C-6), 123.6 (q, $^1J_{CF}$ = 272.6 Hz, CF$_3$), 95.7 (C-2), 54.2 (C-7), 33.3 (C-8), 24.3 (C-9). **^{19}F NMR** (565 MHz, CD$_3$CN): δ[ppm] = -62.66 (CF$_3$). **ATR-IR**: $\tilde{\nu}$ [cm^{-1}] = 3300, 2959, 2870, 1744, 1720, 1713, 1596, 1525, 1440, 1369, 1313, 1207, 1167, 1131, 1075, 1057, 1033, 979, 937, 842, 787, 776, 758, 701, 679. 646, 548, 518, 499, 382. **HRMS** (ESI$^+$): m/z = 400.017 (400.0016 calculated for [M+H]$^+$). **R$_f$** = 0.22 (PE/EA 10:1 v/v).

2-Iodo-6-(trifluoromethyl)phenol 46b

The compound was prepared according to general procedure **8** using carbamate **51** (2.98 g, 7.46 mmol). After 20 h stirring and purification by column chromatography (PE/CH$_2$Cl$_2$ 35:1 v/v), iodophenol derivative **46b** (1.77 g, 6.15 mmol, 82 %) was furnished as colorless liquid.

C$_7$H$_4$F$_3$IO
288.0077 g/mol
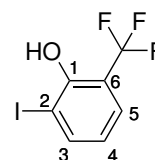
^{1}H NMR (600 MHz, DMSO-d_6): δ [ppm] = 9.82 (s, 1H, OH), 8.01 (dd, $^3J_{HH}$ = 7.9 Hz, $^4J_{HH}$ = 0.9 Hz, 1H, H-3), 7.57 (dd, $^3J_{HH}$ = 7.8 Hz, $^4J_{HH}$ = 1.2 Hz, 1H, H-5), 6.83 (t, $^3J_{HH}$ = 6.8 Hz, 1H, H-4). **^{13}C NMR** (151 MHz, DMSO-d_6): δ[ppm] = 154.5 (C-1), 143.4 (C-3), 126.8 (q, $^3J_{CF}$ = 5.2 Hz, C-5), 123.3 (q, $^1J_{CF}$ = 273.0 Hz, CF$_3$), 122.1 (C-4), 118.6 (q, $^2J_{CF}$ = 30.0 Hz, C-6), 90.5 (C-2). **^{19}F NMR** (565 MHz, DMSO-d_6): δ[ppm] = -60.93 (CF$_3$). **ATR-IR**: $\tilde{\nu}$ [cm^{-1}] = 3608, 3477, 1600, 1449, 1308, 1246, 1180, 1117, 1084, 1070, 1053, 967, 919, 836, 780, 736, 676, 602, 568, 539, 501, 389. **MS** (EI): m/z = 287.92 (287.92 calculated for [M]$^{+\cdot}$). **R$_f$** = 0.22 (PE/EA 35:1 v/v).

2,4-diiodo-6-(trifluoromethyl)phenol 49

A solution of 2-trifluoromethylphenol **37d** (1.6 g, 10 mmol) in methanol (21 mL) was added to a suspension of calcium carbonate (1.5 g, 15 mmol) in demin. water (4 mL). Subsequently, iodine monochloride (0.53 mL, 1.6 mmol, 10 mmol) was added dropwise and the reaction mixture was stirred at roomtemperature for 3 h. The crude product mixture was purified by column chromatography (CH$_2$Cl$_2$/PE gradient 1:4 to 1:0) to give the diiodinated phenol **49** (1.6 g, 3.9 mmol, 78 % rel. to ICl) as yellow crystals.

^{1}H NMR (600 MHz, DMSO-d_6): δ [ppm] = 10.15 (s, 1H, OH), 8.30 (d, $^4J_{HH}$ = 2.1 Hz, 1H, H-3), 7.79 (d, $^4J_{HH}$ = 2.1 Hz, 1H, H-5). **^{13}C NMR** (151 MHz, DMSO-d_6): δ[ppm] = 154.7 (C-1), 150.1 (C-3), 134.8 (q, $^3J_{CF}$ = 5.2 Hz, C-5), 122.2 (q, $^1J_{CF}$ = 273.9 Hz, CF$_3$), 120.2 (q, $^2J_{CF}$ = 29.7 Hz, C-6), 92.7 (C-2), 83.4 (C-4). **^{19}F NMR** (565 MHz, DMSO-d_6): δ[ppm] = -61.26 (CF$_3$). **ATR-IR**: $\tilde{\nu}$ [cm^{-1}] = 3442, 3079, 1801, 1776, 1587, 1449, 1399, 1296, 1263, 1240, 1146, 1123, 1104, 1060, 903, 875, 839, 790, 743, 684, 656, 606, 541, 517, 489. **R$_f$** = 0.43 (PE/CH$_2$Cl$_2$ 4:1 v/v).
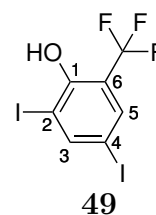
49

C$_7$H$_3$F$_3$I$_2$O
413.9041 g/mol

4-Iodo-2-(trifluoromethyl)phenol 48

Under inert atmosphere, an ice-cooled solution of 2,4-diiodo-6-(trifluoromethyl)phenol **49** (0.59 mg, 1.4 mmol) in dry tetrahydrofurane (7 mL) was slowly added to a suspension of sodium hydride (36 mg, 1.5 mmol) in dry tetrahydrofurane (7 mL), at 0 °C. The mixture was stirred for 15 min at 0 °C, cooled to -95 °C and treated with *n*-butyllithium (1.6 M in hexane, 0.89 mL, 1.4 mmol). After 15 min stirring, the mixture was warmed to 0 °C, acidified with hydrochloric acid (1 M) and extracted with dichloromethane three times. The combined extracts were dried over sodium sulfate and the solvent was removed under reduced pressure. Finally, column-chromatographic purification (CH$_2$Cl$_2$) yielded 4-iodo-2-(trifluoromethyl)phenol **48** (0.22 g, 77 mmol, 54 %) as yellowish oil.
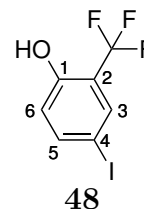
48

C$_7$H$_4$F$_3$IO
288.0077 g/mol

^{1}H NMR (600 MHz, DMSO-d_6): δ [ppm] = 10.86 (s, 1H, OH), 7.75 (dd, $^3J_{HH}$ = 8.5 Hz, $^4J_{HH}$ = 2.3 Hz, 1H, H-5), 7.73 (d, $^4J_{HH}$ = 2.2 Hz, 1H, H-3), 6.86 (d, $^3J_{HH}$ = 8.6 Hz, 1H, H-6). **^{13}C NMR** (151 MHz, DMSO-d_6): δ[ppm] = 155.7 (C-1), 142.2 (C-5), 134.4 (q, $^3J_{CF}$ = 5.7 Hz, C-3), 122.9 (q, $^1J_{CF}$ = 272.9 Hz, CF$_3$), 119.6 (C-6), 117.7 (q, $^2J_{CF}$ = 31.0 Hz, C-2), 79.9 (C-4). **^{19}F NMR** (565 MHz, DMSO-d_6): δ[ppm] = -60.41 (CF$_3$). **ATR-IR**: $\tilde{\nu}$ [cm^{-1}] = 3491, 3253, 3064, 2960, 2087, 1899, 1650, 1603, 1591, 1493, 1411, 1367, 1314, 1284, 1249, 1221, 1162, 1117, 1101, 1047, 951, 889, 841, 818, 764, 717, 669, 620, 579, 526, 496, 464. **HRMS** (ESI$^+$): m/z = 286.9184 (286.9186 calculated for [M-H]$^-$). **R$_f$** = 0.29 (PE/CH$_2$Cl$_2$ 4:1 v/v).

7-(Trifluoromethyl)benzofuran-2-ylmethanol 45b

According to general procedure **9**, iodophenol derivative **46b** (1.7 g, 6.0 mmol), TMG (2.3 mL, 2.1 g, 18 mmol), Pd(Ph$_3$)$_2$Cl$_2$ (0.21 g, 0.30 mmol), CuI (0.11 g, 0.60 mmol) and 2-propin-1-ol (0.39 mL, 0.37 g, 6.6 mmol) were used to obtain benzofuranyl analogue **45b** (1.1 g, 5.0 mmol, 84 %) as slightly orange solid.

C$_{10}$H$_7$F$_3$O$_2$

216.1592 g/mol

^{1}H NMR (600 MHz, DMSO-d_6): δ [ppm] = 7.93 (d, $^3J_{HH}$ = 7.8 Hz, 1H, H-4), 7.61 (d, $^3J_{HH}$ = 7.6 Hz, 1H, H-6), 7.41 (dt, $^3J_{HH}$ = 7.8 Hz, $^4J_{HH}$ = 0.6 Hz, 1H, H-5), 6.95-6.92 (m, 1H, H-3), 5.59 (t, $^3J_{HH}$ = 5.9 Hz, 1H, OH), 4.63 (dd, $^3J_{HH}$ = 5.9 Hz, $^4J_{HH}$ = 0.5 Hz, 2H, H-8). **^{13}C NMR** (151 MHz, DMSO-d_6): δ[ppm] = 160.3 (C-2), 149.6 (q, $^3J_{CF}$ = 1.7 Hz, C-7a), 130.0 (C-3a), 125.9 (C-4), 123.4 (q, $^1J_{CF}$ = 272.0 Hz, CF$_3$), 122.9 (C-5), 120.9 (q, $^3J_{CF}$ = 4.5 Hz, C-6), 112.7 (q, $^2J_{CF}$ = 33.4 Hz, C-7), 103.4 (C-3), 56.0 (C-8). **^{19}F NMR** (565 MHz, DMSO-d_6): δ[ppm] = -59.55 (CF$_3$). **ATR-IR**: $\tilde{\nu}$ [cm^{-1}] = 3210, 2963, 2927, 1621, 1601, 1434, 1356, 1333, 1305, 1273, 1236, 1207, 1166, 1141, 1113, 1055, 1020, 970, 955, 924, 858, 829, 792, 766, 745, 721, 657, 629, 577, 486, 413. **MS** (EI$^+$): m/z = 216.04 (216.05 calculated for [M]$^{+\cdot}$). **R$_f$** = 0.12 (PE/CH$_2$Cl$_2$ 2:1 v/v).
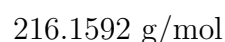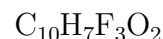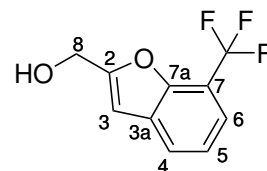
2-(Chloromethyl)-7-(trifluoromethyl)benzofuran 77b

The compound was prepared according to general procedure **3**. Alcohol **45b** (1.1 g, 4.9 mmol), triethylamine (1.3 mL, 0.95 g, 9.4 mmol) and methanesulfonyl chloride (0.51 mL, 0.76 g, 6.6 mmol) were used to obtain chloride **77b** (0.66 g, 2.8 mmol, 57 %) as yellowish liquid.

C$_{10}$H$_6$ClF$_3$O

234.6022 g/mol

^{1}H NMR (600 MHz, DMSO-d_6): δ [ppm] = 7.99 (d, $^3J_{HH}$ = 7.8 Hz, 1H, H-4), 7.70 (d, $^3J_{HH}$ = 7.6 Hz, 1H, H-6), 7.48-7.44 (m, 1H, H-5), 7.20 (s, 1H, H-3), 5.06 (s, 2H, H-8). **^{13}C NMR** (151 MHz, DMSO-d_6): δ[ppm] = 154.7 (C-2), 149.9 (C-7a), 129.4 (C-3a), 126.7 (C-4), 123.4 (C-5), 123.2 (q, $^1J_{CF}$ = 272.0 Hz, CF$_3$), 122.2 (q, $^3J_{CF}$ = 4.4 Hz, C-6), 112.9 (q, $^2J_{CF}$ = 33.5 Hz, C-7), 106.7 (C-3), 37.3 (C-8). **^{19}F NMR** (565 MHz, DMSO-d_6): δ[ppm] = -59.66 (CF$_3$). **ATR-IR**: $\tilde{\nu}$ [cm^{-1}] = 3119, 2980, 1888, 1711, 1665, 1619, 1601, 1432, 1359, 1336, 1309, 1279, 1236, 1184, 1161, 1135, 1106, 1056, 975, 947, 916, 890, 849, 830, 795, 761, 748, 711, 696, 643, 613, 576, 522, 499, 481, 449, 383. **MS** (EI): m/z
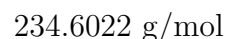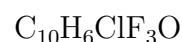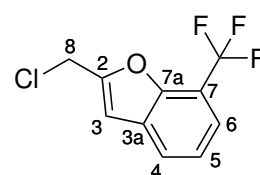
= 234.01 (234.01 calculated for [M]$^{+\cdot}$). $\mathbf{R_f}$ = 0.88 (CH$_2$Cl$_2$).

2-(Azidomethyl)-7-(trifluoromethyl)benzofuran 73b

According to general procedure **4**, chloride **77b** (628 mg, 2.68 mmol) and sodium azide (478 mg, 7.35 mmol) were used, followed by purification via column chromatography (PE/CH$_2$Cl$_2$ 10:1 v/v), to prepare azide **73b** (511 mg, 2.12 mmol, 79 %) as colorless liquid.

C$_{10}$H$_6$F$_3$N$_3$O
241.1732 g/mol
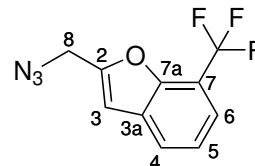
¹H NMR (500 MHz, DMSO-d_6): δ [ppm] = 8.00 (d, $^3J_{HH}$ = 7.8 Hz, 1H, H-4), 7.69 (d, $^3J_{HH}$ = 7.6 Hz, 1H, H-6), 7.48-7.43 (m, 1H, H-5) 7.15 (s, 1H, H-3), 4.75 (s, 2H, H-8). **¹³C NMR** (126 MHz, DMSO-d_6): δ[ppm] = 154.2 (C-2), 149.9 (C-7a), 129.5 (C-3a), 126.5 (C-4), 123.3 (C-5), 123.2 (q, $^1J_{CF}$ = 272.1 Hz, CF$_3$), 121.8 (q, $^3J_{CF}$ = 4.4 Hz, C-6), 112.9 (q, $^2J_{CF}$ = 33.4 Hz, C-7), 106.1 (C-3), 46.2 (C-8). **¹⁹F NMR** (565 MHz, DMSO-d_6): δ[ppm] = -59.70 (CF$_3$). **ATR-IR**: $\tilde{\nu}$ [cm^{-1}] = 3675, 3116, 2971, 2929, 2109, 2091, 2070, 1882, 1824, 1708, 1656, 1622, 1600, 1431, 1359, 1337, 1310, 1276, 1244, 1226, 1201, 1174, 1150, 1111, 1052, 974, 958, 935, 875, 852, 826, 791, 763, 743, 723, 671, 634, 577, 556, 526, 500, 485, 437, 395. **MS** (EI): m/z = 241.10 (241.05 calculated for [M]$^{+\cdot}$). $\mathbf{R_f}$ = 0.26 (PE/CH$_2$Cl$_2$ 10:1 v/v).

7-(1,1-Dimethylpropyl)benzofuran-2-yl)methanamine 43b

The compound was prepared according to general procedure **5**, using azide **73b** (475 mg, 2.05 mmol) and Pd/C (50 mg). Purification was performed via column chromatography (CH$_2$Cl$_2$/CH$_3$OH gradient 99:1 to 9:1 v/v) to obtain amine **43b** (334 mg, 1.55 mmol, 79 %) as colorless liquid.

C$_{10}$H$_8$NO
215.1752 g/mol
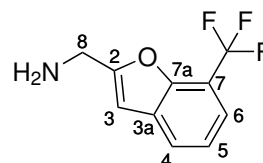
¹H NMR (600 MHz, DMSO-d_6): δ [ppm] = 7.90 (d, $^3J_{HH}$ = 7.8 Hz, 1H, H-4), 7.57 (d, $^3J_{HH}$ = 7.6 Hz, 1H, H-6), 7.41-7.36 (m, 1H, H-5), 6.87 (s, 1H, H-3), 3.89 (d, $^3J_{HH}$ = 0.8 Hz, 2H, H-8). **¹³C NMR** (151 MHz, DMSO-d_6): δ[ppm] = 163.0 (C-2), 149.4 (C-7a), 130.3 (C-3a), 125.5 (C-4), 122.7 (C-5), 123.4 (q, $^1J_{CF}$ = 271.3 Hz, CF$_3$), 120.4 (q, $^3J_{CF}$ = 4.4 Hz, C-6), 112.6 (q, $^2J_{CF}$ = 33.1 Hz, C-7), 101.9 (C-3), 45.4 (C-8). **¹⁹F NMR** (565 MHz, DMSO-d_6): δ[ppm] = -59.52 (CF$_3$). **ATR-IR**: $\tilde{\nu}$ [cm^{-1}] = 3675, 3294, 2922, 1621, 1601, 1463, 1435, 1360, 1327, 1264, 1242, 1219, 1163, 1111, 1055, 937, 855, 812, 744, 707,

691, 656, 629, 595, 490. **MS** (EI): m/z = 215.10 (215.06 calculated for $[M]^{+\cdot}$). $\mathbf{R_f}$ = 0.14(CH_2Cl_2/CH_3OH 19:1 v/v).

Benzyl 2-(3-((7-(trifluoromethyl)benzofuran-2-yl)methyl)ureido benzoate 89b

The compound was prepared according to general procedure **6** using triphosgene (0.54 g, 1.8 mmol), benzyl anthranilate (0.41 g, 1.8 mmol), triethylamine (0.53 mL, 0.39 g, 3.8 mmol) and amine **43b** (0.33 g, 1.3 mmol). After purification via column chromatography (silica, petroleum ether/ethyl acetate gradient 7:1 to 1:1 v/v), ureide **89b** (0.49 g, 1.0 mmol, 80 %) was obtained as colorless, fluffy solid.
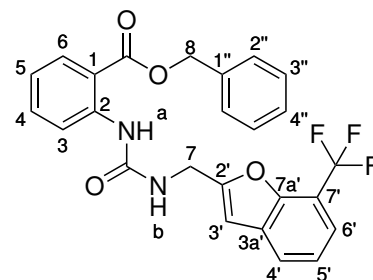
$C_{25}H_{19}F_3N_2O_4$
468.4322 g/mol

¹H NMR (600 MHz, CD_3CN): δ [ppm] = 10.14 (s, 1H, NH-a), 8.46 (dd, $^3J_{HH}$ = 8.5 Hz, $^4J_{HH}$ = 0.8 Hz, 1H, H-3), 8.02 (dd, $^3J_{HH}$ = 8.0 Hz, $^4J_{HH}$ = 1.6 Hz, 1H, H-6), 7.83 (d, $^3J_{HH}$ = 7.8 Hz, 1H, H-4'), 7.57 (d, $^3J_{HH}$ = 7.6 Hz, 1H, H-6'), 7.52 (ddd $^3J_{HH}$ = 8.7 Hz, 7.4 Hz, $^4J_{HH}$ = 1.6 Hz, 1H, H-4), 7.49-7.44 (m, 2H, H-2"), 7.43-7.39 (m, 2H, H-3"), 7.38-7.34 (m, 2H, H-4", H-5'), 7.01 (ddd, $^3J_{HH}$ = 8.2 Hz, 7.2 Hz, $^4J_{HH}$ = 1.1 Hz, 1H, H-5), 6.82 (s, 1H, H-3'), 6.45 (t, $^3J_{HH}$ = 4.9 Hz, 1H, NH-b), 5.34 (s, 2H, H-8), 4.55 (dd, $^3J_{HH}$ = 5.9 Hz, $^4J_{HH}$ = 1.0 Hz, 2H, H-7). **¹³C NMR** (151 MHz, CD_3CN): δ[ppm] = 168.9 (COO), 158.9 (C-2'), 155.6 (CONH), 151.2 (C-7a'), 144.1 (C-2), 137.1 (C-1"), 135.2 (C-4), 131.7 (C-6), 131.3 (3a'), 129.6 (C-3"), 129.2 (C-4"), 129 (C-2"), 126.5 (C-4'), 123.9 (CF3), 123.7 (C-5'), 121.9 (q, $^3J_{CF}$ = 271.3 Hz, C-6'), 121.8 (C-5), 120.5 (C-3), 115.3 (C-1), 114.5 (C-7'), 104.3 (C-3'), 67.6 (C-8), 37.9 (C-7). **¹⁹F NMR** (565 MHz, DMSO-d_6): δ[ppm] = -61.40 (CF$_3$). **ATR-IR**: $\tilde{\nu}$ [cm^{-1}] = 3338, 3311, 3035, 2954, 1712, 1649, 1583, 1550, 1453, 1430, 1327, 1307, 1290, 1251, 1243, 1164, 1114, 1089, 1051, 1041, 943, 807, 765, 740, 710, 694, 677, 625, 601, 523, 488, 455. **HRMS** (ESI⁺): m/z = 469.1365 (469.1370 calculated for $[M+H]^+$). $\mathbf{R_f}$ = 0.32 (PE/EA 7:1 v/v).

2-(3-((7-(Trifluoromethyl)benzofuran-2-yl)methyl)ureido)benzoic acid 33b

The compound was prepared according to general procedure **5** using benzoate **89b** (383 mg, 817 µmol) and Pd/C (38 mg). The reaction mixture was stirred for 20 h and the crude product was recrystallised by solvent diffusion to obtain carboxylic acid **33b** (308 mg, 814 µmol, 100 %) as colorless crystals.

$C_{18}H_{12}F_3N_2O_4$
378.3072 g/mol

¹H NMR (500 MHz, DMSO-d_6): δ [ppm] = 13.50 (brs, 1H, COOH) 10.77 (brs, 1H, NH-a), 8.36 (dd, $^3J_{HH}$ = 8.5 Hz, $^4J_{HH}$ = 1.1 Hz, 1H, H-3), 8.10 (brs, 1H, NH-b), 7.95-7.89 (m, 2H, H-6, H-4'), 7.60 (d, $^3J_{HH}$ = 7.6 Hz, 1H, H-6'), 7.46-7.38 (m, 2H, H-4, H-5'), 7.97-6.92 (m, 1H, H-5), 6.91 (s, 1H, H-3'), 4.49 (d, $^3J_{HH}$ = 5.6 Hz, 2H, H-7). **¹³C NMR** (126 MHz, DMSO-d_6): δ[ppm] = 169.8 (COOH), 158.4 (C-2'), 154.8 (CONH), 149.5 (C-7'a), 142.7 (C-2), 133.0 (C-4), 131.0 (C-6), 130.0 (C-3'a), 125.8 (C-4'), 123.4 (q, $^1J_{CF}$ = 272.1 Hz, CF₃)) 123.0 (C-5'), 120.8 (q, $^3J_{CF}$ = 4.4 Hz, C-6') 120.1 (C-5), 118.9 (C-3), 116.5 (C-1), 112.7 (q, $^2J_{CF}$ = 33.6 Hz, C-7'), 103.4 (C-3'), 36.8 (C-7). **¹⁹F NMR** (565 MHz, DMSO-d_6): δ[ppm] = -59.47 (CF₃). **ATR-IR**: $\tilde{\nu}$ [cm⁻¹] = 3330, 2928, 2883, 2652, 2559, 1687, 1651, 1561, 1430, 1412, 1325, 1293, 1267, 1241, 1171, 1131, 1118, 1085, 1051, 945, 817, 755, 740, 733, 707, 667, 612, 597, 560, 522, 482, 456, 418 **HRMS** (ESI⁺): m/z = 377.0745 (377.0755 calculated for [M-H]⁻). **Mp** = 179.5 °C. **R$_f$** = 0.22 (CH₂Cl₂/CH₃OH 9:1 v/v).

6.6.12 Synthesis of benzofuranyl-based target compounds 33c and 36

2-(2-Methylbutan-2-yl)phenyl cyclopentylcarbamate 52

According to general procedure **7**, 2-(2-methylbutan-2-yl)phenol **37b** (3.50 mL, 3.43 g, 20.9 mmol) and cyclopentyl isocyanate (4.65 mL, 4.58 g, 41.3 mmol) were used to obtain carbamate **52** (5.73 g, 20.8 mmol, 100 %) as white solid.

¹H NMR (600 MHz, CD₃CN): δ [ppm] = 7.33 (dd, $^3J_{HH}$ = 7.9 Hz, $^4J_{HH}$ = 1.5 Hz, 1H, H-3), 7.20 (ddd, $^3J_{HH}$ = 7.7 Hz, 7.7 Hz, $^4J_{HH}$ = 1.6 Hz, 1H, H-5), 7.13 (ddd, $^3J_{HH}$ = 7.7 Hz, 7.7 Hz, $^4J_{HH}$ = 1.3 Hz, 1H, H-4), 6.97 (dd, $^3J_{HH}$ = 7.9 Hz, $^4J_{HH}$ = 1.3 Hz, 1H, H-6), 6.08 (d, $^3J_{HH}$ = 4.4 Hz, 1H, NH), 3.95 (sext, $^3J_{HH}$ = 7.0 Hz, 1H, H-11), 1.95-1.88 (m, 2H, H-12a), 1.76 (q, $^3J_{HH}$ = 7.5 Hz, 2H, H-8), 1.75-1.68 (m, 2H, H-13a), 1.63-1.57 (m, 2H, H-13b), 1.55-1.48 (m, 2H, H-12b), 1.31 (s, 6H, H-10), 0.62 (t, $^3J_{HH}$ = 7.5 Hz, 3H, H-9). **¹³C NMR** (151 MHz, CD₃CN): δ[ppm] = 155.2 (C=O), 150.8 (C-1), 140.8 (C-2), 129.2 (C-3), 127.6 (C-5), 125.8 (C-4), 125.6 (C-6), 54.0 (C-11), 39.0 (C-7), 34.9 (C-8), 33.5 (C-12), 28.6 (C-10), 24.3 (C-13), 9.8 (C-9). **ATR-IR**: $\tilde{\nu}$ [cm⁻¹] = 3293, 2953, 2868, 2264, 2043, 1994, 1960, 1703, 1578, 1531, 1485, 1442, 1361, 1305, 1274, 1198, 1088, 1025, 989, 937, 898, 765, 751, 640. **HRMS** (ESI⁺): m/z = 276.1954 (276.1958 calculated for [M+H]⁺). **R$_f$** = 0.40 (PE/EA 10:1 v/v).

$C_{17}H_{25}NO_2$

275.3920 g/mol
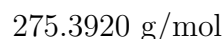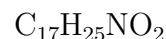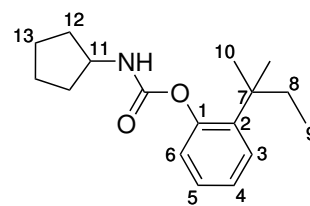
2-(2-Methylbutan-2-yl)-6-(trimethylsilyl)phenyl cyclopentylcarbamate 56

In an inert atmosphere, a solution of trimethylsilyl trifluoromethanesulfonate (4.0 mL, 4.9 g, 22 mmol, 1.05 eq.) in diethyl ether (30 mL) was added dropwise to a solution of compound **52** (5.76 g, 20.9 mmol, 1 eq.) and tetramethylethylenediamine (TMEDA, 3.5 mL, 2.7 g, 23 mmol, 1.1 eq.) in diethyl ether (160 mL). After 1 h stirring at room temperature, the reaction mixture was cooled to -78 °C, treated with trimethylsilyl chloride (3.3 mL, 2.8 g, 26 mmol, 1.2 eq.) and stirred at -78 °C for 1 h. TMEDA (6.3 mL, 4.9 g,

$C_{20}H_{33}NO_2Si$

347.5740 g/mol

42 mmol, 2.0 eq.) and *sec*-butyllithium solution (1.4 M in cyclohexane; 33 mL, 46 mmol, 2.2 eq.) were added successively to the mixture that was afterwards stirred at -78 °C for 1 h. Finally, the thawing reaction mixture was treated with methanol (2.0 mL) and hydrochlorid acid (2M, 125 mL, 0.25 mmol, 11 eq.) and stirred until room temperature was reached. The phases were seperated, the aqueous phase was extracted with diethyl ether three times and the combined organic extracts were washed with sat. sodium bicarbonate solution. After reextraction of the seperated aqueous phase the combined organic phases were dried over sodium sulfate, concentrated in vacuo and purified by column chromatography (petroleum ether/dichloromethane 3:1 v/v). Compound **56**
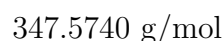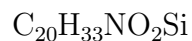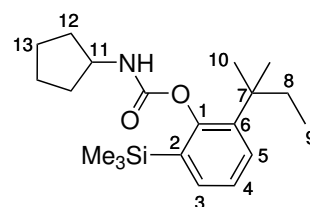
(6.43, 18.5 mmol, 88 %) was obtained as white solid.

¹H NMR (500 MHz, CD$_3$CN): δ [ppm] = 7.41-7.33 (m, 2H, H-3, H-5), 7.17 (t, $^3J_{HH}$ = 7.5 Hz, 1H, H-4), 6.11 (d, $^3J_{HH}$ = 6.7 Hz, 1H, NH), 3.91 (sext, $^3J_{HH}$ = 6.7 Hz, 1H, H-11), 1.94-1.84 (m, 2H, H-12b), 1.82-1.74 (m, 3H, H-10a), 1.75-1.68 (m, 2H, H-13b), 1.69-1.61 (m, 3H, H-10b), 1.63-1.57 (m, 2H, H-13a), 1.57-1.49 (m, 2H, H-12a), 1.37-1.24 (m, 9H, Si(CH$_3$)$_3$). **¹³C NMR** (126 MHz, CD$_3$CN): δ[ppm] = 155.9 (C=O), 155.5 (C-1), 141.1 (C-2), 136.0 (C-6), 134.3 (C-5), 131.2 (C-3), 126.1 (C-4), 54.0 (C-11), 39.4 (C-7), 35.5 (C-8), 33.6 (C-12), 29.3 (C-10), 24.1 (C-13), 9.9 (C-9), -0.1 (Si(CH$_3$)$_3$). **ATR-IR**: $\tilde{\nu}$ [cm^{-1}] = 3319, 2956, 2869, 1731, 1704, 1569, 1533, 1455, 1401, 1365, 1302, 1246, 1179, 1113, 1089, 1061, 1029, 999, 956, 862, 836, 778, 754, 688, 628, 565, 527. **HRMS** (ESI$^+$): m/z = 348.2357 (348.2353 calculated for [M+H]$^+$). **R$_f$** = 0.23 (PE/CH$_2$Cl$_2$ 2:1 v/v).

2-Iodo-6-(2-Methylbutan-2-yl) cyclopentylcarbamate 53

Under nitrogen atmosphere, a 0 °C cooled solution of compound **56** (5.51 g, 15.9 mmol, 1.0 eq.) in dry dichloromethane (200 mL) was carefully treated with a solution of iodo monochloride (3.35 g, 20.6 mmol, 1.3 eq.) in dry dichloromethane (20 mL). The reaction mixture was stirred for 3 h while warming up to room temperature and afterwards washed with sat. sodium thiosulfate solution twice. The combined aqueous phases were extracted with dichloromethane three times and the combined extracts

C$_{17}$H$_{24}$INO$_2$
401.2885 g/mol

were washed with brine. Dehydration over sodium sulfate, concentration in vacuo and purification via column chromatography (PE/CH$_2$Cl$_2$ 2:1 v/v) finally furnished iodide **53** (6.38 g, 15.9 mmol, 100 %) as white solid.
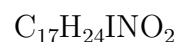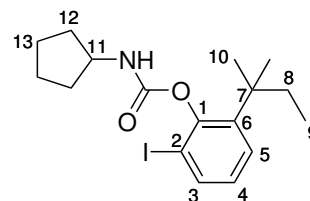
¹H NMR (500 MHz, CD$_3$CN): δ [ppm] = 7.72 (dd, $^3J_{HH}$ = 7.8 Hz, $^4J_{HH}$ = 1.4 Hz, 1H, H-3), 7.36 (dd, $^3J_{HH}$ = 8.0 Hz, $^4J_{HH}$ = 1.4 Hz, 1H, H-5), 6.82 (t, $^3J_{HH}$ = 7.9 Hz, 1H, H-4), 6.21 (d, $^3J_{HH}$ = 6.0 Hz, 1H, NH), 3.95 (sext, $^3J_{HH}$ = 7.0 Hz, 1H, H-11), 1.96-1.87 (m, 2H, H-8), 1.78-1.68 (m, 4H, H-13), 1.65-1.55 (m, 4H, H-12), 1.29 (s, 6H, H-10), 0.61 (t, $^3J_{HH}$ = 7.5 Hz, 3H, H-9). **¹³C NMR** (126 MHz, CD$_3$CN): δ[ppm] = 153.6 (C=O), 150.8 (C-1), 143.8 (C-6), 138.5 (C-3), 130.1 (C-5), 127.9 (C-4), 96.0 (C-2), 54.1 (C-11), 39.7 (C-7), 35.1 (C-8), 33.5 (C-12), 28.7 (C-10), 24.3 (C-13), 9.8 (C-9). **ATR-IR**: $\tilde{\nu}$ [cm^{-1}] = 3280, 2960, 2865, 1749, 1714, 1561, 1538, 1455, 1420, 1377, 1362, 1296, 1242, 1207, 1088, 1025, 986, 936. **HRMS** (ESI$^+$): m/z = 402.0925 (402.0924 calculated for [M+H]$^+$). **R$_f$** = 0.20 (PE/CH$_2$Cl$_2$ 2:1 v/v).

N-cyclopentyl-2-hydroxy-3-(2-methylbutan-2-yl)benzamide 54

The undesired compound was prepared, following the synthesis procedure described for 2-iodo-6-(trifluoromethyl) cyclopentylcarbamate **51**, using trimethylsilyl trifluoromethanesulfonate (3.8 mL, 4.6 g, 20.9 mmol, 1.05 eq.), carbamate **52** (5.47 g, 19.9 mmol, 1 eq.), tetramethylethylenediamine (TMEDA, 3.3 mL, 2.5 g, 22 mmol, 1.1 eq.) in the first step, TMEDA (6.0 mL, 4.6 g, 40 mmol, 2 eq.) and *n*-butyllithium solution (1.6 M in hexane; 40 mmol, 2 eq.) in the second step, iodine (6.30 g, 24.8 mmol, 1.25 eq.) and hydrochloric acid (2M, 238 mL).

$C_{17}H_{25}NO_2$
275.3920 g/mol

Purification was performed by column chromatography (PE/ethyl acetate gradient 60:1 to 45:1 v/v). Compound **54** (2.80 g, 10.2 mmol, 51 %) was obtained as colorless solid.
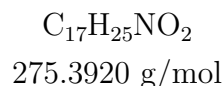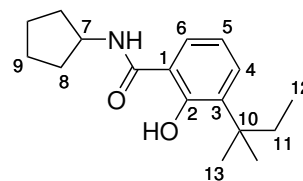
¹H NMR (600 MHz, DMSO-d_6): δ [ppm] = 13.82 (s, 1H, OH), 8.61 (t, $^3J_{HH}$ = 7.4 Hz, 1H, NH), 7.76 (dd, $^3J_{HH}$ = 8.1 Hz, $^4J_{HH}$ = 1.5 Hz, 1H, H-6), 7.28 (dd, $^3J_{HH}$ = 7.7 Hz, $^4J_{HH}$ = 1.6 Hz, 1H, H-4), 6.78 (t, $^3J_{HH}$ = 7.8 Hz, 1H, H-5), 4.25 (sext, $^3J_{HH}$ = 6.9 Hz, 1H, H-7), 1.94-1.88 (m, 2H, H-8a), 1.85 (q, $^3J_{HH}$ = 7.4 Hz, 2H, H-11), 1.76-1.65 (m, 2H, H-9a) 1.62-1.50 (m, 4H, H-8b, H-9b), 1.30 (s, 6H, H-13), 0.56 (t, $^3J_{HH}$ = 7.5 Hz, 3H, H-12). **¹³C NMR** (151 MHz, DMSO-d_6): δ[ppm] = 170.4 (CONH), 160.3 (C-2), 135.3 (C-3), 131.9 (C-4), 125.2 (C-6), 117.2 (C-5), 113.7 (C-1), 50.8 (C-10), 40.1 (C-7), 38.1 (C-8), 27.4 (C-13), 23.6 (C-9), 9.5 (C-12). **ATR-IR**: $\tilde{\nu}$ [cm⁻¹] = 3341, 2955, 2871, 1817, 1600, 1579, 1537, 1475, 1454, 1424, 1382, 1366, 1323, 1284, 1247, 1196, 1165, 1136, 1097, 1059, 844, 825, 800, 779, 750, 713, 674, 624, 603, 573, 551, 535, 404. **HRMS** (ESI⁺): m/z = 276.1962 (276.1958 calculated for [M+H]⁺). R_f = 0.23 (PE/EA 30:1 v/v).

Besides, *N*-cyclopentyl-2-hydroxy-5-iodo-3-(2-methylbutan-2- yl)benzamide **55** (552 mg, 1.38 mmol, 7 %) was obtained as yellowish solid.

¹H NMR (500 MHz, DMSO-d_6): δ [ppm] = 13.99 (s, 1H, OH), 8.76 (d, $^3J_{HH}$ = 7.1 Hz, 1H, NH), 8.14 (d, $^4J_{HH}$ = 2.1 Hz, 1H, H-6), 7.46 (d, $^4J_{HH}$ = 2.1 Hz, 1H, H-4), 4.28-4.19 (m, 1H, H-7), 1.95-1.86 (m, 2H, H-8a), 1.83 (q, $^3J_{HH}$ = 7.5 Hz, 2H, H-11), 1.76-1.65 (m, 2H, H-9a) 1.63-1.49 (m, 4H, H-8b, H-9b), 1.28 (s, 6H, H-13), 0.56 (t, $^3J_{HH}$ = 7.4 Hz, 3H, H-12). **¹³C NMR** (126 MHz, DMSO-d_6): δ[ppm] = 169.0 (CONH), 160.2 (C-2), 139.8


55

$C_{17}H_{24}INO_2$
401.2885 g/mol
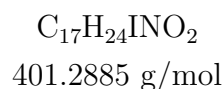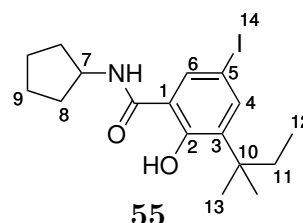
(C-4), 138.5 (C-3), 133.1 (C-6), 115.9 (C-1), 80.2 (C-5), 51.0 (C-7), 38.3 (C-10), 31.7 (C-8), 27.2 (C-13), 23.7 (C-9), 9.5 (C-12). **ATR-IR**: $\tilde{\nu}$ [cm^{-1}] = 3358, 2954, 2916, 2751, 2593, 1609, 1589, 1565, 1534, 1476, 1452, 1424, 1361, 1323, 1280, 1246, 1200, 1165, 1140, 1126, 1080, 1057, 992, 904, 893, 866, 851, 804, 774, 723, 678, 631, 574, 558, 530, 518, 433. **HRMS** (ESI$^+$): m/z = 402.0944 (402.0924 calculated for [M+H]$^+$). **R$_f$** = 0.34 (PE/EA 30:1 v/v).

2-Iodo-6-(2-methylbutan-2-yl)phenol 46c

The compound was prepared according to general procedure **8** using carbamate **53** (6.36 g, 15.9 mmol). After 4 h stirring and purification by column chromatography (PE/CH$_2$Cl$_2$ 5:1 v/v), iodophenol derivative **46c** (4.25 g, 14.7 mmol, 92 %) was furnished as colorless liquid.
^{1}H NMR (600 MHz, DMSO-d_6): δ [ppm] = 8.25 (s, 1H, OH), 7.58 (dd, $^3J_{HH}$ = 7.8 Hz, $^4J_{HH}$ = 1.5 Hz, 1H, H-3), 7.13 (dd, $^3J_{HH}$ = 7.8 Hz, $^4J_{HH}$ = 1.4 Hz, 1H, H-5), 6.61 (t, $^3J_{HH}$ = 7.8 Hz, 1H, H-4), 1.82 (q, $^3J_{HH}$ = 7.5 Hz, 2H, H-8), 1.28 (s, 6H, H-10), 0.56 (t, $^3J_{HH}$ = 7.5 Hz, 3H, H-9). **^{13}C NMR** (151 MHz, DMSO-d_6): δ[ppm] = 154.3 (C-1), 137.6 (C-6), 136.7 (C-3), 128.1 (C-5), 122.2 (C-4), 91.3 (C-2), 38.7 (C-7), 32.4 (C-8), 27.6 (C-10), 9.5 (C-9). **ATR-IR**: $\tilde{\nu}$ [cm^{-1}] = 3475, 2961, 2930, 2874, 1587, 1464, 1425, 1377, 1362, 1326, 1302, 1267, 1238, 1224, 1181, 1167, 1139, 1086, 1058, 1006, 842, 816, 784, 767, 734, 713, 590, 560. **MS** (EI): m/z = 290.03 (290.02 calculated for [M]$^{+\cdot}$). **R$_f$** = 0.54 (PE/CH$_2$Cl$_2$ 2:1 v/v).
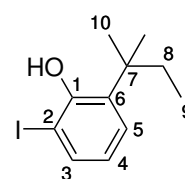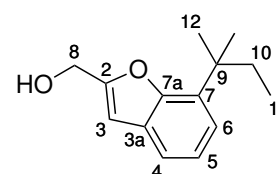
C$_{11}$H$_{15}$IO
290.1445 g/mol

7-(2-Methylbutan-2-yl)benzofuran-2-ylmethanol 45c

According to general procedure **9**, iodophenol derivative **46c** (1.13 g, 3.88 mmol), TMG (1.5 mL, 1.3 g, 12 mmol), Pd(Ph$_3$)$_2$Cl$_2$ (146 mg, 194 μmol), CuI (74 mg, 0.39 mmol) and 2-propin-1-ol (0.24 mL, 0.23 g, 4.1 mmol) were used to obtain benzofuranyl analogue **45c** (738 mg, 3.38 mmol, 87 %) as yellowish liquid.
**^{1}H NMR** (400 MHz, DMSO-d_6): δ [ppm] = 7.43 (dd, $^3J_{HH}$ = 7.5 Hz, $^4J_{HH}$ = 1.3 Hz, 1H, H-4), 7.13 (t, $^3J_{HH}$ = 7.6 Hz, 1H, H-5), 7.07 (dd, $^3J_{HH}$ = 7.6 Hz, $^4J_{HH}$ = 1.3 Hz, 1H, H-6), 6.70 (s, 1H, H-3), 5.44 (t, $^3J_{HH}$ = 5.9 Hz, 1H, OH), 4.57 (dd, $^3J_{HH}$ = 5.8 Hz, $^4J_{HH}$ = 0.4 Hz, 2H, H-8), 1.90 (q,

C$_{14}$H$_{18}$O$_2$
218.2960 g/mol

$^3J_{HH}$ = 7.5 Hz, 2H, H-10), 1.40 (s, 6H, H-12), 0.59 (t, $^3J_{HH}$ = 7.5 Hz, 3H, H-11). **^{13}C NMR** (101 MHz, DMSO-d_6): δ[ppm] = 157.6 (C-2), 152.4 (C-7a), 132.3 (C-7), 128.5 (C-3a), 122.5 (C-5), 121.6 (C-6), 119.0 (C-4), 103.0 (C-3), 56.3 (C-8), 37.4 (C-9), 33.6 (C-10), 27.2 (C-12), 9.3 (C-11). **ATR-IR**: $\tilde{\nu}$ [cm^{-1}] = 3313, 2963, 2875, 1610, 1461, 1414, 1378, 1363, 1298, 1270, 1217, 1167, 1134, 1062, 1009, 943, 908, 853, 811, 745, 617. **HRMS** (ESI$^+$): m/z = 257.0931 (257.0938 calculated for [M+K]$^+$). **R$_f$** = 0.32 (CH$_2$Cl$_2$).

Methyl 2-(((((7-(2-methylbutan-2-yl)benzofuran-2-yl)methoxy)carbonyl)-amino)benzoate 71

All reaction steps were performed under nitrogen atmosphere. Methyl anthranilate **62** (0.13 mL, 0.15 g, 1.0 mmol) was dissolved in dry tetrahydrofurane (8 mL) and added slowly to a solution of triphosgene (148 mg, 500 µmol) in dry tetrahydrofurane (0.5 mL). After careful, dropwise addition of dry triethylamine (0.28 mL, 0.20 g, 2.0 mmol), the reaction mixture was stirred for 1 h at room temperature. Subsequently, excess phosgene was removed by degassing and volatile reaction components were evaporated. The solid residue was
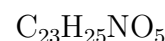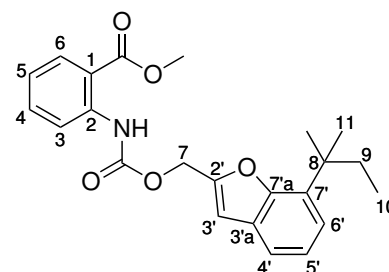
C$_{23}$H$_{25}$NO$_5$
395.4550 g/mol

suspended in dry tetrahydrofurane (8 mL). Alcohol **45c** (175 mg, 800 µmol) was added to a suspension of sodium hydride (26 mg, 1.1 mmol) in dry tetrahydrofurane (8 mL), stirred for 15 min at room temperature and the supernatant was added to the prepared isocyanate suspension. The reaction mixture was stirred for 15 h, diluted with water and extracted with dichloromethane three times. Dehydration of the combined organic phases over sodium sulfate and subsequent evaporation of the solvents afforded the crude product that was finally purified via column chromatography (PE/EA 15:1 v/v). Methylester **71** (250 mg, 632 µmol, 79%) was finally obtained as colorless solid.

^{1}H NMR (500 MHz, DMSO-d_6): δ [ppm] = 10.31 (brs, 1H, NH), 8.12 (d, $^3J_{HH}$ = 8.5 Hz, 1H, H-3), 7.92 (dd, $^3J_{HH}$ = 7.9 Hz, $^4J_{HH}$ = 1.7 Hz, 1H, H-6), 7.63 (ddd, $^3J_{HH}$ = 8.7 Hz, 7.3 Hz, $^4J_{HH}$ = 1.6 Hz, 1H, H-4), 7.50 (dd, $^3J_{HH}$ = 7.5 Hz, $^4J_{HH}$ = 1.4 Hz, 1H, H-4'), 7.18 (t, $^3J_{HH}$ = 7.6 Hz, 1H, H-5'), 7.19-7.15 (m, 1H, H-5), 7.14 (dd, $^3J_{HH}$ = 7.7 Hz, $^4J_{HH}$ = 1.4 Hz, 1H, H-6'), 6.98 (s, 1H, H-3'), 5.36 (s, 2H, H-7), 3.82 (s, 3H, OCH$_3$) 1.88 (q, $^3J_{HH}$ = 7.5 Hz, 2H, H-9) 1.39 (s, 6H, H-11), 0.56 (t, $^3J_{HH}$ = 7.4 Hz, 3H, H-10). **^{13}C NMR** (126 MHz, DMSO-d_6): δ[ppm] = 167.7 (COO), 152.6 (C-2'/C-7'a),

152.5 (C-2'/C-7'a), 151.3 (CONH), 139.8 (C-2), 134.2 (C-4), 132.5 (C-7'), 130.7 (C-6), 128.0 (C-3'a), 122.9 (C-5), 122.7 (C-5'), 122.5 (C-6'), 119.6 (C-3), 119.5 (C-4'), 116.7 (C-1), 106.6 (C-3'), 58.9 (C-7), 52.4 (OCH$_3$), 37.4 (C-8), 33.5 (C-9), 27.2 (C-11), 9.2 (C-10). **ATR-IR**: $\tilde{\nu}$ [cm^{-1}] = 3273, 2962, 2877, 1737, 1693, 1590, 1525, 1451, 1435, 1414, 1364, 1304, 1261, 1239, 1204, 1165, 1142, 1093, 1036, 995, 949, 852, 816, 747, 698, 622, 527. **HRMS** (ESI$^+$): m/z = 418.1623 (418.1625 calculated for [M+Na]$^+$). **R$_f$** = 0.30 (PE/EA 15:1 v/v).

2-(((((7-(2-Methylbutan-2-yl)benzofuran-2-yl)methoxy)carbonyl)amino)-benzoic acid 36

The compound was prepared according to general procedure **8**, using methyl ester **71** (190 mg, 480 µmol). The reaction mixture was stirred for 1 h at 50 °C. The crude product was purified by column chromatography (PE/EA 35:1 v/v) and recrystallisation by solvent diffusion. Carboxylic acid **36** (130 mg, 341 µmol, 71 %) was furnished as colorless crystals.

C$_{22}$H$_{23}$NO$_5$
381.4280 g/mol

^{1}H NMR (600 MHz, DMSO-d_6): δ [ppm] = 13.88 (brs, 1H, COOH), 11.28 (brs, 1H, NH), 8.26 (d, $^3J_{HH}$ = 8.4 Hz, 1H, H-3), 7.97 (dd, $^3J_{HH}$ = 7.9 Hz, $^4J_{HH}$ = 1.7 Hz, 1H, H-6), 7.58 (ddd, $^3J_{HH}$ = 8.7 Hz, 7.3 Hz, $^4J_{HH}$ = 1.7 Hz, 1H, H-4), 7.49 (dd, $^3J_{HH}$ = 7.6 Hz, $^4J_{HH}$ = 1.3 Hz, 1H, H-4'), 7.18 (t, $^3J_{HH}$ = 7.6 Hz, 1H, H-5'). 7.13 (dd, $^3J_{HH}$ = 7.6 Hz, $^4J_{HH}$ = 1.3 Hz, 1H, H-6'), 7.10 (td, $^3J_{HH}$ = 7.6 Hz, $^4J_{HH}$ = 1.2 Hz, 1H, H-5), 6.98 (s, 1H, H-3'), 5.35 (s, 2H, H-7), 1.87 (q, $^3J_{HH}$ = 7.5 Hz, 2H, H-9) 1.39 (s, 6H, H-11), 0.56 (t, $^3J_{HH}$ = 7.4 Hz, 3H, H-10). **^{13}C NMR** (151 MHz, DMSO-d_6): δ[ppm] = 169.7 (COOH), 152.6 (C-7'a), 152.4 (C-2'), 151.4 (CONH), 140.8 (C-2), 133.8 (C-4), 132.6 (C-7'), 131.3 (C-6), 128.1 (C-3'a), 123.0 (C-5'), 122.5 (C-6'), 121.9 (C-5), 119.5 (C-4'), 118.1 (C-3), 116.6 (C-1), 106.5 (C-3'), 58.8 (C-7), 37.5 (C-8), 33.5 (C-9), 27.2 (C-11), 9.2 (C-10). **ATR-IR**: $\tilde{\nu}$ [cm^{-1}] = 2970, 2902, 2169, 2161, 1977, 1739, 1718, 1698, 1668, 1604, 1588, 1528, 1452, 1412, 1375, 1301, 1258, 1208, 1165, 1140, 1066, 1037, 950, 902, 879, 853, 827, 803, 751, 698, 680, 662, 647, 626, 612, 557, 528, 504, 482, 468 451, 440, 428, 409, 393, 386. **HRMS** (ESI$^+$): m/z = 404.1469 (404.1468 calculated for [M+Na]$^+$). **R$_f$** = 0.42 (CH$_2$Cl$_2$/CH$_3$OH 9:1 v/v).
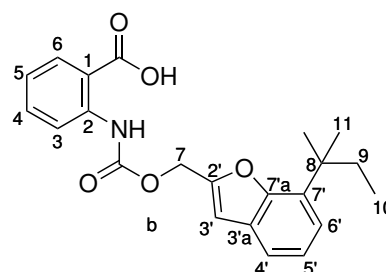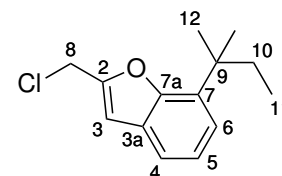
2-(Chloromethyl)-7-(2-Methylbutan-2-yl)benzofuran 77c

The compound was prepared according to general procedure **3**. Alcohol **45c** (0.80 g, 3.7 mmol), triethylamine (1.0 mL, 0.74 g, 7.3 mmol) and methanesulfonyl chloride (0.33 mL, 0.48 g, 4.2 mmol) were used, followed by column chromatography (PE/CH$_2$Cl$_2$ 5:1 v/v), to obtain chloride **77c** (0.25 g, 1.1 mmol, 29 %) as colorless oil.

C$_{14}$H$_{17}$ClO
236.7390 g/mol

In another approach, dest. thionyl chloride (70 µL, 0.11 g, 0.96 mmol, 1.6 eq.) was added dropwise to a solution of alcohol **45c** (0.13 g, 0.61 mmol) in dry tetrahydrofurane (2 mL). The reaction mixture was stirred for 90 min at 50 °C and mixed with dichloromethane, water and brine afterwards. The seperated aqueous phase was extracted with dichloromethane three times and all combined organic phases were dehydrated over sodium sulfate. Evaporation of the volatile components and subsequent column chromatography (PE/CH$_2$Cl$_2$ 5:1 v/v) afforded chloride **77c** (0.49 g, 0.12 mmol, 80 %) as colorless oil.

¹H NMR (500 MHz, DMSO-d_6): δ [ppm] = 7.49 (dd, $^3J_{HH}$ = 7.4 Hz, $^4J_{HH}$ = 1.4 Hz, 1H, H-4), 7.19 (t, $^3J_{HH}$ = 7.5 Hz, 1H, H-5), 7.15 (dd, $^3J_{HH}$ = 7.6 Hz, $^4J_{HH}$ = 1.4 Hz, 1H, H-6), 6.96 (s, 1H, H-3), 4.99 (s, 2H, H-8), 1.90 (q, $^3J_{HH}$ = 7.5 Hz, 2H, H-10), 1.58 (s, 6H, H-12), 0.59 (t, $^3J_{HH}$ = 7.5 Hz, 3H, H-11). **¹³C NMR** (126 MHz, DMSO-d_6): δ[ppm] = 152.8 (C-2), 151.9 (C-7a), 132.5 (C-7), 128.0 (C-3a), 123.0 (C-5), 122.7 (C-6), 119.6 (C-4), 106.4 (C-3), 38.1 (C-8), 37.5 (C-9), 33.6 (C-10), 27.2 (C-12), 9.2 (C-11). **ATR-IR**: $\tilde{\nu}$ [cm^{-1}] = 2963, 2876, 1606, 1461, 1413, 1378, 1363, 1328, 1278, 1255, 1217, 1200, 1171, 1143, 1125, 1070, 1043, 1006, 961, 902, 849, 816, 778, 747, 711, 639, 608, 522, 489. **MS** (EI): m/z = 236.10 (236.10 calculated for [M]$^{+\cdot}$). **R$_f$** = 0.42 (PE/CH$_2$Cl$_2$ 10:1 v/v).

2-(Azidomethyl)-7-(2-methylbutan-2-yl)benzofuran 73c

According to general procedure **4**, chloride **77c** (556 mg, 2.34 mmol) and sodium azide (458 mg, 7.05 mmol) were used, followed by purification via column chromatography (PE/CH$_2$Cl$_2$ 10:1 v/v), to prepare azide **73c** (523 mg, 2.15 mmol, 91 %) as colorless crystals.

¹H NMR (500 MHz, DMSO-d_6): δ [ppm] = 7.49 (dd, $^3J_{HH}$ = 7.5 Hz, $^4J_{HH}$ = 1.3 Hz, 1H, H-4), 7.19 (t, $^3J_{HH}$ = 7.5 Hz, 1H, H-5), 7.15 (dd, $^3J_{HH}$ = 7.6 Hz, $^4J_{HH}$ = 1.3 Hz, 1H, H-6), 6.92 (s, 1H, H-3), 4.64 (s, 2H, H-8), 1.91 (q, $^3J_{HH}$ = 7.5 Hz, 2H, H-10), 1.41 (s, 6H, H-12), 0.59 (t, $^3J_{HH}$ = 7.5 Hz, 3H, H-11). **¹³C NMR** (126 MHz, DMSO-d_6): δ[ppm] = 152.8 (C-2), 151.3 (C-7a), 132.5 (C-7), 128.0 (C-3a), 123.0 (C-5), 122.5 (C-6), 119.5 (C-4), 105.9 (C-3), 46.5 (C-8), 37.4 (C-9), 33.6 (C-10), 27.2 (C-12), 9.2 (C-11). **ATR-IR**: $\tilde{\nu}$ [cm⁻¹] = 3062, 2964, 2876, 2093, 1609, 1487, 1461, 1414, 1378, 1363, 1344, 1322, 1276, 1237, 1201, 1166, 1134, 1071, 1043, 1006, 948, 909, 876, 851, 812, 780, 745, 684, 637, 613, 555, 523, 495. **MS** (EI): m/z = 243.14 (243.14 calculated for [M]⁺·). **R_f** = 0.23 (PE/CH₂Cl₂ 10:1 v/v).

$C_{14}H_{17}N_3O$

243.3100 g/mol
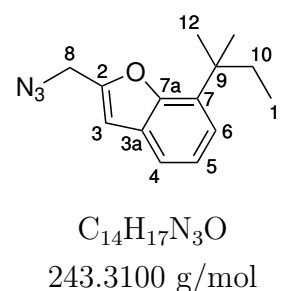
7-((2-Methylbutan-2-yl)benzofuran-2-yl)methanamine 43c

The compound was prepared according to general procedure **5**, using azide **73c** (500 mg, 2.05 mmol) and Pd/C (50 mg). Purification was performed via column chromatography (CH₂Cl₂/CH₃OH gradient 99:1 to 19:1 v/v) to obtain amine **43c** (278 mg, 1.28 mmol, 62 %) as colorless liquid.

$C_{14}H_{19}NO$

217.3120 g/mol

¹H NMR (500 MHz, DMSO-d_6): δ [ppm] = 7.39 (dd, $^3J_{HH}$ = 7.5 Hz, $^4J_{HH}$ = 1.2 Hz, 1H, H-4), 7.19 (t, $^3J_{HH}$ = 7.6 Hz, 1H, H-5), 7.03 (dd, $^3J_{HH}$ = 7.6 Hz, $^4J_{HH}$ = 1.2 Hz, 1H, H-6), 6.63 (t, $^4J_{HH}$ = 0.93 Hz, 1H, H-3), 3.84 (d, $^3J_{HH}$ = 0.9 Hz, 2H, H-8), 1.91 (brs, 2H, NH₂), 1.89 (q, $^3J_{HH}$ = 7.4 Hz, 2H, H-10), 1.40 (s, 6H, H-12), 0.59 (t, $^3J_{HH}$ = 7.5 Hz, 3H, H-11). **¹³C NMR** (101 MHz, DMSO-d_6): δ[ppm] = 160.1 (C-2), 152.1 (C-7a), 132.1 (C-7), 128.8 (C-3a), 122.4 (C-5), 121.1 (C-6), 118.6 (C-4), 101.3 (C-3), 39.3 (C-8), 37.4 (C-9), 33.6 (C-10), 27.3 (C-12), 9.3 (C-11). **ATR-IR**: $\tilde{\nu}$ [cm⁻¹] = 3301, 3060, 2963, 2875, 1607, 1461, 1414, 1378, 1362, 1296, 1261, 1217, 1166, 1139, 1070, 951, 852, 807, 745, 664, 619, 524, 412, 382. **MS** (EI): m/z = 217.16 (217.15 calculated for [M]⁺·). **R_f** = 0.17 (CH₂Cl₂/CH₃OH 19:1 v/v).
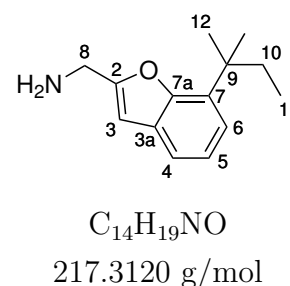
Besides, bis((7-(2-methylbutan-2-yl)benzofuran-2-yl)-methyl)amine **83** (150 mg, 0.359 mmol, 35 %) was obtained as colorless liquid.

¹H NMR (400 MHz, DMSO-d_6): δ [ppm] = 7.41 (dd, $^3J_{HH}$ = 7.6 Hz, $^4J_{HH}$ = 1.2 Hz, 1H, H-4), 7.13 (t, $^3J_{HH}$ = 7.6 Hz, 1H, H-5), 7.06 (dd, $^3J_{HH}$ = 7.6 Hz, $^4J_{HH}$ = 1.3 Hz, 1H, H-6), 6.70 (s, 1H, H-3), 3.94 (s, 2H, H-8), 1.90 (q, $^3J_{HH}$ = 7.4 Hz, 2H, H-10), 1.40 (s, 6H, H-12), 0.58 (t, $^3J_{HH}$ = 7.4 Hz, 3H, H-11). **¹³C NMR** (101 MHz, DMSO-d_6): δ[ppm] = 156.6 (C-2), 152.3 (C-7a), 132.2 (C-7), 128.6 (C-3a), 122.5 (C-5), 121.4 (C-6), 118.8 (C-4), 103.2 (C-3), 45.1 (C-8), 37.4 (C-9), 33.6 (C-10), 27.3 (C-12), 9.3 (C-11). **ATR-IR**: $\tilde{\nu}$ [cm⁻¹] = 3675, 2963, 2931, 2876, 1775, 1609, 1459, 1414, 1378, 1362, 1297, 1261, 1217, 1165, 1140, 1071, 1043, 950, 854, 809, 744, 704. **HRMS** (ESI⁺): m/z = 418.2741 (418.2741 calculated for [M+H]⁺). **R_f** = 0.62 (CH₂Cl₂/CH₃OH).
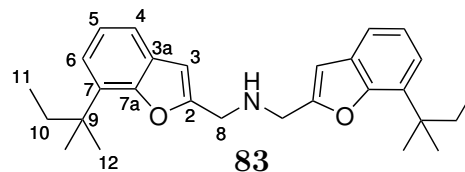
$C_{28}H_{35}NO_2$

417.5930 g/mol

Benzyl 2-(3-((7-(2-methylbutan-2-yl)benzofuran-2-yl)methyl)ureido) benzoate 89c

The compound was prepared according to general procedure **6** using triphosgene (0.24 g, 0.80 mmol), benzyl anthranilate (363 mg, 1.60 mmol), triethylamine (0.44 mL, 0.32 g, 3.2 mmol) and amine **43c** (278 mg, 1.28 mmol). Ureide **89c** (485 mg, 1.03 mmol, 81 %) was obtained as colorless solid.

$C_{29}H_{30}N_2O_4$

470.5690 g/mol

¹H NMR (300 MHz, CD₃CN): δ [ppm] = 10.10 (s, 1H, NH-a), 8.44 (dd, $^3J_{HH}$ = 8.6 Hz, $^4J_{HH}$ = 0.9 Hz, 1H, H-3), 7.99 (dd, $^3J_{HH}$ = 8.0 Hz, $^4J_{HH}$ = 1.6 Hz, 1H, H-6), 7.49 (ddd, $^3J_{HH}$ = 8.8 Hz, 7.3 Hz, $^4J_{HH}$ = 1.8 Hz, 1H, H-4), 7.46-7.29 (m, 7H, H-6, H-4', H-2", H-3", H-4"), 7.12 (t, $^3J_{HH}$ = 7.6 Hz, 1H, H-5'). 7.11-7.06 (m, 1H, H-6') 6.97 (ddd, $^3J_{HH}$ = 8.2 Hz, 7.3 Hz, $^4J_{HH}$ = 1.2 Hz, 1H, H-5), 6.61-6.58 (m, 1H, H-3'), 6.37 (t, $^3J_{HH}$ = 5.7 Hz, 1H, NH-b), 5.31 (s, 2H, H-12), 4.49 (dd, $^3J_{HH}$ = 5.9 Hz, $^4J_{HH}$ = 0.7 Hz, 2H, H-7), 1.95-1.86 (m, 2H, H-9) 1.39 (s, 6H, H-11), 0.56 (t, $^3J_{HH}$ = 7.5 Hz, 3H, H-10). **¹³C NMR** (75 MHz, CD₃CN): δ[ppm] = 168.9 (COO), 156.1 (CONH), 155.7 (C-2'), 154.2 (C-7'a), 144.2 (C-2), 137.1 (C-1"), 135.2 (C-4), 133.8 (C-7'), 131.7 (C-6), 129.6 (C-3"), 129.2 (C-4"), 129.0 (C-2"), 128.7 (C-3'a), 123.7 (C-5'), 122.8 (C-6'), 121.7 (C-5), 120.6 (C-3), 119.9 (C-4'), 115.3 (C-1), 103.8 (C-3'), 67.6 (C-12), 38.2 (C-7), 36.2 (C-8), 34.8 (C-9), 27.8 (C-11), 9.7 (C-10).

ATR-IR: $\tilde{\nu}$ [cm^{-1}] = 3287, 2962, 2874, 1681, 1660, 1586, 1545, 1448, 1414, 1377, 1304, 1273, 1242, 1163, 1147, 1110, 1079, 1044, 948, 910, 856, 809, 753, 746, 718, 698, 677, 622, 587, 570, 536, 528, 504, 441. **HRMS** (ESI$^+$): m/z = 471.2278 (471.2278 calculated for [M+H]$^+$). **R$_f$** = 0.48 (CH$_2$Cl$_2$).

2-(3-((7-(2-Methylbutan-2-yl)benzofuran-2-yl)methyl)ureido)benzoic acid 33c

The compound was prepared according to general procedure **5** using benzoate **89c** (1.03 g, 2.19 mmol) and Pd/C (100 mg). After 19 h stirring and multiple purification steps using column chromatography (PE/CH$_2$Cl$_2$/CH$_3$COOH 16:4:1 v/v and CH$_2$Cl$_2$/CH$_3$OH 50:1 v/v), carboxylic acid **33c** (774 mg, 2.03 mmol, 93 %) was furnished as white solid.

C$_{22}$H$_{24}$N$_2$O$_4$
380.4440 g/mol

^{1}H NMR (500 MHz, DMSO-d_6): δ [ppm] = 13.30 (s, 1H, COOH) 10.30 (s, 1H, NH-a), 8.38 (dd, $^3J_{HH}$ = 8.4 Hz, $^4J_{HH}$ = 0.5 Hz, 1H, H-3), 8.12-8.00 (m, 1H, NH-b), 7.91 (dd, $^3J_{HH}$ = 7.9 Hz, $^4J_{HH}$ = 1.7 Hz, 1H, H-6), 7.48 (ddd, $^3J_{HH}$ = 8.7 Hz, 7.3 Hz, $^4J_{HH}$ = 1.6 Hz, 1H, H-4), 7.41 (dd, $^3J_{HH}$ = 7.6 Hz, $^4J_{HH}$ = 1.1 Hz, 1H, H-4'), 7.13 (t, $^3J_{HH}$ = 7.6 Hz, 1H, H-5'), 7.06 (dd, $^3J_{HH}$ = 7.6 Hz, $^4J_{HH}$ = 1.1 Hz, 1H, H-6'), 7.00-6.94 (m, 1H, H-5), 6.67 (s, 1H, H-3'), 4.45 (d, $^3J_{HH}$ = 5.7 Hz, 2H, H-7), 1.88 (q, $^3J_{HH}$ = 7.4 Hz, 2H, H-9), 1.39 (s, 6H, H-11), 0.57 (t, $^3J_{HH}$ = 7.4 Hz, 3H, H-10). **^{13}C NMR** (126 MHz, DMSO-d_6): δ[ppm] = 169.5 (COOH), 155.4 (CONH), 154.7 (C-2'), 152.2 (C-7'a), 142.9 (C-2), 140.6 (C-1"), 133.6 (C-4), 132.2 (C-7'), 130.8 (C-6), 128.6 (C-3'a), 122.6 (C-5'), 121.4 (C-6'), 120.2 (C-5), 119.2 (C-3), 118.8 (C-4'), 114.8 (C-1), 102.7 (C-3'), 37.4 (C-7), 36.9 (C-8), 33.6 (C-9), 27.2 (C-11), 9.3 (C-10). **ATR-IR**: $\tilde{\nu}$ [cm^{-1}] = 3230, 2962, 2875, 1683, 1659, 1606, 1586, 1557, 1466, 1452, 1413, 1384, 1321, 1266, 1237, 1161, 1088, 1044, 949, 922, 859, 807, 745, 717, 696, 657, 630, 612, 565, 524, 482, 452, 425, 406. **HRMS** (ESI$^+$): m/z = 381.1806 (381.1809 calculated for [M+H]$^+$). **Mp** = 138.3 °C. **R$_f$** = 0.43 (CH$_2$Cl$_2$/CH$_3$OH 50:1).
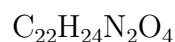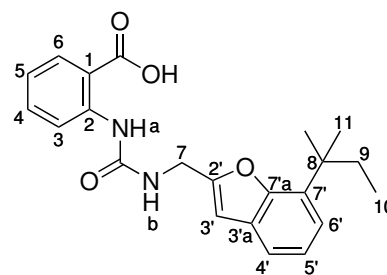
6.6.13 Synthesis of reference compound 18

Methyl 2-(phenylamino)benzoate 100

In a nitrogen atmosphere, aniline (0.16 mL, 0.16 g, 1.8 mmol, 1.7 eq.), tris(dibenzylideneacetone)dipalladium (0.18 g, 0.20 mmol, 0.2 eq.), 2,2'-bis(diphenylphosphino)-1,1'-binaphthalene (0.25 g, 0.40 mmol, 0.4 eq.) and potassium carbonate (0.38 g, 2.7 mmol, 2.7 eq.) were successively added to a solution of methyl 2-bromobenzoate **98** (0.22 g, 1.0 mmol) in 13 mL dry 1,2-dimethoxyethane. After the reaction mixture was stirred for three days under reflux, it was diluted with dichloromethane and

$C_{14}H_{13}NO_2$
227.2630 g/mol

filtrated. The filtrate was washed with water three times and the aqueous phase was reextracted with dichloromethane three times. The combined organic phases were dried over sodium sulphate and the solvent was evaporated under reduced pressure. Finally, the crude product was purified by column chromatography (PE/EA 50:1 v/v) and methyl fenamate **100** (0.24 g, 1.0 mmol, 99 %) was obtained as yellowish oil.
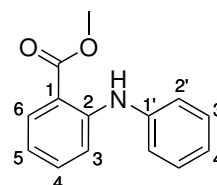
^{1}H NMR (400 MHz, DMSO-d_6): δ [ppm] = 9.32 (s, 1H, NH), 7.90 (dd, $^3J_{HH}$ = 8.0 Hz, $^4J_{HH}$ = 1.7 Hz, 1H, H-6), 7.41 (ddd, $^3J_{HH}$ = 8.8 Hz, $^3J_{HH}$ = 7.1 Hz, $^4J_{HH}$ = 1.8 Hz, 1H, H-4), 7.41-7.32 (m, 2H, H-3'), 7.29-7.20 (m, 3H, H-2', H-3), 7.09 (tt, $^3J_{HH}$ = 7.3 Hz, $^4J_{HH}$ = 1.2 Hz, 1H, H-4'), 6.81 (ddd, $^3J_{HH}$ = 8.1 Hz, $^3J_{HH}$ = 7.1 Hz, $^4J_{HH}$ = 1.1 Hz, 1H, H-5), 3.85 (s, 3H, CH$_3$). **^{13}C NMR** (101 MHz, DMSO-d_6): δ[ppm] = 168.1 (COO), 146.7 (C-2), 140.4 (C-1'), 134.5 (C-4), 131.4 (C-6), 129.5 (C-3'), 123.3 (C-4'), 121.5 (C-2'), 117.7 (C-5), 114.2 (C-3), 112.0 (C-1), 52.0 (CH$_3$). **ATR-IR**: $\tilde{\nu}$ [cm^{-1}] = 3318, 3036, 2949, 1682, 1590, 1576, 1512, 1452, 1434, 1318, 1255, 1229, 1189, 1161, 1139, 1081, 1044, 1028, 965, 884, 743, 692, 643, 579, 490. **HRMS** (ESI$^+$): m/z = 228.1019 (228.1019 calculated for [M+H]$^+$). **R$_f$** = 0.72 (CH$_2$Cl$_2$).

2-(Phenylamino)benzoic acid 18

The compound was prepared according to general procedure **8**, using methyl ester **100** (235 mg, 1.03 mmol) with the exception of stirring under reflux for 15 h. The crude product was recrystallised by solvent diffusion to obtain carboxylic acid **18** (220 mg, 1.03 mmol, 100 %) as colorless crystals.

¹H NMR (400 MHz, DMSO-d_6): δ [ppm] = 13.07 (brs, 1H, COOH) 9.64 (s, 1H, NH), 7.90 (dd, $^3J_{HH}$ = 8.0 Hz, $^4J_{HH}$ = 1.7 Hz, 1H, H-6), 7.39 (ddd, $^3J_{HH}$ = 8.7 Hz, $^3J_{HH}$ = 7.1 Hz, $^4J_{HH}$ = 1.7 Hz, 1H, H-4), 7.39-7.32 (m, 2H, H-3'), 7.27-7.20 (m, 3H, H-2', H-3), 7.07 (tt, $^3J_{HH}$ = 7.3 Hz, $^4J_{HH}$ = 1.2 Hz, 1H, H-4'), 6.78 (ddd, $^3J_{HH}$ = 8.1 Hz, $^3J_{HH}$ = 7.1 Hz, $^4J_{HH}$ = 1.1 Hz, 1H, H-5). **¹³C NMR** (101 MHz, DMSO-d_6): δ[ppm] = 170.0 (COO), 147.0 (C-2), 140.5 (C-1'), 134.2 (C-4), 131.9 (C-6), 129.5 (C-3'), 123.1 (C-4'), 121.4 (C-2'), 117.4 (C-5), 113.7 (C-3), 112.6 (C-1). **ATR-IR**: $\tilde{\nu}$ [cm⁻¹] = 3329, 2558, 1652, 1588, 1574, 1505, 1434, 1408, 1323, 1250, 1163, 1150, 1075, 1041, 1025, 886, 801, 742, 692, 642, 537, 489, 417. **HRMS** (ESI⁺): m/z = 214.0861 (214.0863 calculated for [M+H]⁺). **Mp** = 185.9 °C. **R$_f$** = 0.48 (CH$_2$Cl$_2$/CH$_3$OH 9:1 v/v).
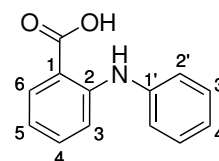
$C_{13}H_{11}NO_2$

213.2360 g/mol

6.6.14 Synthesis of benzamido derivative 94a

Methyl 2-benzamidobenzoate 101a

According to general procedure **1**, the compound was prepared using benzoic acid **102a** (0.72 g, 5.9 mmol), oxalyl chloride (0.61 mL, 0.90 g, 7.1 mmol), methyl anthranilate **62** (0.54 mL, 0.63 g, 4.2 mmol) and dry triethyl amine (0.91 mL, 0.66 g, 6.5 mmol). Column-chromatographic purification (PE/CH$_2$Cl$_2$ 3:1 v/v) finally yielded methyl ester **101a** (1.1 g, 4.2 mmol, 99 %) as colorless solid.
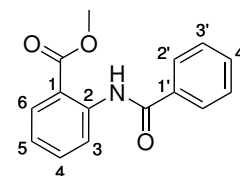
$C_{15}H_{13}NO_3$

255.2730 g/mol

¹H NMR (400 MHz, DMSO-d_6): δ [ppm] = 11.62 (s, 1H, NH) 8.58 (dd, $^3J_{HH}$ = 8.4 Hz, $^4J_{HH}$ = 1.2 Hz, 1H, H-3), 8.02 (dd, $^3J_{HH}$ = 8.0 Hz, $^4J_{HH}$ = 1.6 Hz, 1H, H-6), 7.99-7.94 (m, 2H, H-2'), 7.69 (ddd, $^3J_{HH}$ = 8.7 Hz, 7.3 Hz, $^4J_{HH}$ = 1.7 Hz, 1H, H-4'), 7.69-7.57 (m, 3H, H-3', H-4), 7.25 (ddd, $^3J_{HH}$ = 8.0 Hz, 7.4 Hz, $^4J_{HH}$ = 1.2 Hz, 1H, H-5), 3.90 (s, 3H, OCH$_3$). **¹³C NMR** (101 MHz, DMSO-d_6): δ[ppm] = 168.1 (COO), 164.8 (CONH), 140.3 (C-2), 134.4 (C-4'), 134.3 (C-1'), 132.2 (C-4), 130.7 (C-6), 129.0 (C-3'), 127.1 (C-2'), 123.4 (C-5), 120.8 (C-3), 117.0 (C-1), 52.7 (OCH$_3$). **ATR-IR**: $\tilde{\nu}$ [cm⁻¹] = 3264, 2949, 1693, 1668, 1607, 1590, 1532, 1494, 1454, 1433, 1323, 1296, 1269, 1252, 1235, 1190, 1178, 1146, 1110, 1080, 1046, 1026, 998, 966, 931, 896, 873, 795, 767, 698, 674, 665, 687, 530, 503, 400. **HRMS** (ESI⁺): m/z = 256.1016 (256.0968 calculated for [M+H]⁺). **R$_f$** = 0.41 (CH$_2$Cl$_2$/PE 1:1 v/v).

2-Benzamidobenzoic acid 94a

The compound was prepared according to general procedure **8**, using methyl ester **101a** (205 mg, 803 µmol). The crude product was recrystallised by solvent diffusion to obtain carboxylic acid **94a** (135 mg, 560 µmol, 70 %) as colorless crystals.

$C_{14}H_{11}NO_3$

241.2460 g/mol

^{1}H NMR (400 MHz, DMSO-d_6): δ [ppm] = 11.62 (s, 1H, NH) 8.58 (dd, $^3J_{HH}$ = 8.4 Hz, $^4J_{HH}$ = 1.2 Hz, 1H, H-3), 8.02 (dd, $^3J_{HH}$ = 8.0 Hz, $^4J_{HH}$ = 1.6 Hz, 1H, H-6), 7.99-7.94 (m, 2H, H-2'), 7.69 (ddd, $^3J_{HH}$ = 8.7 Hz, 7.3 Hz, $^4J_{HH}$ = 1.7 Hz, 1H, H-4'), 7.69-7.57 (m, 3H, H-3', H-4), 7.25 (ddd, $^3J_{HH}$ = 8.0 Hz, 7.4 Hz, $^4J_{HH}$ = 1.2 Hz, 1H, H-5), 3.90 (s, 3H, OCH$_3$). **^{13}C NMR** (101 MHz, DMSO-d_6): δ[ppm] = 168.1 (COO), 164.8 (CONH), 140.3 (C-2), 134.4 (C-4'), 134.3 (C-1'), 132.2 (C-4), 130.7 (C-6), 129.0 (C-3'), 127.1 (C-2'), 123.4 (C-5), 120.8 (C-3), 117.0 (C-1), 52.7 (OCH$_3$). **ATR-IR**: $\tilde{\nu}$ [cm^{-1}] = 2852, 2787, 2609, 1682, 1640, 1607, 1587, 1575, 1537, 1496, 1450, 1401, 1328, 1314, 1266, 1228, 1183, 1160, 1148, 1081, 1043, 900, 851, 777, 756, 704, 682, 653, 616, 587, 539, 527. **HRMS** (ESI$^-$): m/z = 240.0673 (240.0666 calculated for [M-H]$^-$). **R$_f$** = 0.41 (CH$_2$Cl$_2$/PE 1:1 v/v). **Mp** = 179.5 °C.
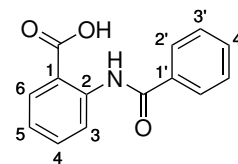
6.6.15 Synthesis of pyrrole-2-carboxamido derivative 94b

Methyl 2-(1*H*-pyrrole-2-carboxamido)benzoate 101b

According to general procedure **1**, the compound was prepared using 1*H*-pyrrole-2-carboxylic acid **102**cmpdCcoupledRings (0.33 g, 3.0 mmol), oxalyl chloride (0.31 mL, 0.46 g, 3.6 mmol), methyl anthranilate **62** (0.31 mL, 0.36 g, 2.4 mmol) and triethyl amine (0.46 mL, 0.33 g, 3.3 mmol). Column-chromatographic purification (CH$_2$Cl$_2$/CH$_3$OH 400:1 v/v) finally yielded methyl ester **101b** (0.54 g, 2.2 mmol, 93 %) as colorless solid.
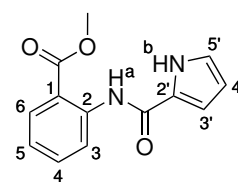
$C_{13}H_{12}N_2O_3$

244.2460 g/mol

^{1}H NMR (500 MHz, DMSO-d_6): δ [ppm] = 11.89 (s, 1H, NH-b), 11.38 (s, 2H, NH-a), 8.58 (dd, $^3J_{HH}$ = 8.5 Hz, $^4J_{HH}$ = 1.2 Hz, 1H, H-3), 8.00 (dd, $^3J_{HH}$ = 7.9 Hz, $^4J_{HH}$ = 1.6 Hz, 1H, H-6), 7.65 (ddd, $^3J_{HH}$ = 8.7 Hz, 7.2 Hz, $^4J_{HH}$ = 1.7 Hz, 1H, H-4), 7.17 (td, $^3J_{HH}$ = 7.7 Hz, $^4J_{HH}$ = 1.2 Hz, 1H, H-5), 7.04 (m, 1H, H-5'), 6.84 (dt, $^3J_{HH}$ = 3.5 Hz, $^4J_{HH}$ = 1.7 Hz, 1H, H-3'), 6.24 (dt, $^3J_{HH}$ = 3.8 Hz, 2.0 Hz, 1H, H-4'), 3.91 (s, 3H, CH$_3$. **^{13}C NMR** (126 MHz, DMSO-d_6): δ[ppm] = 168.1 (COO),

158.7 (CONH), 140.9 (C-2), 134.4 (C-4), 130.7 (C-6), 126.0 (C-2'), 123.6 (C-5'), 122.3 (C-5), 119.9 (C-3), 115.5 (C-1), 110.6 (C-3'), 109.4 (C-4'), 52.6 (CH$_3$). **ATR-IR**: $\tilde{\nu}$ [cm^{-1}] = 3262, 1694, 1645, 1605, 1588, 1551, 1528, 1450, 1436, 1400, 1311, 1276, 1255, 1231, 1166, 1123, 1092, 1078, 1051, 954, 887, 866, 832, 801, 770, 739, 695, 670, 603, 522, 497, 403. **HRMS** (ESI$^+$): m/z = 245.0934 (245.0921 calculated for [M+H]$^+$). **R$_f$** = 0.75 (CH$_2$Cl$_2$/CH$_3$OH 199:1 v/v).

2-(1*H*-pyrrole-2-carboxamido)benzoic acid 94b

The compound was prepared according to general procedure **8**, using methyl ester **101b** (131 mg, 536 µmol). The crude product was purified by column chromatography (CH$_2$Cl$_2$/CH$_3$OH/acetic acid 95:5:1 v/v/v) and subsequently recrystallised via solvent diffusion to obtain carboxylic acid **94b** (119 mg, 517 mmol, 97 %) as colorless crystals.
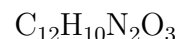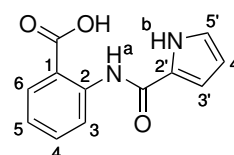
C$_{12}$H$_{10}$N$_2$O$_3$
230.2230 g/mol

¹H NMR (400 MHz, DMSO-d_6): δ [ppm] = 13.74 (brs, 1H, COOH), 11.96-11.84 (m, 2H, NH-a, NH-b), 8.68 (dd, $^3J_{HH}$ = 8.5 Hz, $^4J_{HH}$ = 1.2 Hz, 1H, H-3), 8.03 (dd, $^3J_{HH}$ = 8.0 Hz, $^4J_{HH}$ = 1.7 Hz, 1H, H-6), 7.62 (ddd, $^3J_{HH}$ = 8.7 Hz, 7.2 Hz, $^4J_{HH}$ = 1.7 Hz, 1H, H-4), 7.13 (ddd, $^3J_{HH}$ = 8.2 Hz, 7.3 Hz, $^4J_{HH}$ = 1.2 Hz, 1H, H-5), 7.03 (td, $^3J_{HH}$ = 2.7 Hz, $^4J_{HH}$ = 1.3 Hz, 1H, H-5'), 6.78 (ddd, $^3J_{HH}$ = 3.9 Hz, $^4J_{HH}$ = 2.5 Hz, 1.4 Hz, 1H, H-3'), 6.23 (dt, $^3J_{HH}$ = 3.7 Hz, 2.7 Hz, 1H, H-4'). **¹³C NMR** (101 MHz, DMSO-d_6): δ[ppm] = 170.2 (COO), 158.7 (CONH), 141.7 (C-2), 134.4 (C-4), 131.3 (C-6), 126.2 (C-2'), 123.6 (C-5'), 122.0 (C-5), 119.3 (C-3), 115.4 (C-1), 110.3 (C-3'), 109.5 (C-4'). **ATR-IR**: $\tilde{\nu}$ [cm^{-1}] = 3249, 2967, 2863, 2632, 2558, 2495, 1652, 1606, 1581, 1550, 1526, 1470, 1449, 1401, 1314, 1277, 1243, 1162, 1129, 1092, 1052, 960, 879, 834, 770, 743, 722, 704, 693, 662, 610, 596, 553, 523, 512, 410. **HRMS** (ESI$^-$): m/z = 229.0624 (239.0619 calculated for [M-H]$^-$). **R$_f$** = 0.20 (CH$_2$Cl$_2$/CH$_3$OH 9:1 v/v).

6.6.16 Synthesis of 2-(pyrrole-1-carboxamido)benzoic acid 94c

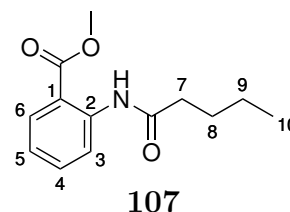### Methyl 2-(1*H*-pyrrole-1-carboxamido)benzoate 101c

The compound was prepared according to general procedure **10** using triphosgene (0.89 g, 3.0 mmol), methyl 2-aminobenzoate **62** (0.39 mL, 0.45 g, 3.0 mmol), tri-

ethylamine (0.87 mL, 6.3 mmol)), pyrrole **103c** (0.29 mL, 4.2 mmol)) and *n*-butyllithium (1.6 M in hexane; 2.8 mL, 4.5 mmol). After column-chromatographic purification (PE/EA 20:1 v/v), ureide **101c** (0.33 g, 1.3 mmol, 44 %) was obtained as colorless crystals.
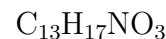
$C_{13}H_{12}N_2O_3$
244.2500 g/mol
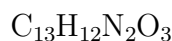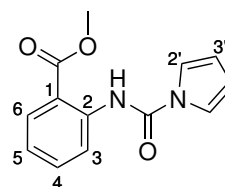
^{1}H NMR (400 MHz, DMSO-d_6): δ [ppm] = 11.06 (s, 1H, NH), 8.16 (dd, $^3J_{HH}$ = 8.3 Hz, $^4J_{HH}$ = 1.2 Hz, 1H, H-3), 7.98 (dd, $^3J_{HH}$ = 7.9 Hz, $^4J_{HH}$ = 1.6 Hz, 1H, H-6), 7.69 (ddd, $^3J_{HH}$ = 8.4 Hz, 7.4 Hz, $^4J_{HH}$ = 1.7 Hz, 1H, H-4), 7.46 (t, $^3J_{HH}$ = 2.3 Hz, 1H, H-2'), 7.28 (ddd, $^3J_{HH}$ = 7.9 Hz, 7.3 Hz, $^4J_{HH}$ = 1.2 Hz, 1H, H-5), 6.37 (t, $^3J_{HH}$ = 2.3 Hz, 1H, H-3'), 3.87 (s, 3H, OCH$_3$. **^{13}C NMR** (101 MHz, DMSO-d_6): δ[ppm] = 167.8 (COO), 148.1 (CONH), 138.9 (C-2), 134.2 (C-4), 130.7 (C-6), 124.0 (C-5), 121.8 (C-3), 118.9 (C-1), 118.8 (C-2'), 112.3 (C-3'), 52.6 (OCH$_3$). **ATR-IR**: $\tilde{\nu}$ [cm^{-1}] = 3245, 3163, 3137, 3120, 2955, 2849, 1738, 1720, 1684, 1607, 1593, 1531, 1474, 1450, 1435, 1330, 1301, 1289, 1261, 1233, 1191, 1170, 1139, 1100, 1088, 1071, 1043, 956, 865, 805, 757, 729, 695, 671, 603, 588, 524, 505. **HRMS** (ESI$^+$): m/z = 267.0728 (267.0719 calculated for [M+Na]$^+$). **R$_f$** = 0.70 (CH$_2$Cl$_2$/PE 1:1 v/v).

Besides, methyl 2-pentanamidobenzoate **107** (156 mg, 665 µmol, 22 %) was obtained as colorless sirup. **^{1}H NMR** (400 MHz, DMSO-d_6): δ [ppm] = 10.25 (s, 2H, NH), 8.17 (dd, $^3J_{HH}$ = 8.5 Hz, $^4J_{HH}$ = 1.2 Hz, 1H, H-3), 7.93 (dd, $^3J_{HH}$ = 7.9 Hz, $^4J_{HH}$ = 1.7 Hz, 1H, H-6), 7.61 (ddd, $^3J_{HH}$ = 8.7 Hz, 7.2 Hz, $^4J_{HH}$ = 1.7 Hz, 1H, H-4), 7.14 (ddd, $^3J_{HH}$ = 8.2, 7.4 Hz, $^4J_{HH}$ = 1.2 Hz, 1H, H-5), 4.11 (t, $^3J_{HH}$ = 6.6 Hz, 2H, H-7),

107

$C_{13}H_{17}NO_3$
235.1208 g/mol

3.86 (s, 3H, OCH$_3$, 1.65-1.55 (m, 2H, H-8), 1.44-4.30 (m, 2H, H-9), 0.91 (t, $^3J_{HH}$ = 7.4 Hz, 3H, H-10). **^{13}C NMR** (101 MHz, DMSO-d_6): δ[ppm] = 167.8 (COO), 153.0 (CONH), 140.4 (C-2), 134.4 (C-4), 130.7 (C-6), 122.3 (C-5), 119.0 (C-3), 115.9 (C-1), 64.6 (C-7), 52.5 (OCH$_3$), 30.4 (C-8), 18.6 (C-9), 13.6 (C-10). **ATR-IR**: $\tilde{\nu}$ [cm^{-1}] = 3304, 1257, 2874, 1734, 1692, 1589, 1524, 1450, 1435, 1314, 1260, 1239, 1209, 1163, 1144, 1094, 1057, 1041, 963, 840, 751, 699, 675, 528, 510. **HRMS** (ESI$^+$): m/z = 274.1030 (274.0840 calculated for [M+K]$^+$). **R$_f$** = 0.28 (PE/EA 30:1 v/v).

2-(1*H*-pyrrole-1-carboxamido)benzoic acid 94c

The compound was prepared according to general procedure **8**, using methyl ester **101c** (154 mg, 631 µmol). The crude product was recrystallised by solvent diffusion to obtain carboxylic acid **94c** (144 mg, 627 mmol, 99%) as colorless crystals.

$C_{12}H_{10}N_2O_3$

230.2230 g/mol
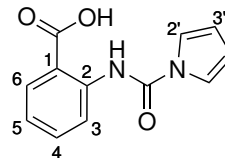
¹H NMR (500 MHz, DMSO-d_6): δ [ppm] = 13.89 (brs, 1H, COOH), 11.83 (s, 1H, NH), 8.35 (dd, $^3J_{HH}$ = 8.4 Hz, $^4J_{HH}$ = 1.1 Hz, 1H, H-3), 8.04 (dd, $^3J_{HH}$ = 7.9 Hz, $^4J_{HH}$ = 1.6 Hz, 1H, H-6), 7.68 (ddd, $^3J_{HH}$ = 8.6 Hz, 7.3 Hz, $^4J_{HH}$ = 1.6 Hz, 1H, H-4), 7.43 (t, $^3J_{HH}$ = 2.3 Hz, 1H, H-2'), 7.24 (td, $^3J_{HH}$ = 7.6 Hz, $^4J_{HH}$ = 1.2 Hz, 1H, H-5), 6.37 (t, $^3J_{HH}$ = 2.3 Hz, 1H, H-3'). **¹³C NMR** (126 MHz, DMSO-d_6): δ[ppm] = 169.9 (COO), 147.7 (CONH), 140.1 (C-2), 134.3 (C-4), 131.2 (C-6), 123.3 (C-5), 120.1 (C-3), 118.6 (C-2'), 117.6 (C-1), 112.4 (C-3'). **ATR-IR**: $\tilde{\nu}$ [cm⁻¹] = 3107, 2988, 2901, 1700, 1608, 1592, 1540, 1481, 1452, 1381, 1330, 1312, 1271, 1208, 1162, 1145, 1102, 1072, 959, 876, 863, 835, 812, 750, 726, 693, 653, 604, 583, 524. **HRMS** (ESI⁻): m/z = 229.0550 (229.0619 calculated for [M-H]⁻). **R$_f$** = 0.2 (CH$_2$Cl$_2$/CH$_3$OH 9:1 v/v). Decomposes at 193.0 °C.

6.6.17 Synthesis of 2-(Pyrrolidine-1-carboxamido)benzoic acid 94d

Methyl 2-(pyrrolidine-1-carboxamido)benzoate 101d

The compound was prepared according to general procedure **6**, using triphosgene (0.89 g, 3.0 mmol), methyl anthranilate **62** (0.39 mL, 0.45 g, 3.0 mmol), triethylamine (0.87 mL, 6.3 mmol) and pyrrolidine **103d** (0.22 mL, 2.7 mmol). Ureide **101d** (0.66 g, 2.6 mmol, 88 %) was obtained as colorless solid.

$C_{13}H_{16}N_2O_3$

248.2820 g/mol
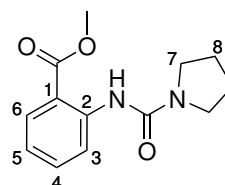
¹H NMR (500 MHz, DMSO-d_6): δ [ppm] = 10.26 (s, 1H, NH), 8.50 (dd, $^3J_{HH}$ = 8.6 Hz, $^4J_{HH}$ = 1.2 Hz, 1H, H-3), 7.94 (dd, $^3J_{HH}$ = 8.0 Hz, $^4J_{HH}$ = 1.7 Hz, 1H, H-6), 7.55 (ddd, $^3J_{HH}$ = 8.7 Hz, 7.2 Hz, $^4J_{HH}$ = 1.7 Hz, 1H, H-4), 7.01 (ddd, $^3J_{HH}$ = 7.9 Hz, 7.3 Hz, $^4J_{HH}$ = 1.2 Hz, 1H, H-5), 3.87 (s, 3H, OCH$_3$), 3.39 (t, $^3J_{HH}$ = 6.4 Hz, 4H, H-2'), 1.90 (brs, 4H, H-3'). **¹³C NMR** (126 MHz, DMSO-d_6): δ[ppm] = 168.5 (COO), 152.8 (CONH), 143.0 (C-2), 134.4 (C-4), 130.5 (C-6), 120.5 (C-5), 118.7 (C-3), 113.5 (C-1), 52.5 (OCH$_3$),
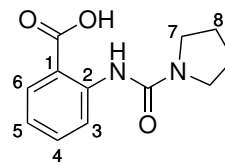
45.5 (C-3'), 24.9 (C-2'). **ATR-IR**: $\tilde{\nu}$ [cm^{-1}] = 3270, 2970, 2945, 2872, 2847, 1693, 1667, 1607, 1589, 1535, 1451, 1439, 1368, 1338, 1298, 1256, 1232, 1199, 1177, 1161, 1144, 1100, 1073, 1045, 969, 876, 748, 699, 671, 609, 529, 517, 505. **HRMS** (ESI$^+$): m/z = 249.1231 (249.1231 calculated for [M+H]$^+$). **R$_f$** = 0.20 (CH$_2$Cl$_2$/CH$_3$OH 99:1 v/v).

2-(Pyrrolidine-1-carboxamido)benzoic acid 94d

The compound was prepared according to general procedure **8**, using methyl ester **101d** (603 mg, 2.43 mmol). The crude product was recrystallised by solvent diffusion to obtain carboxylic acid **94d** (556 mg, 2.37 mmol, 98%) as colorless crystals.

C$_{12}$H$_{14}$N$_2$O$_3$
234.2550 g/mol

^{1}H NMR (500 MHz, DMSO-d_6): δ [ppm] = 13.47 (brs, 1H, COOH), 10.67 (s, 1H, NH), 8.51 (dd, $^3J_{\mathrm{HH}}$ = 8.6 Hz, $^4J_{\mathrm{HH}}$ = 1.1 Hz, 1H, H-3), 7.95 (dd, $^3J_{\mathrm{HH}}$ = 8.0 Hz, $^4J_{\mathrm{HH}}$ = 1.7 Hz, 1H, H-6), 7.51 (ddd, $^3J_{\mathrm{HH}}$ = 8.8 Hz, 7.2 Hz, $^4J_{\mathrm{HH}}$ = 1.7 Hz, 1H, H-4), 7.01-6.95 (m, 1H, H-5), 3.38 (t, $^3J_{\mathrm{HH}}$ = 6.7 Hz, 4H, H-2'), 1.90 (brs, 4H, H-3'). **^{13}C NMR** (126 MHz, DMSO-d_6): δ[ppm] = 170.2 (COO), 152.9 (CONH), 143.4 (C-2), 134.1 (C-4), 131.0 (C-6), 120.2 (C-5), 118.4 (C-3), 114.0 (C-1), 45.3 (C-3'), 24.9 (C-2'). **ATR-IR**: $\tilde{\nu}$ [cm^{-1}] = 3115, 2969, 2877, 2603, 2530, 1640, 1602, 1581, 1532, 1446, 1402, 1378, 1342, 1295, 1223, 1159, 1146, 1074, 983, 885, 777, 745, 719, 697, 656, 607, 518. **HRMS** (ESI$^+$): m/z = 257.0901 (257.0897 calculated for [M+Na]$^+$). **R$_f$** = 0.21 (CH$_2$Cl$_2$/CH$_3$OH 9:1 v/v). **Mp** = 172.9 °C.
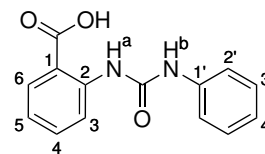
2-(3-Phenylureido)benzoic acid 94e

The compound was prepared in one step according to general procedure **11**, using phenyl isocyanate **104e** (0.32 mL, 3.0 mmol) and 2-aminobenzoic acid **105** (370 mg, 2.70 mmol). The crude product was recrystallised via solvent diffusion. Target compound **94e** (691 mg, 2.70 mmol, 700 %) was furnished as colorless, fluffy solid.

C$_{14}$H$_{12}$N$_2$O$_3$
256.2610 g/mol

^{1}H NMR (400 MHz, DMSO-d_6): δ [ppm] = 13.37 (brs, 1H, COOH), 10.35 (s, 1H, NH-a), 9.79 (s, 1H, NH-b), 8.36 (dd, $^3J_{\mathrm{HH}}$ = 8.6 Hz, $^4J_{\mathrm{HH}}$ = 1.2 Hz, 1H, H-3), 7.95 (dd, $^3J_{\mathrm{HH}}$ = 8.0 Hz, $^4J_{\mathrm{HH}}$ = 1.8 Hz, 1H, H-6), 7.54 (ddd, $^3J_{\mathrm{HH}}$ = 8.7 Hz, 7.2 Hz, $^4J_{\mathrm{HH}}$ = 1.7 Hz, 1H, H-4), 7.54-7.48 (m, 2H, H-2'), 7.32-7.24 (m, 2H, H-3'), 7.04 (dt, $^3J_{\mathrm{HH}}$ = 7.6 Hz, $^4J_{\mathrm{HH}}$ = 1.2 Hz, 1H, H-5), 6.98 (tt,

$^3J_{HH}$ = 7.4 Hz, $^4J_{HH}$ = 1.3 Hz, 4H, H-4'). **^{13}C NMR** (101 MHz, DMSO-d_6): δ[ppm] = 169.5 (COO), 152.3 (CONH), 142.3 (C-2), 139.8 (C-1'), 133.8 (C-4), 131.0 (C-6), 128.7 (C-3'), 122.1 (C-5), 120.9 (C-4'), 119.9 (C-3), 118.8 (C-2'), 115.5 (C-1). **ATR-IR**: $\tilde{\nu}$ [cm^{-1}] = 3334, 3300, 1663, 1598, 1583, 1540, 1521, 1497, 1473, 1454, 1443, 1414, 1329, 1305, 1274, 1227, 1173, 1151, 1097, 1044, 946, 832, 756, 748, 689, 672, 644, 570, 512, 425. **HRMS** (ESI$^-$): m/z = 255.0774 (255.0775 calculated for [M-H]$^-$). **R$_f$** = 0.08 (CH$_2$Cl$_2$/CH$_3$OH 19:1 v/v). **Mp** = 176.4 °C.

2-(3-Cyclopentylureido)benzoic acid 94f

The compound was prepared in one synthesis step according to general procedure **11**, using cyclopentyl isocyanate **104f** (1.0 mL, 8.9 mmol) and 2-aminobenzoic acid **105** (247 mg, 1.80 mmol) and multiple column-chromatographic purification steps (CH$_2$Cl$_2$/CH$_3$OH 19:1 v/v and CH$_2$Cl$_2$), followed by recrystallisation via solvent diffusion. Target compound **94f** (44 mg, 0.18 mmol, 10 %) was furnished as colorless crystals.

C$_{13}$H$_{16}$N$_2$O$_3$
248.2820 g/mol
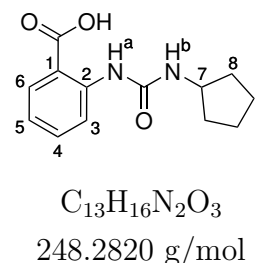
^{1}H NMR (300 MHz, DMSO-d_6): δ [ppm] = 13.22 (brs, 1H, COOH), 10.02 (s, 1H, NH-a), 8.39 (dd, $^3J_{HH}$ = 8.6 Hz, $^4J_{HH}$ = 1.1 Hz, 1H, H-3), 7.89 (dd, $^3J_{HH}$ = 7.9 Hz, $^4J_{HH}$ = 1.7 Hz, 1H, H-6), 7.46 (ddd, $^3J_{HH}$ = 8.8 Hz, 7.2 Hz, $^4J_{HH}$ = 1.8 Hz, 1H, H-4), 7.40 (d, $^3J_{HH}$ = 7.0 Hz, 1H, NH-b), 6.93 (ddd, $^3J_{HH}$ = 8.2 Hz, 7.2 Hz, $^4J_{HH}$ = 1.2 Hz, 1H, H-5), 3.93 (sext, $^3J_{HH}$ = 6.7 Hz, 1H, H-7), 1.91-1.74 (m, 2H, H-8a), 1.73-1.57 (m, 2H, H-9a), 1.57-1.33 (m, 4H, H-8b, H-9b). **^{13}C NMR** (75 MHz, DMSO-d_6): δ[ppm] = 169.5 (COO), 154.3 (CONH), 143.3 (C-2), 133.7 (C-4), 130.9 (C-6), 119.8 (C-5), 119.2 (C-3), 114.3 (C-1), 51.2 (C-1'), 32.5 (C-2'), 23.3 (C-3'). **ATR-IR**: $\tilde{\nu}$ [cm^{-1}] = 3296, 2961, 2973, 1685, 1656, 1607, 1584, 1541, 1475, 1448, 1409, 1364, 1347, 1318, 1292, 1248, 1163, 1088, 1043, 966, 953, 878, 814, 803, 753, 741, 697, 655, 628, 552, 524, 421. **HRMS** (ESI$^+$): m/z = 249.1233 (249.1234 calculated for [M+H]$^+$). **R$_f$** = 0.23 (CH$_2$Cl$_2$/CH$_3$OH 9:1 v/v). **Mp** = 169.8 °C.

Besides, 2-(cyclopentylamino)-4*H*-benzo[1,3]oxazin-4-one **131** (0.11 g, 0.46 mmol, 26 %) was obtained as colorless sirup.

¹H NMR (400 MHz, DMSO-d_6): δ [ppm] = 8.04 (d, $^3J_{HH}$ = 7.2 Hz, 1H, NH), 7.86 (dd, $^3J_{HH}$ = 7.9 Hz, $^4J_{HH}$ = 1.6 Hz, 1H, H-3), 7.65 (ddd, $^3J_{HH}$ = 8.6 Hz, 7.2 Hz, $^4J_{HH}$ = 1.6 Hz, 1H, H-4), 7.19 (d, $^3J_{HH}$ = 8.2 Hz, 1H, H-6), 7.15 (ddd, $^3J_{HH}$ = 8.0 Hz, 7.2 Hz, $^4J_{HH}$ = 1.1 Hz, 1H, H-5), 4-11 (sext, $^3J_{HH}$ = 6.7 Hz, 1H, H-9), 1.97-1.83 (m, 2H, H-10a), 1.73-1.60 (m, 2H, H-11a), 1.61-1.45 (m, 4H, H-10b, H-11b). **¹³C NMR** (101 MHz, DMSO-d_6): δ[ppm] = 159.7 (C-7), 153.7 (C-8) 150.8 (C-2), 136.8 (C-4), 128.1 (C-3), 123.9 (C-6), 122.9 (C-5), 112.6 (C-1), 52.5 (C-9), 32.0 (C-10), 23.4 (C-11). **ATR-IR**: $\tilde{\nu}$ [cm⁻¹] = 3294, 3068, 2957, 2867, 1734, 1627, 1600, 1567, 1537, 1473, 1361, 1344, 1328, 1300, 1268, 1240, 1188, 1153, 1105, 1040, 1026, 1011, 989, 952, 867, 756, 686, 627, 578, 531, 506. **HRMS** (ESI⁺): m/z = 231.1124 (231.1128 calculated for [M+H]⁺). **R$_f$** = 0.26 (CH$_2$Cl$_2$).


131
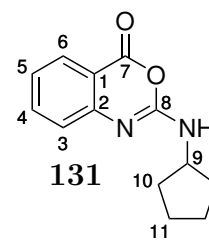
C$_{13}$H$_{16}$N$_2$O$_3$
248.2820 g/mol

6.6.18 Synthesis of phenylacetamido derivative 94g

Methyl 2-(2-phenylacetamido)benzoate 101g

According to general procedure **1**, the compound was prepared using phenylacetic acid **102g** (0.21 g, 1.5 mmol), oxalyl chloride (0.15 mL, 0.23 g, 1.8 mmol), methyl anthranilate **62** (0.14 mL, 0.16 g, 1.1 mmol) and dry triethyl amine (0.23 mL, 0.17 g, 1.7 mmol). Column-chromatographic purification (PE/CH$_2$Cl$_2$ 2:1 v/v) finally yielded methyl ester **101g** (0.30 g, 1.1 mmol, 100 %) as colorless solid.
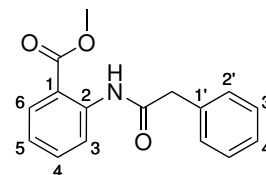

C$_{16}$H$_{15}$NO$_3$
269.3000 g/mol

¹H NMR (600 MHz, DMSO-d_6): δ [ppm] = 10.62 (s, 1H, NH), 8.23 (dd, $^3J_{HH}$ = 8.3 Hz, $^4J_{HH}$ = 1.2 Hz, 1H, H-3), 7.88 (dd, $^3J_{HH}$ = 7.9 Hz, $^4J_{HH}$ = 1.7 Hz, 1H, H-6), 7.59 (ddd, $^3J_{HH}$ = 8.6 Hz, 7.3 Hz, $^4J_{HH}$ = 1.7 Hz, 1H, H-4), 7.38-7.34 (m, 4H, H-2', H-3'), 7.30-7.25 (m, 1H, H-4'), 7.18 (ddd, $^3J_{HH}$ = 8.2 Hz, 7.3 Hz, $^4J_{HH}$ = 1.2 Hz, 1H, H-5), 3.76 (s, 3H, OCH$_3$), 3.74 (s, 2H, CH$_2$), **¹³C NMR** (151 MHz, DMSO-d_6): δ[ppm] = 169.4 (CONH), 167.4 (COOH), 139.4 (C-2), 135.1 (C-1'), 133.8 (C-4), 130.5 (C-6), 129.4 (C-C-2'), 128.5 (C-3'), 126.8 (C-4'), 123.3 (C-5), 121.2 (C-3), 118.1 (C-1), 52.28 (OCH$_3$), 44.1 (CH$_2$). **ATR-IR**: $\tilde{\nu}$ [cm⁻¹] = 3258, 2951, 1697, 1682, 1604, 1584, 1524, 1491, 1444, 1432, 1300, 1267, 1243, 1192, 1164, 1142, 1121, 1089, 1074, 1043, 1029, 966, 955, 919, 885, 758, 720, 69, 675, 649, 552, 502, 390. **HRMS** (ESI⁺): m/z = 292.0952 (292.0944 calculated for [M+Na]⁺). **R$_f$** = 0.42 (CH$_2$Cl$_2$).

2-(2-Phenylacetamido)benzoic acid 94g

The compound was prepared according to general procedure **8**, using methyl ester **101g** (0.12 g, 0.45 mmol). The crude product was recrystallised by solvent diffusion to obtain carboxylic acid **94g** (86 mg, 0.34 mmol, 76 %) as colorless crystals.

$C_{15}H_{13}NO_3$

194.2740 g/mol
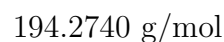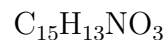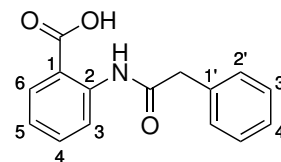
^{1}H NMR (400 MHz, DMSO-d_6): δ [ppm] = 13.57 (brs, 1H, COOH), 11.13 (s, 1H, NH), 8.50 (dd, $^3J_{HH}$ = 8.5 Hz, $^4J_{HH}$ = 1.2 Hz, 1H, H-3), 7.94 (dd, $^3J_{HH}$ = 7.9 Hz, $^4J_{HH}$ = 1.7 Hz, 1H, H-6), 7.57 (ddd, $^3J_{HH}$ = 8.7 Hz, 7.2 Hz, $^4J_{HH}$ = 1.7 Hz, 1H, H-4), 7.39-7.32 (m, 5H, H-2', H-3', H-4'), 7.13 (ddd, $^3J_{HH}$ = 8.2 Hz, 7.3 Hz, $^4J_{HH}$ = 1.2 Hz, 1H, H-5), 3.75 (s, 2H, CH$_2$). **^{13}C NMR** (101 MHz, DMSO-d_6): δ[ppm] = 169.5 (COO), 169.4 (CONH), 140.8 (C-2), 134.8 (C-1'), 134.1 (C-4), 131.1 (C-6), 129.5 (C-C-2'), 128.6 (C-3'), 127.0 (C-4'), 122.7 (C-5), 119.8 (C-3), 116.4 (C-1), 44.7 (CH$_2$). **ATR-IR**: $\tilde{\nu}$ [cm^{-1}] = 2987, 1873, 1688, 1668, 1602, 1584, 1527, 1490, 1468, 1450, 1407, 1314, 1298, 1262, 1251, 1162, 1155, 1139, 1089, 1044, 1027, 959, 889, 804, 760, 717, 696, 658, 889, 804, 760, 717, 686, 658, 647, 536, 511, 424. **HRMS** (ESI$^+$): m/z = 278.0792 (278.0788 calculated for [M+Na]$^+$). **R$_f$** = 0.26 (CH$_2$Cl$_2$/CH$_3$OH 9:1 v/v).

6.6.19 Synthesis of indole-3-carboxamido derivative 94h

Methyl 2-(1H-indole-3-carboxamido)benzoate 101h

According to general procedure **1**, the compound was prepared using 1H-indole-3-carboxylic acid **102h** (0.16 g, 1.0 mmol), oxalyl chloride (0.10 mL, 0.15 g, 1.2 mmol), methyl anthranilate (90 µL, 0.11 g, 0.70 mmol) and dry triethyl amine (0.15 mL, 0.11 g, 1.1 mmol). Column-chromatographic purification (silica gel, CH$_2$Cl$_2$) finally yielded methyl ester **101h** (0.15 g, 0.49 mmol, 70 %) as colorless solid.

$C_{17}H_{14}N_2O_3$

294.3100 g/mol
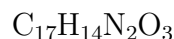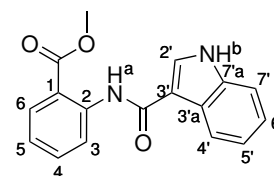
^{1}H NMR (400 MHz, DMSO-d_6): δ [ppm] = 11.88 (brs, 1H, NH-b), 11.30 (s, 1H, NH-a), 8.64 (dd, $^3J_{HH}$ = 8.5 Hz, $^4J_{HH}$ = 1.2 Hz, 1H, H-3), 8.22-8.16 (m, 1H, H-4'), 8.08 (s, 1H, H-2'), 8.01 (dd, $^3J_{HH}$ = 7.9 Hz, $^4J_{HH}$ = 1.7 Hz, 1H, H-6), 7.65 (ddd, $^3J_{HH}$ = 8.7 Hz, $^3J_{HH}$ = 7.2 Hz, $^4J_{HH}$ = 1.7 Hz, 1H, H-4), 7.55-7.50 (m, 1H, H-7'), 7.26-7.16 (m, 2H, H-5', H-6'), 7.17 (ddd, $^3J_{HH}$ = 8.2 Hz, $^3J_{HH}$ = 7.3 Hz,

$^4J_{HH}$ = 1.2 Hz, 1H, H-5), 3.91 (s, 3H, CH$_3$).

2-(1*H*-indole-3-carboxamido)benzoic acid 94k

The compound was prepared according to general procedure **8**, using methyl ester **101h** (131 mg, 442 µmol). The crude product was washed with water and dichloromethane to obtain carboxylic acid **94h** (106 mg, 375 µmol, 85 %) as light red crystals.
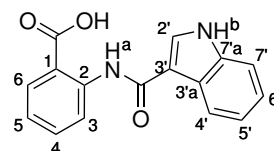
C$_{16}$H$_{12}$N$_2$O$_3$
280.2830 g/mol

^{1}H NMR (400 MHz, DMSO-d_6): δ [ppm] = 13.69 (brs, 1H, COOH) 11.91 (s, 1H, NH-b), 11.83 (s, 1H, NH-a), 8.76 (dd, $^3J_{HH}$ = 8.5 Hz, $^4J_{HH}$ = 1.2 Hz, 1H, H-3), 8.25-8.18 (m, 1H, H-4'), 8.05 (dd, $^3J_{HH}$ = 8.0 Hz, $^4J_{HH}$ = 1.7 Hz, 1H, H-6), 8.03 (d, $^3J_{HH}$ = 3.0 Hz, 1H, H-2'), 7.63 (ddd, $^3J_{HH}$ = 8.7 Hz, $^3J_{HH}$ = 7.2 Hz, $^4J_{HH}$ = 1.7 Hz, 1H, H-4), 7.52 (dt, $^3J_{HH}$ = 8.1 Hz, $^4J_{HH}$ = 0.9 Hz, 1H, H-7'), 7.27-7.16 (m, 2H, H-5', H-6'), 7.13 (ddd, $^3J_{HH}$ = 8.2 Hz, $^3J_{HH}$ = 7.3 Hz, $^4J_{HH}$ = 1.2 Hz, 1H, H-5). **^{13}C NMR** (126 MHz, DMSO-d_6): δ[ppm] = 170.14 (COOH) 162.9 (CONH), 142.1 (C-2), 136.6 (C-7'a), 134.2 (C-4), 131.3 (C-6), 128.8 (C-2'), 125.4 (C-3'a), 122.5 (C-6'), 121.8 (C-5), 121.0 (C-5'), 120.5 (C-4'), 119.7 (C-3), 115.4 (C-1), 112.4 (C-3'), 111.1 (C-3'). **ATR-IR**: $\tilde{\nu}$ [cm^{-1}] = 3298, 2815, 2548, 1657, 1604, 1579, 1522, 1465, 1447, 1406, 1361, 1315, 1253, 1235, 1175, 1155, 1145, 1107, 1089, 1046, 1026, 1012, 1012, 961, 899, 883, 869, 841, 764, 751, 737, 696, 674, 659, 638, 606, 578, 557, 541, 528, 504, 420. **HRMS** (ESI$^-$): m/z = 279.1787 (279.0775 calculated for [M-H]$^-$). **Mp** = 233.0 °C. **R$_f$** = 0.08 (CH$_2$Cl$_2$/CH$_3$OH 9:1 v/v).

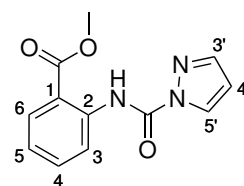## 6.6.20 Synthesis of 2-(1*H*-pyrazole-1-carboxamido)benzoic acid 94i

Methyl 2-(1*H*-pyrazole-1-carboxamido)benzoate 101i

The compound was prepared according to general procedure **10** using triphosgene (0.44 g, 1.5 mmol), methyl 2-aminobenzoate **62** (0.39 mL, 3.0 mmol), triethylamine (0.83 mL, 6.0 mmol)), pyrazole **42i** (0.35 mL, 4.9 mmol)) and *n*-butyllithium (1.6 M in hexane; 2.4 mL, 3.9 mmol). After column-chromatographic purification (PE/CH$_2$Cl$_2$ 1:2 v/v), ureide **101i** (0.64 g, 2.6 mmol, 87 %) was obtained as colorless crystals.

¹H NMR (400 MHz, DMSO-d_6): δ [ppm] = 12.39 (s, 1H, NH), 8.55 (dd, $^3J_{HH}$ = 8.5 Hz, $^3J_{HH}$ = 1.2 Hz, 1H, H-3), 8.47 (dd, $^3J_{HH}$ = 2.8 Hz, $^4J_{HH}$ = 0.7 Hz, 1H, H-3'), 8.06 (dd, $^3J_{HH}$ = 8.0 Hz, $^4J_{HH}$ = 1.7 Hz, 1H, H-6), 7.95 (dd, $^3J_{HH}$ = 1.6 Hz, $^4J_{HH}$ = 0.7 Hz, 1H, H-1'), 7.72 (ddd, $^3J_{HH}$ = 8.7 Hz, 7.4 Hz, $^4J_{HH}$ = 1.7 Hz, 1H, H-4), 7.27 (ddd, $^3J_{HH}$ = 8.3 Hz, 7.4 Hz, $^4J_{HH}$ = 1.2 Hz, 1H, H-5), 6.65 (dd, $^3J_{HH}$ = 2.8 Hz, $^3J_{HH}$ = 1.6 Hz, 1H, H-2'), 3.92 (s, 3H, OCH₃).

$C_{12}H_{11}N_3O_3$
245.2380 g/mol

¹³C NMR (101 MHz, DMSO-d_6): δ[ppm] = 167.4 (COO), 146.8 (CONH), 143.3 (C-1'), 139.2 (C-2), 134.7 (C-4), 131.0 (C-6), 129.3 (C-3'), 123.5 (C-5), 119.6 (C-3), 116.3 (C-1), 109.7 (C-2'), 52.7 (OCH₃). **ATR-IR**: $\tilde{\nu}$ [cm⁻¹] = 3187, 3136, 3120, 2998, 2952, 1726, 1698, 1589, 1532, 1513, 1468, 1451, 1388, 1336, 1299, 1264, 1247, 1228, 1203, 1186, 1163, 1142, 1090, 1063, 1026, 953, 911, 873, 846, 809, 785, 752, 735, 694, 672, 642, 605, 593, 526, 504. **HRMS** (ESI⁺): m/z = 268.0693 (268.0693 calculated for [M+Na]⁺). **R$_f$** = 0.44 (PE/CH₂Cl₂ 1:1 v/v).

2-(1*H*-pyrazole-1-carboxamido)benzoic acid 94i

The compound was prepared according to general procedure **8**, using methyl ester **101i** (476 mg, 1.94 mmol). The crude product was purified by multiple column-chromatographic steps (PE/EA 30:1:1 v/v/v) and finally recrystallised by solvent diffusion to obtain carboxylic acid **94i** (151 mg, 653 µmol, 33 %) as colorless crystals.
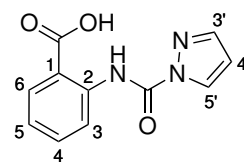
$C_{11}H_9N_3O_3$
231.2110 g/mol

¹H NMR (400 MHz, DMSO-d_6): δ [ppm] = 13.51 (brs, 1H, COOH), 12.61 (s, 1H, NH), 8.55 (dd, $^3J_{HH}$ = 8.4 Hz, $^3J_{HH}$ = 1.1 Hz, 1H, H-3), 8.46 (dd, $^3J_{HH}$ = 2.8 Hz, $^4J_{HH}$ = 0.7 Hz, 1H, H-3'), 8.06 (dd, $^3J_{HH}$ = 8.0 Hz, $^4J_{HH}$ = 1.7 Hz, 1H, H-6), 7.91 (m, 1H, H-1'), 7.69 (ddd, $^3J_{HH}$ = 8.8 Hz, 7.3 Hz, $^4J_{HH}$ = 1.8 Hz, 1H, H-4), 7.24 (m, 1H, H-5), 6.63 (dd, $^3J_{HH}$ = 2.7 Hz, $^3J_{HH}$ = 1.6 Hz, 1H, H-2'), 3.92 (s, 3H, OCH₃). **¹³C NMR** (101 MHz, DMSO-d_6): δ[ppm] = 168.6 (COO), 146.9 (CONH), 143.6 (C-1'), 139.0 (C-2), 134.3 (C-4), 131.4 (C-6), 129.3 (C-3'), 123.2 (C-5), 119.4 (C-3), 117.2 (C-1), 109.6 (C-2'). **ATR-IR**: $\tilde{\nu}$ [cm⁻¹] = 2871, 2636, 2563, 1800, 1761, 1739, 1678, 1604, 1587, 1534, 1515, 1471, 1452, 1417, 1384, 1337, 1319, 1298, 1268, 1250, 1204, 1165, 1149, 1090, 1063, 1030, 999, 952, 913, 873, 848, 755, 735, 699, 665, 644, 607, 593, 559, 527, 416. **HRMS** (ESI⁺): m/z = 254.0536 (254.0536 calculated for [M+Na]⁺). **R$_f$** = 0.14 (PE/CH₂Cl₂ 9:1 v/v). **Mp** = 106.2 °C.

6.6.21 2-(1*H*-pyrazole-1-carboxamido)benzoic acid 94j

Methyl 2-(1*H*-pyrazole-1-carboxamido)benzoate 101j

The compound was prepared according to general procedure **10** using triphosgene (0.89 g, 3.0 mmol), methyl 2-aminobenzoate **62** (0.39 mL, 3.0 mmol), triethylamine (0.87 mL, 6.3 mmol)), indole **42j** (0.39 mL, 3.9 mmol)) and *n*-butyllithium (1.6 M in hexane; 2.8 mL, 3.9 mmol). After column-chromatographic purification (PE/EA gradient 60:1 to 40:1 v/v), ureide **101j** (582 mg, 2.0 mmol, 66 %) was obtained as colorless solid.

$C_{17}H_{14}N_2O_3$

294.3100 g/mol
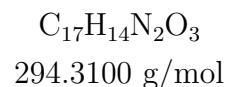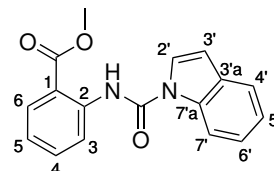
^{1}H NMR (400 MHz, DMSO-d_6): δ [ppm] = 11.04 (s, 1H, NH), 8.25 (dd, $^3J_{HH}$ = 8.2 Hz, $^4J_{HH}$ = 1.0 Hz, 1H, H-7'), 8.19 (dd, $^3J_{HH}$ = 8.4 Hz, $^4J_{HH}$ = 1.2 Hz, 1H, H-3), 7.99 (dd, $^3J_{HH}$ = 7.9 Hz, $^4J_{HH}$ = 1.6 Hz, 1H, H-6), 7.89 (d, $^3J_{HH}$ = 3.7 Hz, 1H, H-2'), 7.70 (ddd, $^3J_{HH}$ = 8.5 Hz, 7.4 Hz, $^4J_{HH}$ = 1.8 Hz, 1H, H-4), 7.67 (d, $^3J_{HH}$ = 7.7 Hz, 1H, H-4'), 7.33 (ddd, $^3J_{HH}$ = 8.8 Hz, 7.4 Hz, $^4J_{HH}$ = 1.5 Hz, 1H, H-6'), 7.31-7.22 (m, 2H, H-5, H-5'), 6.85 (dd, $^3J_{HH}$ = 3.8 Hz, $^4J_{HH}$ = 0.8 Hz, 1H, H-3'), 3.85 (s, 3H, OCH$_3$). **^{13}C NMR** (101 MHz, DMSO-d_6): δ[ppm] = 167.8 (COO), 149.3 (CONH), 139.2 (C-2), 135.3 (C-7'a), 134.1 (C-4), 130.7 (C-6), 129.8 (C-3'a), 124.5 (C-2'), 124.2 (C-6'), 123.9 (C-5), 122.6 (C-5'), 121.9 (C-3), 121.1 (C-4'), 119.1 (C-1), 114.9 (C-7'), 107.7 (C-3'), 52.6 (OCH$_3$). **ATR-IR**: $\tilde{\nu}$ [cm^{-1}] = 3261, 2950, 1714, 1677, 1604, 1590, 1534, 1474, 1449, 1434, 1325, 1299, 1260, 1240, 1205, 1166, 1144, 1121, 1088, 1045, 1016, 966, 935, 880, 856, 842, 805, 767, 751, 741, 722, 697, 670, 610, 581, 527, 502, 425, 403. **HRMS** (ESI$^+$): m/z = 295.1074 (295.1077 calculated for [M+H]$^+$). **R$_f$** = 0.38 (PE/EA 20:1 v/v).

Besides, methyl 2-pentanamidobenzoate **107** (109 mg, 464 µmol, 15 %) was obtained as colorless sirup. The analytical data are in accordance with the data that are listed above.

2-(1*H*-pyrazole-1-carboxamido)benzoic acid 94j

The compound was prepared according to general procedure **8**, using methyl ester **101j** (189 mg, 642 µmol). The crude product was purified by recrystallisation via solvent diffusion to obtain carboxylic acid **94j** (180 mg, 642 µmol, 100 %) as colorless crystals.

$C_{16}H_{12}N_2O_3$
280.2830 g/mol
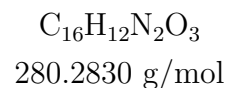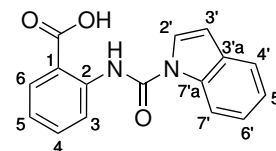
¹H NMR (400 MHz, DMSO-d_6): δ [ppm] = 13.85 (brs, 1H, COOH) 11.77 (s, 1H, CONH), 8.39 (dd, $^3J_{HH}$ = 8.4 Hz, $^4J_{HH}$ = 1.2 Hz, 1H, H-3), 8.27 (d, $^3J_{HH}$ = 8.3 Hz, 1H, H-7'), 8.05 (dd, $^3J_{HH}$ = 7.9 Hz, $^4J_{HH}$ = 1.7 Hz, 1H, H-6), 7.83 (d, $^3J_{HH}$ = 3.8 Hz, 1H, H-2'), 7.69 (ddd, $^3J_{HH}$ = 8.7 Hz, 7.4 Hz, $^4J_{HH}$ = 1.8 Hz, 1H, H-4), 7.66 (d, $^3J_{HH}$ = 7.7 Hz, 1H, H-4'), 7.33 (ddd, $^3J_{HH}$ = 8.4 Hz, 7.1 Hz, $^4J_{HH}$ = 1.4 Hz, 1H, H-6'), 7.29-7.20 (m, 2H, H-5, H-5'), 6.85 (d, $^3J_{HH}$ = 3.6 Hz, 1H, H-3'). **¹³C NMR** (101 MHz, DMSO-d_6): δ[ppm] = 170.0 (COO), 149.0 (CONH), 140.4 (C-2), 135.2 (C-7'a), 134.2 (C-4), 131.2 (C-6), 129.8 (C-3'a), 124.2 (C-2', C-6'), 123.2 (C-5), 122.6 (C-5'), 121.1 (C-4') 120.3 (C-3) 117.6 (C-1), 114.8 (C-7'), 107.8 (C-3'). **ATR-IR**: $\tilde{\nu}$ [cm^{-1}] = 3164, 3129, 3049, 1707, 1686, 1666, 1608, 1592, 1543, 1475, 1447, 1368, 1326, 1300, 1250, 1197, 1174, 1158, 1142, 1124, 1080, 1015, 981, 880, 872, 833, 744, 711, 651, 610, 546, 522, 511, 418. **HRMS** (ESI$^+$): m/z = 281.0924 (281.0921 calculated for [M+H]$^+$). **R$_f$** = 0.19 (CH$_2$Cl$_2$/CH$_3$OH 9:1 v/v). Decomposes at 205.4 °C.

2-(3-(naphthalen-1-yl)ureido)benzoic acid 94k

The compound was prepared in one step according to general procedure **11**, using 1-naphthyl isocyanate **104k** (0.19 mL, 1.2 mmol) and 2-aminobenzoic acid **105** (0.27 g, 2.0 mmol). The crude product was purified via column chromatography (CH$_2$Cl$_2$/CH$_3$OH 15:1 v/v) and finally recrystallised via solvent diffusion. Target compound **94k** (0.37 g, 1.2 mmol, 100 %) was furnished as colorless crystals.

$C_{18}H_{14}N_2O_3$
306.3210 g/mol
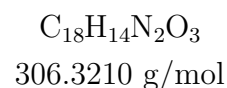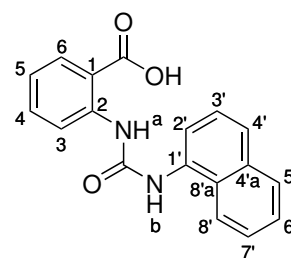
**¹H NMR** (400 MHz, DMSO-d_6): δ [ppm] = 11.64 (brs, 1H, NH-a), 9.55 (s, 1H, NH-b), 8.34 (dd, $^3J_{HH}$ = 8.5 Hz, $^4J_{HH}$ = 1.1 Hz, 1H, H-3), 8.20-8.09 (m, 1H, H-8'), 8.00-7.87 (m, 2H, H-6, H-5'), 7.73 (d, $^3J_{HH}$ = 8.2 Hz, 1H, H-4), 7.69 (d, $^3J_{HH}$ = 7.4 Hz, 1H, H-2'), 7.58-7.50 (m, 2H, H-6', H-7'), 7.49 (t, $^3J_{HH}$ = 8.2 Hz, 1H, H-3'), 7.44 (ddd, $^3J_{HH}$ = 8.6 Hz,

$^3J_{HH}$ = 7.1 Hz, $^4J_{HH}$ = 1.7 Hz, 1H, H-4), 6.97 (t, $^3J_{HH}$ = 7.6 Hz, 1H, H-5). **^{13}C NMR** (151 MHz, DMSO-d_6): δ[ppm] = 169.8 (COOH), 153.6 (CONH), 142.1 (C-2), 134.2 (C-8'a), 133.8 (C-4'a), 132.5 (C-4), 131.0 (C-6), 128.3 (C-1'), 128.1 (C-5'), 125.9-125.6 (C-3', C-6', C-7'), 124.6 (C-4'), 122.9 (C-8'), 121.5 (C-2'), 120.5 (C-5), 119.5 (C-3), 117.1 (C-1). **ATR-IR**: $\tilde{\nu}$ [cm^{-1}] = 3186, 3056, 1666, 1583, 1505, 1474, 1447, 1391, 1342, 1318, 1290, 1271, 1251, 1162, 865, 780, 752, 657, 618, 542, 524, 493, 449, 418. **HRMS** (ESI$^+$): m/z = 345.0616 (345.0636 calculated for [M+K]$^+$). Decomposes at 189.5 °C. **R$_f$** = 0.26 (**R$_f$** = 0.52 (PE/CH$_2$Cl$_2$ 1:2 v/v).

6.6.22 Synthesis of 3-(3-(naphthalen-1-yl)ureido)isonicotinic acid 97

Under inert atmosphere, 3-aminoisonicotinic acid **130** (0.28 g, 2.0 mmol, 1 eq.) was suspended in dry tetrahydrofurane (2 mL) and 1-naphthyl isocyanate **104k** (0.16 mL, 1.1 mmol, 0.9 eq.) was added dropwise. The reaction mixture was stirred under reflux for 20 h and treated with a small amount of methanol, subsequently. After evaporating the solvent, the crude product was purified by column chromatography (CH$_2$Cl$_2$/CH$_3$OH/CH$_3$COOH 100:10:3 v/v) to obtain carboxylic acid **97** (82mg, 0.27 mmol, 24 %) as colorless solid.
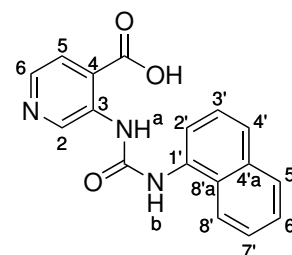
C$_{17}$H$_{13}$N$_3$O$_3$
307.3090 g/mol

^{1}H NMR (600 MHz, DMSO-d_6): δ [ppm] = 12.46 (brs, 1H, NH-a), 9.51 (s, 1H, NH-b), 9.42 (s, 1H, H-2) 8.17-8.12 (m, 1H, H-8'), 8.09 (d, $^3J_{HH}$ = 4.9 Hz, 1H, H-6), 8.94-7.89 (m, 1H, H-5'), 7.74 (d, $^3J_{HH}$ = 4.9 Hz, 1H, H-5), 7.71 (d, $^3J_{HH}$ = 8.2 Hz, 1H, H-4'), 7.65 (d, $^3J_{HH}$ = 7.4 Hz, 1H, H-2'), 7.55-7.50 (m, 2H, H-6', H-7'), 7.48 (t, $^3J_{HH}$ = 7.8 Hz, 1H, H-3'). **^{13}C NMR** (151 MHz, DMSO-d_6): δ[ppm] = 167.9 (COOH), 153.8 (CONH), 141.4 (C-2), 141.1 (C-6), 137.4 (C-3), 134.6 (C-8'a), 133.8 (C-4'a), 130.5 (C-4), 128.4 (C-1'), 128.0 (C-5'), 125.8 (C-6'), 125.7 (C-3'), 125.4 (C-7'), 124.4 (C-4'), 124.0 (C-5), 123.2 (C-8'), 121.6 (C-2'). **ATR-IR**: $\tilde{\nu}$ [cm^{-1}] = 3264, 2921, 2851, 1665, 1630, 1582, 1547, 1504, 1428, 1380, 1345, 1309, 1275, 1258,1238, 792, 770, 741, 711, 674. **HRMS** (ESI$^+$): m/z = 308.1040 (308.1030 calculated for [M+H]$^+$). **R$_f$** = 0.02 (CH$_2$Cl$_2$/CH$_3$OH 9:1 v/v).

6.6.23 Synthesis of benzodioxole derivative 96

2,2-Difluorobenzo[1,3]dioxole-4-carbaldehyde 114

In an inert atmosphere, a solution of 2,2-difluoro-1,3-benzodioxole **113** (1.4 mL, 1.8 g, 11 mmol) in dry tetrahydrofuran (18mL) was cooled to -75 °C and treated dropwise with a *sec*-butyllithium solution (1.4 M in cyclohexane; 11 mL, 15 mmol) and dry *N,N*-dimethylformamide (0.94 mL, 0.89 g, 12 mmol). The reaction solution was stirred for 2.5 h to room temperature. After solvent evaporation under reduced pressure, the residue was treated with hydrochloric acid (1 M, 2 mL) and extracted with

$C_8H_4F_2O_3$
186.0129 g/mol

diethyl ether three times. The combined organic phases were washed twice with brine, dried over sodium sulphate and freed from solvent under reduced pressure. The crude product was purified via column chromatography (CH_2Cl_2/PE 2:1 v/v) to finally give aldehyde **114** (1.3 g, 7.1 mmol, 63 %) as colorless liquid.

¹H NMR (600 MHz, DMSO-d_6): δ [ppm] = 10.07 (s, 1H, COH), 7.73 (dd, $^3J_{HH}$ = 8.1 Hz, $^4J_{HH}$ = 1.2 Hz, 1H, H-7), 7.71 (dd, $^3J_{HH}$ = 8.0 Hz, $^4J_{HH}$ = 1.2 Hz, 1H, H-5), 7.42 (t, $^3J_{HH}$ = 8.0 Hz, 1H, H-6). **¹³C NMR** (151 MHz, DMSO-d_6): δ[ppm] = 188.1 (COH), 143.7 (C-1), 141.9 (C-3), 131.7 (t, $^1J_{CF}$ = 254.8 Hz, C-2), 125.3 (C-5), 124.8 (C-6), 120.1 (C-4), 115.4 (C-7). **¹⁹F NMR** (565 MHz, DMSO-d_6): δ[ppm] = -48.68 (CF$_3$). **ATR-IR**: $\tilde{\nu}$ [cm^{-1}] = 3102, 2841, 2748, 1699, 1646, 1607, 1464, 1395, 1243, 1214, 1149, 1114, 1086, 1061, 1046, 995, 976, 895, 869, 858, 772, 721, 686, 653, 613, 593, 564, 453, 386. **MS** (EI): m/z = 186.00 (186.01 calculated for [M]$^{+\cdot}$). **R$_f$** = 0.55 (CH_2Cl_2/PE 1:2 v/v).
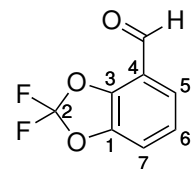
2,2-Difluoro-5-nitrobenzo[1,3]dioxole-4-carbaldehyde 119

Ice-cooled nitric acid (65 % 14 mL) and ice-cooled sulphuric acid (95 %, 11.5 mL) were successively added to 2,2-Difluoro-1,3-benzodioxole-4-carbaldehyde **114** (2.24 g, 12.1 mmol) at 0 °C. The reaction mixture was stirred for three hours at room temperature, poured into demin. ice water (100 mL) and extracted three times with ethyl acetate. Subsequently, the combined organic phases were washed twice with brine, three times with saturated sodium bicarbonate solution and again with brine. Drying over sodium
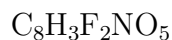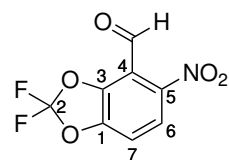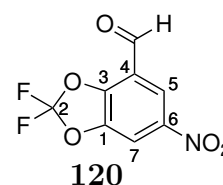
$C_8H_3F_2NO_5$
231.1108 g/mol

sulfate was followed by solvent evaporation under reduced pressure. Final column-chromatographic purification (PE/EA 7:1 v/v) afforded desired product **119** (1.19 g, 5.14 mmol, 43 %) as yellowish crystals.

¹H NMR (600 MHz, DMSO-d_6): δ [ppm] = 10.16 (s, 1H, COH), 8.18 (d, $^3J_{HH}$ = 8.8 Hz, 1H, H-6), 7.85 (d, $^3J_{HH}$ = 8.8 Hz, 1H, H-7). **¹³C NMR** (151 MHz, DMSO-d_6): δ[ppm] = 185.9 (COH), 147.2 (C-5), 144.2 (C-1), 141.6 (C-3), 131.9 (t, $^1J_{CF}$ = 257.8 Hz, C-2), 122.4 (C-6), 116.3 (C-4), 113.2 (C-7). **¹⁹F NMR** (565 MHz, DMSO-d_6): δ[ppm] = -47.95 (CF$_3$). **ATR-IR**: $\tilde{\nu}$ [cm⁻¹] = 3369, 3111, 2943, 2874, 2644, 1691, 1601, 1530, 1461, 1389, 1378, 1347, 1251, 1169, 1141, 1090, 1009, 983, 960, 883, 846, 829, 780, 751, 720, 672, 645, 619, 605, 578, 536, 490, 444. **HRMS** (ESI⁺): m/z = 232.0058 (232.0052 calculated for [M+H]⁺). **R$_f$** = 0.30 (PE/EA 12:1 v/v).

Besides, 2,2-difluoro-6-nitrobenzo[1,3]dioxole-4-carbaldehyde **120** (1.46 g, 6.33 mmol, 53 %) was obtained as yellowish crystals.

¹H NMR (600 MHz, DMSO-d_6): δ [ppm] = 10.12 (s, 1H, COH), 8.68-8.66 (m, 2H, H-5, H-7). **¹³C NMR** (151 MHz, DMSO-d_6): δ[ppm] = 187.1 (COH), 146.0 (C-6), 144.2 (C-1/3), 144.0 (C-1/3), 131.9 (t, $^1J_{CF}$ = 258.5 Hz, C-2), 121.9 (C-5), 119.3 (C-4), 110.8 (C-7). **¹⁹F NMR** (565 MHz, DMSO-d_6): δ[ppm] = -47.68 (CF$_3$). **ATR-IR**: $\tilde{\nu}$ [cm⁻¹] = 3117, 3085, 2880, 1698, 1652, 1538, 1478,

120

C$_8$H$_3$F$_2$NO$_5$
231.1108 g/mol

1452, 1399, 1377, 1342, 1302, 1224, 1165, 1131, 1070, 1003, 942, 896, 885, 839, 784, 743, 720, 702, 615, 560, 542, 455, 383. **MS** (EI): m/z = 231.06 (231.00 calculated for [M]⁺·). **R$_f$** = 0.17 (PE/EA 12:1 v/v).

2,2-Difluoro-5-nitrobenzo[1,3]dioxole-4-carboxylic acid 126

Potassium permanganate (2.29 g, 14.5 mmol) was dissolved in demin. water (60 mL). At 60 °C, a solution of 2,2-difluoro-5-nitro-1,3-benzodioxole-4-carbaldehyde (3.36 g, 14.3 mmol) in acetone (36 mL) was added dropwise for 20 min. Acetone was evaporated and the residual aqueous solution was stirred for 75 min under reflux. The hot mixture was filtered and the solid residue was washed with hot water. After the filtrate was acidified with hydrochloric acid (1 M) to pH 1, it was extracted three times with

C$_8$H$_3$F$_2$NO$_6$
247.1098 g/mol

dichloromethane and the combined organic phases were dried over sodium sulphate. Solvent evaporation under reduced pressure was followed by column-chromatographic
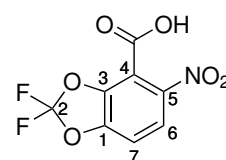
purification (CH$_2$Cl$_2$/acetic acid 20:1 v/v) of the crude product. Carboxylic acid **126** (3.31 g, 13.4 mmol, 92 %) was obtained as colorless crystals.

^{1}H NMR (600 MHz, DMSO-d_6): δ [ppm] = 8.06 (d, $^3J_{HH}$ = 8.8 Hz, 1H, H-6), 7.75 (d, $^3J_{HH}$ = 8.8 Hz, 1H, H-7). **^{13}C NMR** (151 MHz, DMSO-d_6): δ[ppm] = 161.6 (COOH), 146.5 (C-5), 142.7 (C-1), 140.8 (C-3), 131.4 (t, $^1J_{CF}$ = 257.7 Hz, C-2), 122.1 (C-6), 113.3 (C-4), 111.7 (C-7). **^{19}F NMR** (565 MHz, DMSO-d_6): δ[ppm] = -47.93 (CF$_3$). **ATR-IR**: $\tilde{\nu}$ [cm^{-1}] = 3107, 2641, 1988, 1727, 1656, 1611, 1544, 1466, 1350, 1232, 1179, 1126, 1069, 976, 879, 831, 761, 720, 706, 645, 610, 445, 405. **HRMS** (ESI$^+$): m/z = 285.9497 (285.9560 calculated for [M+H]$^+$). **R$_f$** = 0.30 (CH$_2$Cl$_2$/CH$_3$OH/CH$_3$COOH 19:1:1 v/v/v).

Methyl 2,2-Difluoro-5-nitrobenzo[1,3]dioxole-4-carboxylate 127

According to general procedure **1**, the compound was prepared with the exception of using tetrahydrofurane instead of dichloromethane and methanol (4 eq.) instead of anthranilic acid. 2,2-Difluoro-5-nitrobenzo[1,3]dioxole-4-carboxylic acid **126** (3.26 g, 13.0 mmol), oxalyl chloride (1.4 mL, 16 mmol), methanol (2.2 mL, 1.7 g, 52 mmol) and dry triethyl amine (3.7 mL, 2.7 g, 26 mmol). Column-chromatographic purification (CH$_2$Cl$_2$/PE 2:1 v/v) finally yielded methyl ester **127** (3.17 g, 12.2 mmol, 92 %) as yellowish solid.

C$_9$H$_5$F$_2$NO$_6$
261.1368 g/mol

^{1}H NMR (600 MHz, DMSO-d_6): δ [ppm] = 8.13 (d, $^3J_{HH}$ = 8.8 Hz, 1H, H-6), 7.82 (d, $^3J_{HH}$ = 8.8 Hz, 1H, H-7), 3.93 (s, 3H, OCH$_3$). **^{13}C NMR** (151 MHz, DMSO-d_6): δ[ppm] = 160.8 (COO), 146.7 (C-5), 142.6 (C-1), 141.2 (C-3), 131.4 (t, $^1J_{CF}$ = 258.3 Hz, C-2), 122.5 (C-6), 112.5 (C-7), 111.1 (C-4), 53.9 (OCH$_3$). **^{19}F NMR** (565 MHz, DMSO-d_6): δ[ppm] = -47.77 (CF$_3$). **ATR-IR**: $\tilde{\nu}$ [cm^{-1}] = 3108, 2960, 1741, 1658, 1611, 1541, 1462, 1437, 1374, 1347, 1289, 1222, 1167, 1121, 1065, 994, 927, 878, 829, 807, 758, 719, 675, 646, 620, 557, 445, 379. **MS** (EI$^+$): m/z = 261.01 (261.08 calculated for [M]$^{+\cdot}$). **R$_f$** = 0.70 (CH$_2$Cl$_2$).
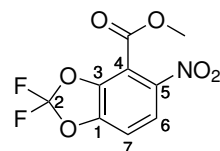
Methyl 5-amino-2,2-difluorobenzo[1,3]dioxole-4-carboxylate 112

According to general procedure **5**, the compound was prepared
using compound **127** (1.06 g, 4.04 mmol) and Pd/C (10 mg).
After 4 h stirring, purification was performed via column chro-
matography (CH_2CH_2/PE 1:1 v/v gradient to pure CH_2CH_2) to
obtain arylamine **112** (789 mg, 3.42 mmol, 85 %) as yellowish
solid.

$C_9H_7F_2NO_4$
231.1548 g/mol
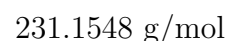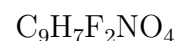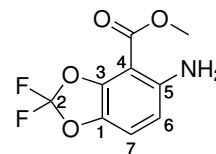
¹H NMR (600 MHz, DMSO-d_6): δ [ppm] = 7.33 (d, $^3J_{HH}$ =
9.1 Hz, 1H, H-7), 6.71 (s, 2H, NH₂), 6.55 (d, $^3J_{HH}$ = 9.0 Hz, 1H,
H-6), 3.84 (s, 3H, OCH₃). **¹³C NMR** (151 MHz, DMSO-d_6): δ[ppm] = 165.1 (COO),
148.6 (C-5), 142.7 (C-1), 128.9 (C-3), 132.6 (t, $^1J_{CF}$ = 121.1 Hz, C-2), 116.1 (C-7),
110.5 (C-6), 95.6 (C-4), 51.9 (OCH₃). **ATR-IR**: $\tilde{\nu}$ [cm⁻¹] = 3108, 2960, 1741, 1658,
1611, 1541, 1462, 1437, 1374, 1347, 1289, 1222, 1167, 1121, 1065, 994, 927, 878, 829,
807, 758, 719, 675, 646, 620, 557, 445, 379. **ATR-IR**: $\tilde{\nu}$ [cm⁻¹] = 3513, 3379, 3204,
3020, 2956, 2848, 1701, 1654, 1614, 1492, 1462, 1436, 1364, 1341, 1279, 1245, 1222,
1192, 1117, 1053, 1016, 916, 879, 805, 782, 722, 704, 650, 623, 607, 500, 403. **HRMS**
(ESI⁺): m/z = 232.0421 (232.0422 calculated for [M+H]⁺). **R_f** = 0.50 (CH_2Cl_2). **Mp**
= 71.6 °C.

**Methyl 2,2-difluoro-5-(1*H*-pyrrole-1-carboxamido)benzo[1,3]dioxole-4-
carboxylate 129**

The compound was prepared according to general pro-
cedure **10** using triphosgene (299 mg, 1.01 mmol), me-
thyl 5-amino-2,2-difluorobenzo [1,3]-dioxol-4-carboxylate **112**
(231 mg, 999 µmol), triethylamine (0.30 mL, 2.2 mmol)),
pyrrole **103c** (0.10 mL, 1.5 mmol)) and *n*-butyllithium (1.6 M
in hexane; 0.95 mL, 1.5 mmol). After column-chromatographic
purification (PE/EA gradient 12:1 to 4:1 v/v), ureide **129**
(125 mg, 386 µmol, 39 %) was obtained as colorless solid.

$C_{14}H_{10}F_2N_2O_5$
324.2398 g/mol
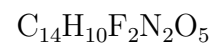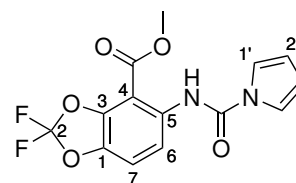
¹H NMR (600 MHz, DMSO-d_6): δ [ppm] = 10.55 (s, 1H, NH) 7.70 (d, $^3J_{HH}$ = 8.8 Hz,
1H, H-7), 7.60 (d, $^3J_{HH}$ = 8.8 Hz, 1H, H-6), 7.46 (t, $^3J_{HH}$ = 2.3 Hz, 2H, H-1'), 6.33
(t, $^3J_{HH}$ = 2.3 Hz, 2H, H-2'), 3.84 (s, 3H, OCH₃). **¹³C NMR** (151 MHz, DMSO-d_6):
δ[ppm] = 163.1 (COO), 148.9 (CONH), 142.4 (C-1), 140.2 (C-3), 133.3 (C-5), 131.3
(t, $^1J_{CF}$ = 253.5 Hz, C-2), 119.9 (C-6), 119.0 (C-1'), 113.8 (C-7), 112.1 (C-2'), 108.7

(C-4), 52.9 (OCH$_3$). **ATR-IR**: $\tilde{\nu}$ [cm^{-1}] = 3278, 3239, 3129, 3093, 2961, 1722, 1695, 1644, 1611, 1567, 1449, 1375, 1332, 1284, 1269, 1238, 1214, 1138, 1097, 1069, 1042, 1008, 986, 954, 932, 887, 871, 862, 834, 807, 793, 729, 712, 681, 656, 618, 600, 531, 488, 462, 415, 394. **HRMS** (ESI$^+$): m/z = 325.0631 (325.0641 calculated for [M+H]$^+$). **R$_f$** = 0.28 (PE/EA 8:1 v/v).

2,2-Difluoro-5-(1*H*-pyrrole-1-carboxamido)benzo[1,3]dioxole-4-carboxylic acid 96

The compound was prepared according to general procedure **8** using methyl ester **129** (0.11 mg, 0.33 mmol). The obtained crude product was purified by column chromatography (CH$_2$Cl$_2$/CH$_3$OH gradient 19:1 to 9:1 v/v) and subsequently recrystallised by solvent diffusion to obtain carboxylic acid **96** (92 mg, 0.30 µmol, 90 %) as colorless solid.

C$_{13}$H$_8$F$_2$N$_2$O$_5$

310.2128 g/mol

¹H NMR (600 MHz, DMSO-d_6): δ [ppm] = 11.17 (brs, 1H, COOH) 7.82 (d, $^3J_{\text{HH}}$ = 8.9 Hz, 1H, H-6), 7.66 (d, $^3J_{\text{HH}}$ = 8.9 Hz, 1H, H-7), 7.44 (t, $^3J_{\text{HH}}$ = 2.3 Hz, 2H, H-1'), 6.34 (t, $^3J_{\text{HH}}$ = 2.3 Hz, 2H, H-2'). **¹³C NMR** (151 MHz, DMSO-d_6): δ[ppm] = 165.1 (COOH), 148.5 (CONH), 142.8 (C-3), 139.6 (C-1), 134.5 (C-5), 131.4 (t, $^1J_{\text{CF}}$ = 253.8 Hz, C-2), 118.8 (C-1'), 118.0 (C-6), 113.7 (C-7), 112.1 (C-2'), 108.0 (C-4). **ATR-IR**: $\tilde{\nu}$ [cm^{-1}] = 3097, 2922, 2853, 1708, 1683, 1639, 1614, 1578, 1468, 1448, 1410, 1370, 1330, 1258, 1237, 1205, 1159, 1102, 1072, 1041, 1003, 977, 950, 873, 861, 829, 798, 764, 731, 705, 620, 608, 584, 534, 496, 460, 411, 400. **HRMS** (ESI$^+$): m/z = 348.9979 (349.0033 calculated for [M+K]$^+$). **R$_f$** = 0.05 (CH$_2$Cl$_2$/CH$_3$OH 19:1 v/v).
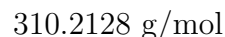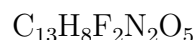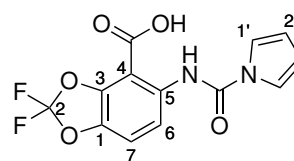
Bibliography

[1] Christopherson, R. I.; Lyons, S. D.; Wilson, P. K. Inhibitors of de Novo Biosynthesis as Drugs. *Acc. Chem. Res.* **2002**, *35*, 961-971.

[2] Munier-Lehmann, H.; Vidalain, P.-O.; Tangy, F; Janin, Y. L. On Dihydroorotate Dehydrogenases and Their Inhibitors and Uses. *J. Med. Chem.* **2013**, *56*, 3148–3167.

[3] Sykes, D. B. The emergence of dihydroorotate dehydrogenase (DHODH) as a therapeutic target in acute myeloid leukemia. *Expert Opin. Ther. Targets* **2018**, *22*, 893-898.

[4] Lolli, M. L.; Sainas, S.; Pippione, A. C.; Giorgis, M.; Boschi, D.; Dosio, F. Use of human Dihydroorotate Dehydrogenase (hDHODH) Inhibitors in Autoimmune Diseases and New Perspectives in Cancer Therapy. *Recent Pat. Anticancer. Drug Discov.* **2018**, *13*, 86–105.

[5] Madak, J. T.; Bankhead, A.; Cuthbertson, C. R.; Showalter, H. D.; Neamati, N. Revisiting the role of dihydroorotate dehydrogenase as a therapeutic target for cancer. *Pharmacol. Ther.* **2019**, *195*, 111– 131.

[6] Boschi, D.; Pippione, A. C.; Sainas, S.; Lolli, M. L. Dihydroorotate dehydrogenase inhibitors in anti-infective drug research. *Eur. J. Med. Chem.* **2019**, 111681.

[7] Fairbanks, L. D.; Bofill, M.; Ruckemann, K.; Simmonds, H. A. Importance of ribonucleotide availability to proliferating T-lymphocytes from healthy humans: Disproportionate expansion of pyrimidine pools and contrasting effects of de novo synthesis inhibitors. *J. Biol. Chem.* **1995**, *270*, 29682–29689.

[8] Quéméneur, L.; Gerland, L.-M.; Flacher, M.; Ffrench, M.; Revillard, J.-P.; Genestier, L. Differential Control of Cell Cycle, Proliferation and Survival of Primary T Lymphocytes by Putine and Pyrimidine Nucleotides. *J. Immunol.* **2003**, *170*, 4986-4995.

[9] Villa, E.; Ali, E.S.; Sahu, U. Ben-Sahra, I. Cancer Cells Tune the Signaling Pathways to Empower de Novo Synthesis of Nucleotides. *Cancers* **2019**, *11(5)*, 688.

[10] Lafita-Navarro, M. C.; Venkateswaran, N.; Kilgore, J. A.; Kanji, S.; Han, J.; Barnes, S.; Williams, N. S.; Buszczak, M.; Burma, S.; Conacci-Sorrell, M. Inhibition of the *de novo* pyrimidine biosynthesis pathway limits ribosomal RNA

transcription causing nucleolar stress in glioblastoma cells. *PLOS Genet.* **2020**, *16*, 1–28.

[11] Wachsman, M.; Hamzeh, F. M.; Assadi, N. B.; Lietman, P. S. Antiviral activity of inhibitors of pyrimidine *de-novo* biosynthesis. *Antivir. Chem. Chemother.* **1996**, *7*, 7-13.

[12] Okesli, A.; Khosla, C.; Bassik, M. C. Human Pyrimidine Nucleotide Biosynthesis as a Target for Antiviral Chemotherapy. *Curr Opin Biotechnol.* **2017**, *48*, 127-134.

[13] Evans, D. R.; Guy, H. I. Mammalian Pyrimidine Biosynthesis: Fresh Insights into an Ancient Pathway. *J. Biol. Chem.* **2004**, *279*, 33035–33038.

[14] Debing, Y.; Neyts, J.; Delang, L. The future of antivirals: broad-spectrum inhibitors. *Curr. Opin. Infect. Dis.* **2015**, *28*, 596-602.

[15] Bekerman, E.; Einav, S. Combating emerging viral threats - Broad-spectrum antiviral drugs are under development to treat emerging viral diseases such as Ebola and dengue for which no specific, licensed treatments exist. *Science* **2015**, *348*, 282-283.

[16] Ka-Wai Hui, E. Reasons for the increase in emerging and re-emerging viral infectious diseases. *Microbes Infect.* **2006**, *8*, 905–916.

[17] Zhao, L.; Seth-Pasricha, M.; Stemate, D.; Crespo-Bellido, A.; Gagnon, J.; Draghi, J.; Duffy, S. Existing host range mutations constrain further emergence of RNA viruses. *J. Virol.* **2019**, *93*, e01385-18.

[18] WHO. WHO Coronavirus (COVID-19) Dashboard - 18th January 2022. https://covid19.who.int.

[19] Mehand, M. S.; Al-Shorbaji, F.; Millett, P.; Murgue, B. The WHO R&D Blueprint: 2018 review of emerging infectious diseases requiring urgent research and development efforts. *Antiviral Res.* **2018**, *159*, 63-67.

[20] ter Horst, S.; Conceicao-Neto, N.; Neyts, J.; Rocha-Pereira, J. Structural and functional similarities in bunyaviruses: Perspectives for pan-bunya antivirals. *Rev. Med. Virol.* **2019**, *29*, e2039.

[21] Houghes, J. P.; Rees, S.; Kalindjian, S. B.; Philpott, K. L. Principles of early drug discovery. *Br. J. Pharmacol.* **2011**, *162*, 1239-1249.

[22] Wilson, G. L.; Lill, M. A. Integrating structure-based and ligand-based approaches for computational drug design. Future Med. Chem. **2011**, *3*, 735-750.

[23] Chung, T. D. Y.; Terry, D. B., Smith, L. H. In Vitro and In Vivo Assessment of ADME and PK Properties During Lead Selection and Lead Optimization – Guidelines, Benchmarks and Rules of Thumb. In: The Assay Guidance Manual. Eli Lilly & Company and the National Center for Advancing Translational Sciences, **2015**.

[24] Thomas, G. An Introduction to Drugs and their Action. In: Fundamentals of Medicinal Chemistry. Wiley, **2003**, 37-56.

[25] Sakai, J. B. Pharmacokinetics: The Absorption, Distribution, and Excretion of Drugs. In: Practical Pharmacology for the Pharmacy Technician. Lippincott Williams & Wilkins, **2009**.

[26] Murakami, T. Absorption sites of orally administered drugs in the small intestine. *Expert Opin. Drug Discov.* **2017**, *12*, 1219-1232.

[27] Di, L.; Artursson, P.; Avdeef, A.; Benet, L. Z.; Houston, J. B.; Kansy, M.; Kerns, E. H.; Lennernäs, H.; Smith, D. A.; Sugano, K. The Critical Role of Passive Permeability in Designing Successful Drugs. *ChemMedChem* **2020**, *15*, 1862-1874.

[28] Wanat, K. Biological barriers, and the influence of protein binding on the passage of drugs across them.*Mol. Biol. Rep.* **2020**, *47*, 3221–3231.

[29] Kansy, M.; Senner, F.; Gubernator, K. Physicochemical High Throughput Screening: Parallel Artificial Membrane Permeation Assay in the Description of Passive Absorption Processes. *J. Med. Chem.* **1998**, *41*, 1007-1010.

[30] Johanson, G. Modeling of Disposition. In: Comprehensive Toxicology. Second Edition, Elsevier, **2010**, 153–177.

[31] Thomas, G. Quantitative structure-activity relationships (QSARS). In: Fundamentals of Medicinal Chemistry. Wiley, **2003**, 71-94.

[32] Kok-Yong, S.; Lawrence, L. Drug Distribution and Drug Elimination, In: Basic Pharmacokinetic Concepts and Some Clinical Applications. IntechOpen, **2015**.

[33] Aldred, E. Drug Excretion. In: Pharmacology: A handbook for complementary healthcare professionals. Churchill Livingstone, **2009**, ISBN: 9780-4430-6896-0.

[34] Fanos, V.; Cataldi, L. Renal Transport of Antibiotics and Nephrotoxicity: a Review. *J Chemother* **2001**, *13*, 461-472.

[35] Appell, K.; Baldwin, J. J.; Egan, W. J. Combinatorial Chemistry and High-Throughput Screening in Drug Discovery and Development. *Sep Sci Technol* **2001**, *3*, 23-56.

[36] Coleman, M. D. Drug Biotransformational Systems - Origins and Aims. In: Human Drug Metabolism - An Intoduction. Wiley-Blackwell, **2010**, 13-22.

[37] Coleman, M. D. How Oxidative Systems Metabolize Substrates. In: Human Drug Metabolism - An Intoduction. Wiley-Blackwell, **2010**, 13-22.

[38] Marques Netto, C. G. C.; Palmeira, D. J.; Brondani, P. B.; Andrade, L. H. Enzymatic reactions involving the heteroatoms from organic substrates. *An. Acad. Bras. Cienc.* **2018**, *90*, 943-992.

[39] Ortiz de Montellano, P. R. Hydrocarbon hydroxylation by cytochrome P450 enzymes. *Chem Rev.* **2010**, *110*, 932-948.

[40] Coleman, M. D. Role of Metabolism in Drug Toxicity. In: Human Drug Metabolism - An Intoduction. Wiley-Blackwell, **2010**, 213-268.

[41] Shakya, A. K.; Al-Najjar, B. O.; Deb, P. K.; Naik, R. R.; Tekade, R. K. Chapter 8 - First-Pass Metabolism Considerations in Pharmaceutical Product Development. In: Dosage Form Design Considerations. Academic Press, **2018**, 259–286.

[42] Jia, L.; Liu, X. The conduct of drug metabolism studies considered good practice (II): in vitro experiments. *Curr. Drug Metab.* **2007**, *8*, 822-829.

[43] Coleman, M. D. Induction of Cytochrome P450 Systems. In: Human Drug Metabolism - An Intoduction. Wiley-Blackwell, **2010**, 65-92.

[44] Thomas, G. Selected Examples of Drug Action at some Common Target Areas. In: Fundamentals of Medicinal Chemistry. Wiley, **2003**, 71-94.

[45] Caldwell, G. W.; Yan, Z.; Lang, W.; Masucci, J. A. The IC$_{50}$ Concept Revisited. *Curr. Top. Med. Chem.* **2012**, *12*, 1282–1290.

[46] Guengerich, F. P. Mechanisms of Drug Toxicity and Relevance to Pharmaceutical Development. *Drug Metab. Pharmacokinet.* **2011**, *26*, 3-14.

[47] Dörwald, F. Z. Lead Optimization. In: Lead Optimization for Medicinal Chemists: Pharmacokinetic Properties of Functional Groups and Organic Compounds. Wiley-VCH, **2012**.

[48] Cecchelli, R.; Berezowski, V.; Lundquist, S.; Culot, M.; Renftel, M.; Dehouck, M.-P.; Fenart, L. Modelling of the blood–brain barrier in drug discovery and development. *Nat. Rev. Drug Discov.* **2007**, *6*, 650–661.

[49] Klebe, G. Wirkstoffdesign: Entwurf und Wirkung von Arzneistoffen, 2nd edition, Spektrum Akademischer Verlag, Heidelberg **2009**.

[50] Bissantz, C.; Kuhn, B.; Stahl, M. A Medicinal Chemist's Guide to Molecular Interactions. *J. Med. Chem.* **2010**, *53*, 5061-5084.

[51] Ullrich, A.; Knecht, W.; Fries, M.; Löffler, M. Recombinant expression of N-terminal truncated mutants of the membrane bound mouse, rat and human flavoenzyme dihydroorotate dehydrogenase. *Eur J Biochem* **2001**, *268*, 1861-1868.

[52] Raushel, F. M.; Thoden, J. B.; Reinhart, G. D.; Holden, H. M. Carbamoyl phosphate synthetase: a crooked path from substrates to products. *Curr Opin Chem Biol.* **1998**; *2(5)*, 624-632.

[53] Lane, A. N.; Fan, T. W.-M. Regulation of mammalian nucleotide metabolism and biosynthesis. *Nucleic Acids Res.* **2015**,*43(4)*, 2466-2485.

[54] Connolly, G. P.; Duley, J. A. Uridine and its nucleotides: biological actions, therapeutic potentials. *Trends Pharmacol Sci.* **1999**, *20(5)*, 218-25.

[55] Nyhan, W. L. Nucleotide Synthesis via Salvage Pathway. In: ELS. John Wiley & Sons, Chichester, **2014**, p. 1-7.

[56] Bhagavan, N. V. Medical Biochemistry, 4. Auflage; Harcourt/Academic Press: San Diego, 2002.

Bibliography

[57] Yang, W. Nucleases: Diversity of Structure, Function and Mechanism. *Q Rev Biophys.* **2011**, *44(1)*, 1-93.

[58] Cao, D. L. J.; McCabe, J.; Kim, B.; Pizzorno, G. Abnormalities in uridine homeostatic regulation and pyrimidine nucleotide metabolism as a consequence of the deletion of the uridine phosphorylase gene. *J Biol Chem.* **2005**, *280(22)*, 21169–75.

[59] Hoogenraad, N. J.; Lee, D. C. Effect of uridine on de novo pyrimidine biosynthesis in rat hepatoma cells in culture. *J. Biol. Chem.* **1974**, *249*, 2763–2768.

[60] Fang, J.; Uchiumi, T.; Yagi, M.; Matsumoto, S.; Amamoto, R.; Takazaki, S.; Yamaza, H.; Nonaka, K.; Kang, D. Dihydro-orotate dehydrogenase is physically associated with the respiratory complex and its loss leads to mitochondrial dysfunction. *Biosci. Rep.* **2013**, *33*, e00021.

[61] Crofts, A. R. The cytochrome bc1 complex: function in the context of structure. *Annu. Rev. Physiol.* **2004**, *66*, 689–733.

[62] Alberts, B.; Johnson, A.; Lewis, J.; Raff, M.; Roberts, K.; Walter, P. Electron-Transport Chains and Their Proton Pumps. In: Molecular Biology of the Cell. 4th edition, Garland Science, New York, **2002**. Available from: https://www.ncbi.nlm.nih.gov/books/NBK21054/

[63] Alcázar-Fabra, M.; Navas, P.; Brea-Calvo, G. Coenzyme Q biosynthesis and its role in the respiratory chain structure. *Biochim. Biophys. Acta - Bioenerg.* **2016**, *1857*, 1073–1078.

[64] Janeway, C. A.; Travers, P.; Walport, M. *et al.* The front line of host defense. In: Immunobiology: The Immune System in Health and Disease. 5th edition. Garland Science, New York, **2001**. ID: NBK27118

[65] Janeway, C. A.; Travers, P.; Walport, M. *et al.* The production of armed effector T cells. In: Immunobiology: The Immune System in Health and Disease. 5th edition. Garland Science, New York, **2001**. ID: NBK27118

[66] Bachmann, M. F.; Kopf, M. On the role of the innate immunity in autoimmune disease. *J Exp Med.* **2001**, *193(12)*, F47-F50.

[67] Alberts, B.; Johnson, A.; Lewis, J. *et al.* T Cells and MHC Proteins. In: Molecular Biology of the Cell. 4th edition. Garland Science, New York, **2002**. ID: NBK26926

[68] Leech, S. Molecular mimicry in autoimmune disease. *Arch Dis Child* **1998**, *79*, 448-451.

[69] Janeway, C. A.; Travers, P.; Walport, M. *et al.* Autoimmune responses are directed against self antigens. In: Immunobiology: The Immune System in Health and Disease. 5th edition. Garland Science, New York, **2001**. ID: NBK27118

[70] Cusick, M. F.; Libbey, J. E.; Fujinami, R. S. Molecular Mimicry as a Mechanism of Autoimmune Disease. *Clinic Rev Allerg Immunol* **2012**, *42*, 42102–111.

[71] Allison, C. A. Immunosuppressive drugs: the first 50 years and a glance forward. *Immunopharmacology* **2000**, *47*, 63-83.

[72] Cann, A. J. Replication of Viruses. In: Encyclopedia of Virology. 3rd edition. Academic Press **2008**, 406–412.

[73] Chinchar, V. G. Replication of Viruses. In: Encyclopedia of Virology. 2nd edition. Elsevier, **1999**, 1471–1478.

[74] Modrow, S.; Falke, D.; Truyen, U.; Schaetzl, H. Molecular virology. Springer-Verlag, Heidelberg, 2013.

[75] Rouse, B.; Sehrawat, S. Immunity and immunopathology to viruses: what decides the outcome?. *Nat Rev Immunol* **2010**, *10*, 514–526.

[76] Lee, K.-Y.; Rhim, J.-W.; Kang, J.-H. Hyperactive immune cells (T cells) may be responsible for acute lung injury in influenza virus infections: a need for early immune-modulators for severe cases. *Med. Hypotheses* **2011**, *76*, 64-69.

[77] Luban, J. Sattler, R. A.; Mühlberger, E.; Graci, J. D.; Cao, L.; Weetall, M.; Trotta, C.; Colacino, J. M.; Bavari, S.; Strambio-De-Castillia, C.; Suder, E. L.; Wang, Y.; Soloveva, V.; Cintron-Lue, K.; Naryshkin, N. A.; Pykett, M.; Welch, E. M.; O'Keefe, K.; Kong, R.; Goodwin, E.; Jacobson, A.; Paessler, S.; Peltz, S. W. al. The DHODH inhibitor PTC299 arrests SARS-CoV-2 replication and suppresses induction of inflammatory cytokines. *Virus Res.* **2021**, *292*, 198246.

[78] 1. Lucas-Hourani, M.; Dauzonne, D.; Jorda, P.; Cousin, G.; Lupan, A.; Helynck, O.; Caignard, G.; Janvier, G.; André-Leroux, G.; Khiar, S.; Escriou, N.; Desprès, P.; Jacob, Y.; Munier-Lehmann, H.; Tangy, F.; Vidalain, P.-O. Inhibition of Pyrimidine Biosynthesis Pathway Suppresses Viral Growth through Innate Immunity. *PLOS Pathog.* **2013**, *9*, 1–18.

[79] Luthra, P.; Naidoo, J.; Pietzsch, C. A.; De, S.; Khadka, S.; Anantpadma, M.; Williams, C. G.; Edwards, M. R.; Davey, R. A.; Bukreyev, A.; Ready, J. M.; Basler, C. F. Inhibiting pyrimidine biosynthesis impairs Ebola virus replication through depletion of nucleoside pools and activation of innate immune responses. *Antiviral Res.* **2018**. *158*, 288-302.

[80] Alberts, B.; Johnson, A.; Lewis, J.; Raff, M.; Roberts, K.; Walter, P. *Molekularbiologie der Zelle*, 5. Auflage WILEY-VCH Verlag, Weinheim **2011**, S. 1191-1260.

[81] Römer, L.; Klein, C.; Dehner, A.; Kessler, H.; Buchner, J. p53 - ein natürlicher Krebskiller: Einsichten in die Struktur und Therapiekonzepte. *Angew. Chem.* **2006**, *118*, 6590-6611.

[82] Ben-Sahra, I.; Howell, J. J.; Asara, J. M.; Manning, B. D. Stimulation of *de novo* pyrimidine synthesis by growth signaling through mTOR and S6K1. *Science* **2013**, *339*, 1323-1328.

[83] Khutornenko, A. A.; Roudko, V. V.; Chernyak, B. V.; Vartapetian, A. B.; Chumakov, P. M.; Evstafieva, A. G.; Pyrimidine biosynthesis links mitochondrial respiration to the p53 pathway. *Proc. Natl. Acad. Sci.* **2010**, *107*, 12828-12833.

[84] Mollick,R.; Laín, S. Modulating pyrimidine ribonucleotide levels for the treatment of cancer. *Cancer Metab.* **2020**, *8*, 12.

[85] Llanos-Cuentas, A.; Casapia, M.; Chuquiyauri, R.; Hinojosa, J.-C.; Kerr, N.; Rosario, M.; Toovey, S.; Arch, R. H.; Phillips, M. A.; Rozenberg, F. D.; Bath, J.; Ng, C. L.; Cowell, A. N.; Winzeler, E. A.; Fidock, D. A.; Baker, M.; Möhrle, J. J.; Hooft van Huijsduijnen, R.; Gobeau, N.; Araeipour, N.; Andenmatten, N.; Rückle, T.; Duparc, S. Antimalarial activity of single-dose DSM265, a novel plasmodium dihydroorotate dehydrogenase inhibitor, in patients with uncomplicated Plasmodium falciparum or Plasmodium vivax malaria infection: a proof-of-concept, open-label, phase 2a study. *Lancet Infect. Dis.* **2018**, *18*, 874-883.

[86] Walse, B.; Dufe, V.; Svensson, B.; Fritzson, I.; Dahlberg, L.; Khairoullina, A.; Wellmar, U.; Al-Karadaghi, S. The structures of human dihydroorotate dehydrogenase with and without inhibitor reveal conformational flexibility in the inhibitor and substrate binding sites. *Biochemistry* **2008**, *47*, 8929–8936.

232

[87] Liu, S.; Neidhardt, E. A.; Grossman, T. H.; Ocain, T.; Clardy, J. Structures of human dihydroorotate dehydrogenase in complex with antiproliferative agents. *Structure* **2000**, *8*, 25–33.

[88] Reis, R. A. G.; Calil, F. A.; Feliciano, P. R.; Pinheiro, M. P.; Nonato, M. C. The dihydroorotate dehydrogenases: Past and present. *Arch. Biochem. Biophys.* **2017**, *632*, 175–191.

[89] Loffler, M.; Carrey, E. A.; Knecht, W. The pathway to pyrimidines: The essential focus on dihydroorotate dehydrogenase, the mitochondrial enzyme coupled to the respiratory chain. *Nucleosides Nucleotides Nucleic Acids* **2020**, 1–25.

[90] Boukalova, S.; Hubackova, S.; Milosevic, M.; Ezrova, Z.; Neuzil, J.; Rohlena, J. Dihydroorotate dehydrogenase in oxidative phosphorylation and cancer. *Biochim. Biophys. Acta Mol. Basis Dis.* **2020**, *1866*, 165759.

[91] Hail, N.; Chen, P.; Kepa, J. J.; Bushman, L. R.; Shearn, C. Dihydroorotate dehydrogenase is required for N-(4-hydroxyphenyl)retinamide-induced reactive oxygen species production and apoptosis. *Free Radic Biol & Med* **2010**, *49*, 109–116.

[92] 1. Dexter, D. L.; Hesson, D. P.; Ardecky, R. J.; Rao, G. V.; Tippett, D. L.; Dusak, B. A.; Paull, K. D.; Plowman, J.; DeLarco, B. M.; Narayanan, V. L., Forbes, M. Activity of a Novel 4-Quinolinecarboxylic Acid, NSC 368390 [6-Fluoro-2-(2'-fluoro-1,1'-biphenyl-4-yl)-3-methyl-4-quinolinecarboxylic Acid Sodium Salt], against Experimental Tumors. *Cancer Res.* **1985**, *45*, 5563–5568.

[93] Chen, S. F.; Ruben, R. L.; Dexter, D. L. Mechanism of action of the novel anticancer agent 6-fluoro-2-(2'-fluoro-I,r-biphenyl-4-yl)-3-methyl-4-quinolinecarboxylic acid sodium salt (NSC 368390): inhibition of de novo pyrimidine nucleotide biosynthesis. *Cancer Res.* **1986**, *46*, 5014-5019.

[94] Schwartsmann, G.; Dodion. P.; Vermorken, J. B.; Ten, B. H. W. W.; Joggi, J.; Winograd, B.; Gall, H.; Simonetti, G.; van der Vijgh, W. J. F.; van Hennik, M. B.; Crespeigne, N.; Pinedo, H. M. Phase I study of Brequinar sodium (NSC 368390) in patients with solid malignancies. *Cancer Chemother Pharmacol* **1990**; *25*, 345-351.

[95] Urba, S.; Doroshow, J.;, Cripps, C.; Robert, F.; Velez-Garcia, E.; Dallaire, B.; Adams, D.; Carlson, R.; Grillo-Lopez, A.; Gyves, J. Multicenter Phase II trial of brequinar sodium in patients with advanced squamous-cell carcinoma of the head and neck. *Cancer Chemother Pharmacol* **1992**, *31*, 167-169.

[96] Natale, R.; Wheeler, R.; Moore, M.; Dallaire, B.; Lynch, W.; Carlson, R. Grillo-Lopez, A.; Gyves, J. Multicenter Phase II trial of brequinar sodium in patients with advanced melanoma. *Ann Oncol* **1992**, *3*, 659-660.

[97] Maroun, J.; Ruckdeschel, J.; Natale, R.; Morgan, R.; Dallaire, B.; Sisk, R.; Gyves, J. Multicenter Phase II study of brequinar sodium in patients with advanced lung cancer. *Cancer Chemother Pharmacol* **1993**, *32*, 64-66.

[98] Moore, M.; Maroun, J.; Robert, F,: Natale, R.; Neidhart, J.; Dallaire, B.; Sisk, R.; Gyves, J. Multicenter Phase II study of brequinar sodium in patients with advanced gastrointestinal cancer. *Invest New Drugs* **1993**, *11*, 61-65.

[99] Cody, R.; Stewart, D.; DeForni, M.; Moore, M.; Dallaire, B.; Azarnia, N.; Gyves, J. Multicenter Phase II study of brequinar sodium in patients with advanced breast cancer. *Am J Clin Oncol* **1993**, *16*, 526-528.

[100] Davis, J. P.; Cain, G. A.; Pitts, W. J.; Magolda, R. L.; Copeland, R. A. The Immunosuppressive Metabolite of Leflunomide Is a Potent Inhibitor of Human Dihydroorotate Dehydrogenase. *Biochemistry* **1996**, *35*, 1270-1273.

[101] Keen, H. I.; Conaghan, P. G.; Tett, S. E. Safety evaluation of leflunomide in rheumatoid arthritis. *Expert Opin. Drug Saf.* **2013**, *12*, 581-588.

[102] Osiri, M.; Shea, B.; Robinson, V.; Suarez-Almazor, M.; Strand, V.; Tugwell, P.; Wells, G. Leflunomide for the treatment of rheumatoid arthritis: a systematic review and metaanalysis. *J Rheumatol.* **2003**, *30*, 1182-1190.

[103] Bartlett, R. R.; Schleyerbach, R. Immunopharmacological profile of a novel isoxazol derivative, HWA 486, with potential antirheumatic activity — I. Disease modifying action on adjuvant arthritis of the rat, *Int. J. Immunopharmacol.* **1985**, *7*, 7-18.

[104] Greene, S.; Watanabe, K.; Traatz-Trulson, J.; Lou, L. Inhibition of dihydroorotate dehydrogenase by the immunosuppressive agent leflunomide. *Biochem. Pharmacol.* **1995**, *50*, 861-867.

[105] Cao, L.; Weetall, M.; Bombard, J.; Qi, H.; Arasu, T.; Lennox, W.; Hedrick, J.; Sheedy, J.; Risher, N.; Brooks, P. C.; Trifillis, P.; Trotta, C.; Moon, Y. C.; Babiak, J.; Almstead, N. G.; Colacino, J. M.; Davis, T. W.; Peltz, S. W. Discovery of Novel Small Molecule Inhibitors of VEGF Expression in Tumor Cells Using a Cell-Based High Throughput Screening Platform. *PLoS One* **2016**, *11*, e0168366.

[106] Cao, L.; Weetall, M.; Trotta, C.; Cintron, K.; Ma, J.; Kim, M. J.; Furia, B.; Romfo, C.; Graci, J. D.; Li, W.; Du, J.; Sheedy, J.; Hedrick, J.; Risher, N.; Yeh, S.; Qi, H.; Arasu, T.; Hwang, S.; Lennox, W.; Kong, R.; Petruska, J.; Moon, Y.-C.; Babiak, J.; Davis, T. W.; Jacobson, A.; Almstead, N. G.; Branstrom, A.; Colacino, J. M.; Peltz, S. W. Targeting of Hematologic Malignancies with PTC299, A Novel Potent Inhibitor of Dihydroorotate Dehydrogenase with Favorable Pharmaceutical Properties. *Mol Cancer Ther* **2019**, *18*, 3-16.

[107] Bender Ignacio, R. A.; Lee, J. Y.; Rudek, M. A.; Dittmer, D. P.; Ambinder, R. F.; Krown, S. E. A Phase 1b/Pharmacokinetic Trial of PTC299, a Novel Post-Transcriptional VEGF Inhibitor, for AIDS-Related Kaposi's Sarcoma: AIDS Malignancy Consortium Trial 059. *J Acquir Immune Defic Syndr.* **2016**, *72*, 52–57.

[108] ClinicalTrials.gov. Bethesda (MD): National Library of Medicine(US). Identifier NCT04439071, A Study to Evaluate Efficacy and Safety of PTC299 in Hospitalized Participants With Coronavirus (COVID-19) (FITE19). First submitted: 17.06.2020; cited: 18.01.2021. Available from: https://clinicaltrials.gov/ct2/keydates/NCT04439071

[109] Leban, J.; Kralik, M.; Mies, J.; Gassen, M.; Tentschert, K.; Baumgartner, R. SAR, species specificity, and cellular activity of cyclopentene dicarboxylic acid amides as DHODH inhibitors. *Bioorg. Med. Chem. Lett.* **2005**, *15*, 4854–4857.

[110] ClinicalTrials.gov. Bethesda (MD): National Library of Medicine(US). Identifier NCT03722576, Vidofludimus Calcium for Primary Sclerosing Cholangitis (PSC). First posted: 29.10.2018; cited: 18.01.2021. Available from: https://clinicaltrials.gov/ct2/show/NCT03722576

[111] ClinicalTrials.gov. Bethesda (MD): National Library of Medicine(US). Identifier NCT03451084, A Dose Optimisation Study of ASLAN003 in Acute Myeloid Leukemia. First posted: 01.03.2018; cited: 18.01.2021. Available from: https://clinicaltrials.gov/ct2/show/NCT03451084

Bibliography

[112] ClinicalTrials.gov. Bethesda (MD): National Library of Medicine(US). Identifier NCT04379271, A Study to Evaluate the Efficacy, Safety and Tolerability of IMU-838 as Addition to Investigator's Choice of Standard of Care Therapy, in Patients With Coronavirus Disease 19 (COVID-19). First posted: 07.05.2020; cited: 18.01.2021. Available from: https://clinicaltrials.gov/ct2/keydates/NCT04379271

[113] Wang, Q.-Y.; Bushell, S.; Qing, M.; Xu, H. Y.; Bonavia, A.; Nunes, S.; Zhou, J.; Poh, M. K.; Florez de Sessions, P.; Niyomrattanakit, P.; Dong, H.; Hoffmaster, K.; Goh, A.; Nilar, S.; Schul, W.; Jones, S.; Kramer, L.; Compton, T.; Shi, P.-Y. Inhibition of dengue virus through suppression of host pyrimidine biosynthesis. *J Virol.* **2011**; *85*, 6548–6556.

[114] Karle, J. M.; Anderson, L. W.; Erlichman, C.; Cysyk, R. L. Serum uridine levels in patients receiving n-(phosphonacetyl)-l-aspartate. Cancer Res. **1980**, *40*, 2938–2940.

[115] Ng, S. B.; Buckingham, K. J.; Lee, C.; Bigham, A. W.; Tabor, H. K.; Dent, K. M.; Huff, C. D.; Shannon, P. T.; Jabs, E. W.; Nickerson, D. A.; Shendure, J.; Bamshad, M. J. Exome sequencing identifies the cause of a mendelian disorder, *Nat. Genet.* **2010**, *42*, 30-35.

[116] Al Kaissi, A.; Roetzer, K. M.; Ulz, P.; Heitzer, E.; Klaushofer, K.; Grill, F. Extra phenotypic features in a girl with Miller syndrome, *Clin. Dysmorphol.* **2011**, *20*, 66-72.

[117] Rainger, J.; Bengani, H.; Campbell, L.; Anderson, E.; Sokhi, K.; Lam, W.; Riess, A.; Ansari, M.; Smithson, S.; Lees, M.; Mercer, C.; McKenzie, K.; Lengfeld, T.; Querol, B. G.; Branney, P.; McKay, S.; Morrison, H.; Medina, B.; Robertson, M.; Kohlhase, J.; Gordon, C.; Kirk, J.; Wieczorek, D.; FitzPatrick, D. R. Miller (Genée–Wiedemann) syndrome represents a clinically and biochemically distinct subgroup of postaxial acrofacial dysostosis associated with partial deficiency of DHODH, *Hum. Mol. Genet.* 2012, *21*, 3969–3983.

[118] Le, T.; Ziemba, A.; Urasaki, Y.; Hayes, E.; Brotman, S.; Pizzorno, G. Disruption of Uridine Homeostasis Links Liver Pyrimidine Metabolism to Lipid Accumulation. J. Lipid Res. **2013**, *54*, 1044-1057.

[119] Zhou, J.; Quah, J. Y.; Ng, Y.; Chooi, J.-Y.; Toh, S. H.-M.; Lin, B.; Tan, T. Z.; Hosoi, H.; Osato, M.; Seet, Q.; Ooi, A. G. L.; Lindmark, B.; McHale, M.; Chng, W.-J. ASLAN003, a potent dihydroorotate dehydrogenase inhibitor for differentiation of acute myeloid leukemia. *Haematologica* **2019**, *105*, 2286–2297.

[120] Baumgartner, R.; Walloschek, M.; Kralik, M.; Gotschlich, A.; Tasler, S.; Mies, J.; Leban, J. Dual Binding Mode of a Novel Series of DHODH Inhibitors. *J. Med. Chem.* **2006**, *49*, 1239-1247.

[121] Costeira-Paulo, J.; Gault, J.; Popova, G.; Ladds, M. J. G. W.; van Leeuwen, I. M. M.; Sarr, M.; Olsson, A.; Lane, D. P.; Laín, S.; Marklund, E. G.; Landreh, M. Lipids Shape the Electron Acceptor-Binding Site of the Peripheral Membrane Protein Dihydroorotate Dehydrogenase. *Cell Chem. Biol.* **2018**, *25*, 309-317.

[122] Fohrmann, N. C. Master thesis. *University of Hamburg* **2016**.

[123] Fritzson, I.; Svensson, B.; Al-Karadaghi, S.; Walse, B.; Wellmar, U.; Nilsson, U. J.; da Graça Thrige, D.; Jönsson, S. Inhibition of Human DHODH by 4-Hydroxycoumarins, Fenamic Acids, and N-(Alkylcarbonyl)anthranilic Acids Identified by Structure-Guided Fragment Selection. *ChemMedChem* **2010**, *5*, 608-617.

[124] Meier, C.; Winkler, M.; Pfaff, K.; Fohrmann, N. C.; Querat, G.; de Lamballerie, X. DHODH inhibitors and their use as antiviral agents. Publication date 2020/11/12. WO/2020/225330 A1.

[125] Pfaff, K. Dissertation. *University of Hamburg* **2018**.

[126] Zeng, F.; Li, S.; Yang, G.; Luo, Y.; Qi, T.; Liang, Y.; Yang, T.; Zhang, L.; Wang, R.; Zhu, L.; Li, H.; Xu, X. Design, synthesis, molecular modeling, and biological evaluation of acrylamide derivatives as potent inhibitors of human dihydroorotate dehydrogenase for the treatment of rheumatoid arthritis. *Acta Pharm. Sin. B* **2020**, in press.

[127] Smith, D. A.; Allerton, C.; Kalgutkar, A. S.; van de Waterbeemd, H.; Walker, D. K. Physicochemistry . In: Pharmacokinetics and Metabolism in Drug Design. Wiley-VCH, **2012**, 1-17.

Bibliography

[128] Davis, M. G.; Manners, C. N.; Payling, D. W.; Smith, D. A.; Wilson, C. A. J. Gastrointestinal absorption of the strongly acidic drug proxicromil. *J. Pharm. Sci.* **1984**, *73*, 949-53.

[129] Lombardo, F.; Shalaeva, M. Y.; Tupper, K. A.; Gao, F. ElogD$_{oct}$. A Tool for Lipophilicity Determination in Drug Discovery. 2. Basic and Neutral Compounds. *J. Med. Chem.* **2001**, *44*, 2490–2497.

[130] van Bremen, R. B.; Li, Y. Caco-2 cell permeability assays to measure drug absorption. *Expert Opin. Drug Metab. Toxicol.* **2005**, *1*, 175-185.

[131] Cui, H.-M.; Zhang, Q. Y.; Wang, J.-L.; Chen, J.-L.; Zhang, Y.-L.; Tong, X. L. Poor permeability and absorption affect the activity of four alkaloids from Coptis. *Mol. Med. Rep.* **2015**, *12*, 7160-7168.

[132] Stockdale, T. P.; Challinor, C. L.; Lehmann, R. P.; De Voss, J. J.; Blanchfield, J. T. Caco-2 Monolayer Permeability and Stability of Chamaelirium luteum (False Unicorn) Open-Chain Steroidal Saponins. *ACS Omega* **2019**, *4*, 7658–7666.

[133] Lipinski, C. A.; Lombardo, F.; Dominy, B. W.; Feeney, P. J. Experimental and computational approaches to estimate solubility and permeability in drug discovery and development settings. *Adv. Drug Deliv. Rev.* **1997**, *23*, 3-25.

[134] Ghose, A. K.; Viswanadhan, V. N.; Wendoloski, J. J. A Knowledge-Based Approach in Designing Combinatorial or Medicinal Chemistry Libraries for Drug Discovery. *J. Combin. Chem.* **1999**, 55–68.

[135] Schmitz, H.; Kohler, B.; Laue, T.; Drosten, C.; Veldkamp, P. J.; Gunther, S.; Emmerich, P.; Geisen, H. P.; Fleischer, K.; Beersma, M. F.; Hoerauf, A. Monitoring of clinical and laboratory data in two cases of imported Lassa fever. *Microbes Infect.* **2002**, *4*, 43–50.

[136] Vrbanac, J., Slauter, R. ADME in Drug Discovery. In: A Comprehensive Guide to Toxicology in Nonclinical Drug Development. Second Edition, Elsevier Inc., **2017**, 39–67.

[137] Richardson, S. J.; Bai, A.; Kulkarni, A. A.; Moghaddam, M. F.; Efficiency in Drug Discovery: Liver S9 Fraction Assay As a Screen for Metabolic Stability. *Drug Metab. Lett.* **2016**, *10*, 83–90.

238

[138] Maiti, M.; Maiti, M.; Rozenski, J.; De Jonghe, S.; Herdewijn, P. Aspartic acid based nucleoside phosphoramidate prodrugs as potent inhibitors of hepatitis C virus replication. *Org. Biomol. Chem.* **2015**, *13*, 5158.

[139] Zhu, Y.; Liu, X.; Zhang, Y.; Wang, Z.; Lasanajak, Y.; Song, X. Anthranilic Acid as a Versatile Fluorescent Tag and Linker for Functional Glycomics. *Bioconjug. Chem.* **2018**, *29*, 3847–3855.

[140] Manna, J. D.; Richardson, S. J.; Moghaddam, M. F. Implementation of a novel ultra fast metabolic stability analysis method using exact mass TOF-MS. *Bioanalysis* **2017**, *9*, 359-368.

[141] Sicho, M.; Stork, C.; Mazzolari, A.; de Bruyn Kops, C.; Pedretti, A.; Testa, B.; Vistoli, G.; Svozil, D. Kirchmair, J. FAME 3: Predicting the Sites of Metabolism in Synthetic Compounds and Natural Products for Phase 1 and Phase 2 Metabolic Enzymes. *J. Chem. Inf. Model.* **2019**, *59*, 3400–3412.

[142] Steiner, K.; Schwab, H. Recent Advances in rational approaches for enzyme engineering. *Comput. Struct. Biotechnol. J.* **2012**, *2*, e201209010.

[143] Syren, P.-O.; Hult, K. Amidases Have a Hydrogen Bond that Facilitates Nitrogen Inversion, but Esterases Have Not. *Chem. Cat. Chem.* **2011**, *3*, 853-860.

[144] Dörwald, F. Z. Amides. In: Lead Optimization for Medicinal Chemists: Pharmacokinetic Properties of Functional Groups and Organic Compounds. Wiley-VCH, **2012**.

[145] Ross, M. K.; Crow, J. A. Human carboxylesterases and their role in xenobiotic and endobiotic metabolism. *J. Biochem. Mol. Toxicol.* **2007**, *21*, 187-96.

[146] Bradshaw, P. R.; Wilson, I. D.; Gill, R. U.; Butler, P. J.; Dilworth, C.; Athersuch, T. J. Metabolic Hydrolysis of Aromatic Amides in Selected Rat, Minipig, and Human In Vitro Systems. *Sci. Rep.* **2018**, *8*, 2405.

[147] Satoh, T.; Hosokawa, M. Carboxylesterases: Structure, Function and Polymorphism. *Biomol. Ther.* **2009**, **17**, 335-347.

[148] Yan, B. Hydrolytic Enzymes. In: Metabolism of Drugs and Other Xenobiotics. Wiley-VCH 2012, p. 165–198.

Bibliography

[149] Das, P.; Deng, X.; Zhang, L.; Roth, M. G.; Fontoura, B. M. A.; Phillips, M. A.; de Brabander, J. K. SAR-Based Optimization of a 4-Quinoline Carboxylic Acid Analogue with Potent Antiviral Activity. *ACS Med. Chem. Lett.* **2013**, *4*, 517-521.

[150] Munier-Lehmann, H.; Lucas-Hourani, M.; Guillou, S.; Helynck, O.; Zanghi, G.; Noel, A.; Tangy, F.; Vidalain, P. O.; Janin, Y. L. Original 2-(3-alkoxy-1H-pyrzol-1-yl)pyrimidine derivatives as inhibitors of human dihydroorotate dehydrogenase (DHODH). *J. Med. Chem.* **2015**, *58*, 860-877.

[151] Stetsenko, A.; Guskov, A. An Overview of the Top Ten Detergents Used for Membrane Protein Crystallization. *Crystals* **2017**, *7*, 197.

[152] Chattopadhyay, G.; Varadarajan, R. Facile measurement of protein stability and folding kinetics using a nano differential scanning fluorimeter. *Protein Science* **2019**, *28*, 1127-1134.

[153] Knecht, W.; Löffler, M.; Species-related inhibition of human and rat dihydroorotate dehydrogenase by immunosuppressive isoxazol and cinchoninic acid derivatives. *Biochem. Pharmacol.* **1998**, *56*, 1259-1264.

[154] Kumari, S.; Carmona, A. V.; Tiwari, A. K.; Trippier, P. C. Amide Bond Bioisosteres: Strategies, Synthesis, and Successes. *J. Med. Chem.* **2020**, *63*, 12290–12358.

[155] Shah, P.; Westwell, A. D. The role of fluorine in medicinal chemistry. *J. Enzyme Inhib. Med.* **2007**, *22*, 527-540.

[156] Kourounakis, A. P.; Xanthopoulos, D.; Tzara, A. Morpholine as a privileged structure: A review on the medicinal chemistry and pharmacological activity of morpholine containing bioactive molecules. *Med. Res. Rev.* **2020**, *40*, 709-752.

[157] Friesner, R. A.; Banks, J. L.; Murphy, R. B.; Halgreen, T. A.; Klicic, J. J.; Mainz, D. T.; Repasky, M. P.; Knoll, E. H.; Shelley, M.; Perry, J. K.; Shaw, D. E.; Francis, P.; Shenkin, P. S. Glide: A New Approach for Rapid, Accurate Docking and Scoring. 1. Method and Assessment of Docking Accuracy. *J. Med. Chem.* **2004**, *47*, 1739-1749.

[158] Beno, B. R.; Yeung, K.-S.; Bartberger, M. D.; Pennington, L. D.; Meanwell, N. A. A Survey of the Role of Noncovalent Sulfur Interactions in Drug Design. *J. Med. Chem* **2015**, *58*, 4383-4438.

[159] Tamargo, J.; Le Heuzey, J.-Y.; Mabo, P. Narrow therapeutic index drugs: a clinical pharmacological consideration to flecainide. *Eur. J. Clin. Pharmacol.* **2015** 71, 549-567.

[160] Gerber, L. Bachelor Thesis. *University of Hamburg* **2019**.

[161] Gallo, R. D. C. ; Gebara, K. S.; Muzzi, R. M.; Raminelli, C. Efficient and selective iodination of phenols promoted by iodine and hydrogen peroxide in water. *J. Braz. Chem. Soc.* **2010**, *21*, 770–774.

[162] Ferreira, I.; Gallo, R. D. C.; Casagrande, G.; Pizzuti, L. Efficient and eco-friendly synthesis of iodinated aromatic building blocks promoted by iodine and hydrogen peroxide in water: a mechanistic investigation by mass spectrometry. *Tetrahedron Lett.* **2012**, *53*, 5372–5375.

[163] Horne, S.; Weeratunga, G.; Rodrigo, R. The regiospecific *p*-deiodination of 2,4-di-iodo phenols; a new synthesis of aflatoxin B$_2$. *J. Chem. Soc. Chem. Commun.*, 1990, *1*, 39–41.

[164] Kauch, M.; Hoppe, D. Synthesis of substituted phenols by directed *ortho*-lithiation of *in situ* *N*-silyl-protected *O*-aryl *N*-monoalkylcarbamates", *Can. J. Chem.* **2001**, *79*, 1736–1746.

[165] Kauch, M.; Hoppe, D. Synthesis of Halogenated Phenols by Directed *ortho*-Lithiation and *ipso*-Iododesilylation Reactions of *O*-Aryl *N*-Isopropylcarbamates. *Synthesis* **2006**, *10*, 1578–1589.

[166] Snieckus, V. Directed Ortho Metalation. Tertiary Amide and Carbamate Directors in Synthetic Strategies for Polysubstituted Aromatics. *Chem. Rev.* **1990**, *90*, 879-933.

[167] Schuemacher, A. C.; Hoffmann, R. W. Condensation Between Isocyanates and Carboxylic Acids in the Presence of 4-Dimethylaminopyridine (DMAP), a Mild and Efficient Synthesis of Amides. *Synthesis* **2001**, *2*, 243-246.

[168] Clayden, J.; Ortholithiation. In: Organolithiums: Selectivity for Synthesis. Pergamon, **2002**.

Bibliography

[169] Kuliszewska, E.; Hammerschmidt, F. On the rearrangement of *N*-aryl-*N*-Boc-phosphoramidates to *N*-Boc-protected *o*-aminoarylphosphonates. *Monatsh. Chem.* **2018**, *149*, 87-98.

[170] Botta, M.; Corelli, F.; Gasparrini, F.; Messina, F.; Mugnaini, C. Chiral azole derivatives. 4.1 Enantiomers of bifonazole and related antifungal agents: synthesis, configuration assignment, and biological evaluation, *J. Org. Chem.* **2000**, *65*, 4736–4739.

[171] Sonogashira, K.; Tohda, Y.; Hagihara, N. A convenient synthesis of acetylenes: catalytic substitutions of acetylenic hydrogen with bromoalkenes, iodoarenes and bromopyridines. *Tetrahedron Lett.* **1975**, *16*, 4467–4470.

[172] Candiani, I.; DeBernardinis, S.; Cabri, W.; Marchi, M.; Bedeschi, A.; Penco, S. A Facile One-Pot Synthesis of Polyfunctionalized 2-Unsubstituted Benzo[*b*]furans. *Synlett* **1993**, *1993*, 269-270.

[173] Sun, W.; Pelletier, J. C. Efficient conversion of primary and secondary alcohols to primary amines. *Tetrahedron Lett.* **2007**, *48*, 7745-7746.

[174] Larock, R. C. Comprehensive Organic Transformations. Wiley & Sons, **1989**, 419–420.

[175] Yamakoshi, H.; Kanoh, N.; Kudo, C.; Sato, A.; Ueda, K.; Muroi, M.; Kon, S.; Satake, M.; Ohori, H.; Ishioka, C.; Oshima, Y.; Osada, H.; Chiba, N.; Shibata, H.; Iqabuchi, Y. Ksrp/fubp2 Is A Binding Protein Of Go-y086, A Cytotoxic curcumin Analogue, *J. Med. Chem.* **2010**, *1*, 273–276.

[176] Merck. IR Spectrum Table & Chart. https://www.sigmaaldrich.com/DE/en/technical-documents/technical-article/analytical-chemistry/photometry-and-reflectometry/ir-spectrum-table.

[177] Ding, R.; He, Y. Wang, X. Xu, J.; Chen, Y. Feng, M. Qi, C. Treatment of Alcohols with Tosyl Chloride Does Not always Lead to the Formation of Tosylates. *Molecules* **2011**, *16*, 5665-5673.

[178] Clayden, J.; Greeves, N.; Warren, S. Elimination Reactions. In: Organic Chemistry. Second Edition, Oxford University Press, **2012**.

[179] Oulette, R. J.; Rawn, J. D. Alcohols: Reactions and Synthesis. In: Organic Chemistry. Second Edition, Academic Press, **2018**.

242

[180] Kara, B. Y.; Kilbas, B. Göksu, H. Selectivity and activity in catalytic hydrogenation of azido groups over Pd nanoparticles on aluminum oxy-hydroxide. *New J. Chem.* **2016**, DOI: 10.1039/C6NJ01925K.

[181] Lange, M.; Pettersen, A. L.; Undheim, K. Synthesis of secondary amines by reductive dimerization of azides. Tetrahedron **1998**, *54*, 5745-5752.

[182] An, I.-H.; Seong, H.-R.; Ahn, K. H. Reductive Dimerization of Azides to Secondary Amines under Hydrogenation Conditions. *Bull. Korean Chem. Soc.* **2004**, *25*, 420-422.

[183] Dayal, B.; Salen, G.; Toome, B.; Tint, G. S.; Shefer, S.; Padia, J. Lithium hydroxide/aqueous methanol: mild reagent for the hydrolysis of bile acid methyl esters. Steroids 1990, 55, 233-237.

[184] Soom, N. A.; Thiemann, T. Hydrogenation of Alkenes with NaBH$_4$, CH$_3$CO$_2$H, Pd/C in the Presence of O- and N-Benzyl Functions. *Int. J. Org. Chem.* **2016**, *6*, 1-11.

[185] Kahn, E. S.; Rheingold, A. L.; Shupack, S. I. Synthesis and properties of palladium(II) complexes with sulfur ligands. *J. crystallogr. spectrosc. res.* **1993**, *23*, 697-710.

[186] Rijono, D. Master Thesis. *University of Hamburg*, 2020.

[187] Rijono, D.; Fohrmann, N. C.; Winkler, M.; Pfeffer, I.; Wilmanns, M.; Meier, C. Manuscript in preparation.

[188] Guram, A. S.; Buchwald, S. L. Palladium-Catalyzed Aromatic Aminations with in situ Generated Aminostannanes. *J. Am. Chem. Soc.* **1994**, *116*, 7901-7902.

[189] Paul, F.; Patt, J.; Hartwig, J. F. Palladium-Catalyzed Formation of Carbon-Nitrogen-Bonds. Reaction Intermediates and Catalyst Improvements in the Hetero Cross-Coupling of Aryl Halides and Tin Amides. *J. Am. Chem. Soc.* **1994**, *116*, 5969-5970.

[190] Laubach, A. Dissertation. *University of Hamburg* **2021**.

[191] Ruiz-Castillo, P.; Buchwald, S. L. Applications of Palladium-Catalyzed C-N Cross-Coupling Reactions. *Chem. Rev.* **2016**, *116*, 12564-12649.

[192] Hofmann, M. Bachelor Thesis. *University of Hamburg* **2018**.

Bibliography

[193] Schlosser, M.; Gorecka, J.; Castagnetti, E. A Homologous Series of *O-* and *N*-Functionalized 2,2-Difluoro-1,3-benzodioxoles: an Exercise in Organometallic Methodology. *Eur. J. Org. Chem.* **2003**, 452–462.

[194] Sainz-Díaz, C. I. A New Approach to the Synthesis of 2-Nitrobenzaldehyde. Reactivity and Molecular Structure Studies. *Monatsh. Chem.* **2002**, *133*, 9-22.

[195] Samant, B. S.; Sukhthankar, M. G., Synthesis and Comparison of Antimalarial Activity of Febrifugine Derivatives Including Halofuginone. *Med. Chem.* **2009**, *5*, 298.

[196] Fry, A. A Tracer Study of the Reaction of Isocyanates with Carboxylic Acids. *J. Am. Chem. Soc.* **1953**, *75*, 2686-2688.

[197] Sheehan, J. C.; Daves, G. D. Benzoxazone Formation in the Reaction of Anthranilic Acid with Isocyanates. *J. Org. Chem.* **1964**, *29*, 3599-3601.

[198] Palfreyman, J. Magnetic Nanoparticle Functionalization. In: Magnetic Nanoparticles in Biosensing and Medicine. Cambridge University Press, **2019**, 68-90.

[199] Bennion, B. J.; Be, N. A.; McNerney, M. W.; Lao, V.; Carlson, E. M.; Valdez, C. A.; Malfatti, M. A.; Enright, H. A.; Nguyen, T. H.; Lightstone, F. C.; Carpenter, T. S. Predicting a Drug's Membrane Permeability: A Computational Model Validated With in Vitro Permeability Assay Data. *J. Phys. Chem.* **2017**, *121*, 5228–5237.

[200] Ölschläger, S.; Gabriel, M.; Schmidt-Chanasit, J.; Meyer, M.; Osborn, E.; Conger, N. G.; Allan, P. F.; Günther, S. Complete sequence and phylogenetic characterisation of Crimean-Congo hemorrhagic fever virus from Afghanistan. *J. Clin. Virol.* **2011**, *50*, 90-92.

[201] Lecompte, E.; Fichet-Calvet, E.; Daffis, S.; Koulémou, K.; Sylla, O.; Kourouma, F.; Doré, A.; Soropogui, B.; Aniskin, V.; Allali, B.; Kouassi, K. S.; Lalis, A.; Koivogui, L.; Günther, S.; Denys, C.; ter Meulen, J. Mastomys natalensis and Lassa fever, West Africa. *Emerg. Infect. Dis.* **2006**, *12*, 1971-1974.

[202] Günther, S.; Asper, M.; Röser, C.; Luna, L. K.; Drosten, C.; Becker-Ziaja, B.; Borowski, P.; Chen, H. M.; Hosmane, R. S. Application of real-time PCR for testing antiviral compounds against Lassa virus, SARS coronavirus and Ebola virus in vitro. *Antiviral Res.* **2004**, *63*, 209-215.

[203] Zhang, Y.; Huo, M.; Zhou, J.; Xie, S. PKSolver: An add-in program for pharmacokinetic and pharmacodynamic data analysis in Microsoft Excel. *Comput. Methods Programs Biomed.* **2010**, *99*, 306–314.

List of hazards and precautionary statements

01	02	03	04	05	06	07	08	09

Substance	GHS-code	H-statement	P-statement
Acetic acid	02, 05	226, 314	280, 305/351/338, 310
Acetone	02, 07	225, 319, 336	210, 241, 243, 305/351/338, 403/235
Acetonitrile	02, 07	225, 302/312/332, 319	210, 261, 280, 305/351/338, 370/378, 403/235
Acrylamide	06, 08	301/311, 315, 317, 319, 332, 340, 350, 361, 402	201, 280, 301/310, 305/351/338, 308/313
2-Aminobenzoic acid	05	318, 280, 305/358/338	280, 305/351/338
3-Aminoisonicotinic acid	07	315, 319, 335	261, 264, 271, 280, 302/352, 304/340, 305/351/338, 312, 321, 332/313, 337/313, 362, 403/233, 405, 501
Ammonium peroxodisulfate	03, 07, 08	272, 302, 315, 317, 319, 334, 335	210, 280, 301312, 302/352, 304/340/312, 305/351/338
Aniline	05, 06, 08, 09	301/311/331, 317, 318, 341, 351, 372, 410	273, 280, 301/310, 302/352/312, 304/340/311, 305/351/338
Benzoic acid	05, 08	315, 318, 372	260, 264, 280, 302/352, 305/351/338, 314

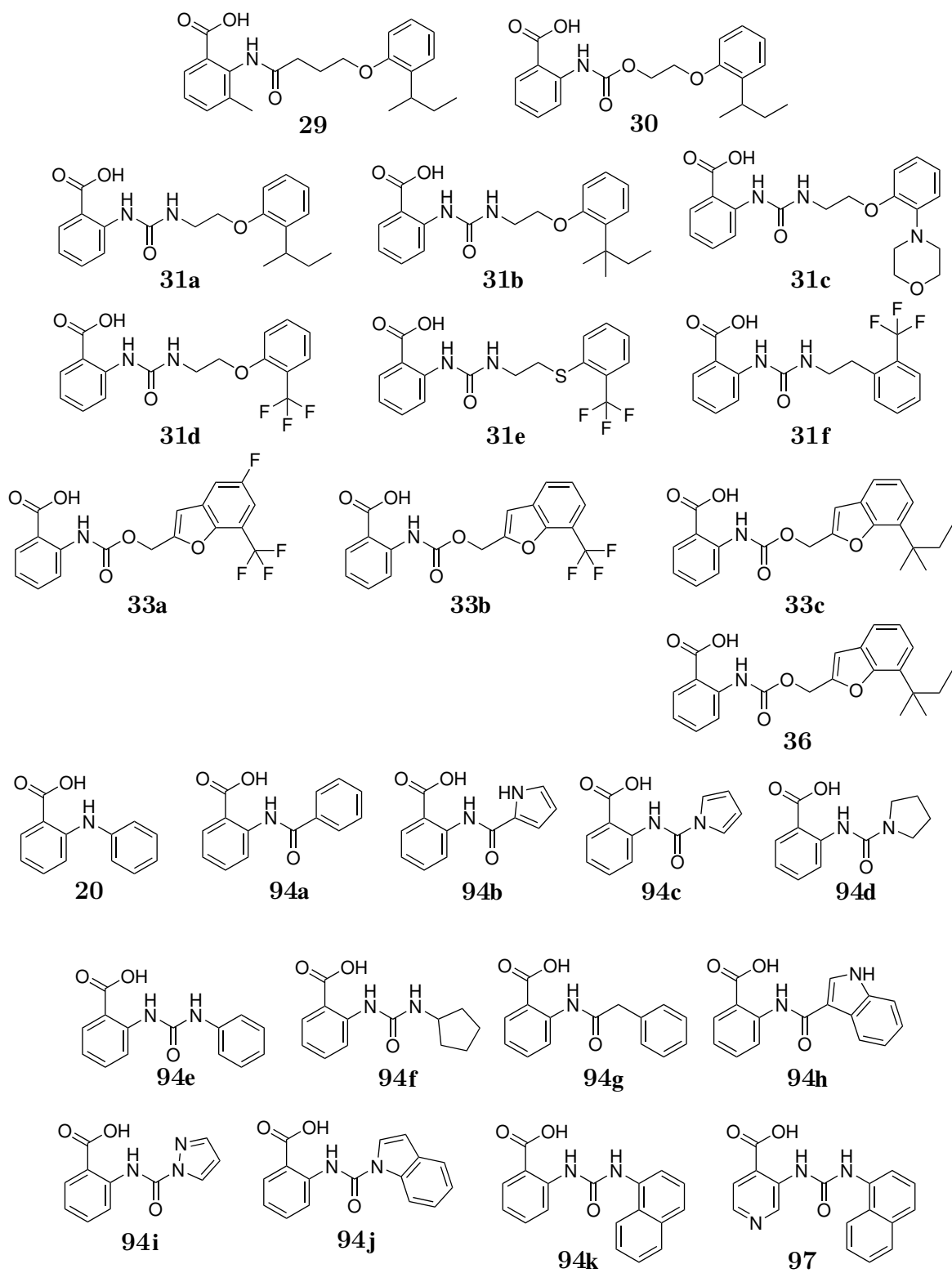|			
Benzyl 2-aminobenzoate	07	315, 319, 335	261, 264, 271, 280, 302/352, 304/340, 305/351/338, 312, 321, 332/313, 337/313, 362, 403/233, 405, 501
2-Bromoethanol	05, 06	301/311/331, 314	261, 270, 280, 303/361/353, 304/340/310, 305/351/338
2-(Butan-2-yl)phenol	05, 07, 09	302, 312, 314, 318, 332, 411	260, 261, 264, 270, 271, 273, 280, 301/312, 301/330/331, 301/352, 303/361/353, 304/312, 304/340, 305/351/338, 310, 312, 321, 322, 330, 363, 391, 401, 501
n-Butyllithium (1.6 M in hexane)	02, 05, 07, 08, 09	225, 250, 261, 304, 314, 336, 361f, 373, 411	210, 222, 231/232, 261, 273, 422
sec-Butyllithium (1.4 M in cyclohexane)	02, 05, 07, 08, 09	225, 250, 260, 304, 314, 336, 410	210, 222, 223, 231/232, 370/378, 422
Celite	07, 08	319, 335, 373	261, 305/351/338
Chloroform	06, 08	302, 315, 319, 331, 336, 351, 361d, 372	260, 261, 280, 301/312/330, 304/340/311, 305/351/338, 403/233
3-Chloroperoxybenzoic acid	02, 03, 05, 07	226, 242, 271, 302, 314, 315, 317, 318, 319, 335	210, 220, 221, 233, 234, 240, 241, 242, 243, 260, 261, 264, 270, 272, 280, 283, 301/312, 301/330/331, 302/352, 303/361/353, 304/340, 305/351/338, 306/360, 310, 312, 321, 330, 332/313, 333/313, 337/313, 362/363, 370/378, 371/380/375, 403/233, 403/235, 405, 411, 420, 501

248

Copper(I) iodide	05, 07, 09	302, 315, 317, 318, 335, 410	280, 301/330/331, 305/351/338
Cyclopentyl isocyanate	02, 07, 08	226, 302, 332, 335, 319, 312, 315, 334	280, 261, 304/341, 342/311, 302/352, 261, 301/312, 304/340, 280, 305/351/338, 210
Dichloromethane	07, 08	315, 319, 335, 336, 351, 371	260, 280, 305/351/338
2,6-Dichlorophenol-indophenol	07	302, 315, 319, 332	261, 264, 270, 271, 280, 301/312, 302/352, 304/340, 305/351/338, 312, 321, 330, 332/313, 337/313, 362, 403/233, 405, 501
Diethyl ether	02, 07	224, 302, 336	210, 240, 403/235
2,2-Difluoro-1,3-benzodioxole	07	315, 317, 319, 335	280, 302/352, 305/351/338
L-Dihydroorotate	07	315, 319, 335	261, 264, 271, 280, 302/352, 304/340, 305/351/338, 312, 321, 332/313, 337/313, 362, 403/233, 405, 501
N,*N*-Diisopropylethylamine	02, 05, 06	225, 302, 318, 331, 335	210, 280, 301/312/330, 304/340/311, 305/351/338/310
4-(Dimethylamino)-pyridine	06	301, 310, 315, 319, 335	280, 301/310/330, 302/352/310, 304/340/312, 305/351/338, 337/313
N,*N*-Dimethylformamide	02, 07, 08	226, 312/332, 319, 360	201, 280, 305/351/338, 308/313
Disodium hydrogen phosphate	05, 07	318, 319	264, 280, 305/351/338, 310, 337/313
Dry ice	-	281	-
Ethyl acetate	02, 07	225, 319, 336	210, 261, 280, 240, 241, 303/361/353, 305/351/338, 304/340, 405, 501a

4-Fluoro-2-(trifluoro-methyl)phenol	05, 07	302, 312, 314, 315, 319, 332, 335	260, 261, 264, 270, 271, 280, 301312, 301/330/331, 302/352, 303/361/353, 304/312, 304/340, 305/351/338, 310, 312, 321, 322, 330, 332/313, 334/313, 362, 363, 403/233, 405, 501
Formic acid	02, 05, 07	331, 302, 314, 318, 226	210, 280, 303/361/353, 305/351/338, 301/330/331, 304/340, 405, 501a
Hydrochloric acid (25 %)	05, 07	290, 314, 335	234, 261, 271, 280, 303/361/353, 305/351/338
Hydrogen	02, 04	220, 280	210, 377, 381, 403
Imidazole	05, 07, 08	302, 314, 360D	201, 202, 260, 264, 270, 280, 281, 301/312, 301/330/331, 303/361/353, 304/P340, 305/351/338, 308/313, 310, 321, 330, 363, 405, and 501
Indole	06, 09	302, 311, 319, 400	264, 273, 280, 301/312, 305/352/312, 305/351/338
Iodine	07, 09	400, 312, 332	261, 273, 280, 271, 304/340, 312, 363, 322, 302/352, 501a
Iodine monochloride	05, 07	314, 335	261, 271, 280, 301/330/331, 303/351/338, 305/351/338
Kanamycin sulfate	08	360	201, 308/313
Methanesulfonyl chloride	02, 06	301, 311, 330, 314	260, 301/310, 303/361/353, 305/351/338, 320, 361, 405, 501
Methanol	02, 06, 08	225, 301/311/331, 370	210, 280, 302/352, 403/235

2-(2-Methylbutan-2-yl)phenol	05, 06, 07, 09	302, 311, 314, 318, 332, 410, 411	260, 261, 264, 270, 271, 273, 280, 301/312, 301/330/331, 302/352, 303/361/353, 304/312, 304/340, 305/351/338, 310, 312, 321, 322, 330, 361, 363, 391, 405, 501
Methyl 2-aminobenzoate	07	315, 319	280, 305/351/338
Methyl 2-amino-3-methylbenzoate	07	315, 319	264, 280, 337/313, 305/351/338, 302/352, 332/313, 362
Methyl chloroformate	02, 05, 06	225, 302/312, 314, 330	210, 280, 301/330/331, 303/361/353, 304/340/310, 305/351/338/310
Molecular sieves	07	315, 319	305/351/338
2-(4-Morpholino)phenol	05, 07	302, 315, 318, 335	261, 280, 305/351/338
1-Naphthyl isocyanate	07, 08	302/312/332, 315, 317, 319, 334, 335	261, 264, 280, 301/312, 302/352/312, 305/351/338
Nitrogen	04	280	403
Oxalyl chloride	02, 05, 06	260, 301/331, 314	223, 231/232, 280, 303/361/353, 304/340/310, 305/351/338, 402/404
Permanganate staining solution	08, 09	341, 361, 411	201, 202, 273, 280, 308/313, 391, 405, 501
Petroleum ether	02, 07, 08, 09	225, 304, 315, 336, 361f, 373, 411	201, 210, 273, 301/310, 303/361/353, 331, 403/233
Phenylacetic acid	07	319	305/315/338
Phenyl isocyanate	02, 05, 06, 08	226, 302, 314, 317, 330, 334	210, 280, 301/312, 303/361/353, 304/340/310, 305/351/338

Potassium *tert*-butoxide	02, 05	228, 260, 314	210, 231, 232, 260, 280, 303/361/353, 305/351/338, 402/404
Potassium carbonate	07	315, 319, 335	261, 264, 271, 280, 302/352, 305/351/338
Potassium permanganate	03, 05, 07, 08, 09	272, 302, 314, 361f, 373, 410	210, 220, 280, 301/330/331, 303/361/353, 305/351/338, 310
Prop-2-in-1-ol	02, 05, 06, 08, 09	226, 301, 310, 314, 330, 373, 411	210, 273, 280, 303/361/353, 304/340/310, 305/351/338, 403/235, 403/233, 405
Pyrazole	05, 06, 08	302, 311, 315, 318, 373, 412	273, 280, 301/312/330, 302/352/312, 305/351/338/310, 314
Pyrrole	02, 05, 06	226, 301, 318, 332	210, 233, 280, 301/310, 304/340/312, 305/351/338
Pyrrole-2-carboxylic acid	07	315, 319, 335	261, 305/351/338
Pyrrolidine	02, 05, 07	225, 302/332, 314	210, 280, 301/312, 303/361/353, 304/340/310, 305/351/338
ROTI®Mark Standard	07	305/351/338	338, 337/313
Sodium azide	06, 08, 09	300/310, 373, 410	273, 280, 301/310/330, 305/352/310, 391, 501
Sodium dodecyl sulfate	02, 05, 07, 09	228, 302/332, 315, 318, 335, 412	210, 273, 280, 301/312, 304/340/312, 305/351/338
Sodium hydride	02, 05	228, 260, 314	210, 223, 280, 231/232, 335/334, 370/378, 422, 402/404
Sodium hydroxide	05	290, 314	234, 260, 280, 303/361/353, 304/340/310, 305/351/338

Sulfuric acid (conc.)	05	314, 290	280, 301, 330, 331/309, 310, 305/351/338
Tetra-*N*-butylammonium iodide	07	302	264, 270, 301/312, 501
Tetrahydrofurane	02, 07, 08	225, 302, 319, 335, 336, 351	201, 202, 210, 301/312, 305/351/338, 308/313, 403/233
N,N,N',N'-Tetra-methylethylenediamine	02, 05, 06	225, 301/331, 314	210, 233, 280, 303/361/353, 304/340/310, 305/351/338, 403/233
N,N,N',N'-Tetramethylguanidine	02, 05, 07	226, 290, 302, 314	210, 233, 280, 301/312, 303/361/353, 305/351/338
Thionyl chloride	05, 06	302, 314, 331, 335	261, 280, 301/312, 303/361/353, 304/340/310, 305/351/338
Toluene	02, 07, 08	225, 304, 315, 336, 361d, 373, 412	201, 210, 273, 301/310, 303/361/353, 331, 403/233
Trichloromethane	06, 08	302, 315, 319, 331, 336, 351, 361d, 372	201, 301/312, 302/352, 304/340/311, 305/351/338, 308/313
Triethylamine	02, 05, 06	225, 302, 311/331, 314, 335	210, 280, 301/361/353, 304/340/310, 305/351/338, 403/233
2-(Trifluoromethyl)-phenol	02, 05, 07	228, 302/312/332, 315, 318, 335	210, 261, 280, 305/351/338
Trimethylsilyl chloride	02, 05, 06	225. 301/331, 312, 314	210, 261, 280, 301/310, 305/351/338, 310
Trimethylsilyl trifluo-romethanesulfonate	02, 05, 07	226, 314, 335	210, 280, 301/330/331, 304/340, 305/351/338, 308/310

Triphosgene	05, 06	314, 330	260, 280, 284, 305/351/338, 310
Triton X-100	05, 07, 09	302, 315, 318, 410	264, 273, 280, 301/312, 302/352, 305/351/338
Vanillin	07	319	305/351/338
Vanillin staining solution	02, 05, 07, 08	302, 314, 360, 371, 372, 373, 340, 335, 336, 401, 225	501, 273, 260, 270, 202, 240, 210, 233, 201, 243, 241, 242, 271, 264, 280, 370/378, 308/311, 303/361/353, 301/330/331, 301/312/330, 304/340/310, 305/351/338/310, 403/233, 403/235, 405.
Zwittergent 3-10 (3-(decyldimethyl-ammonio)propane-1-sulfonate)	07	315, 319, 335	261, 264, 271, 280, 302/352, 304/340, 305/351/338, 312, 321, 332/313, 337/313, 362, 403/233, 405, 501

List of target compounds

29

30

31a

31b

31c

31d

31e

31f

33a

33b

33c

36

20

94a

94b

94c

94d

94e

94f

94g

94h

94i

94j

94k

97

Acknowledgment

Declaration on Oath

I hereby declare on oath, that I have written the present dissertation by my own and have not used other than the acknowledged resources and aids. The submitted written version corresponds to the version on the electronic storage medium. I hereby declare that I have not previously applied or pursued for a doctorate (Ph.D. studies).

Hiermit versichere ich an Eides statt, die vorliegende Dissertation selbst verfasst und keine anderen als die angegebenen Hilfsmittel benutzt zu haben. Die eingereichte schriftliche Fassung entspricht der auf dem elektronischen Speichermedium. Ich versichere, dass diese Dissertation nicht in einem früheren Promotionsverfahren eingereicht wurde.

....

Place, Date   Nora Constanze Laubach, M. Sc.